Modelling the Interaction Between Titania Surfaces and Strong-binding Peptides

by

Adam Skelton

A thesis submitted in partial fulfilment of the requirements for the degree of Doctor of Philosophy in Chemistry

University of Warwick

Deparment of Chemistry

April 2008

Abstract

The aim of this thesis is to understand the interactions of peptides with surfaces so that we can potentially exploit this information in the control of adsorption of biomolecules on surfaces. The study concentrates on titania surfaces which have specific applications, *e.g.* in biosensors and titania implants. A peptide, RKLPDA, which was experimentally found to be strong-binding to titania is studied by molecular dynamics [1].

The interaction of the rutile (110) surface with water is considered and molecular dynamics simulations are performed using the Bandura/Predota model for titania [2, 3] and TIP3P water[4, 5]. It is found that there is significant water structuring both perpendicular to the surface and in the orientation of the water molecules due to the surface. It is shown that the results agree with X-ray truncation rod experiments[6] and other simulations that use SPC/E water.

MD simulations of the RKLPDA peptide in water are made using the Charmm27/TIP3P force-field. It is found that the water structuring at the charged groups, Asp, Arg and Lys is significant and likely to influence its behaviour, especially when close to the structured water at titania. Experimental decreases in binding affinity of the peptide on titania upon mutation of the Pro for Ala have been suggested in terms of an increase in the flexibility of the backbone. The work described in this thesis suggests that the Lys-backbone carbonyl and Lys/Asp interactions are responsible for experimentally observed increases of the Lys-mutant compared to the unmutated peptide.

MD simulations of the RKLPDA peptide adsorbed onto the titania surface with explicit water molecules are performed. It is shown that the charged groups bind to the structured water layers, not the surface itself, in a 'horseshoe' structure first proposed by Sano and Shiba [1]. Examples are shown where the Lys-mutant stays bound to the surface but the unmutated peptide does not, and the where the unmutated peptide binds to the surface but the Pro-mutant does not. These follow the trends shown by experiment and indicates a conformational aspect to binding.

Contents

List of Figures

Acknowledgements

I would like to acknowledge my Supervisor Tiffany Walsh without whom I may not have embarked on such a scientific journey. I would like to thank the old and new members of the theory and computational group who have certainly helped in providing a positive and entertaining workplace. These include Dave Haggart, James Burnside, Christian Dietrich, Dan Jones, Susana Tomasio, Sara Fortuna, Becky Notman, Bibo Jiang and Dan Harding. Robert Hawtin and Kazim Yusaf are certainly in this category but were also very helpful at the start of my PhD, providing well needed programming and computer assistance. I would like to thank Anna Anastasi for proof-reading my thesis. A special thanks to David Quigley and Taining Liang for hours of helpful scientific discussion. Also, vital to my PhD have been the computer facilities provided by the National Grid Service and Centre for Scientific Computing. I would also like to acknowledge the EPSRC Consortium 'Modelling of the Biological Interface with Materials' and Warwick PGF for their funding.

Last and certainly not least, I would like to thank my parents Yvonne and Roger Skelton, and Hanne Kinnunen for their continual support throughout the PhD.

Declaration

This thesis represents original material, and is the author's own work. No part of this thesis has been previously created or published by a person other than the author, unless otherwise acknowledged in the text. This thesis has not been submitted for a degree at an establishment other than the University of Warwick. Part of the work presented in this thesis has also appeared in the following publication: A. A. Skelton and T. R. Walsh. Mol. Simulat. **33**,379 (2007)

List of Abbreviations

QCM	Quartz crystal microbalance
NMR	Nuclear magnetic resonance
CD	Circular dichroism
NOE	Nuclear Overhauser effect
FTIR	Fourier transform infra-red
AFM	Atomic Force microscopy
GP1	gold binding peptide 1
IRAS	infrared reflection-absorption spectroscopy
IgG	Immunoglobulin
GOx	glucose oxidase
SAMS	self-assembling monolayers
RP-HPLC	reversed phase high performance liquid chromatography
HSA	human serum albumin
(P)DFT	(Periodic) Density functional theory
LDA	Local Density Approximation
KE	Kinetic energy
MD	Molecular dynamics
MC	Monte Carlo
PW91	Perdew-Wang 91
NMA	N-methylacetamide
CPMD	Car-Parrinello Molecular Dynamics
ASP	Atomic solvation parameters
UHV	Ultra high vacuum
TPD	temperature programmed desorption
HREELS	high resolution electron energy loss spectroscopy
XPS	X-ray photoelectron spectroscopy
GGA	Generalized Gradient Approximation
BLYP	Becke, Lee, Yang, and Parr
VDW	Van der Waals
RPBE	revised Perdew-Burke-Ernzerhof
NVT	fixed number of atoms, volume and temperature
NVT	fixed number of atoms, pressure and temperature
AMBER	Assisted Model Building with Energy Refinement
CHARMM	Chemistry At Harvard Molecular Mechanics
AMOEBA	Atomic Multipole Optimized Energetics for Biomolecular Applications
SPC/E	extended simple point charge
OEG	Oligoetylene oxide
PMF	potential of mean force
CNT	carbon nanotubes
CHelpG	Charges from Electrostatic Potentials using a Grid based method

HFWL	Hartree Fock and Wilson Levy
RMSD	root mean squared deviation
COM	centre of mass
SGMD	self-guided molecular dynamic
REMD	replica exchange molecular dynamics
PE	Poisson equation
GB	Generalised Born
RDF	radial distribution functions
LW	Liang and Walsh

Glossary

This Glossary will show the notation used for peptides. Throughout the thesis each peptide residues will be assigned three-letter or one-letter codes. They are shown in Table . For example tri-alanine will be labelled AAA.

Residue	Three letter	One letter	Polar/Nonpolar	Charge at pH=7
Alanine	Ala	A	nonpolar	neutral
Arginine	Arg	R	polar	positive
Asparagine	Asn	N	polar	neutral
Aspartic acid	Asp	D	polar	negative
Cysteine	Cys	C	polar	neutral
Glutamic acid	Glu	E	polar	negative
Glutamine	Gln	Q	polar	neutral
Glycine	Gly	G	nonpolar	neutral
Histidine	His	H	polar	neutral
Isoleucine	Ile	I	nonpolar	neutral
Leucine	Leu	L	nonpolar	neutral
Lysine	Lys	K	polar	positive
Methionine	Met	M	nonpolar	neutral
Phenylalanine	Phe	F	nonpolar	neutral
Proline	Pro	P	nonpolar	neutral
Serine	Ser	S	polar	neutral
Threonine	Thr	T	polar	neutral
Tryptophan	Trp	W	nonpolar	neutral
Tyrosine	Tyr	Y	nonpolar	neutral
Valine	Val	V	nonpolar	neutral

Chapter 1

Introduction

1.1 Motivation to study the interaction between peptides/proteins and inorganic surfaces

Over the last 20 years, much research effort has been invested into studying the interactions between proteins, peptides and amino acids with inorganic surface for many different reasons [9, 10]. First, these interactions can be undesirable. Adsorption of fibrinogen to surgical implants causes blood coagulation [11] and must be minimimized. In chromatography [12] and food separation by membrane separation techniques [13], protein interaction can cause blockages. In enzymatic reactions in glass vessels, enzymes can be rendered inactivated by adsorption onto the glass surface [14]. The main aim of research in these fields is therefore to understand the interaction between proteins and surfaces so that different materials can be used in order to minimise these interactions.

The second reason is that these interactions can actually be used in biotechnology. Applications include: nanoassembly [15], control of crystal growth [16, 17] and biosensors[18, 19, 20, 21]. In this instance, the aim of research is to understand the interaction between proteins/peptides and surfaces to find peptides which selectively bind to some surfaces but not others. This selectivity can then be manipulated to develop new materials and

devices [8, 22].

Lastly, protein/peptide interactions with surfaces are studied to gain fundamental information about the biophysics/chemistry of proteins/peptides.

The motivation for the present study is all three of the above. Surgical implants and biosensors both rely on the interaction between peptides and titania surfaces; we aim to gain an understanding of protein/peptide-surface interactions that may help developers of biosensors to control the adsorption. For surgical implants, it is the uncontrolled non-specific adsorption which should be understood so it can be avoided. These two applications will be described in more detail later in this chapter. Of course, as theoretical scientists we also want to gain fundamental insight into the nature of the interaction with the surface, the conformational changes upon adsorption and the role of the solvent in adsorption.

Before discussing the studies of the interaction between proteins and peptides with surfaces and giving more detail about applications, a summary about proteins and peptides will be given. This knowledge is a requisite for understanding these studies and more importantly the present study.

1.2 Amino acids, peptides and proteins

Amino acids are the building blocks of peptides and proteins. They contain both an amine and a carboxyl functional group. A structure is shown in Figure 1.1.

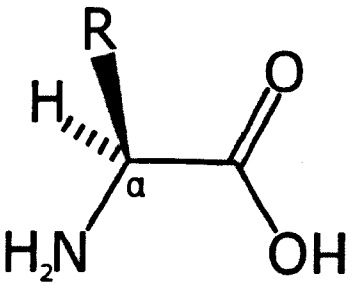

Figure 1.1: A generic amino acid. R denotes a general side-chain. The α-carbon is indicated by α.

In α-amino acids, the amino and carboxylate groups are attached to the same carbon, called the α-carbon. There are 20 different naturally occurring amino acids and they differ only by the group which is connected to the α-carbon (corresponding to R in Figure 1.1. Peptides are polymers of amino acids formed by an amide bond (peptide bond) between the carboxylate group of one amino acid and amine group of another. Proteins are macromolecular polymers of amino acids. They form three dimensional (3D) folded structures which are essential for their function. In the case of proteins this polymerisation is performed by enzymes (large protein catalysts) in biological systems.

1.2.1 Primary and secondary structure of peptides

The primary structure of a protein or peptide is the sequence of residues in the chain. Since there are 20 naturally occurring amino acids, the number of different peptides of a given size (even a small peptides) is massive *e.g* there are 20^6 possible hexapeptide sequences. The secondary structure of a protein or peptide is the conformation it adopts. This is mainly governed by the torsions of the backbone. Each residue will have a different effect on the backbone torsions and this will depend on the size of the side chain, the interaction of the side chain with the solvent and the hydration of the backbone and side chain. Also, in the case of Pro (a ring made up partly of the side chain, partly made up of backbone) a change in the chemistry of the backbone itself will have an effect. These issues will be discussed further in relation to the peptide studied presently in later chapters.

1.2.2 The backbone dihedral angles: ϕ, ψ and ω.

There are three principal torsions per residue in a peptide. These are shown in Figure 1.2. These three torsions are quite different in the angles they tend to adopt. The ω dihedral is the torsion angle around the peptide bond, is usually trans and and usually assumes a value of about 180°. It is therefore the ϕ and ψ angles that dictate the back-

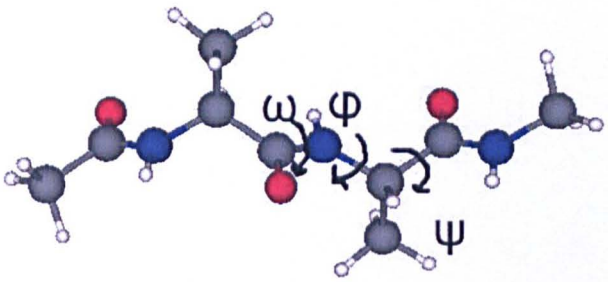

Figure 1.2: The three principal backbone dihedral angles in the alanine dipeptide.

bone conformation of a peptide. The notation used to describe the torsional state around a particular peptide bond is (ϕ, ψ) (in degrees).

1.2.3 α-helices, β-sheets (β-hairpins) and random coil conformations

In peptides and proteins, particular backbone torsions and combinations of backbone torsions are favoured. To give an idea about the backbone torsions which are usually adopted, a typical Ramachandran plot is shown in Figure 1.3.

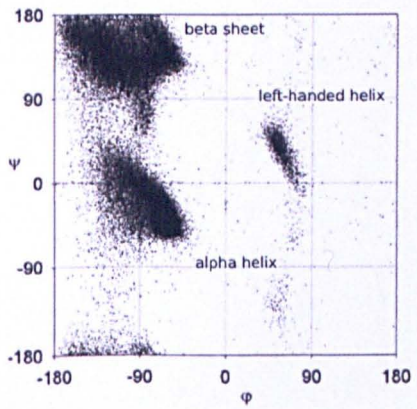

Figure 1.3: A typical Ramachandran plot taken from Ho *et al.* [7].

This shows the correlation between ϕ and ψ torsions of the same residue. It can be seen that the two main regions are approximately (-60,-45), labelled α-helix and approximately (-135,135), labelled β-sheet. An-α-helix is formed when a number of adjacent residues have a (-60,-45) torsional configuration. A β-strand is formed when a number

of adjacent residues have a (-135,135) torsional configuration. A random coil configuration occurs when there a mixture of these two states (or completely different states). The main conformations which have been considered in the present study are the α-helix, β-strand and mixtures of the two; Figure 1.4 shows the hexapeptide used in this study in α-helix (all torsional states (-60,-45)) (a) and β-strand (all torsional states (-135,-135))(b).

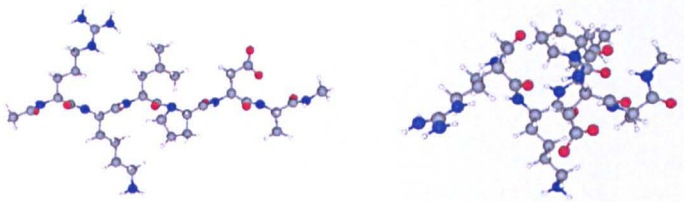

[a] [b]

Figure 1.4: RKLPDA hexapeptide where all the amino acids have torsions [a](-135,135) (β-strand) and [b](-60,-45) (α-helix).

It can be seen that they are quite different; β-strands are extended structures and α-helices more compact structures. In proteins β-sheets are common, which are two β-strands connected by hydrogen bonds between backbone carbonyls and backbone amines. α-helices are also very common and are stabilized by hydrogen bonds within the helix. It will be shown in Chapter 4, that backbone conformation is crucial to modelling peptides in water and when adsorbed onto surfaces. In a hexapeptide, the conformational space that can be sampled is massive and it is helpful to have some knowledge about the common conformations that are adopted as a starting point.

1.2.4 pK_a of amino acids.

The pK_a is very important when considering the physical and chemical properties of peptides and proteins. This is especially true when there are side chains which have groups which can gain/lose protons depending on the pH of the solution. The pK_a can

be explained by considering equations 1.1, 1.2 and 1.3.

$$HA \rightleftharpoons H^+ + A^- \tag{1.1}$$

$$K_a = \frac{[H^+][A^-]}{[HA]} \tag{1.2}$$

$$p K_a = -\log_{10} K_a \tag{1.3}$$

In equation 1.1, the HA denotes any group with a proton that can dissociate. Equation 1.2 shows that the K_a depends on amount of this group that can dissociate compared to the amount which cannot (square brackets, [], denote concentrations of species from Equation 1.1). If there is a large amount of dissociation, this value will be large. Equation 1.3 gives the pK_a as the log of K_a. If there is a large amount of dissociation (strongly acidic), this value will be large and negative. This value will increase to positive numbers with less acidity. The pKa therefore gives a measure of the extent of dissociation and can give information about whether a particular group is in the dissociated or undissociated state in a given solution.

This obviously has to be taken into consideration when deciding which model/force field to use *i.e.* to consider the pH of interest and to use a model which can capture the correct chemistry. pKa is also important for surfaces, especially ones which have the capacity to adsorb water (associatively or dissociatively) or have protons which can dissociate.

For the purpose of this work, we will only consider the the pKa of the side chains of Lys, Leu and Asp and not the terminus group pKa's since they are involved in a peptide

bond (either with another amino acid or blocking group). These pKa values are given in Table 1.1 At a pH of 7, any group with a pKa lower than 7 will dissociate and any

Table 1.1: pK_a of selected charged-group side chains. Values taken from Ref. [23]

Arg	12.5
Lys	10.8
Asp	4.1

group with a higher pKa will not. In the model used in this study, the Asp has a pKa lower than 7 and so is dissociated. The Lys and Arg are undissociated and therefore are positively charged because they have a pKa higher than 7.

1.3 Experimental characterisation techniques

To give an idea about how experimentalists study peptides on surfaces, a short summary of the different techniques used and what information can be obtained will be given.

1.3.1 Quartz crystal microbalance (QCM) and Quartz crystal microbalance/dissipation (QCM/D).

QCM is a method of measuring the amount of an adsorbate on a surface and so lends itself well to studying peptides on surfaces. QCM uses a quartz crystal coated with an electrode and the surface of interest. It measures the change in frequency of a piezoelectric quartz crystal when it is disturbed by the adsorbate. From this change in frequency, the amount of peptide on that surface can be deduced.

QCM/D measures the decay due to energy being dissipated by the adsorbate. The decay is indicative of the visco-elastic properties of the adsorbed layer and therefore gives further information about conformational changes in the internal structure of the adsorbate.

QCM and QCM/D are useful for measuring the affinity of peptides on the surface. They cannot however give information about its specific conformation.

1.3.2 Surface plasmon resonance (SPR)

Surface plasmons are surface electromagnetic waves that propagate parallel along a surface. These oscillations are very sensitive to any change of the surface such as the adsorption of molecules to that surface. Plasmons are created when the surface is irradiated with p-polarized light and the intensity of reflected light is reduced at a specific incident angle due to the resonance energy transfer between evanescent wave and surface plasmons. A linear relationship is found between resonance energy and the concentration of the adsorbed molecule. SPR can be used for measuring equilibrium constants of binding as well as binding kinetics. It cannot however be used for measuring peptide/protein conformation.

1.3.3 Nuclear magnetic resonance (NMR) and Circular dichroism (CD) experiments.

NMR and CD experiments can be used to obtain information about the solution structure of peptides. Nuclear Overhauser effect (NOE) experiments can provide through-space information on the proximity of different groups and therefore can give information on hydrogen bonding [24]. Also the geometry around the α-carbon affects the coupling constants and chemical shifts, so information on torsion angles can be inferred from these. A secondary structure will also impart a distinct response to circularly polarized light to its respective molecules. Circular dichroism spectra can therefore be used to estimate the fraction of a molecule that is in the α-helix conformation, the β-sheet conformation, the β-turn conformation or random coil conformation [25, 26].
NMR and CD can not give information about conformation of peptides/proteins on the surfaces at the moment but can give the information about conformation of pep-

tides/proteins in solution which can be used for inferring the behaviour of proteins on surfaces. CD however averages over a collection of molecules and therefore it cannot be deduced whether there is a certain amount of α/β character in individual molecules or a distribution over all of the molecules. Also, it cannot be deduced which part of the molecule has a particular conformation. In NMR, there are similar problems and the conformations have to be inferred which could be prone to misinterpretations.

1.3.4 Infra-red (IR) spectroscopy experiments.

IR spectra can give information about the modes of binding of peptides and amino acids by comparing absorption of peptides in solution and in the presence of the surface. It can be used to infer the quantity of adsorption [27]. Information about secondary structure of proteins can also be obtained by Fourier transform infra-red (FTIR) by deconvolution of peaks and comparison to secondary structure of known proteins [28]. The problem with this approach could be that different proteins have motifs in different environments affecting the validity of the interpretation.

1.3.5 Atomic Force microscopy (AFM)

AFM is often used for imaging proteins on surfaces [29]. It involves a cantilever with a sharp tip at its end. The tip is deflected by forces between the tip and the sample, leading to a deflection of the cantilever which can be recorded. AFM is useful for giving information on protein ordering and clustering on the surface and can sometimes image processes in real time . It cannot however, give information about the conformational changes. It also cannot give binding affinities directly although the number of clustering units can be counted to give an idea of binding amount.

1.4 Applications of peptide/protein-surface binding.

As alluded to earlier, there are many biotechnological reasons for studying the interaction between peptides and surfaces. Some of the more important applications will be outlined.

1.4.1 Immobilized Enzymes.

Biosensors are relevant to the present study and are one of the main motivations for studying the interaction between peptides and titania. Biosensors are biological devices which can measure the quantity of a substance. They are usually enzymes immobilized onto inorganic supports and can be used to test the amount of substrate present [21]. Biosensors are used commercially for such applications as blood glucose tests and environmental water testing. The inorganic support is necessary for detection of substrate using opto-electronic techniques.

In order for biosensors to be useful, the enzyme must retain its activity after adsorption. It therefore must not be denatured and must bind with the active sites exposed. This is shown schematically in Figure 1.5.

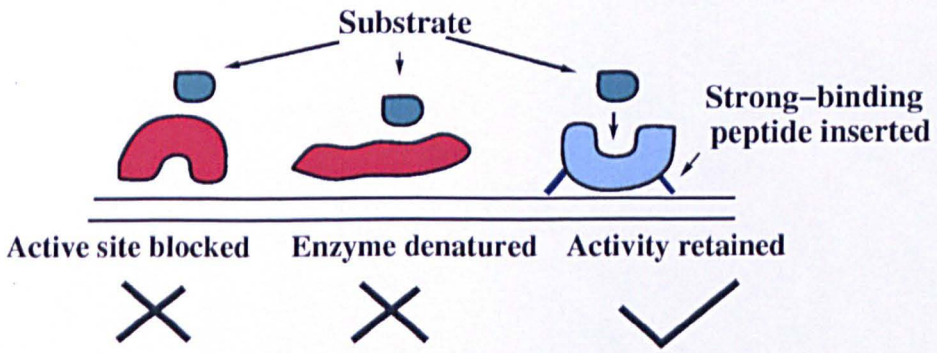

Figure 1.5: Schematic showing the two situations where the activity of an enzyme immobilized on the surface decreases.

This means that there must be some specificity to the binding which would arise if parts of the outer part of the protein were stronger in binding to the surface than other parts. One of the motivations for modelling and experiments in peptide-surface interactions

is to investigate why some peptides bind more strongly than others in order to gain an understanding of this specificity.

Studies have investigated the change in activity when enzymes are adsorbed onto various surfaces. It has been shown that loss of activity is caused by both situations; denaturing the peptide and blocking the site. It was found that the activity of α-chymotrysin adsorbed on a teflon surface changed, inducing helix promotion (observed in the CD spectra) and caused a loss in activity [30]. On the other hand when α-chymotrysin was adsorbed on montmorillonite, a charged surface, the secondary structure was not found to change yet the activity decreased [31]. However, it was found that imino/amino functions, located close to the entrance of active site were bound to the negatively-charged surface indicating a blocking of the active site was responsible for the loss of activity.

1.4.2 Controlled immobilization of enzyme onto surface.

To ensure that an enzyme retains activity after binding, strong binding peptides can be genetically inserted into permissive sites in proteins in order to make the proteins strong binding. Permissive sites are parts of the protein which are amenable to insertion of peptides without causing conformational changes. This has been performed [32] for a DNA binding enzyme on CuO_2. It was shown that DNA could then be used as a template for enzyme mediated binding of CuO_2 nano-particles.

1.4.3 Biomimetics.

It has been observed that in Nature, molecules like proteins (or collections of molecules) exert great control over the assembly of inorganic materials [33]. It is therefore an aim to mimic this control. Therefore the motivation behind much of the research into the biomolecule-inorganic interface is to understand how it occurs in Nature so that this knowledge can be used to assist the development of biotechnology [34]. The next two applications which will be outlined are biomimetic.

1.4.3.1 Controlled crystal growth.

Protein/peptide induced crystal growth and control involves an interaction between the protein and an inorganic material. There are many cases in Nature which involve protein-controlled crystal growth; many studies have been made to attempt to mimic this control[35, 36, 37, 38]. Firstly, studies have been made where the proteins which are thought to be involved in controlled crystal growth are extracted and tested regarding their ability to control crystal growth in isolation [39]. In a study by Belcher *et al.* [16], it was shown that soluble poly-ionic proteins, extracted from abalone shell could be used to control the phase *i.e.* calcite or aragonite.

Other studies have taken these proteins and tested the conformation in order to gain an insight into what makes a good crystalliser [40]. These studies are interesting because the secondary structure of inorganic-binding peptides were studied. Most other studies of conformation concentrate on peptides whose sequence is found in proteins. They are therefore in the same vein as the present study (especially in Chapter 4), where the conformation is studied in order to give clues about the binding.

CD and NMR spectra were used to study the solution properties of a protein, p288 peptide which regulates nucleation of inorganic crystals (NaCl, KCl, $CuSO_4$)[40]. Mollusk shell proteins which are responsible for aragonite polymorph formation and stabilization were also studied[41]. In both of these studies, it was concluded that the reasons for strong binding are an unfolded and unstable structure *i.e.* the tendency to adopt planar backbone configurations. It was suggested that these unstable structures are stabilized by intermolecular interactions with the surface/ions. Also, the ability to interact with Ca ions and to the newly formed aragonite surface via charged peptide sites and therefore location of charged parts of the peptide were also deemed to be important.

These ideas have been taken into consideration in the present study.

Some researchers have completely disregarded natural crystallisers and found new sequences by a combinatorial method (see Section 1.5.3.1).This usually involves finding strong-binding peptides and testing them for crystallisation properties. This work can

provide new opportunities in nanotechnology as well as give insight into the process of naturally occurring crystallisers.

Naik *et al.* investigated the crystallising properties of three strong-binding peptides [42] to Ag (see Section 1.4.3.2). Two peptides were found to cause the precipitation of silver particles and one did not. The peptides with crystallising properties differed from the one that did not in that they were neutral compared to the basic non-crystalliser. It was also shown that pure amino acids did not form crystals even though they were shown to bind. It was thought that binding was not the only essential ingredient for crystallising but a reduction step was also necessary.

In order to study crystal growth, Brown *et al.* studied protein-mediated control of gold as a model system [17]. Phage display was used to find strong-binding peptides and these were tested with a solution of gold where a pink colour formed due to gold crystals forming. It was found that two of the peptides which accelerated crystal formation contained the same tetrapeptides SEKL and GASL. It was found that these peptides caused the formation of large, thin, hexagonal crystals and it was proposed that the shape of the crystals gave an explanation for the acceleration of crystal growth ; the crystal growth was biased by the peptide adsorbing onto faces other than (111) (found by electron diffraction); (111) being the least energetically favourable face for growth. It was postulated however that this alteration of shape was by regulation of pH rather than binding to this face because acidic conditions also caused thin crystals when there was no preferential binding to (111) compared to other faces. Further experiments were performed where the parts of the peptide which were responsible for binding to gold were removed. It was found that the thin crystals were formed but at a slower rate. It was therefore suggested that two functions were necessary for crystal formation; a binding function and pH function. The part responsible for binding brings the part responsible for regulating pH into close proximity to the gold. This argument was strengthened when this peptide was combined (within the same peptide) with a strong binding peptide that did not cause crystallisation. In this case, the peptide produced

long crystals at a quick rate. This paper is very interesting because it shows that the functionality of peptides does not just rely on its power to bind but there can other functions too. Strong binding however is vital because it brings the peptide to the site of action so that its function can be realised.

Strong binders to calcite [43] (found by phage display), HTQNMRMYEPWF and DVFSSFNLKHMR were found to slow down crystallisation but did not distort their shape due to binding to all faces. The authors also tested a peptide rich in Asp and Glu (negatively-charged residues) because proteins known to change crystallisation are rich in these residues (the strong binders only had one each). It was found that this peptide slowed down the rate and distorted the crystal structure.

The control of crystal binding relies on peptide binding of peptides to surfaces but also relies on other phenomena such as binding of ions and nucleation. Therefore although insight into such processes can be gained from work such as the present study, extra areas of research have to also be used for their understanding.

1.4.3.2 Assembly of crystal composites.

A more direct application is the assembly of crystal composites, where peptide/inorganic interactions can be used for controlling the placement of inorganic materials in order to make ordered materials on the nanometer scale. For this to occur, peptides which selectively bind to some materials but not others must be found.

The field of nano-electronics is of great commercial and scientific interest because of the need for making electronic devices smaller and more complicated. For this reason work has been performed studying the interaction between peptides and semiconductor materials. Whaley *et al.* highlight the use of specific peptide-surface interactions for the directed assembly of nanocrystals [15]. In the study, the authors found strong binding peptides to GaAs(110), GaAs(111)A, GaAs(111)B, InP(100) and Si(100) by phage display and it was suggested that this was a way to synthesise semiconductor devices on the nanoscale. It was shown by x-ray photoelectron spectroscopy (XPS) of

phages bound to the peptides as well as streptavidin-labelled colloidal gold (the amount of colloidal gold could be detected by XPS) that there was specificity not only between different materials but between different faces of materials. For example, for a given sequence, the amount of peptide that was bound was 12 times greater for GaAs(100) than GaAs(111)A.

Other materials that have been used for semiconductors are carbon nanotubes and graphite. Wang *et al.* [44] found strong binding peptides and discovered that certain peptides could bind to nanotubes but not graphite, showing specificity between allotropes. It was suggested that binding peptides could be used to manipulate, sort, disperse and separate nanotubes, which could be key to exploiting their use in electronics.

It is not only semiconductor materials with applications in nano-electronics which have been studied in relation to nano-assembly. Naik *et al.* tested the applicability of peptides found to be strong binders to silver by depositing silver onto an ordered array of peptides supported by a glass substrate [42]. The silver only deposited onto parts of the substrate patterned by the peptide. This showed that that peptides can be used as a way of spatially controlling the deposition of inorganic material. A study of the adsorption of a gold binding peptide (GP1) on gold and platinum were compared using QCM [45]. The authors found that the binding rate of adsorption was greater for gold than platinum and the rate of desorption was greater for platinum than gold. The result of this was a greater binding affinity to gold than platinum and the significance of rates of adsorption/desorption will be discussed further in Chapter 5. Surfaces containing strips of Gold and Platinum were made and it was found that the peptide bound selectively to the Gold (proving a higher affinity for gold than platinum). These studies show selectivity for different but similar Noble metal surfaces and the ability to direct the immobilization of nanoscale objects.

Another type of material of great commercial use are liquid crystals and the interaction between peptides and inorganic materials have been manipulated in order to produce such materials. Liquid crystals systems composed of an A7 phage bound to ZnS

nanocrystals were formed [46]. The binding of phage to ZnS was mediated by a peptide found to be a strong binder by phage display. The phages are rod-shaped and order in a particular phase which could be changed by a magnetic field. It was suggested that these systems can be used to organize electronic, optical and magnetic materials.
Although, much research effort has been made in finding applications for protein/peptide-inorganic interactions, in order to fully exploit such interactions a greater understanding of such interactions must be gained.

1.5 Understanding the mechanism of adsorption.

This section will start with the broad subject of molecular self assembly; peptide/surface interactions being one part of this broad subject. We will then focus on protein-surface interactions before moving onto the most relevant subject of peptide-surface interactions. The work performed on titania will be kept until the next section in order to fully appreciate its significance.

1.5.1 Molecular Self-assembly.

Molecular self-assembly is the automatic building of molecules of complexity on the nanoscale. Firstly, for controlled self-assembly to occur, molecules must be built using covalent bonds in a specific way so that they have the correct function to selectively form aggregates by non-bonded interactions[47, 48]. It is not a far stretch to notice that this is the methodology/philosophy adopted in peptide/surface studies *i.e.* finding the amino acid sequences that can selectively bind to a surface and subsequently used to control self assembly. A paper by Whitesides *et al.* discusses some of the factors involved in non-bonded self assembly [47]. The weak non-bonded interactions must be be strong enough (or numerous enough) to overcome interaction of the solvent and the entropic advantage of dissociating. It is suggested, however, that entropic disadvantages to self assembly are reduced by increasing the solvent entropy by displacing structured

water and by having rigid molecules. Both points are highly relevant to the present study as will be discussed later. It is suspected that rigid molecules are better binders because they do not lose so much conformational entropy on binding because their entropy was lower in the first place. It will in fact be seen that rigidity, conformation and solvent entropies all have significant effects in the present study. Proteins are so useful because they lend themselves to molecular self assembly and this leads us to the next subsection.

1.5.2 The Interactions between Proteins and Surfaces.

Since one of the reasons for studying peptide adsorption on surfaces is to have a better understanding of protein-surface interactions, the experimental work in this field will be reviewed. The main proteins which appear in the literature are albumin, immunoglobulin, fibrinogen and lysozyme; partly because they are good test systems and partly because they have some significance/applications *i.e.* blood clotting proteins (see later). Firstly many reviews have been written about proteins on solid surfaces[9, 10] and it is worth highlighting some of the important issues which are addressed within these reviews.

In the review by Hlady and Buijs [10], the fundamental issues of protein adsorption are discussed. The authors highlight the importance of intermolecular forces, such as Coulombic forces, van der Waals forces, Lewis acid-base forces, and entropically-based effects such as hydrophobic interactions, conformational entropy and restricted mobilities. It is also postulated that the adsorption process depends on intramolecular forces within the protein molecules that might lead to an alteration of protein conformation. All of these forces are considered in the present study; intermolecular forces are certainly shown to be important and conformational entropy although not calculated will be considered.

Another interesting point that is made regards conformational changes of proteins when adsorbed on surface. Most experimental observations measure the properties of many

hundreds of thousands of protein molecules, therefore the behaviour of individual molecules cannot be deduced using these methods. Hlady and Buijs [10] also state that they cannot resolve picosecond timescales[10]. These are the opposite problems to modelling and it highlights the need for modelling studies such as the present one to fill in the gaps that experimentalists cannot access.

Despite these issues, many studies have measured the conformational changes that proteins undergo when adsorbed on a surface using a variety of experimental methods[49]. Many insights into the mechanism of adsorption have been derived from such studies and investigations into the difference between hydrophobic and hydrophilic surfaces are particularly revealing. Lu and Park [28] used FTIR to study how hydrophobicity affects conformational change of fibrinogen on different surfaces of varying hydrophobicity (measured by contact angle). It was shown that α-helical structures were changed into unordered structures and the content of β-turns was increased upon the protein adsorption. It was also shown that this conformational change increased with hydrophobicity. Conformational changes were also measured by CD spectra [30], where it was found that α-chymotrypsin and cutinase showed more pronounced conformational changes when adsorbed onto hydrophobic teflon than hydrophilic silica. This was rationalised by stating that the hydrophobic core is likely to be induced to move to the surface of the protein upon exposure to the surface due to the hydrophobic interactions; this will cause massive conformational change. This puts into perspective the work by Walsh [50] in comparison of hydrophobic and hydrophilic surfaces; studying the conformational changes of small peptides can give insight into the processes of larger proteins by elucidating the nature of such interactions.

It has been found that proteins that have a high internal stability only bind to hydrophilic surfaces if there is an electrostatic attraction, but can usually bind to hydrophobic surfaces regardless; these surfaces causing even 'hard' proteins to deform. Proteins with low internal stability however absorb on all surfaces because of a gain in conformational entropy upon adsorption *i.e.* if the peptide changes its configuration, this can happen in

many different ways and therefore the opportunity for binding increases. Adsorption isotherms were obtained by absorption spectroscopy; measuring the extinctions at 278 nm to determine concentrations [51]. Four proteins of different internal stability were adsorbed onto hematite and silica and the softer proteins showed a stronger binding affinity than the hard proteins. It was also shown that when proteins were adsorbed, desorbed and re-adsorbed, the binding affinity increased for the softer proteins but not the harder ones which was attributed to conformational changes making proteins more susceptible to binding. Desorption, remodelling and re-adsorption of the peptide at the peptide-inorganic interface has been observed in the present study and therefore it can help to explain the smaller scale aspects of such phenomena.

It has been found that pH also has a significant effect on the conformation of proteins adsorbed on surfaces. Liedberg *et al.* used infrared reflection-absorption spectroscopy (IRAS) to study the conformation of 3-Lactoglobulin adsorbed on gold [52]. It was shown that at pH 4.5, the protein adsorbed in the native form but at pH 6-10 it adsorbed in a flat, unfolded state. This shows a complexity and subtlety which must be addressed when considering modelling such systems and it will be shown in Chapter 5 that modellers have considered such issues but are far from fully addressing them.

Another aspect of protein adsorption which is considered to be very important is the interaction of different proteins with each other when they adsorb onto the surface. For these types of studies Atomic Force Microscopy (AFM) is useful since protein clusters are able to be resolved. AFM was also used to study adsorption of Immunoglobulin (IgG) and glucose oxidase (GOx) onto a graphite surface (a hydrophobic surface) [29]. Immunoglobulin adsorbs in patches that do not get larger indicating that the surface-protein interaction is more important than protein-protein interactions. Glucose oxidase on the other hand adsorbed with limited nucleation sites along step edges which grew, indicating stronger protein-protein interactions than surface-protein interactions. These differences ware rationalised by examining the different chemistries of the proteins. IgG has hydrophobic groups and a small overall charge which assists adsorption to the

hydrophobic surface. GOx however is highly charged and has more hydrophilic groups. It was postulated that the GOx adsorbs to step edges which are more hydrophilic due to oxidation.

Clustering behaviour of proteins was modelled [53] using a 2D model which randomly put particles onto a mesh. Mulheran and Robbie compared the islands formed with AFM images and conclude that there must be diffusion of particles on the surface. Clustering is an important issue when considering protein/peptide adsorption since in realistic situations, there are many proteins in the solution available for interaction with other proteins. These issues could not be addressed however in the present study due to computational limitations of using fully atomistic models.

Another phenomenon which has been extensively discussed is the reversibility of protein adsorption and seems to be related to the type of surface, the conformational change upon adsorption and the type of residue which is bound to the surface [54]. The concept of reversibility is borne out of the relationship between the concentration and adsorption amount (isotherm). If there is reversible adsorption, the isotherm can be fit to a Langmuir curve. This cannot be achieved however if the adsorption is irreversible. Reversibility is an issue which has been considered in the present study in relation to peptide binding to the surface directly or via water and will be discussed in Chapter 5.

Whereas the studies discussed in this section so far have involved whole proteins, some studies have involved studying the constituent peptides as a way of determining the epitope of binding (the part of the peptide responsible for binding). Sakayama *et al.* studied digested β-lactoglobulin on stainless steel [55]. This approach emphasises one of the reasons for modelling peptides on surfaces *i.e.* explaining why certain peptides are strong/weak binders and relating this information to parts of proteins conceived to bind. In this case it was found that a particular sequence bound strongly to the surface and it was reasoned that this sequence was involved in binding of the whole protein to the surface. This leads us to the next section on peptide-surface interactions.

1.5.3 Peptide-surface Interactions.

By studying the constituent peptides within proteins, an understanding of protein-surface interactions can be achieved. Apart from this, there are other reasons for studying peptide-surface interactions and these will be outlined later. First of all, since there are so many different peptide sequences, there has to be a systematic way of selecting strong binding peptides. The main techniques for screening large peptide libraries are phage display and cell-surface display, which are known as combinatorial search techniques [17].

1.5.3.1 Phage display experiments.

In order to help the explanation of phage display, a schematic of the process is shown in Figure 1.6.

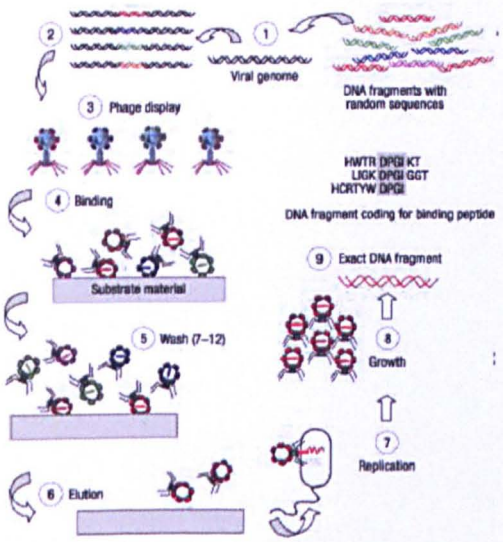

Figure 1.6: A schematic showing the phage display process, taken from Sarikaya *et al.* [8].

Phage display experiments involve inserting random sequences of nucleic acids into a bacteriophage (a virus)[17, 8]. The altered virus will then express different small peptide sequences onto their coat. Commercially-available libraries have a typical diversity of around 10^8 unique peptide sequences. The phage library is then exposed to

the target inorganic material under aqueous conditions (Figure 1.6, 4), and then washed (Figure 1.6,5). The phages with the strong binding peptides will remain bound to the surface after the wash. This washing/exposure cycle is repeated ~ 5 times before bound phages are eluted from the surface (Figure 1.6, 6). The eluted phages are amplified by infecting the host (Figure 1.6, 7). This completes a round of biopanning. After three to five rounds of biopanning, individual clones are sequenced to obtain the amino acid sequence of the strongest binding peptides in the library used. It should be noted that the need to find strong binders does not end there. If binders can be found that bind to some materials but not others, many more uses can be made for these peptides (as discussed in Section 1.4.3.2).

1.5.4 Experimental findings from Phage display.

Many phage display and cell surface display experiments have been performed for different surfaces [56, 57, 58, 59, 34]. This section will concentrate on a small selection of these studies with the emphasis on the sequence and composition of these peptides. It is important to compare how different surfaces will favour different residue compositions and sequence orders, to try to understand the factors which effect peptide binding. This work is central to the thesis because we are comparing directly with phage display results for TiO_2. It will be shown that the insights gained from these studies are very useful for drawing conclusions on the present work. They will therefore be thoroughly discussed, categorising the results into different kinds of inorganic materials. The results for TiO_2 will be discussed in Section 1.6.3. In this work, many studies were made where mutations were made to test their effect. In this case, the unmutated peptide will be called the wildtype peptide.

1.5.4.1 Noble metals.

The first phage display work performed involved Noble metals[8] such as gold, silver and platinum. It was found that hydrophobic and hydroxyl containing polar (serine and

threonine) amino acids were important.

Three strong binding peptides to silver nanoparticles were found by phage display[42] (AYSSGAPPMPPF, NPSSLFRYLPSD and SLATQPPRTPPV). All three binders contained hydrophobic and hydroxyl containing polar amino acids. They also contained Pro - a group which confers backbone rigidity.

Phage display performed by Brown, found hydroxyl containing amino acids Ser and Thr to be also important for gold binding also [60] and another investigated the binding of a strong binding (GBP1- MHGKTQATSGTIQS) peptide on gold. This will be outlined because it highlights some of the important concepts in peptide binding. Firstly, a kinetic study was made to study the gold binding adsorption/desorption kinetics of strong binding peptides using surface plasmon resonance (SPR) and QCM [45]. Using QCM and fitting to Langmuir isotherms, the authors were able calculate the Gibbs free energy of adsorption. They found a value similar to thiol-based self-assembling monolayers (SAMS) on gold used as linkers to biological molecules and so concluded that these peptides could be used as an alternative to SAMS with the advantage of operating under physiological conditions. Using SPR, it was found that two adsorption rates were found showing two different mechanisms of binding thought to be different gold domains (maybe defects), only one desorption rate was found. This shows the possibility that the state/topology of a surface in general may effect binding although the small differences in rate show that the general features of binding are preserved with morphology. In Chapter 5, modelling studies which investigate further into these gold-binding peptides will be outlined.

1.5.4.2 Metal Oxides.

The surfaces which should be the most relevant to the present study are the metal oxides since they are chemically related to titania and hydrophilic just as TiO_2. However, the studies show very diverse sequences; showing how difficult it is to predict the strength of binders and how complicated such processes are [61].

Cell-surface display was used to find binders to Cu_2O and ZnO[62] and statistical analysis was performed. This work goes into great detail about sequence specificity which is central to this section and the whole project. The analysis revealed that Cu_2O binders are enriched in Trp, Gly, Met and Arg and depleted in Leu, Tyr, Pro, Ser and Thr. ZnO binders were enriched in Thr, Gly and Arg and depleted in Tyr, Pro and Ser showing similar compositional biases for both oxides. However they showed positional differences which were found to be statistically significant. Two classes of binders were found for both oxides, Class I Cu_2O binders were hydrophilic and contained RR motifs, Class II Cu_2O binders were more hydrophobic containing W. Class I ZnO binders were like Class I Cu_2O binders but RK motifs were more numerous than RR motifs. Class II ZnO binders were hydrophobic but contained Leu and Val residues. The authors state that the existence of different kinds of binders highlights the idea that there may be different solutions to the problem of metal oxide binding. It was found for both oxides that the RXXR motif was significant. The specificity of six ZnO binding peptides (type I and II) were tested against gold electrochemically patterned with stripes of Cu_2O and ZnO. It was found that four of them bound to ZnO more strongly, but two of the ZnO binders surprisingly bound to Cu_2O more strongly than ZnO. One of these however contained the RR motif found to be prevalent in the Cu_2O binders. Three of the peptides were also found to bind to gold; one of these was not so surprising since it contained an SSS motif; Ser being important for gold binding [60]. None of the peptides bound to $Cu(OH)_2$. This shows that hydroxylation state may be important to binding. It will be shown later that hydroxylation state will be considered in this study and could have an effect in binding of peptides to titania.

An independent study was made finding ZnO binders by cell surface display[63]. It was found that His, Arg, Asp and Met were over-represented. Motifs, THNK, R/T-HXK-D/Q, R-X_2-RS and PXRS were common. These motifs are similar to the motif found to be a strong binder to titania (RKLPDA) and in the study above in that there are two charged groups separated by other amino acids. Therefore, there is some agreement be-

tween different studies for ZnO binders and the possibility that there is some similarities between different oxide surfaces.

Strong-binding peptides to SiO_2 were found by phage display and it was found that His was over represented for these peptides[64]. It was suggested that the imidazole ring can interact with aromatic, hydrophobic and charged groups and this could account for the abundance of His in strong binders and suggests a conformational factor *i.e* that strong binding does not just rely on strong binding groups but more subtle factors. This would account for residue order specificity and not just compositional specificity of peptides. It will be shown in Chapters 4 and 5 that this is the case for peptide binding to titania. It was found that out of fifteen strong binding dodeca-peptides, thirteen peptides had His in positions 1 and nine had His at position 6 showing this positional bias.

From these studies it seems that ZnO and CuO_2 (see later for TiO_2) are very similar in their binding (involving charged groups) but SiO_2 is quite different (aromatic groups). This is not however conclusive since in phage display only a fraction of sequence space can be sampled.

An attempt to solve this problem was made by Oren *et al.* using a bioinformatics approach to identify strong binding peptides to quartz (SiO_2) surfaces [65]. This involved using experimentally-characterised binders: strong, moderate and weak binders (dodecapeptides). An algorithm called a scoring matrix was used in order to calculate how similar the respective binders were to each other and was used to further improve the scoring matrix to take into consideration the specificity of quartz binders. The authors then randomly generated 1,000,000 sequences (theoretically) and used the scoring matrix to test the strength of binding. When the predicted peptides were then synthesised and tested experimentally, it was found that the peptides exhibited the predicted affinities. In fact, it was found that the strongest binders were stronger than any binders found previously. When the new binders were used to optimise the scoring matrix, it was better at characterising known binders and it was suggested that an iterative process could be used to improve the accuracy of the similarity matrices. The amino acid composi-

tion was investigated and it was found that Pro was over-represented in strong binders and Gly under-represented. This agrees with the work by Sano and Shiba [1] which will be outlined in Section 1.6.3 and indicates that Pro which holds the peptide rigid is important for strong binders and Gly which gives the peptide flexibility (similar to Ala in that respect) destabilises binding. However, bulky hydrophobic groups, Thr, Phe and Met were also overrepresented. In order to test whether it was the order of residues or just composition which dictated binding, a classifier was used which was only based on composition. The prediction of strong binders decreased significantly, showing that the sequence is essential.

This type of study is very important for the subject of peptide binding and gave many insights into the understanding of what makes a strong binder. It can also be used to predict sequences and could be the key to finding binders of different strengths since phage display alone can only search on the order of 10^8 sequences. However there are on the order of 10^{15} dodecapeptides, it is conceivable that these types of techniques could search for all of these if enough computational power was available. It should be noted that this type of bioinformatics approach gives us information about what residues are strong binding but tells us nothing about why they are strong binding. For that information physics based modelling studies like in the present study can be employed.

1.5.4.3 Semiconductors.

As already stated, peptide binding to semiconductor materials has been extensively studied. Goede *et al.* also studied adsorption of a peptide found from phage display with GaAs (AQNPSDNNTHTH) to semiconductors[66](GaAs, Si, InP, GaP and Al_xGa_yAs, x and y= 0.0 - 1.1)) and explored some interesting issues. The lattice constant size for the different surfaces was plotted versus peptide adsorption and found to show no correlation. This is surprisingly because the lattice parameters are considered to be important; it seems likely that the different chemistries of the semiconductors can complicate the comparison. However, it was also shown that adsorption depended on electroneg-

ativity between the different atoms in the semiconductor where the strongest binders were ones with the smaller difference. This could however be because GaAs (the surface the peptide was selected against) had a small difference and therefore the best surfaces for binding were ones similar to GaAs. This would still suggest that electronegativity difference is a key factor when considering binding of peptides to semiconductors. Goede *et al.* tested two mutated peptides against GaAs and Si, the first one being the peptide where they mutated the two H groups for A (AQNPSDNNTATA). They found a decrease in binding for GaAs and an increase for Si. This showed that His, a basic residue was important for binding to GaAs but somehow hindered binding to Si. It is possible that the increase in binding to Si was due to conformational differences, revisiting the argument expressed in relation to oxide surfaces.

The other mutant used was one containing the same amino acids but in a randomly different order (TNHDHSNAPTNQ). It was shown that the binding affinity for GaAs stayed the same but for Si increased to the same level as GaAs. It therefore showed that although binding was retained by changing the order, specificity was destroyed. It opens questions about how the spatial conformation of the peptide on the surface can influence binding, because a different order can change the conformation and therefore the lattice matching. The same amino acids are present so it could mean that the same interactions are in place but are less able to bind simultaneously. We must ask what makes the unmutated peptide bind to GaAs but not Si *i.e.* is it constrained to a particular binding configuration that cannot be accommodated by Si? Is this not shown in the mutant? Related issues are investigated in the present study where mutations were made in order to understand experimental changes in binding affinity [1].

1.5.4.4 Carbon Nanotubes and Graphite.

Other types of inorganic surfaces which have been studied are carbon surfaces [67]. These are interesting since they are hydrophobic and it should be expected that completely different sequences will be important for strong binding. Comparison of these

binders should provide insight into the effect of hydrophobicity on protein binding introduced above. This was found to be the case in a study by Wang *et al.* where strong-binding peptides were found for carbon nanotubes using phage display [44]. It was shown that there was an over-representation of His and Trp and it was found that the frequency of these residues increased with detergent concentration (detergent used to decrease non-specific interactions). Mutagenesis was performed and the Trp at the 6th position was replaced by Ser in two of the peptides (HWKHPWGAWDTL and HWSAWWIRSNQS). It was found that the binding affinity decreased to weak binding peptides with mutagenesis showing the importance of Trp in such binding. Also Monte Carlo simulations were performed, which suggested that the low energy structures for the binders were compact, the weak binders extended. The authors concluded that for flexible structures there would be little conformational penalty to adsorb onto the surface. This is in contrast to other studies where strong binders tend to contain Pro which makes the peptide extended and stiff. This difference could be due to the difference between binding peptides to hydrophobic surfaces and hydrophilic surfaces *i.e.* that peptides that bind hydrophobic surfaces tend to change on adsorption. This would compare with large proteins which denature when adsorbed onto hydrophobic surface but not hydrophilic surfaces. It could also be because more hydrophobic side groups will cause the peptide to be more compact in order to keep away from the water.

The studies presented have shown that different materials have different sequences and compositions which will bind to them. They also show that some peptides tend to be stronger binding because of their flexibility whereas others will be stronger binding due to Pro-derived rigidity. This shows that there are different mechanisms which depend on the sequence and type of surface and will probably be explained by the conformations it adopts. Conformation and sequence specificity will be explored in later chapters and attempts will be made to understand such effects.

1.6 Titanium dioxide.

The previous experimental work described so far has involved surfaces other than titania and is useful for giving an overview of the broad subject which is being studied presently. In this section, the titania surface will be focused on [68, 69, 70]. Just as in the previous section, it will start with general subjects of titania, the applications will concentrate on proteins on titania and finally will move onto peptides adsorbed on titania including the experiment which is the key experiment for this project [1].

1.6.1 The nature of the rutile (110) TiO_2 surface.

Firstly, the nature of the surface will be outlined. Figure 1.7 shows the fully hydroxylated [a] and non-hydroxylated surfaces [b].

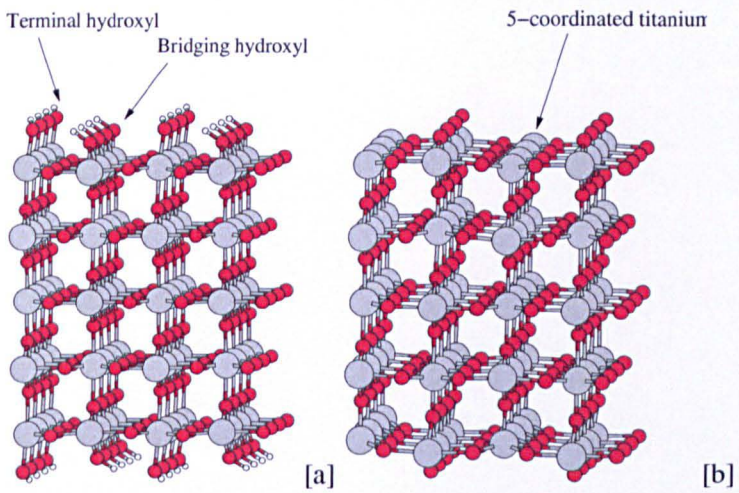

Figure 1.7: The fully hydroxylated [a] and non-hydroxylated [b] surfaces of the rutile TiO_2 (110) surface.

Firstly, the non-hydroxylated surface would be the reconstructed surface where bulk rutile has been cleaved. There are two atom types deemed to be important for adsorption of peptides and water. The 5-coordinated Ti has a partial positive charge, is under-coordinated (with respect to the bulk) and is therefore a site for binding of atoms with a partial negative-charge such as the oxygen of water (water is neutral but the oxygen has

a partial negative-charge because of the polarity of oxygen). The bridging oxygen has a partial negative-charge and binds to atoms with a partial positive charged sites such as water hydrogen. The presence of the bridging oxygen causes the surface to not be flat but corrugated; it will be shown later that this has some significance for its adsorption properties. The hydroxylated surface has an extra hydrogen on the bridging oxygen, making a bridging hydroxyl and an extra hydroxyl group on the the 5-coordinated Ti, making a terminal hydroxyl. The hydrogen and hydroxide group comes from a water which has been dissociated.

It was shown that the isoelectric point of titania is 5 [71, 72]. Therefore it is neutral at pH5, negatively-charged at pH7, and positively charged below pH5. It will be shown that this has significance when considering the interaction with peptides and proteins at different pH's, especially since the pH also affects the dissociation state of the side chains in different ways depending on their pKa. This issue of surface dissociation state will be a large part of Chapter 3, where it will be shown that there is the possibility to actually change the dissociation state and charge of the TiO_2 rutile (110) surface in the model used.

1.6.2 Application for peptides and proteins on titania.

As alluded to earlier, the two main areas where surface-protein interactions on titania are important are implants and biosensors. A review of some of the work in these areas will therefore be given.

1.6.2.1 Biocompatability

Titania and its alloys are used for medical implants. These include bone-anchoring systems, such as dental implants or hip-joint fixation and replacement, as well as for pacemakers and heart valves [73]. Titania is used for many reasons such as a low modulus of elasticity, a high strength-to-weight ratio, excellent resistance to corrosion, but the main reason is that it is biocompatible. This means that it can interface with a

biological material without causing adverse effects.

Experiments were performed where titanium bone implants were inserted into rabbits [74]. It was found that the bone came into direct contact with the titania but mostly a layer of proteoglycan (proteins with one or more covalently attached glycosaminoglycan chains) separated titania from cells. This is in contrast to stainless steel where the cells (via fibrinogen) were found in contact with the metal. It has been suggested that it is surface-protein/peptide interactions which govern these processes. Specific mechanisms have been postulated. It was suggested by Kasemo and Gold [75] that the first point of contact for an implant is the water layer, followed by natural ions moving into the water layer. They suggest that small peptides adsorb, are replaced by proteins and allow whole cells to attach to the implants. This is called the Vroman effect and puts the present study into perspective as we have studied the water layer in conjunction with smaller peptides on the titania surface.

Much work has been put into enhancing the biocompatability of titania [76, 73]. It is therefore desirable to understand selective binding affinities of different peptides. In fact it has been found that preferential adsorption of human serum albumin (HSA) [77] (the most abundant protein in blood) seems to be advantageous for biological acceptance of the material, whereas adsorption of fibrinogen (blood clotting protein) and immunoglobulins (antibody proteins) causes adverse biological responses [11, 78, 79].

1.6.2.2 Titania biosensors

Much effort has been put into the immobilization of enzymes onto titania for biosensor applications. Investigations into the the use of nanoporous TiO_2 for protein immobilization have been made [18, 19, 20, 21]. UV-visible absorption spectroscopy was used to measure the amount of iron(III) cytochrome C (Fe (III) Cyt-c), haemoglobin (Hb), myoglobin and maltase adsorption on titania films. It was found that the adsorbed spectra were the same as the solution spectra showing that no denaturation had occurred for any of the proteins at pH 7. Certain peaks in the spectra were used in order to

give a quantitative measure of adsorption and the authors were able to fit the data to a Langmuir isotherm. It was found that the binding was at its optimum at a pH where the proteins and surface were oppositely charged (negative-surface, positively-charged protein) indicating that the binding was electrostatic. When the lysines of cyt-c were acetelated, and hence lost their positive charge, the binding decreased, which showed that Lys was involved in binding. The desorption of the proteins was also tested by immersing the protein-bound nanoparticles in buffer and it was shown that the desorption constants were one order of magnitude smaller than the adsorption constants. This showed irreversible binding which increased with exposure time of adsorption.
It was shown in the papers by Topoglidis *et al.* that the titania-adsorbed cyt-c could be used as a biosensor for the detection of CO in aqueous solution and the titania adsorbed Hb could be used as a biosensor for the detection of NO. The authors used cyclic voltametry and spectroelectrochemistry to demonstrate this. Some insights into the binding modes of proteins to titania were shown by these studies *e.g.* the presence of Lys binding, but more information was obtained by studies of peptides on titania.

1.6.3 Peptides on titania.

The experiments involving peptides and amino acids on titania are the most applicable to the present study. The first few experiments that will be discussed involve the peptide that has been modelled in the present work.

1.6.3.1 The RKLPDA peptide on titania.

Phage display experiments on Ti metal were performed and 43 12-mer sequences were identified. Of these sequences, 34 were a particular peptide RKLPDAPGMHTW (they named it Ti-12-3-1). The binding affinities of all the sequences were measured by QCM and it was found that Ti-12-3-1 had the highest affinity by many orders of magnitude [1]. The authors performed alanine scanning mutagenesis on the peptide. This involved mutating each residue with alanine, a neutral, non-bulky, chemically inactive group.

Figure 1.8 shows the binding affinities of all the mutants of the Ti-12-3-1 peptide relative to the wildtype Ti-12-3-1 peptide measured by QCM.

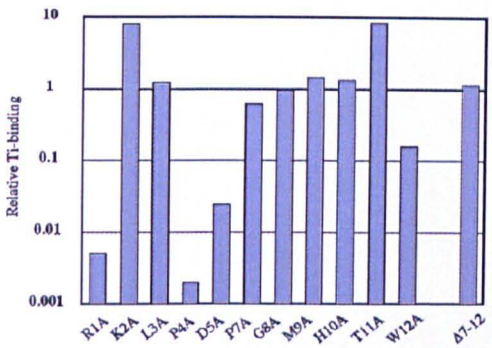

Figure 1.8: Binding affinities of mutants of Ti-12-3-1 peptide relative to that of the wildtype Ti-12-3-1 peptide. Graph taken from Sano and Shiba [1].

It can be seen that when they mutated the Pro (P4A), Asp (D5A) and Arg (R1A), the binding affinity significantly decreased. It was found that when the C-terminal half of the peptide was deleted *i.e.* when they used RKLPDA only (referred to as TBP-1), the binding affinity remained the same. It was therefore concluded that RKLPDA was the part of the peptide responsible for binding. Sano and Shiba postulated a binding configuration in which Asp and Arg were bound to the surface (we will denote it the 'horseshoe' structure), with Asp, a negatively-charged residue bound to positively-charged parts of the surface and Arg, a positively-charged residue, to negatively-charged parts of the surface. The proposed structure is shown in Figure 1.9.

It was reasoned that Pro, being a residue that confers backbone rigidity, was involved in holding the peptide stable on the surface. The binding affinity of ARKLPDA was also tested in order to investigate whether Arg had to be at the N-terminus of the peptide; the extra Ala however had no effect. It was also found that when the the surface was exposed to H_2O_2 (made the surface more hydroxylated) that the binding affinity increased. It will be shown that different levels of hydroxylation have been considered in the present study. The effect of ionic strength on binding was investigated by changing the concentration of the solution and it was shown that the binding affinity was not

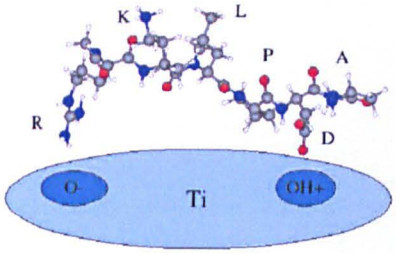

Figure 1.9: Proposed 'horseshoe' binding configuration, suggested by Sano and Shiba [1].

affected. This was in contrast to a peptide that had hydrophobic character which had an increased binding affinity with increased ionic concentration. In this case the negative charge of the surface would be dampened by this ionic charge.

In this study, the interaction of the RKLPDA peptide with rutile (110) has been investigated to gain insight into its strength of binding and why this changes with mutation. From now, when considering this peptide in relation to its mutants, the RKLPDA peptide will be called the wildtype. The TiO_2 surface was studied because in the biological environment, the metallic Ti is covered in an oxide layer consisting of amorphous TiO_2. The first step in understanding this process is therefore to study the single crystal surfaces, since they are simple making it easy to implement modelling studies using such surfaces. The reason we are studying the TiO_2 rutile (110) face in particular is that it the thermodynamically most stable single crystal surface and is therefore the single crystal surface which is most likely to be formed spontaneously [80]. There is also a wealth of information both theoretically and experimentally concerning the rutile (110) surface and therefore it seems the ideal choice of surfaces. For these reasons, a force-field has already been developed for rutile (110) [3]; this is obviously convenient for this study. This study was meant as a precursor for studying more complicated amorphous solids but it will be described later that for the purpose of peptide adsorption behaviour, the

crystallographic orientation, or even degree of crystallinity may not be critical to this study

The same peptide residue was inserted into the N-terminus of subunits of Ferritin and binding was tested using AFM against Au(111), Si, Ti and self assembled monolayers (SAM's) of alkanethiol with different terminal groups[81, 82]. The authors found that Ti was much more strongly bound for the inserted ferretin than wildtype ferretin. A similar enhancement was found for Si. The other surfaces were unaffected. The experiment was repeated with surfactant in order remove non-specific interactions and it was found that this enhancement was greater suggesting that the main interaction is electrostatic (between charged groups and charged parts of the surface).

The phage-bound TBP-1 was also tested against Si, Ag, Au, Cr, Pt, Sn, Zn, Cu and Fe [83]. Sano, Sasaki and Shiba found that the peptide bound to Ti, Ag and Si but not really the others. It was found that when the Arg, Pro, Asp were mutated, the affinities also decreased in the same way as in Ti; when they mutated Lys, the binding affinity increased. These changes were however milder for Si than Ti and Ag. The authors concluded that the mechanism for binding is the same for Si and Ag as Ti. It is surprising that there was binding to Ag, since Ag is a noble metal which does not oxidise in the same way as Ti. The authors suggested that the peptide recognises a common structure shared by all three metals but that it is not necessarily the presence of a hydroxyl moiety, since the peptide did not bind to Fe. Also the ioselectronic points and crystal structures of Ti, Ag and Si are quite different.

It was shown by Sano, Sasaki and Shiba that the TBP-1 mediated mineralisation of Ag nanocrystals from $AgNO_3$ [83]. This is very interesting because it provides a link between the present work and peptide mediated crystallisation. Sano, Sasaki and Shiba compared this to a similar silver-binder and crystalliser RYLPSD [42]. Both peptides have the three residues Arg, Pro and Asp except Asp is in a slightly different position and shows that binding is a key factor in such processes *i.e.* the same electrostatic interactions were available for binding. It was also shown that TBP-1 can mineralise silica

from tetramethyloxysilane solution. When Arg, Pro and Asp were substituted for Ala it was found that the mutation of Pro and Arg impaired silification and that the mutation of Asp had no effect (even though it decreased binding). This could be explained by the difference between the mechanism for strong binding and the mechanism for peptide-mediated crystallisation as highlighted above.

This section outlines the main motivation and idea behind the present work. The original work by Sano and Shiba gives experimental results that can firstly be used to test the model employed. Secondly, in all the papers, no comprehensive explanation has been given for the changes in binding with mutation. This work will strive to fill this gap. The work on insertion of TBP-1 into ferritin gives a direct link between the present work and the controlled immobilisation of proteins. The work on the other surfaces (Ag and Si) gives the opportunity for further modelling efforts in order to understand why it binds to some surfaces and not others. It also poses questions about whether the mechanism is the same for the different surfaces; modelling could help in answering these questions.

1.6.3.2 Other peptides and amino acids.

The next experiments that will be discussed involve different sequences than the one in the present study. However they mainly involve the same residues, and give insight into the conditions required for adsorption. In most cases, this involves the effect of changing the pH and therefore the dissociation state of both surface and amino acids and peptide side chains. Different dissociation states of peptides cannot be tested dynamically at the moment by modelling because of a lack of dissociative models, but this work provides the opportunity for new models to be developed to take into consideration the effect of changing pH dynamically. This has already been done statistically for titania and will be shown in Chapter 3.

Attenuated total reflection infra-red spectroscopy (ATR-IR) was used to study Glu and Asp on amorphous TiO_2 sols [84]. Roddick-Lanzilotta and McQuillan found that Glu

exhibited many different conformations on the surface but Asp only showed one. The authors attribute this to the smaller size of Asp, giving fewer energetically attainable conformations. Asp bound more strongly at low pH (below 3), where the surface is positively charged and Asp is negatively-charged, than neutral pH where Asp and the surface are both negatively-charged. Importantly however, there was some binding at physiological pH despite this apparent electrostatic barrier. Roddick-Lanzilotta and McQuillan do not provide an explanation for this but consider the surface as being homogeneously negatively-charged. We should hovever consider that this is not the case and there are patches of different charge on the surface. The binding of Asp to titania at neutral pH could then be explained. Glu on the other hand was found to be more insensitive to such electrostatic considerations. Since the behaviour of Glu and Asp are so different in their binding (but very similar chemically), it shows that conformation as well as electrostatics is important. Conformational aspects will be a repeated theme in the present study.

Roddick-Lanzilotta and McQuillan studied the adsorption of Lys on TiO_2 [85]. It was found that at physiological pH there was adsorption of K^+ due to favourable electrostatic interactions between K^+ and anionic titania. The difference in binding between different types of surfaces was investigated and IR spectroscopy was used in the investigation of adsorption of Lys onto amorphous TiO_2 and anatase powder. The authors found there was very little difference in the spectra, showing that the general features of adsorption are independent of the polymorph of the crystal. It adds weight to our argument that the adsorption of the RKLPDA peptide on rutile (110) surface can be studied in order to gain insight into the mechanism and sequence specificity of adsorption of the peptide onto Ti particles (a layer of amorphous TiO_2). The authors also state that Gly did not adsorb to titania showing that the side group binds to the surface, not the end groups since Gly also has end groups but a chemically neutral side group.

The effect of pH on binding was investigated to give an idea about the mode of binding of Lys. At pH 11.5, a small amount adsorbs despite repulsion between the C-terminal

carboxylate and TiO_2. At pH 9.8, there is greatest adsorption because of the interaction between the positively-charged amine of Lys and the negatively-charged surface.

The adsorption of oligopeptides of Lys (2-5 units) and poly-lysine (169 units) were also investigated by ATR-IR [27]. It was shown that all peptides adsorbed at pH 7.4. The isotherm was plotted and it was shown that the binding constant per Lys unit increased with increasing size. This at least shows that Lys as part of larger peptides is important for binding on titania. The previous two studies show that Lys does in fact bind to the titania surface via the side group and raises questions about why the mutation of Lys in the RKLPDA peptide does not decrease the binding affinity. It should be assumed therefore that this anomalous behaviour is due to a conformational factor. This subject will be explored in Chapters 4 and 5.

More complicated peptides have also been studied and these give us more insight into conformational factors as well as reiterating the electrostatic nature of the binding of charged residues. Imamura *et al.* measured the isotherms of four different octapeptides with varying amounts and sequences of Asp, Lys and Ala at different pHs on Ti using reversed phase high performance liquid chromatography (RP-HPLC) [86]. The authors separated the contributions into irreversible (qI) and reversible (qII) adsorption modes by fitting to a modified Langmuir equation. They found that $D_4K_0A_4$, $D_4K_1A_3$, $D_4K_3A_1$ and $D_4K_4A_0$ peptides all showed irreversible adsorption below pH 7 but normal Langmuir (reversible) behaviour above pH 7. $D_0K_4A_4$ however only showed reversible adsorption. A suggestion for such behaviour will be given in Chapter 5, in relation to the present work involving the difference between water-mediated binding and direct binding of Asp to titania. It was suggested that at acidic pH, the surface is positively-charged and causes ionisation of Asp groups which is responsible for the high affinity. The authors attribute binding of Lys-rich peptides at pH 7.5 to attractions between positively-charged Lys with the negatively-charged surface agreeing with the studies shown above.

A study by Chen *et al.* found different heptapeptides which are strong binding to TiO_2

[87]: HKKPSKS, TKRNNKR and DQQTSEF. The first two were not surprising since they contained charged residues just as in the RKPLDA peptide. The third peptide however is quite different; containing hydroxylated residues T and S. This could show that there is more than one mechanism for binding as discussed in relation to other oxides. It was found that the peptide HKKPSKS and TKRNNKR also bound to SiO_2 and this can be compared to the cross specificity work of Shiba *et al.* [83] which showed that RKLPDA also bound to SiO_2. These two studies suggest TiO_2 and SiO_2 have some similar characteristics.

As mentioned earlier, molecular self-assembly is deemed to be an important factor in producing nanomaterials. This was investigated in two studies into the molecular organisation of a 16-mer peptide EAK16 (H-AKAKAEAEAKAKAEAE-NH_2)[88], EAK16-RGD (RGD is added to the end of the peptide) and a scrambled version of EAK16-RGD [89] on TiO_2 (and Au) using X-ray Absorption Near Edge Structure (NEXAFS), XPS and IR spectroscopies [89]. It can be seen that EAK16 contains the charged groups K and E already outlined above, RGD was added in order to increase the binding. It was found (by measurement of the C=O stretching frequency which is diagnostic of secondary structure) that all peptides formed a β-sheet structure on the surface and the driving force behind the self organisation was suggested to be interactions between the charged groups K and E and between hydrophobic alanines. This study is interesting because it gives a link to the work on the aggregation of proteins (which should be very important for peptide/protein binding) outlined earlier.

All of these studies, strongly suggest an electrostatic attraction is the main type of binding for charged residues on titania. They all also provide convincing evidence that all the charged groups (R, D and K) are important in binding of peptides other than RKLPDA to titania surfaces, and pose new questions about the conformational effects of Lys.

1.7 Discussion.

The purpose of this chapter was to set the scene for the project. At its heart is the understanding of different factors which influence the binding of peptides/proteins with different surfaces. These include, the hydrophobicity of the surface as well as the nature of the protein/peptide adsorbed to it.

The same issues are relevant when considering both the binding of proteins and the binding of peptides to surfaces. These include the effect of pH, the effect of ionic concentration and the presence of certain residues which bind to the surface *e.g.* charged residues which bind to hydrophilic surfaces. Therefore, by finding and understanding the binding of peptides to different surfaces, insight can be gained about the binding of proteins to such surfaces. There are some fundamental differences however when considering protein binding and peptide binding. For proteins, it is the tertiary structure which is important and therefore there are issues of structural stabilities and irreversible collapse; peptides on the other hand are too small for such considerations. For this reason, we have to be careful about drawing conclusions about the binding of proteins from that of peptides even when the peptide is part of that protein. It will be shown later that perhaps this gap can be bridged by modelling.

Despite these reservations, it has been shown that the understanding of peptide binding has some more direct applications such as controlled assembly of crystal composites. These applications further validate the need for such a study.

In smaller peptides, the residue composition and sequence are vital. For metal oxides, of particular relevance to the present study, a wide variety of types of residues were shown to bind. Of these, charged residues tended to be important showing links to the strong binding peptides found by Sano and Shiba for peptides on titania [1]. Sano and Shiba found that the RKLPDA peptide was a strong binder and an electrostatic interaction between charged residues and charged surfaces was implicated for such binding. Conformational factors have also been suggested.

1.8 Structure of the results chapters

Since this is a large piece of work with many different ideas, the structure of the results chapters should be explained in order to help the reader to follow its logical flow. There are three results chapters each of which is meant as an individual piece of work on its own. They do however follow a logical progression. Chapters 3 and 4 investigate the titania-water interface and peptide-water interface respectively. Chapter 5 investigates the titania-water-peptide interface and although Chapters 3 and 4 are not pre-requisites for obtaining crude results, are essential for gaining and interpreting many of the results in Chapter 5. This aspect will be fully highlighted in the relevant chapters. The next chapter however, will give information about the theoretical and computational methods used for the present study.

Chapter 2

Theoretical methods

In this study, periodic density functional theory and force-field methods were used for quite different purposes. Density functional theory (DFT) takes electrons into consideration, does not require pre-known bond connectivities and requires little parameterisation before use. Force-field methods on the other hand deal only with atomic coordinates, use simpler analytic expressions and must be parameterised for each specific situation. It will be shown later how this parameterisation was performed [90, 91, 3].

2.1 Periodic density functional theory(PDFT)

PDFT was used for this study in order to test the force-fields used. DFT can be used to obtain accurate single-point energies but there are many other methods which can be used which possibly give more accurate energies. However this thesis is not an *ab initio* study and a review of such methods is beyond its scope. The reason why DFT was required in this study was that periodic calculations were used, and the codes available use DFT (CASTEP). DFT is relatively efficient compared to other methods and gives relatively accurate results.

2.1.1 Density functional theory

The key concept that underpins density functional theory (DFT) is that there is a relationship between the total energy of a system and the electron density[92]. It was shown by Hohenberg and Kohn [93] that the ground state energy and other properties are defined by the electron density and therefore energy is a functional of density. This can be written as a sum of two terms.

$$E[\rho(\mathbf{r})] = \int V_{ext}(\mathbf{r})\rho(\mathbf{r})d\mathbf{r} + F[\rho(\mathbf{r})] \tag{2.1}$$

The first term arises from the interaction of the electron density with the external potential $V_{ext}(r)$, typically the Coulomb interaction with the nuclei. $F[\rho(r)]$ is the sum of the kinetic energy of the electrons and the contribution to the energy from inter-electronic interactions.

$F[\rho(r)]$ can be broken up into a sum of three terms.

$$F[\rho(\mathbf{r})] = E_{KE}[\rho(\mathbf{r})] + E_H[\rho(\mathbf{r})] + E_{XC}[\rho(\mathbf{r})] \tag{2.2}$$

where $E_{KE}[\rho(r)]$ is the kinetic energy of a system of non-interacting electrons with the same density as the real system, $E_H[\rho(r)]$ is the electron-electron Coulombic energy and is the classical interaction between two charge densities, and $E_{XC}[\rho(r)]$ has contributions from exchange and correlation. The most popular practical way of doing DFT for molecules is the Kohn-Sham approach [94] where orbitals are reintroduced

The Kohn-Sham equations are given by:

$$\left(-\frac{\nabla^2}{2} - \left(\sum_{A=1}^{M}\frac{Z_A}{r_{1A}}\right) + \int\frac{\rho(\mathbf{r}_2)}{r_{12}}d\mathbf{r}_2 + V_{xc}(\mathbf{r}_1)\right)\psi(\mathbf{r}_1) = \epsilon_i\psi_i(\mathbf{r}_1) \tag{2.3}$$

where the $\psi(\mathbf{r}_1)$ are the Kohn-Sham orbital, Z_A is the nuclear charge, r_{1A} is the nuclear-electron distance, ϵ_i the orbital energies, r_{12} the electron-electron distance and V_{xc} is the

exchange-correlation potential and is defined by:

$$V_{xc}(\mathbf{r}) = \left(\frac{\delta E_{xc}[\rho(\mathbf{r})]}{\delta\rho(\mathbf{r})}\right) \tag{2.4}$$

In practice, the Kohn-Sham equations are solved iteratively in a self-consistent way. First of all the initial density is guessed, then this is used in Equation 2.3 in order to obtain a set of orbitals which in turn yields an improved density that is used in the next iteration.

The exchange correlation functional is a key factor in DFT. It has to be approximated in practice, since the exact expression for this functional is not known. In the Local Density Approximation (LDA), the exchange-correlation functional is constructed to be a functional of the density for a uniform electron gas, and is given by

$$E_{xc}[\rho(\mathbf{r})] = \int \rho(\mathbf{r})\epsilon_{xc}(\rho(\mathbf{r}))d\mathbf{r} \tag{2.5}$$

where $\epsilon_{xc}(\rho(\mathbf{r}))$ is the exchange-correlation energy per electron as a functional of the density of the uniform gas. $\epsilon_{xc}(\rho(\mathbf{r}))$ is then expressed in an analytical form. Since in molecular systems, the electron density is far from spatially uniform, LDA is limited. The exchange correlation functional can be constructed as a function of the density and density gradient in more sophisticated functionals such as PBE. DFT is not the perfect method, and is known to not include dispersion. This can be a problem, and in this study is important since DFT is used to model intermolecular energies and forces. However it has been found that the functional used in this study, RPBE gives accurate results for hydrogen bonding [95] so the water-surface DFT calculations are likely to be reliable (albeit not completely accurate). In the peptide-surface calculations, it is electrostatic interactions that dominate. Since electrostatic interactions are satisfactorily recovered within Kohn-Sham DFT, these peptide-surface calculations should at least be moderately reliable.

2.1.2 Periodic calculations

In this study, an infinite crystalline surface was modelled and therfore periodic boundary conditions had to be incorporated to avoid edge effects. It would be impossible to calculate for all electrons over all space so there must be a way to take the periodicity of the system into account.

In order to do this, a plane-wave basis set of the form $e^{i\mathbf{g}\cdot\mathbf{r}}$ was used. **g** is called the wave-vector and the plane waves in question only contain the periodicity of the atoms in the unit cell at certain wave-vectors. **r** is the cartesian vector.

The cell periodic part of the wave-function, $U(\mathbf{r})$ is given as a linear combination of plane-waves with index j;

$$U(\mathbf{r}) = \sum_j C_j e^{i\mathbf{g}_j\cdot\mathbf{r}} \tag{2.6}$$

g has to be a multiple of the reciprocal space lattice vector. The larger the expansion and therefore the more plane-waves used, the more accurate the calculation will be (equivalent to having a larger basis set for real-space calculations). In the present study, two parameters, cut-off energy and *k*-point sampling had to be considered. The cutoff energy gives a measure of the accuracy of the basis set and largest value of **g** in the expansion will relate to the cut-off energy. For a free particle (where the potential of the ions in the lattice has not been taken into consideration):,

$$-\frac{\hbar^2}{2m}\nabla^2 U(\mathbf{r}) = -\frac{\hbar^2}{2m}\nabla^2 C e^{i\mathbf{g}\cdot\mathbf{r}} = \frac{\mathbf{g}^2\hbar^2}{2m}U(\mathbf{r}) \tag{2.7}$$

and therefore the cut-off Kinetic energy (KE) is

$$KE = \frac{\hbar^2}{2m}\mathbf{g}^2 \tag{2.8}$$

the larger the cut-off energy, the smaller the wavelength of the smallest wavelength

plane-wave ($\mathbf{g} = \frac{2\pi}{\lambda}$) and so the better represented the wavefunction will be.
The wavefunction is the product of the cell-periodic part of the wavefunction and a phase factor and is shown as a Bloch function.

$$\psi_{\mathbf{k}}(\mathbf{r}) = e^{i\mathbf{k}\cdot\mathbf{r}}U(\mathbf{r}) \tag{2.9}$$

where $e^{i\mathbf{k}\cdot\mathbf{r}}$ is the phase factor. In order to represent the solid correctly, the energy at many points in k space should be sampled *i.e.* a DFT calculation has to performed for each value of k. The greater the sampling, the more accurate the calculation. For example a 111 grid would have just one point in each principal axis so would only sample the energy at one *k*-point. A 221 grid however would have two points in the reciprocal x- and y-directions but only one in the reciprocal z-direction so would sample four *k*-points.
It is important to optimise both the *k*-point sampling and the cut-off energy since although a high *k*-point sampling and cut-off energy are more accurate they are more computationally expensive.

2.2 Geometry optimisation

In the present study, geometry optimisations have been used in order to find various local energy minima using force-field or PDFT methods. Most methods calculate the force on each atom and move the atom towards the direction of the force *e.g.* "downhill" in energy. The force is then recalculated and is iterated until a threshold of 'zero' force is reached *i.e.* the forces, geometry and therefore energy is minimized. Geometry optimisations can only be used to find the minimum energy configuration in the region of configuration space close to the starting geometry.

2.3 Force-field methods

As alluded to earlier, force-field methods are used because they use very simple expressions for energy and forces and are therefore much less computationally expensive than *ab initio* and DFT methods. Force-field methods are therefore useful for studying the large systems necessary for the present study. In the study of peptides on surfaces, it is not only important to calculate energies (and minimum energy configurations) but we also want to study how the particles propagate with time and determine the statistical properties of a large number of configurations. This can be performed using Molecular dynamics (MD) and Monte Carlo (MC) simulations which require a large number of force and energy calculations respectively. The size of system and configurational sampling exclude DFT/*ab initio* approaches from being used, therefore force-field methods and specifically MD simulation were used for the main part of the present study. It should be noted that periodic boundary conditions were used for force-field calculations for the same reason as they were used for PDFT.

The force-field potential is a sum of different contributions and is given as:

$$U_{total} = U_{elec} + U_{LJ} + U_B + U_{ang} + U_{di} + U_{imp} \tag{2.10}$$

where U_{total} is the total energy, U_{elec} is the electrostatic contribution, U_{LJ} the Lennard-Jones contribution, U_B the bonding contribution, U_{ang} the angle-bending contribution, U_{di} the dihedral contribution and U_{imp} the improper torsion contribution to the energy. Each contribution to the force-field is a chemically intuitive contribution. These contributions can be separated into intermolecular and intramolecular contributions. All contributions used in the present study will be outlined.

2.3.1 Intermolecular contributions

Intermolecular contributions are crucial for the present study since the peptide-water, peptide-surface, water-surface interactions rely on them. This category also contains

interactions within the peptide but with more than three bonds separation. These contributions therefore effect peptide conformation.

2.3.1.1 Electrostatics - Ewald summation of partial charges

The electrostatics is a leading contribution to the intermolecular forces. In the models used in this study, partial charges are distributed over atomic sites which combine in order to approximate the electrostatic potential (U_{elec}). The basic form of this contribution is a Coloumb dependency

$$U_{elec} = \frac{1}{4\pi\varepsilon_0}\frac{q_1 q_2}{r} \tag{2.11}$$

where q_1 and q_2 are the partial charges, r is the distance between the charges and ϵ_0 the permittivity in free space. The periodic nature of the calculations makes this contribution complicated and the Ewald summation is therefore used in which a point charge interacts with all the other point charges in the periodic box and all point charges in an infinite array of periodic cells [92]. To calculate the energy, a summation is made which takes into consideration all the interactions in the periodic box and the interactions between the central box and all image boxes. A regular summation converges slowly because it contains a mixture of positive and negative terms. The positive terms alone form a divergent series as do the negative terms. The summation is therefore converted into two, more rapidly converging series. These take the form of the charges plus a neutralising Gaussian distribution of equal magnitude, calculated in real space. A cancelling charge is then added which is calculated in reciprocal space.

2.3.1.2 Lennard-Jones Potential

The Lennard-Jones contribution to the potential (U_{LJ}) is made up of a repulsive part which approximates the electronic exchange-repulsion and an attractive part which ap-

proximates the London dispersion interactions at long range;

$$U_{LJ} = 4\epsilon_{ij}\left[\left(\frac{\sigma}{\rho_{ij}}\right)^{12} - \left(\frac{\sigma}{\rho_{ij}}\right)^{6}\right] \tag{2.12}$$

ϵ_{ij} is the depth of well of the function, σ is the separation (ρ_{ij}) where the energy is zero. The repulsive part of the Lennard-Jones contributions is especially important for avoiding close contact of atoms. Dispersion is often less important since it is usually much weaker than the electrostatic contributions *e.g.* In the present study the electrostatic contributions tend to dominate. Dispersion can be important however when strong electrostatic contributions are absent.

2.4 Intramolecular contributions

Intramolecular contributions are particularly important for the peptide in the present study because these exert a massive influence on the peptide conformation.

2.4.0.3 Bond stretching potential

A harmonic potential approximates the bond between two atoms, and a typical analytical form for the bond stretching energy (U_B) is given as:,

$$U_B = \frac{k_b}{2}(l - l_0)^2 \tag{2.13}$$

where k_b is the force constant of the bond, l is the bond distance and l_0 is the ideal bond distance. This potential cannot model bond dissociation.

2.4.1 Angle bending

A harmonic potential is also used to model the angle bending potential (U_{ang});

$$U_{ang} = \frac{k}{2}(\theta - \theta_0)^2 \tag{2.14}$$

where k is the force constant, θ is the angle and θ_0 is the ideal angle. The force constant is usually smaller than the bond force-constant allowing greater flexibility.

2.4.2 Torsional terms

A torsion is defined by four different atoms and gives the dihedral angle between two planes of three atoms. Torsional terms can be very important for peptides since a peptide conformation is mainly governed by the dihedral angles. Therefore care has to be taken when parameterising the torsional terms. The strategy used for such parametrisation will be described in Section 2.7 [90].

2.4.2.1 Dihedral Potential

The dihedral potential (U_{di}) is a periodic function (or multiple functions) of four bonded atoms.

$$U_{di} = A[1 - cos(n\omega - \gamma] \tag{2.15}$$

where ω is the torsional angle, A gives the barrier height, n gives the number of minimum points in the function from 0 to 360° and γ defines the torsion angle corresponding to the minimum energy.

2.4.2.2 Improper Torsions

Improper torsions act on groups of four atoms which are not all connected by bonds. They are usually used to keep certain groups of atoms planar. In this study, they are

used to keep the peptide bond planar and rigid. The improper torsion (U_{imp}) potential is given by

$$U_{imp} = K_{imp}(\phi - \phi_0)^2 \tag{2.16}$$

where ϕ is the out of plane torsional angle, ϕ_0 the equilibrium torsional angle and K_{imp} is the improper force constant.

Torsional parameters are usually much softer than angle bending terms. In the present study, much of the barriers to dihedral rotation actually come from interactions of the peptide with water.

2.5 Parametrisation of Force-fields

This study used two previously derived force-fields, Charmm27/TIP3P for the peptide and peptide-water interactions, and the Bandura force-field for the TiO_2 surface. In order to have confidence in the force-field it is always necessary to understand where the force-field came from and how it has been tested [96].

2.6 Force-fields for TiO_2

The primary source for our preferred force-field for TiO_2 was developed by Matsui and Akoagi [91] and was used to model the bulk solid. The force field that was used included Coulombic potential for the electrostatics and Buckingham potential for dispersion/repulsion. The charges were obtained from previous work on phonon-dispersion relations [97]. The repulsive radius was taken from previous work for magnesium silicates. The other parameters were obtained by fitting to crystal structures and elastic constants of rutile. Molecular dynamics (MD) simulations were performed for rutile, anatase, Brookite and a dense phase called TiO_2 (II). Comparisons were made with structural data from X-ray experiments and good agreement was found with experi-

ment for cell parameters and Ti-O bond bond distances. Kim *et al.* [98] also performed MD on bulk rutile, anatase and Brookite using a modified potential to that of Matsui and Akoagi by fitting to crystal data and physical data. These were mean volume thermal expansivity, bulk modulus and heat capacity. These results show that there is physical basis behind the force-fields, at least for the bulk. Bandura and Kubicki used the force-field described above and modified the parameters in order to take the rutile surface into consideration [3]. Optimisations of three layer non-hydroxylated titania rutile slabs were performed using both parameters. It was found that they were both correct in predicting surface relaxation when compared to data generated from Perdew-Wang 91 DFT calculations (PW91). For hydroxylated structures however, the Matsui potential gave a closer agreement to PW91 optimisations, and Charges from Electrostatic Potentials using a Grid based method (CHelpG) charges of titanium hydroxyl complexes were found to be closer to the Matsui potential and so the charges from the Matsui potential were used as a starting point for their parametrisation. The TiO-H bond parameters were taken from Fleming *et al.* [99] (Gibsite potential). To obtain force constants for Ti-O-H harmonic angle bending terms, generalised gradient approximation- Becke, Lee, Yang, and Parr (GGA-BLYP) DFT vibrational frequencies were calculated for $Ti(OH)_4$; the Ti-O-H harmonic angle bending terms were adjusted so that force-field calculations could reproduce the DFT vibrational calculations.

Predota *et al.* [2] performed molecular dynamics of the rutile-water interface. They used the Bandura and Kubicki [3] force-field and SPC/E water. These simulations will be discussed further in chapter .

2.7 Force-fields for peptide systems

The force-field used in this study was Charmm27 [90]. Throughout the years, a great deal of work has been put into its parametisation and it is important to understand and review the parametrisation processes in order to have some confidence in the model.

The first stage was the optimisation of the parameters. Mackerall *et al.* took the initial values from the previous Charmm parameters. Intramolecular parameters were taken from structural (microwave, electron diffraction and X-ray) and vibrational data (*ab initio* and gas-phase infrared and Raman) for model compounds. They then used these values for optimising intermolecular parameters by studying interaction energies, minimum energy geometries and dipole moments (*ab initio* calculations with water) and condensed phase properties (from MD simulations compared with experimental thermodynamic data such as heats of vapourisation). With improved interaction parameters, structures, vibrational spectra and energy surfaces were reoptimised by adjusting the internal parameters. This iterative process was repeated until convergence.

The reason for using the TIP3P water model was stated in the paper by Mackerall[90]. This was that in the SPC/E water model, a correction is used to account for the lack of polarisation. This is adequate for bulk solvent but leads to inconsistencies when a solute is introduced. The TIP4P leads to good results but is expensive. TIP3P had neither of these problems and the unmodified VDW parameters for solvent-solute interactions are used.

Mackerall *et al.* extensively tested the force-field, mainly for N-methylacetamide (NMA) and alanine dipeptide. The authors pointed out that structural changes can occur in going from the gas phase to condensed phases, notably the C=O and N-H distances can change due hydrogen-bonding. Therefore the parameters they used were ones which can represent condensed phases, but not gas phase structures since the focus for the force-field was condensed phase simulations. They assumed that there would always be hydrogen bonding (with water or internally).

Mackerall *et al.* tested internal parameters by studying minimised structures and vibrational frequencies, and found reasonable agreement with *ab initio* calculations and infra-red (IR) spectra for NMA and dialanine.

Interaction parameters were tested using NMA as a model compound. The interaction energies and geometries of the complexes of NMA with water and the NMA dimer

were compared with *ab initio* calculations, the dipole moment of NMA and the heat of solvation of NMA compared with experiment. Good agreement was found.

Importantly, for the present study, tripeptides, GAL.$(H_2O)_3$, GAV.$(H_2O)_3$ and AAA were tested using crystal simulations and dihedral angles and non-bonded distances of X-ray and simulation structures were compared. It was shown that the torsions or non-bonded distances between peptides did not deviate much from that of the crystal structure but the peptide-water distances showed significant deviation indicating a limitation in the model.

It has just been shown that a great deal of work has been put into validating both the Charmm protein and Bandura/Matsui force-fields. Therefore we can have confidence in the TIP3P water-peptide, peptide intramolecular and surface force-fields. It will be shown that in this thesis, the issues of the validitity of the surface-TIP3P water and surface-peptide interaction parameters will be addressed.

2.8 Molecular Dynamics Simulations

Molecular dynamics was used because it yields dynamical and statistical properties. It uses Newton's equations of motion to calculate the classical trajectory that specifies how the positions and velocities of particles evolve with time.

2.8.1 Integration algorithms

The force on each atom is given by taking the analytical first derivative of each force-field term and partitioning the force into individual Cartesian components for each atom.

$$F_i = \frac{-dU}{d\mathbf{r}_i} \tag{2.17}$$

U is the potential energy and $\mathbf{r_i}$ is the position vector. The trajectory is then obtained by solving the differential equation

$$\frac{d^2\mathbf{r_i}}{dt^2} = \frac{F_i}{m_i} \tag{2.18}$$

where m_i is the particle mass and t is the time. An integration has to be performed to find the positions and velocities of each atom at each time step.

The Leap-frog and Verlet [100] integration algorithms were used in this study. The difference between them is that the leap-frog algorithm explicitly calculates the velocity unlike the Verlet algorithm. To show how these algorithms work, the Leap-frog algorithm will be detailed. The Leap-frog algorithm uses the following relations;

$$\mathbf{r}(t + \delta t) = r(t) + \delta t \mathbf{v}(t + \frac{1}{2}\delta t) \tag{2.19}$$

$$\mathbf{v}(t + \frac{1}{2}\delta t) = \mathbf{v}(t - \frac{1}{2}\delta t) + \delta t \mathbf{a}(t) \tag{2.20}$$

$$\mathbf{v}(t) = \frac{1}{2}[\mathbf{v}(t + \frac{1}{2}\delta t) + \mathbf{v}(t - \frac{1}{2}\delta t)] \tag{2.21}$$

The velocities at time $t+\frac{1}{2}\delta t$, $\mathbf{v}(t+\frac{1}{2}\delta t)$ are calculated from the velocities at time $t-\frac{1}{2}\delta t$, $\mathbf{v}(t-\frac{1}{2}\delta t)$ (equation 2.20) and the accelerations at time t, $\mathbf{a}(t)$ (from Equation 2.18). The positions at $t+\frac{1}{2}\delta t$, $\mathbf{r}(t+\frac{1}{2}\delta t)$ are then obtained from Equation 2.19. The initial velocity (at $t-\frac{1}{2}\delta t$) has to be obtained stochastically and δt is the timestep.

2.8.2 Timesteps

The timestep chosen should be smaller than the fastest mode in the simulation in order to capture all the major information. In this work a timestep of 1 fs was used which is short enough to capure the bond vibrations which connect various atoms to hydrogen.

2.8.3 Thermostat

The simulations performed in the present study were performed at room temperature because this is the temperature relevant to the experiments that we compare with. In an MD simulation there has to be a way of regulating this temperature. Temperature regulation is performed using a thermostat. The Nose-Hoover thermostat was used for the simulations in this study [101, 102, 103]. This thermostat considers a thermal reservoir as an integral part of the system. The reservoir is represented by an additional degree of freedom, $\chi(t)$. The equations of motion are modified to account for this:

$$\frac{d\mathbf{v}(t)}{dt} = \frac{f_i}{m_i} - \chi(t)\mathbf{v}(t) \tag{2.22}$$

χ is controlled by the the first order differential equation

$$\frac{d\chi(t)}{dt} = C(\tau(t) - T_{ext}) \tag{2.23}$$

where C is a constant and is dependent on an effective mass Q, the magnitude of which determines the coupling between the reservoir and the system. τ(t) is the instantaneous temperature of the system at time t which is related to the kinetic energy, k of the system by the following equation:

$$k = \frac{K_B T}{2}(3N) \tag{2.24}$$

where K_B is Boltzmann's constant, and N is the number of molecules in the system. $\chi(t)$ is propagated in time in the same way as the velocity. $\chi(t)$ is then used in order to calculate the acceleration and the leapfrog algorithm is propagated. The Nose-Hoover thermostat was used because it maintains a rigorous canonical ensemble (see Statistical mechanics section later). Other thermostats which scale the velocities can lead to temperature differences between solute and solvent.

2.8.4 Barostat

In the simulations performed, it was desired that the pressure was kept at ambient pressure. The pressure was kept constant using the Nose-Hoover barostat. This was so the volume could fluctuate freely and that the density of water could reach equilibrium during the simulation. The Hoover barostat works in a similar way to the Nose-Hoover thermostat and is used in conjunction with the Nose-Hoover thermostat. There is a fictional mass W analogous to Q and a modification of velocity;

$$\frac{d\mathbf{r}(t)}{dt} = \mathbf{v}(t) + \eta(\mathbf{r}(t) - \mathbf{R}_0) \tag{2.25}$$

where

$$\frac{d\eta(t)}{dt} = \frac{3}{W}V(t)(P(t) - P_{ext}) - \chi(t)\eta(t) \tag{2.26}$$

and gives a dependence of instantaneous pressure P(t) compared to desired pressure P_{ext}. The positions are effectively scaled in response to the difference in pressure. V is volume, $\mathbf{R}_0$ is the system centre of mass. The coupling depends on the value of W.

2.8.5 Fixed atoms

In the simulations discussed in this thesis, the surface was held rigid and the atoms were held fixed in space. The forces on these atoms are not used to propagate the atoms involved.

2.8.6 Car-Parrinello molecular dynamics(CPMD)

In the present study, CPMD was used to compare the dynamics using force-field derived forces with dynamics using DFT-derived forces. CPMD simulates classical dynamics, where the potential is described using quantum mechanical methods. The obvious way

to do this would be to calculate the forces using quantum mechanical methods and use them to integrate Newtons equations of motion like any other MD method (called Born-Oppenheimer MD). However this can be very slow because the ground state electronic configuration has to be found for every time step. In CPMD however, the electronic state is propagated in time just like the atomic positions. This is done by an analogous equation to the atomic equations of motion but moving in Kohn-Sham orbital coefficient space;

$$\mu_k \frac{\mathrm{d}^2 c_k^i}{\mathrm{d}t^2} = -\frac{\partial E}{\partial c_k^{i*}} - \sum_j \lambda_{ij} c_k^j$$

c_k^j are the basis set coefficients. Here, the μ_k can be though of as "fictitious masses" and controls the acceleration of the basis set coefficients, due to the force on the coefficients $-\frac{\mathrm{d}^2 c_k^i}{\mathrm{d}t^2}$. The last term arises from the constraint of orthonormality , with λ_{ij} the undetermined Lagrange multipliers. CPMD then integrates the classical and quantum equations of motion simultaneously.

2.8.7 Monte Carlo simulation and Monte Carlo optimization

Monte Carlo simulation can sample from the same ensembles as MD. It is often used because it does not require the forces on the atoms to be calculated and a reduced set of degrees of freedom can be sampled. For example for peptides, instead of moving all the atoms in Cartesian space, only the important torsions can be moved. This greatly reduces computational cost. MC samples by making random changes to the configuration and calculating the energy at each step. It samples from a canonical ensemble by using the Metropolis criterion which accepts each move on the basis of the energy difference and the calculation of the probability (P) that it will be accepted which is;

$$P = e^{-\beta E_j} \tag{2.27}$$

$$\beta = \frac{1}{k_B T} \tag{2.28}$$

where E_j is the energy, k_B is the Boltzmann constant, T is the temperature. Moves are always accepted if the energy is lower than the previous step. In the present study, MD was used instead of MC because in MC nothing can be deduced about the dynamics of the system. In MC only equilibrium properties can be extracted. However in the systems in the present studies, dynamic information is important. Also, because explicit water molecules were used, MC would not allow a reduced set of degrees of freedom and would be complicated to implement.

2.9 Statistical mechanics

Statistical mechanics is the link between macroscopic and microscopic properties. A macroscopic property is an average over a large number of particles and a timescale that is not conveniently accessed by molecular simulation. Therefore a system evolving in time can be represented by a large number of replications of the system called an ensemble and the time average is replaced by the ensemble average.

The total potential energy tells us how stable a given configuration is. The entropy however is a measure of how many states there are in the region of phase space which are important. In the continuous case it is the volume of phase space *e.g.* a particular set of torsions for a molecule in a particular configuration may have a very low energy, however if this is the only configuration which is very low in energy, it may still not be very populated. In the micro-canonical ensemble, each micro-state has the same energy and is equally likely to be populated. The macrostate which is occupied entirely depends on the volume of that particular state (the number of microstates which it contains). In a physical system (isobaric-isothermic or canonical ensemble), the probability (P) of population of each micro-state depends on the energy, E_j and the temperature in the

following way.

$$P = e^{-\beta E_j} \tag{2.29}$$

where $\beta = 1/k_B T$.

This gives the relative probabilities of a particular state to be populated. The absolute probability however depends on the probability of the other states and is given by the Boltzmann population equation:

$$P_j = \frac{1}{Z} e^{-\beta E_j} \tag{2.30}$$

where

$$Z = \sum e^{-\beta E_j} \tag{2.31}$$

is called the partition function and is the sum over all states. If we could find the energy of all the states (or most of the states sampled evenly), we could calculate the partition function. The partition function gives us the denominator in a probability *i.e.* it normalises the distribution. The Boltzmann population equation tells us that when we increase the temperature, the difference in probability between two micro-states relies less on the difference in their energies. It therefore, makes the volume of configuration space and therefore entropy more important. This is apparent by the following equation:

$$\Delta G = \Delta H - T\Delta S \tag{2.32}$$

Where ΔH is the change in enthalpy (H=E+PV), ΔS is the change in entropy and ΔG is the change in Gibbs free energy in the isobaric-isothermal ensemble. The higher the temperature, the more important entropy is to the Gibbs free energy.

The reason why this is important is that the free energy difference between two states

tells us about how favourable it is for one state at equilibrium to move to another state *i.e.* it tells us the population of both states at equilibrium (the free energy barrier gives us information about the probability of transition from one state to the other).
The entropy can be calculated from the following relation:

$$S = k_B lnW \tag{2.33}$$

where W is the number of microstates available. This therefore takes into consideration only the number of states and does not consider energy. The Gibbs free energy on the other hand is calculated from the partition function which is effectively the Boltzmann weighted number of states and therefore takes into consideration energy and entropy. It is given by:

$$G = -k_B T lnZ \tag{2.34}$$

If we could sample all the possible states, there would be no problem in finding all the probabilities of all the states, and therefore calculating all the desired properties. However, the number of states that would have to be calculated even for a small system would be absolutely massive. Therefore, it is necessary to find a way of reducing the amount of phase space which has to be sampled. Since it is only really the low energy states which are actually important to the partition function (because the high energy parts provide a tiny contribution to the sum), it is only these that need to be explored in detail. In MC, the Metropolis criterion provides this condition since only configurations which are suitable go on to be randomly changed, high energy parts of configuration space are mostly avoided. For MD, the forces dictate the next configuration. High energy parts of the ensemble will not be explored because the force would then be massive and the atoms would be moved to configurations that are lower in energy.

2.9.1 Energy barriers and rates

The rate of any process is governed by the free energy barrier between two sub-ensembles of states. MC is a good way to demonstrate how this arises. In MC (like in MD), sampling can be slowed by the simulation being trapped in local minima. If we were making small modifications, in order for any energy barrier to be overcome, a move that is higher in energy (but within the Metropolis criterion) would have to be made, this would have to happen again and again until the barrier was surmounted. The probability of such a move would be very low since the probability of these moves being selected would be multiplied with every step. This crossing would therefore happen seldomly and the rate would be slow. With MD, the trajectory depends on the force. Since the velocities are scaled with temperature, the movement of atoms in a particular step will be smaller for smaller temperatures. The velocities however, are involved in the evolution of the next step and will decrease in response to reaching a higher energy state. In order for the barrier to be surmounted, the velocities of several atoms in a specific directions must all be favourable. Again the probability of this occurring is very small and the rate of transition would be slow.

These slow rates of crossing are the reason for sampling problems in MD. The time that can be simulated is usually smaller than the rate of barrier crossing for high barriers. For this reason, long time scale methods like metadynamics are currently under development[104].

2.10 Equilibrium

At equilibrium, any process which occurs has to be a reversible process. In a simulation, care has to be taken in order to ensure equilibrium has been reached. Equilibrium usually means that the average energy and forces are constant. In the simulations in this study, it is very important to ensure that the peptide is completely solvated.

There has also been an issue concerning the correct procedure to start a simulation;

especially when the initial conditions are important. In this situation, it is important to reach equilibrium slowly without affecting the initial configuration too much. The procedure used to do this will be shown here since it concerns whether the method used was correct. It involves simulations of the peptide on the surface because this is the most complicated case and it is assumed that this is the most likely case for equilibrium problems to arise. Figure 2.1 shows the potential energy of a peptide/water/surface system which has been geometry optimised at the start but has then been simulated at 298K.

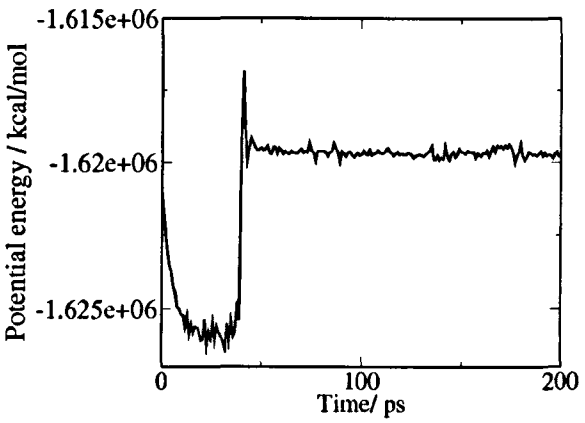

Figure 2.1: Total potential energy versus time for a peptide/water/surface system with no heating schedule.

It can be seen that at the start of the simulation, the energy decreases during the zero Kelvin stage. However, when the simulation is started, the energy increases abruptly. If the initial conditions are very important, this is not a good situation since this increase in energy can disrupt the system. Figure 2.2 on the other hand shows a simulation which has been slowly brought up to temperature (in 50 K increments).

It can be seen that there are steps in potential energy with each 50 K increment but there is no sudden increase in energy. This is because the water around the peptide was able to solvate the peptide sufficiently before the 298K stage of simulation. This therefore shows that it is the most appropriate method for starting a simulation where starting configurations are crucial. The procedure will be outlined in Chapter 5.

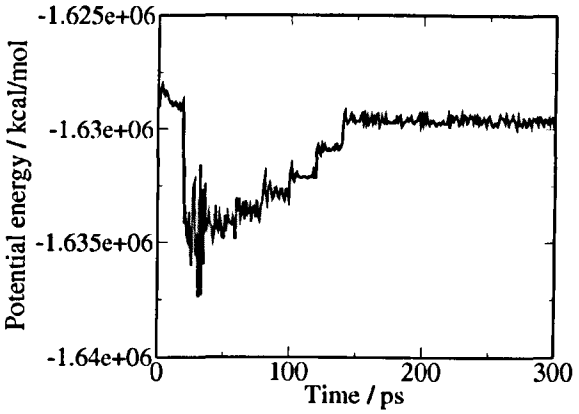

Figure 2.2: Total potential energy versus time for a peptide/water/surface system using a heating schedule.

2.11 Atomic solvation parameters (ASP) implicit solvent model

Implicit solvent models can be used to represent the solvent without explicitly including solvent molecules. The benefit is a decrease in the computational cost while the mean-field effects of solvent (*e.g.* the background dielectric) are accounted for. In this study the Atomic solvation parameters (ASP) [105] model was used in order to find initial configurations for subsequent simulations including explicit water molecules. It was not used to gain any useful phenomenological information and therefore it was not absolutely crucial to choose the best implicit solvent model. ASP was therefore used because it allowed efficient and sensible sampling. The ASP model works by including an extra term to the force-field that is dependent on the the derivative of the free energy of solvation.

$$\Delta G_s = \sum_{atoms,\, i} \Delta\sigma_i A_i \tag{2.35}$$

where σ_i is the atomic solvation parameter for atom i, and A_i is the solvent accessible area for each atom or group. The modification of the force F_i on atom i can be expressed

as

$$F_i = -\frac{\delta(\Delta G_s)}{\delta \mathbf{r}_i} \tag{2.36}$$

where $\mathbf{r}_i$ is the position vector.

The areas, A_i, were found by taking averages for different conformations of different amino acid residues in four different proteins in the Brookhaven database [106]. The atomic solvation parameters were fit to free energy of solvation calculations and are classified into atom types.

2.12 Hierarchy of Modelling

For meaningful modelling, there must be three ingredients all of which depend on each other. These ingredients are in a hierarchy. Firstly, the structural model must be correct. Secondly, the force-field must be correct but means little without the correct structural model. The sampling must be sufficient to gain meaningful information depending on the scientific challenge which needs to be addressed. The sampling of configuration space, however, cannot be correct unless the force-field is correct (see Section 2.9). In this thesis, it will be shown that many of these aspects have been addressed although it would be wrong to state that all of the aspects are perfect. Scientific progress has been made however, creating opportunity for further refinement. It should also be stated that there are many more important aspects which have not been addressed in this thesis such as size effects, chemical changes, ion and pH effects *etc.* Firstly it must be tested whether these effects are crucial for the problem which is being addressed. If not, more complicated models must be developed and employed.

Chapter 3

Interaction of TiO_2 with water

3.1 Introduction

In this chapter, the interaction between water and the rutile (110) surface will be studied. Validations will made by comparing force-field calculations (MD, single point and optimisation) with analogous periodic density functional theory (PDFT) calculations. Also MD simulations of the water/titania surfaces will be shown and comparisons made with X-ray experiments and previous simulation studies.

The main objectives for this chapter are as follows. First, it is an interesting subject in its own right since inorganic-water interfaces are ubiquitous both in nature and technology [107]. Secondly, it is a prerequisite for the work on the peptide-surface interactions because it validates the approach employed with DFT, experiment and other MD simulations. It will be shown in later chapters that the same force-field/structural models will be taken forward for use in the peptide/water/surface simulations.

There is considerable controversy regarding the adsorption behaviour of water on titania (specifically the rutile (110) surface), especially between experimental and theoretical results [68]. The main question involves the extent with which water dissociates on the surface. Firstly, does water adsorb to the surface as molecular water or as a chemically bonded hydroxyl group and proton? If dissociation does occur, does it occur

uniformally on the surface? What is the density of dissociated waters? These issues are fundamental when considering the adsorption of biomolecules on the titania surface since the dissociation state will determine the surface which the adsorbing peptide will interact with. With a given level of dissociation, it must be asked how does molecular water interact with the surface, how does the water structure itself both in terms of position and orientation? This will also influence the adsorption of peptides. Some of these issues will be covered in this Chapter and used in Chapter 5 involving peptide/water/titania systems. It will be shown that the analysis performed in this chapter will also be very useful when considering such systems.

Before discussing the results, some of the previous work will be highlighted in order to gain an understanding of the model necessary to describe the water-titania surface.

3.2 Background

In order to answer some of the questions previously posed, especially involving the dissociation of water on the surface, many studies have been made involving the rutile (110) surface under ultra high vacuum (UHV) conditions [108, 68, 109, 80, 110]. In these studies, a controlled amount of water is added; these usually involve temperature programmed desorption (TPD) studies combined with other techniques such as molecular beam scattering [111], high resolution electron energy loss spectroscopy (HREELS) [112] and work function measurements (and X-ray photoelectron spectroscopy (XPS)) [80]. All of these TPD studies showed separate desorption peaks relating to first layer, second layer and multilayers. All of them indicated little dissociation of water on the rutile(110) surface.

A molecular beam scattering study [111] was interpreted to give kinetic information which could be used to decide whether there was associative or dissociative adsorption, it was concluded that very few molecules dissociate. In a HREELS study[112], a loss feature (at 135K) was observed which is indicative of an O-H group. The amount

was low, indicating water dissociation only at point defects (not the flat surface). This remained low even at room temperature.

Work function measurements using Auger electron spectroscopy [113] were able to give information about the orientational structuring of water (in multilayers) on the surface[80] *i.e.* gives information about the dipole of water. It was stated that a decrease in the work-function with coverage (up to monolayer coverage) was consistent with the oxygens (dipoles) facing towards the 5-coordinated Ti for the first layer but slightly off to facilitate hydrogen bonding to neighbouring oxygen (water or bridging). The work function did not change for higher coverages suggesting that second layer waters bound with their hydrogens directed toward bridging oxygen anion sites and lie nearly parallel to the surface to improve hydrogen bonding between their oxygen atoms and the hydrogen atoms of first layer water molecules. It will be shown later that results of the present study agree with such findings. It was suggested that there is predominantly molecular adsorption because the negatively-charged hydroxyl group would increase the work-function.

Interpretations of STM studies [114] suggested that OH groups were bridging hydroxyls (not terminal) and that water adsorbs dissociatively in oxygen vacancies and via proton transfer to two neighbouring bridging oxygen atoms.

Allegretti *et al.* [109] performed scanned-energy mode photoelectron diffraction and were able to measure the distance between the water oxygen with the 5-coordinated Ti as 2.21 Å. This long bond would also suggest molecular adsorption. This length will be compared with results of the present study.

As outlined, most experimental results suggest little dissociation; mainly molecular adsorption on perfect crystals. In contrast to the experimental work, most theoretical calculations indicated that dissociation of the water molecules is energetically favoured on the perfect TiO_2(110) surface. [115, 116, 117, 118, 119, 120, 121]. Most of these involved static DFT calculations which showed lower binding energies for the dissociated state.

A series of studies investigated different levels of water coverage by static and Car-Parrinello molecular dynamics (CPMD), PDFT calculations [115, 120, 116]. Firstly, one water was placed close to the 5-coordinated Ti in many different initial conditions (0.5 coverage) and simulated by CPMD [116]. The water dissociated, showing that in this model, the dissociated state is more stable at half monolayer coverage.

Lindan *et al.* then added a second water to the surface containing one dissociatively bound water, simulated with CPMD and found that the second water adsorbed associatively. Static calculations were then performed and it was found that the most stable state was this mixed state where there was one dissociated and one molecularly adsorbed water[120, 115]. It was stated that hydrogen bonds made the molecular adsorbed water state lower in energy.

Calculations have also been made to investigate the adsorption of second layer water. Zhang and Lindan [120] performed PDFT single point energy and CPMD calculations of second layer water. One water was put on different sites of three different first layer states: fully dissociated and two mixed mode states (containing first layer molecular and dissociated water) and simulated using CPMD. The authors found interesting proton transfer mechanisms where the proton propagated down the [001] direction with some of the mixed first layer states and that the presence of the extra water molecule changed the first layer state in one case into the less stable fully hydroxylated state.

These multilayer studies are interesting and relevant to the present study, because they bring us closer to understanding the state of the surface when fully submerged in water (when compared with single water studies). They give us insight into further layers of water, the interactions between these waters and the effect that has on dissociation; something that cannot dynamically be done for the atomistic model used here.

A study by Barnard *et al.* was interesting from the point of view of characterising an amorphous phase of titania. DFT was used to study the energetics (100), (001) and (101) surfaces of anatase; and the (100), (110) and (011) surfaces of rutile under different acidic and basic conditions by studying surfaces with a differing coverage of

associative and dissociative water [121]. This study is a step in the right direction considering the need to understand amorphous surfaces *i.e.* understanding many of the different possible surfaces of the different polymorphs of titania. It can be envisaged that future work leading on from the present study could benefit from such an approach since amorphous surfaces are the key to fully understanding the interaction between titanium and peptides (considering titanium oxidises into an amorphous layer of titania). DFT studies which do not use periodic boundary conditions but use clusters to model the surface have also been made. Two such studies involved DFT calculations of water on TiO_2 (110), performed using a cluster model terminated with pseudo hydrogens [122, 123]. Different functionals were used and it found that the results closest to experiment were using GGA functionals (not LDA) and concluded that a small cluster (Ti_7O_9) could be used for these calculations. These types of studies could, in the future, be used to generate more accurate force-fields for solid-water interactions *i.e.* up until now, clusters have been used but there has not been a way of terminating them in order to take into consideration electronic effects of the remaining bulk solid.

It seems that the difference between the theoretical and experimental results could be that although it may be thermodynamically stable for dissociation to occur, it cannot occur (at least under the conditions of the experiment) due to kinetic factors. The limitations of DFT calculations is that they can only consider at most two water molecules and therefore neglect condensed phase effects such as hydrogen bonding and entropy. Also UHV experiments consider each layer at a time giving similar problems. In order to address such issues, atomistic simulation combined with X-ray *in-situ* experiments have been made.

3.2.1 Previous simulation work and related experiments

The simulation work by Predota *et al.* which was combined with X-ray experiments of Zhang *et al.* is very important for the present study since results of our simulations were compared with these studies. Firstly X-ray crystal rod studies were made (used as

a direct analogue of X-ray crystallography for interfacial systems)[6, 124]. This work probed the structure of oxygen atoms in the surface and adsorbed ions. Importantly, the X-ray studies were *in-situ* which meant that information about the surface when submerged with water could be gathered. This is in contrast to the experiments highlighted earlier.

In the work by Predota *et al.*[2, 125, 126, 127], the water/surface interface was simulated using the Bandura force-field (outlined in the theory chapter) to describe the surface and SPC/E for water. Since dissociation could not be described for such force-field simulations, the dissociation state issue could not be addressed dynamically as in *ab initio* or DFT studies. The main idea behind this work was therefore to study the structuring of water on the surface using different levels of hydroxylation (a different simulation for each different degree of hydroxylation). Comparisons between axial densities and X-ray experiments could then be made in order to gain insight into the dissociation state. The molecular dynamics simulation work in the present study follows the work by Predota *et al.* The results of this study will therefore be apparent later.

The second paper of the series by Predota *et al.* involved studying the adsorption of ions onto the rutile(110) surface[128] using the same model and comparing with X-ray experiments. This was interesting because it gave an idea about the hydroxylation state of the surface by testing how close the agreement with experiment was with the different surfaces when considering ion adsorption. It was stated that this comparison suggested that the charged hydroxylated surface model rather than the nonhydroxylated model gave a better approximation to the the real rutile-water interface. This is because in X-ray studies, Rb^+ and Sr^{2+} on rutile(110) single crystal surfaces there was only one peak; corresponding to one adsorption site: the tetra-dentate site in contact with two terminal and two bridging oxygens. The axial density of these ions on the negatively-charged hydroxylated surface only showed one peak; agreeing with experiment.

In contrast, the axial density of the negative non-hydroxylated surface showed an extra shoulder relating to a bidentate site between a bridging and terminal oxygen. Also it

showed little adsorption for the neutral surfaces showing that the negatively-charged surfaces best represent the real surface (at least with respect to ion adsorption). This would agree with electrochemical experiments which showed that the surface is negatively-charged [71, 72].

A recent study investigated water adsorption on TiO_2 nanoparticles (rutile and anatase) [129]. One of the conclusions was that for the rutile nanoparticle, the water coverage and structuring, and crystallinity increased as the nanoparticle size increased becoming more like a flat rutile surface. Understanding water structuring on nanoparticles is very interesting because many studies for peptides/proteins on surfaces have involved nanoparticles. This could therefore be the next step in understanding such processes.

Much of the previous work outlined has been concerned with the nature of the rutile (110) surface. This chapter will continue in this vein as well as being part of the preliminary work for the peptide-surface work in later chapters. As stated, the present study follows the work by Predota *et al.* The reason for repeating such work was that in the present study, it was desirable to use the TIP3P water model [4, 5]. The TIP3P water model [5] was developed with and extensively tested against the CHARMM27 force-field [90] (see Chapter 2) which we intended to use for simulations with peptides and water. We therefore wanted to compare the modified TIP3P model with the SPC/E model, which was the existing water model used for aqueous/TiO_2 interfaces.

3.3 Methods

The details of the methods will be described here. Since it is the first results chapter, particular detail will be used; in later chapters, similar procedures were used so do not necessarily need to be described again.

3.3.1 Force-field

The intermolecular potential used is given by (taking Lorentz-Berthelot mixing rules into consideration):

$$E_{ij} = \sqrt{\epsilon_i \epsilon_j}\left[\left(\frac{r_{mi} + r_{mj}}{2r_{ij}}\right)^{12} - 2\left(\frac{r_{mi} + r_{mi}}{2r_{ij}}\right)^{6}\right] + \frac{q_i q_j}{4\pi\epsilon_o r_{ij}} \tag{3.1}$$

Where E_{ij} is the total intermolecular potential energy. q_i and q_j are the charges on atom i and j, r_{mi} and r_{mj} is the Lennard-Jones minimum distance of atoms i and j and r_{ij} is the distance between atoms i and j. The charges for the TiO_2 surface were taken from Predota *et al.* [2] and the intermolecular force-field parameters are shown in Table 3.1.

Table 3.1: Atomic charges (q) and Lennard-Jones parameters for water and hydroxyl atoms.

atom	q(e)	r_m(Å)	ϵ_i(kcal/mol)
H	0.417	0.2245	0.0460
O	-0.834	1.7682	0.1521
Ti(5-coordinated)-O(water) pair	—	3.7	0.032

As mentioned in Chapter 1, the titania surface is negatively-charged at pH 7. It is therefore desirable to have a model which can take this into consideration. However, as alluded to in the background of this chapter, the exact hydroxylation state is still uncertain. A different charge set was used for neutral and negatively-charged surfaces so that removing a bridging hydrogen or adding a terminal hydroxyl would result in a -1 charge on the surface. These were also taken from Predota *et al.* [2]. The Lennard-Jones parameters for the surface hydrogens and oxygens were taken from the TIP3P hydrogen and oxygen respectively. Initial Lennard-Jones parameters for the titaniums were taken from the Ca^{2+} ion with the knowledge that testing and validation of the model would be made. Lorentz-Berthelot rules were used in order to calculate Van der Waals (VDW) interactions. The TIP3P water parameters were taken from the TINKER package [130, 5] and have VDW parameters for the hydrogens, which we recognise is not the standard

TIP3P force-field. A harmonic potential was used to describe bonding between oxygens and hydrogens for the bridging and terminal hydroxyls, and the parameters are given in Table 3.2 (refer to equation 2.13 for definition).

Table 3.2: Bonding potential parameters.

Bonding pair	l_0(Å)	k_b (kcal/mol)
O-H(terminal)	0.9708	400.00
O-H(bridging)	0.9766	400.00
O-H(water)	0.9572	450.00

3.3.2 Validation of Force-field

In order to test the force-field, periodic density functional theory (PDFT) calculations were performed. All calculations used the CASTEP package [131] with 4 k-points (221 Monkhurst-Pack grid [132]) with a 400 eV cut-off energy using ultrasoft psuedopotentials[108]. We used the revised Perdew-Burke-Ernzerhof (RPBE) functional [133]. For the optimisation of the water on the hydroxylated surface using PDFT, a five layer TiO_2 slab was used with cell dimensions of 6.499 × 6.1874 × 30.0 Å. This corresponds to a 1 × 2 unit cell with a vacuum gap in the z-direction of about 20 Å. The slab was generated by cleaving the experimental bulk structure and optimising using the PDFT with the above conditions. The conditions used for these simulations (k-point, cutoff energy and slab thickness, RPBE functional) were chosen because they were used by Zhang and Lindan [120]. Extensive studies were made to test these conditions and therefore they were deemed to be sufficient to give accurate calculations.

3.3.3 Car-Parrinello Molecular dynamics (CPMD)

A CPMD simulation was performed for 8 ps with a time step of 0.01 ps using the CASTEP package [131]. The canonical (NVT) ensemble was used at a temperature of 300K. 1 k-point was used with a cutoff of 400eV, ultrasoft psuedopotentials [108]

and using the RPBE functional. A cell dimension of 6.499× 6.1874× 30.0 Å was used and all atoms were kept fixed except for bridging and terminal hydroxyls. No water molecules were present in these simulations.

3.3.4 Cutoff selection for simulations

The cutoff we used for the simulations was 12 Å, the same as Predota *et al.* [2]. The first simulations that we ran were ones with three layers of atoms. However it was discovered that this caused problems as the cut-off was larger than the width of the surface. For this reason we used the 5 layer surface for further calculations.

3.3.5 Molecular dynamics simulation details

The molecular dynamics (MD) simulations were performed using the TINKER package [130]. For all simulations a five layer slab was used. No vacuum layer was used in between slab-water cells because it has been shown to be unimportant for atom density profiles [134]. The non-hydroxylated surface (see Figure 1.7b) was a replica of the experimental unit cell [135, 136]. The negative non-hydroxylated surfaces were then made by addition of the desired number of hydroxyls. Here we followed the structural model of Predota *et al.* [2]. The hydroxylated surface (see Figure 1.7a) was derived by placing hydroxyls on all 5-coordinated Ti sites, placing protons on all bridging oxygen sites, and fully optimising using PDFT under the conditions mentioned previously. To give an idea about the structural model of the negatively-charged surfaces, a schematic is shown in Figure 3.1

Negatively-charged hydroxylated surfaces were then made by removing 25% and 12.5% of the bridging hydroxyl protons and again, the structural models of Predota *et al.* were followed. The nonhydroxylated bridging oxygens in this case were fixed. Negative non-hydroxylated surfaces were made by putting hydroxyls on 25% and 12.5% of the 5-coordinated titanium sites as in Predota *et al.* [2]. In order to balance the extra neg-

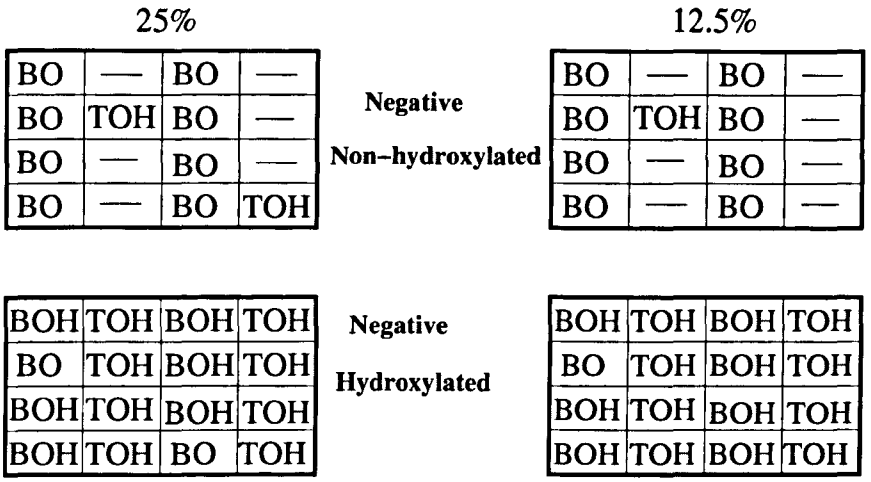

Figure 3.1: Schematic to show the distribution of surface groups for negatively-charged surfaces. TOH represents terminal hydroxyl groups, BO represents bridging oxygen and BOH bridging hydroxyl, taken from Predota *et al.*[2].

ative charge in the cell, Na^+ ions were added to the water. 18 Na^+ ions and 2 Cl^- ions were added to the 25% surfaces and 10 Na^+ ions and 2 Cl^- ions to the 12.5% surfaces. All simulations were done using the isobaric-isothermal (NPT) ensemble at 1 atmosphere pressure and a temperature of 298 K. The simulations were run for 1 ns with a time step of 1 fs with the frames being saved every 500 fs. The Verlet algorithm [100] and 12 Å cutoff were used for all simulations. The initial cell dimension was 25.996 × 24.7496 × 75 Å with vertical axis typically compressing to about 55 Å. 870 water molecules in total were simulated in the cell.

3.4 Results

The results section will cover force-field validation using PDFT and larger scale MD simulations of the water/surface interface.

3.4.1 Validation of force-field

The main purpose for the DFT work was for validation of the force-field. It does however highlight some important issues, which may be over-complicated when considering many water molecules (will be evident later). Sections 3.4.1.1 and 3.4.1.2 consider degrees of freedom of the hydrogens of the hydroxylated surface. Note that no validation was performed for the non-hydroxylated surface alone because the surface was held fixed in all the simulations. Sections 3.4.1.3 and 3.4.1.4 show the validation of the water-surface interactions for both the hydroxylated and nonhydroxylated surfaces; the two extremes of hydroxylation. Negatively-charged surfaces could not be tested using DFT since the unit cell is much larger and is therefore computationally intractable.

3.4.1.1 PDFT calculations of torsion energy profile for surface hydroxyls

Since the terminal hydrogens of the fully hydroxylated surface were able to move, especially when interacting with water, it was desirable to test whether the force-field could accurately describe their rotation (without water).

PDFT single-point energy calculations were made at regular intervals of the dihedral angle corresponding to rotation of one of the terminal hydrogens about the Ti-O axis. To demonstate how the terminal hydrogen atom is rotated Figure 3.2, a plan view of the hydroxylated surface is shown.

The change in potential energy as the hydrogen was rotated was calculated. The same torsional profile was calculated using the force-field and the comparison is shown in Figure 3.3. Zero on the y-axis is given when the hydrogen-bonded pattern is as shown in Figure 3.2

It can be seen that the energy profile follows a similar shape with the highest energy occurring when the hydrogens are closest to each other. The peak at 180° is when the terminal hydrogen and bridging hydrogens are facing towards each other. This agreement gives some validation that the force-field can adequately represent the rotation of terminal hydrogens. The profile shows that there must be a driving force for the

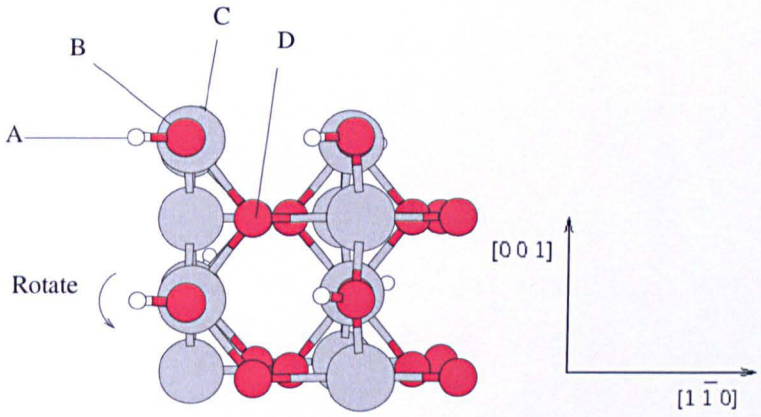

Figure 3.2: Plan view of the TiO_2 (110) surface shown to demonstate how the terminal hydrogen atom is rotated in the torsional energy profile calculation. The four atoms which define the torsion (A-B-C-D) are shown.

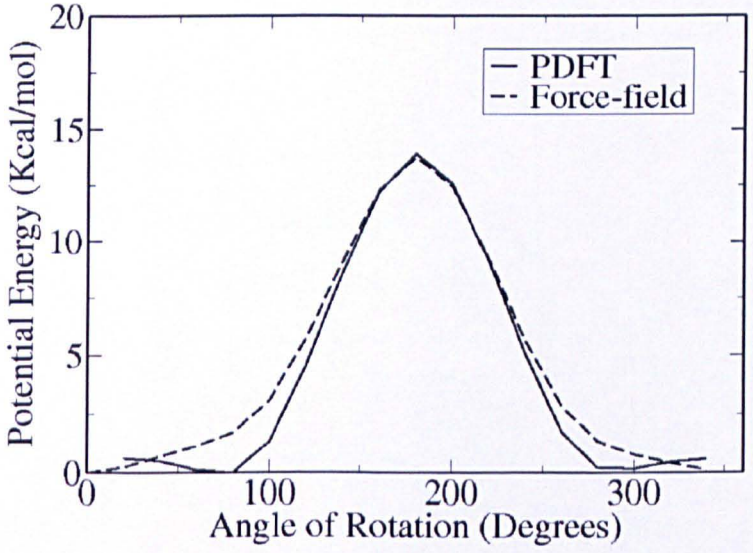

Figure 3.3: Torsional energy profile of terminal hydroxyl using the force-field and PDFT for the fully hydroxylated surface. Zero on the x-axis (torsion angle) is when the hydrogen-bonded pattern is as shown in Figure 3.2.

hydrogens to turn in order to face away from each other.

3.4.1.2 CPMD calculations

It should be assumed that it is not a simple case of terminal hydroxyls moving away from each other independently but that they more likely move in a concerted manner. It should therefore be assumed that when one terminal hydrogen is rotated and approaches another terminal hydrogen that this hydrogen will itself rotate in order to move away. For this reason, CPMD calculations were performed to test this. The same simulations were then made using the force-field *i.e.* the same time-step, cell dimensions and starting conditions. Figure 3.2 shows the atoms defining the torsion which were measured in order to analyze the results of the simulation *i.e.* the rotation of the terminal hydrogen. Figure 3.4 shows the torsion between a terminal hydrogen (Identified as "A" in Figure 3.2), terminal oxygen (Identified as "B" in Figure 3.2), terminal titanium (Identified as "C" in Figure 3.2) and a surface oxygen (Identified as "D" in Figure 3.2) for two adjacent hydrogens as a function of simulation time. Zero on the y-axis is set as the torsion at the start of the simulation, given a hydrogen-bonded pattern as shown in Figure 3.2.

It can be seen that there is mostly an anti-correlation between adjacent hydrogens in both PDFT and classical simulations. This shows that the hydrogens will move away from each other in a periodic manner. It shows agreement between the force-field and PDFT and although there are differences (the movement is more complicated for PDFT), the same qualitative relationships were seen for force-field and DFT methods.

3.4.1.3 PDFT calculations of water on the bare TiO_2 (110) surface

The next two subsections involve water on non-hydroxylated and fully hydroxylated TiO_2 surfaces. Water was optimised on the bare surface using PDFT and the force-field. The results are shown in Figure 3.5; three structures showing the configuration after optimisation with PDFT, and with two slightly different force-fields. Also the

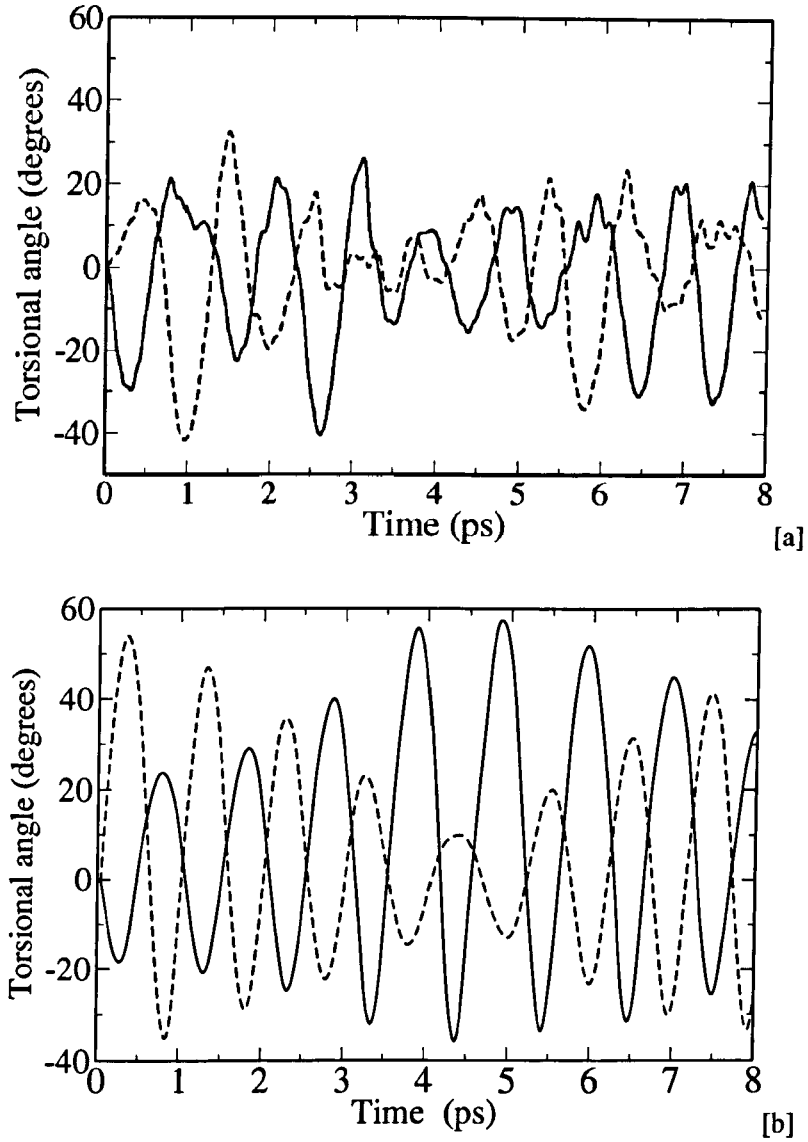

Figure 3.4: Torsional angle for two adjacent terminal hydrogens (solid and dashed lines) as a function of simulation time using CPMD (a) and force-field simulations (b).

distances of the water oxygen and 5-coordinated Ti (D1) and the water hydrogen to bridging oxygen (D2) are shown

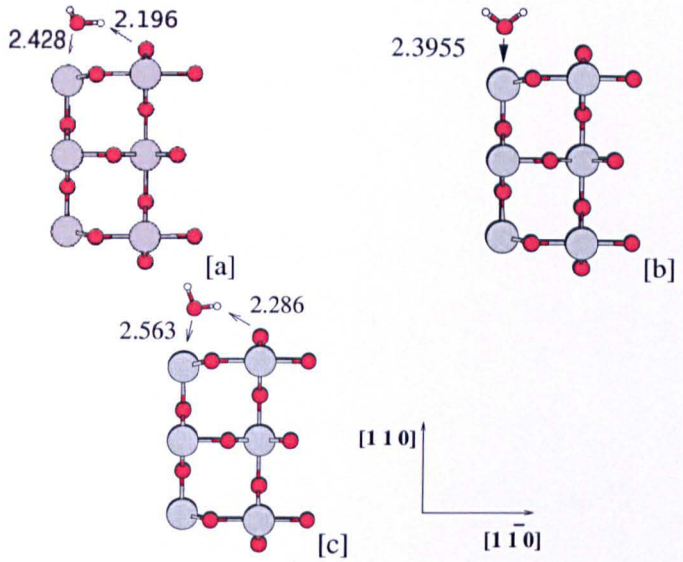

Figure 3.5: Geometries of water adsorbed on the non-hydroxylated surface of TiO_2 rutile (110) after optimization using PDFT (a) and the force-field without (b) and with (c) the extra VDW pairwise interaction. Distances are in Å.

Firstly, it can seen that the PDFT optimisation shows a configuration where the oxygen is facing towards the 5-coordinated surface with its hydrogens towards bridging oxygen. This is in qualitative agreement with the interpretation of work-function measurements by Clendening *et al.* [113].

Similar calculations were performed by Bandura and Kubicki [3] using GGA-PW91 with a 340 eV cutoff (they do not state the k-point grid). D1 and D2 were given as 2.17 Å and 1.73 Å respectively (*c.f.* 2.428 Å and 2.196 Å, present study). This discrepency is probably because of a difference in functional used but could also involve slight differences in structural model or starting conditions. In the present study, a 1 × 2 (6.499 × (2×3.0937)) unit cell was used as opposed to a 1 × 1 (6.497 × 2.959) in the study by Bandura and Kubicki. In order to test this, an optimisation of water on the titania structural model used in the present study using GGA-PW91 with a 340 eV cutoff could be repeated. To put this into context, the measurements by Allegretti *et al.* showed D1

to be 2.21 Å which showed closer agreement to calculations by Bandura and Kubicki. Crystal structure experiments have shown cell parameters as 4.594 × 2.958 [136, 135] again closer to those of Bandura and Kubicki. It should be noted that these cell parameters in the present study were obtained from relaxation of the bulk using the functional and cutoff energy stated above, showing the possible limitations in completely relying on such PDFT techniques. It is clear that much more work needs to performed for providing consistency between experiment, different theoretical results and the work presented here. This should involve investigating the change in result with different cell parameters and different functionals as well as the generation of more experimental results. This should however, be put into the context of the issue of dissociated versus undissociated water before getting too concerned with such accuracy.

It can be seen that the water has not dissociated as predicted by earlier work[120, 115]. However, in those studies CPMD simulations were run, compared with optimisations in the present study. This suggests that there is an energy barrier to dissociation which could be overcome in a CPMD simulation but not in an optimisation (because optimisations search for minima, not transition states).

Optimisations using the force-field were made for comparison with PDFT optimisations. A different structure where the oxygen was facing the 5-coordinated Ti was found, as seen in Figure 3.5[b]. As a result, an extra VDW term with a σ_i of 3.7 Å and ϵ_i of -0.032 kcal/mol, fitted from the Buckingham potential interaction of Predota *et al.* [2] was added between the 5-coordinated titanium and the water oxygen (see Table 3.1). Figure 3.5[c] shows the geometry from the force-field optimisation when the term has been added in comparison to when it was not. It shows a better agreement to the PDFT structure (experiment [113] and other work[2]) with the water hydrogen facing towards the bridging oxygen. Both D1 and D2 are greater than for the PDFT and much greater than other reults.

These results have shown that the force-field gives qualitative agreement with experiment and other theoretical results despite showing slight differences in distances be-

tween the water and surface. Therefore, it was decided to take the force-field forward for use in molecular dynamics simulations since further validations would be made with experiment. It was suspected that condensed phase properties would yield greater complexities than were shown for the single water case. It was thought that the small differences in minimum distances would not be so important when considering such condensed phase properties.

3.4.1.4 PDFT calculations of water on the fully hydroxylated surface

It was decided to test the interaction between water and the fully hydroxylated surface. Optimisations using three different adsorption geometries were performed using PDFT and interaction energies were calculated. The interaction energies were then calculated using the force-field allowing hydroxyl hydrogens to move. Table 3.3 shows the interaction energy of water on the hydroxylated surface calculated using PDFT, the force-field with the PDFT minimized geometry and the using the force-field after minimization using the force-field. It can be seen that despite the energies (PDFT compared to force-field) being different, the relative ordering agrees in all three cases. Figure 3.6 shows

Table 3.3: PDFT and force-field interaction energies before and after force-field optimization for three fully hydroxylated 5-layer TiO_2 surfaces. Min1-Min3 are shown in Figure 3.6.

surface	PDFT kcal mol^{-1}	Force-field (PDF geom) kcal mol^{-1}	After optimization kcal mol^{-1}
min1	-14.10	-17.61	-19.24
min2	-3.33	-6.60	-10.85
min3	-4.95	-8.12	-12.81

the structures after the optimisations.

For the first minimum (Figure 3.6a), calculations show both terminal oxygen donors to the water hydrogens and water oxygen donors to bridging hydrogens. The second set of minima (Figure 3.6b) are both terminal and bridging oxygen donors to water hydrogens. However, it should be noted that another bridging hydrogen also interacts with the water

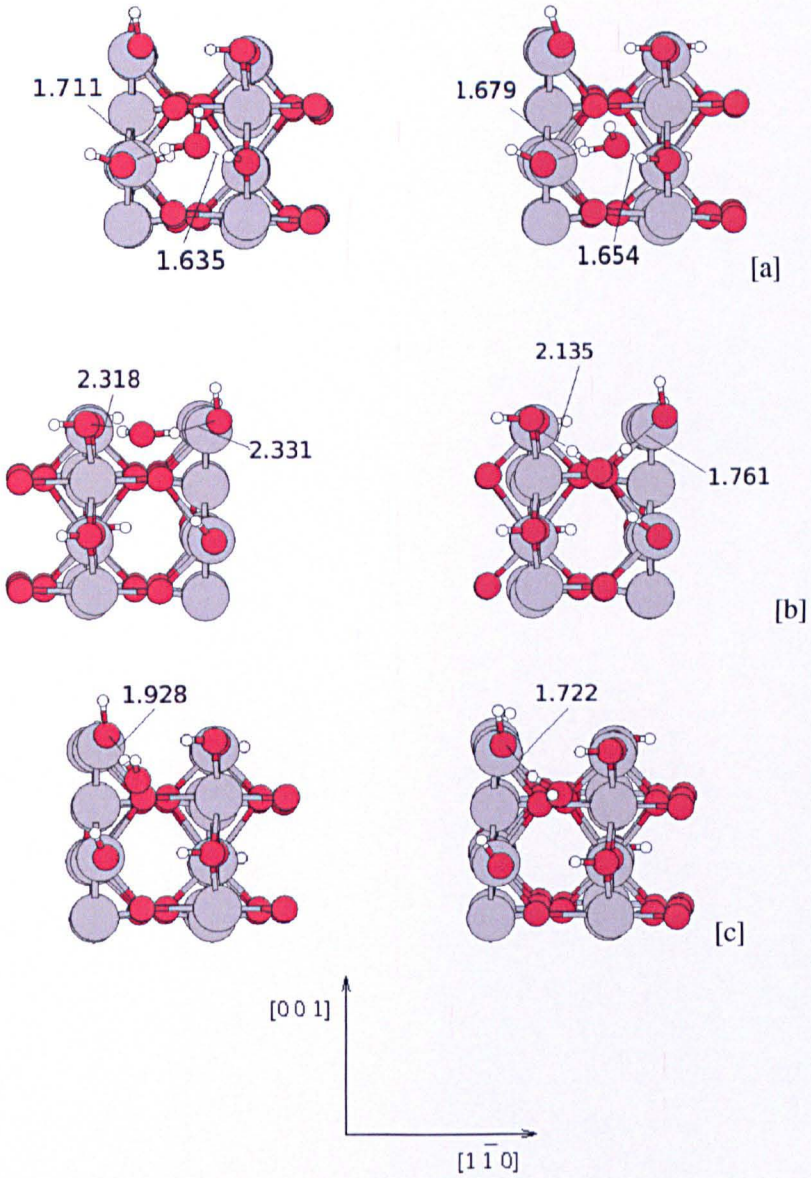

Figure 3.6: Water on the hydroxylated surface of rutile TiO_2 (110) after optimization using PDFT (left) and the force-field with (right) for min1 (a), min2 (b) and min3 (c). Distances are in Å.

oxygen when optimised using the force-field, causing a flattening of the water on the surface. The third set (Figure 3.6c) are both terminal oxygen donors to water hydrogens. In all three cases, the hydrogen-bonded pattern of hydroxyls on the surface have stayed the same; showing qualitative agreement between PDFT and force-field calculations. It should be noted that for all the minimizations performed (hydroxylated and nonhydroxylated), there may be other local minimum configurations available since a comprehensive search was not made. However, these results give enough evidence to support a satisfactory agreement between DFT and force-field, especially since we can not be entirely convinced about the accuracy of DFT methods. The next section will show the validation of the force-field with experiment, helps us to understand the structural model required for modelling water on the rutile (110) surface and gives microscopic detail and insights into the water/surface interface.

3.4.2 TiO_2-water interface

So far we have presented results of single molecules of water on the surface. We must expect however that condensed phase properties of water will give us quite different insights. The work above was a prerequisite for this work and this section presents the main results of the chapter. As stated there is a considerable interaction between water and TiO_2. In the condensed phase and over many time-frames this translates into structuring of water; the correlation of water position and orientation with respect to the surface. In order to gain an idea about the structuring of the water on the surface, axial density profiles of water hydrogen and oxygen were calculated for all kinds of surface considered here. These give the average density over all configurations as a function of vertical distance from the surface plane. The baseline for the surface was taken as the z-position of the 5-coordinated titanium in non-hydroxylated surfaces and the saturated terminal titanium in hydroxylated surfaces. The results are summarised in Figures 3.7 and 3.8 and Table 3.4 (see later). It should be noted that we can make comparisons between hydroxylated and non-hydroxylated surfaces by considering a dissociated wa-

ter in the hydroxylated surface equivalent to a molecularly adsorbed molecule in the non-hydroxylated surface. We can then compare positions of peaks.

The oxygen profile for all the non-hydroxylated surfaces (neutral and negatively-charged) can be seen in Figure 3.7. The profile for the neutral non-hydroxylated surface shows a peak at 1.4 Å which corresponds to the bridging oxygen, a peak at 2.6 Å which is the first layer oxygen and a peak at 3.9 Å for the second water layer. There are also peaks at 5.0 Å and 6.5 Å corresponding to third and fourth layers. The defined peaks show that the water is very ordered on this surface and the ordering propagates far from the surface with the peaks getting smaller and therefore the structuring of the water decreasing as we move away from the surface. The negatively-charged non-hydroxylated surfaces show similar features to the neutral non-hydroxylated surface features with the addition of an extra peak at 2 Å corresponding to the extra terminal oxygens; the density being greater for the 25% surface than 12.5% surface. There are also some other differences between negatively-charged and neutral surfaces. There is a slight increase in the position of the second layer water peak and a large increase in the position of the third water layer peak for the negatively-charged surfaces compared to the neutral surface. Also the second and third peak heights decrease with amount of charge, probably because of the presence of increasing numbers of terminal hydroxyls providing less non-hydroxylated water binding sites. The different charges used for the different surfaces could also contribute to the differences between the non-hydroxylated surfaces. It seems possible that these differences could be significant when considering peptide adsorption onto such surfaces. It is therefore important to find the surface which best represents the real surface.

The hydrogen profile shows a peak at 3 Å corresponding to the first layer of adsorbed water and peaks at 4.4 Å and 5.5 Å which are ascribed to the two hydrogens of the second layer water. The negative non-hydroxylated surfaces give similar features plus the addition of an extra terminal hydroxyl peak at 2.2 Å and increasingly smaller peak heights for the first two water layers with negative charge, again because of less non-

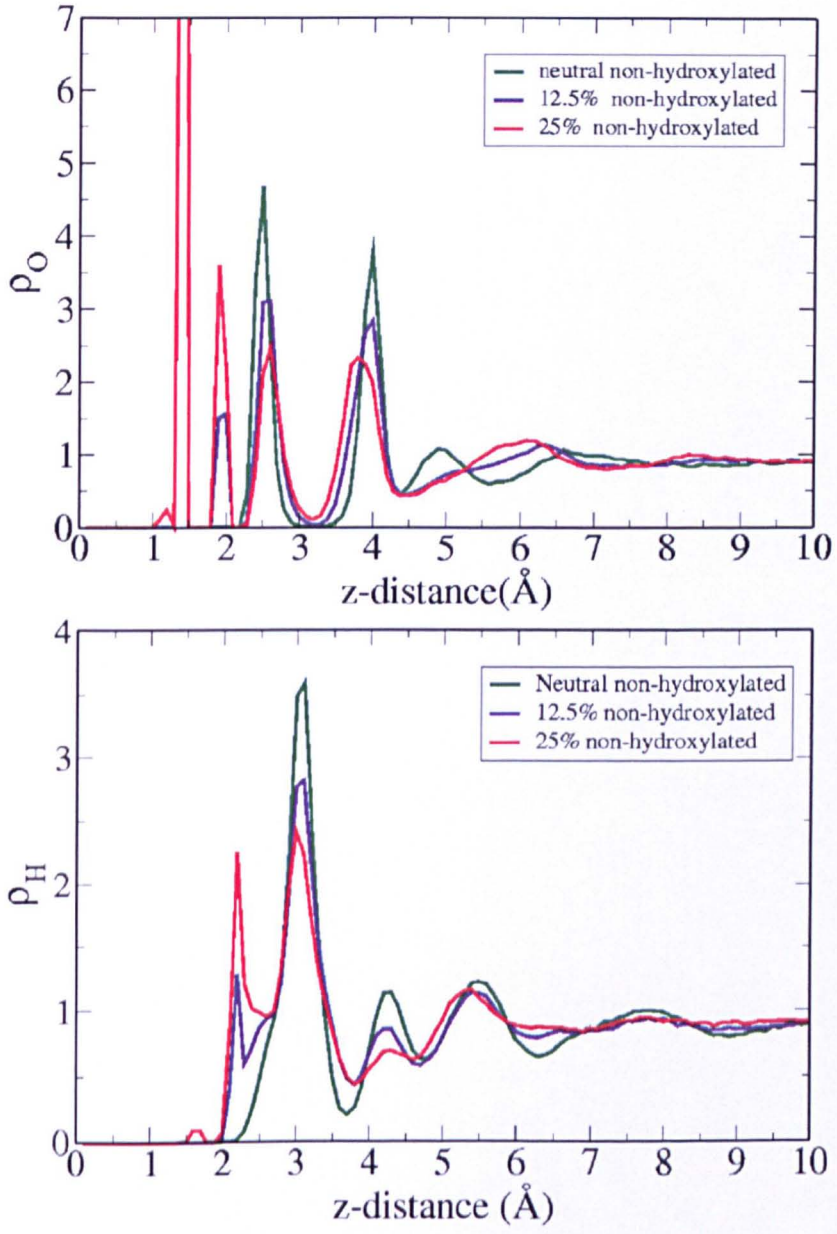

Figure 3.7: Axial density profile (as a function of z-distance) of oxygen (top) and hydrogen (bottom) for the neutral non-hydroxylated, and negative non-hydroxylated surfaces.

hydroxylated water adsorption sites.

Figure 3.8 shows the oxygen and hydrogen profile for all the hydroxylated surfaces (neutral and negatively-charged). The oxygen profile for the hydroxylated surface gives two peaks at 1.4Å and 1.9Å which correspond to the bridging and terminal oxygens respectively. The peak at 3.5Å corresponds to the next layer of water. There are also peaks at 5.9 Å and 8.4 Å showing water structuring out to long distances. The negatively-charged surfaces give similar density profiles but the peak heights decrease with negative charge. This is probably because some of the bridging hydrogens were removed leaving less hydroxylated-surface water adsorption sites.

The hydrogen profile of the neutral hydroxylated surface shows the bridging and terminal hydrogens at 1.6 Å and 2.4 Å. The peaks at 3.4 Å and 4.5 Å correspond to the second layer water and the peaks at 6.2 Å and 8.6 Å are the third and fourth molecularly adsorbed layers. Most of the peaks for negative hydroxylated surfaces follow the other plots and are in the same position as the neutral hydroxylated peaks but decrease with negative charge. However for the 25 % surface there is also a peak at 2.7 Å which is due to the binding of water hydrogens to the exposed bridging oxygens caused by removal of bridging hydrogens in the scheme for modelling negatively-charged hydroxylated surfaces. It should be noticed that this peak is similar in height to the first hydrogen peak of the non-hydroxylated surface. This is just a shoulder for the 12.5 % surface (smaller because less exposed bridging oxygens).

At this point, the equivalent peaks for hydroxylated and non-hydroxylated peaks can be compared (see Table 3.4). It can be seen that the terminal oxygen of the hydroxylated surface peak is at 1.9 Å but the first water oxygen peak of the non-hydroxylated surface is at 2.5 Å. The terminal oxygen is set by the structural model since it is fixed and the difference in peak positions highlights differences in the two models. If we were going to completely trust the model, it could be stated that the dissociation caused the dissociated water oxygen to move much closer than that of the molecular adsorbed water oxygen. This would be a reasonable assumption since a chemical bond would cause a

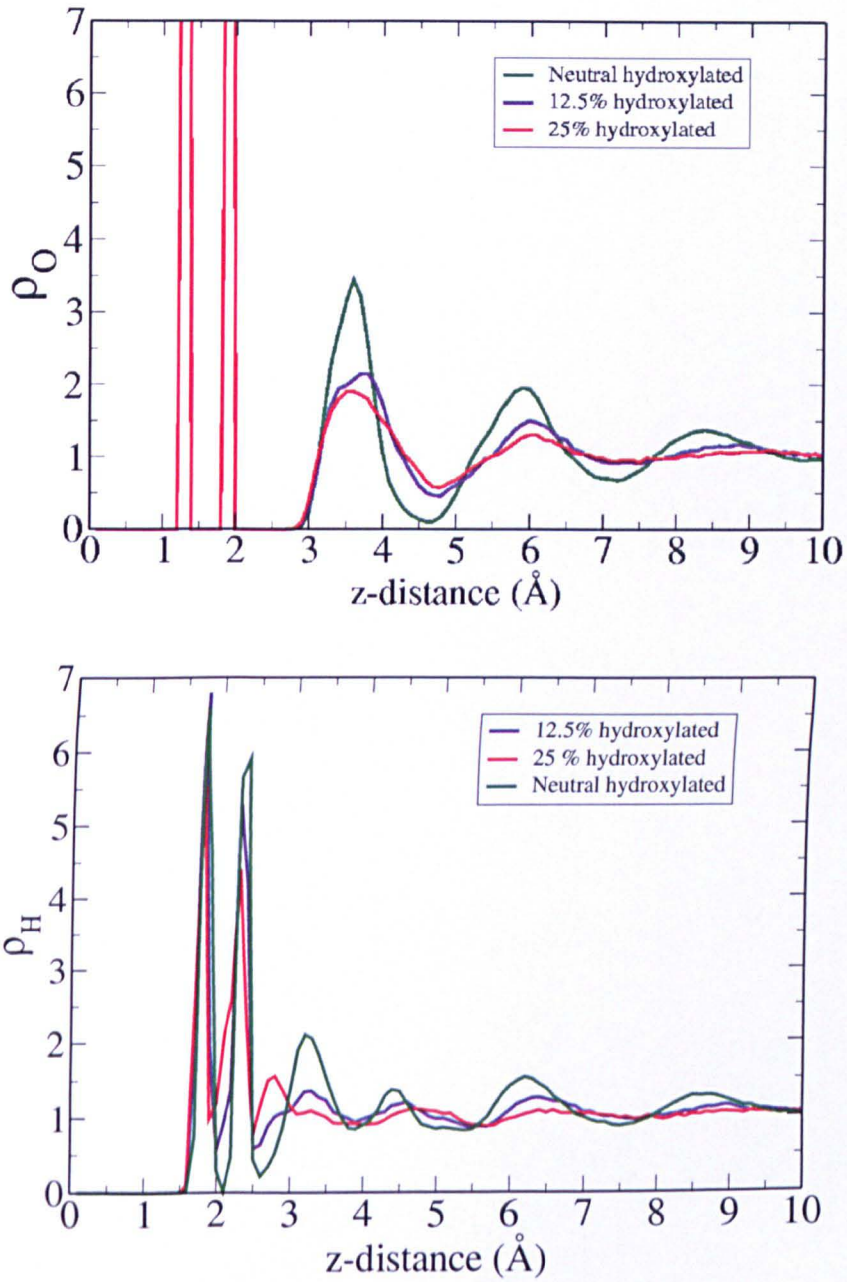

Figure 3.8: Axial density profile (as a function of vertical distance) of oxygen (top) and hydrogen (bottom) for the neutral hydroxylated, and negatively-charged hydroxylated surfaces.

stronger interaction than an electrostatic interaction. As a result of this difference, the next water layer peaks show differences between models; the non-hydroxylated peak is at 4.0 Å and the hydroxylated peaks is at 3.6 Å. This trend also follows for water layers further away from the surface.

It is not just the position of the water but also its orientation with respect to the surface which is of interest since this could have effects when considering the peptide behaviour at the surface. The angular distribution of water was therefore calculated. This is defined by the cosine of the angle between the water dipole and the surface normal and is plotted as a function of distance from the surface. The plots are shown in Figure 3.9. Figure 3.9a shows the angular distribution function for the neutral and negatively-charged non-hydroxylated surfaces. In order to help the interpretation, a snapshot of a simulation is shown in Figure 3.10. The first layer of waters point their dipoles away from the surface and hence the oxygen points toward the titanium as in Figure 3.5. This peak at 2.2 Å corresponds to the first peak in the axial density profile. The second layer water molecules face the opposite direction with the hydrogens facing towards the surface; specifically the hydrogens are pointing towards the bridging oxygens and this is indicated by the depletion at around 3.9 Å. The third layer then reverts to a positive value and the water oxygens are loosely bound to the first layer hydrogens causing the hydrogens to face away from the surface. There is ordering out to 8 Å with depletions followed by peaks, getting less ordered with increasing distance. This decrease in ordering with distance is expected as the surface has less effect on the orientation and the water becomes more like bulk water.

The negatively-charged non-hydroxylated surfaces follow the same pattern as the neutral hydroxylated surface except the distribution is shifted downwards *i.e.* more negative overall. This is caused by a greater tendency for the hydrogen to face the surface *i.e.* rather than the oxygen. An explaination for this is that the partial positive charge on the hydrogens have a greater affinity for more negatively-charged surfaces.

A snapshot of a simulation with hydroxylated surface and water is shown in Figure

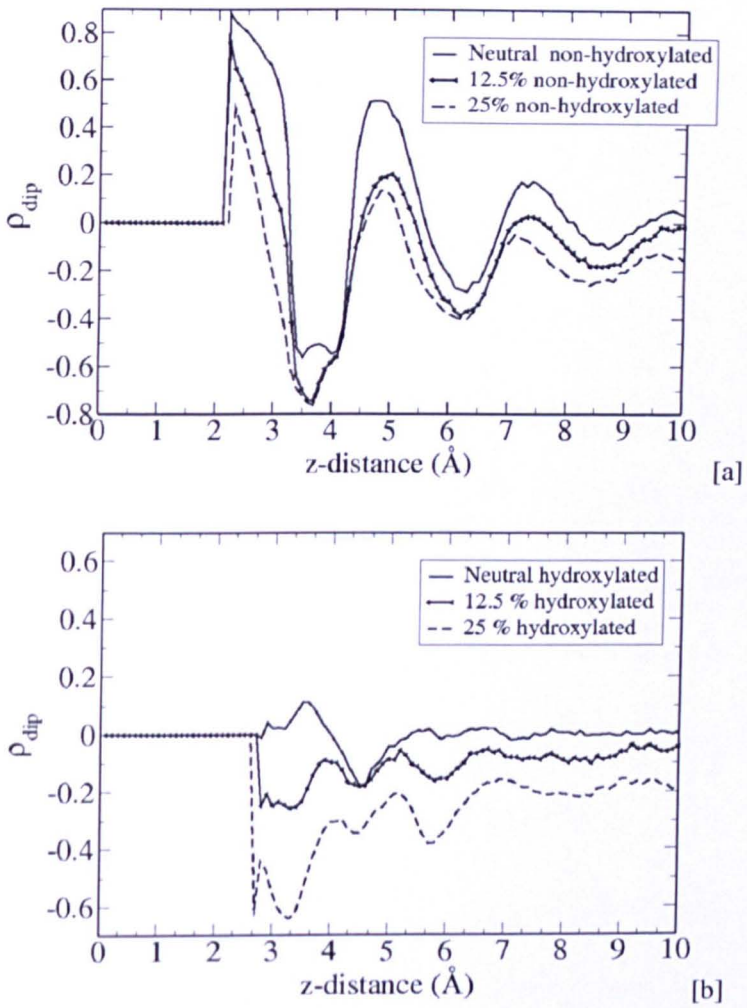

Figure 3.9: Angular distribution of water as a function of vertical distance for the non-hydroxylated surfaces [a] and hydroxylated surfaces [b].

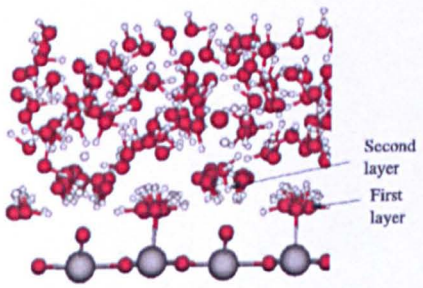

Figure 3.10: A snapshot of a non-hydroxylated surface with water simulation showing the orientation of structured water on the surface.

3.11.

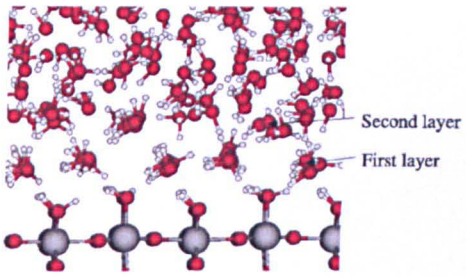

Figure 3.11: A snapshot of a hydroxylated surface with water simulation showing the orientation of structured water on the surface.

There is less orientational ordering for the neutral hydroxylated surface than for the non-hydroxylated surface. This can be explained by considering the number of different possible binding modes available as shown in Figure 3.6. This means that one particular mode is not dominant and therefore there is not a first layer peak as large or defined as in the equivalent non-hydroxylated second layer case. Also, it can be seen in Figure 3.11 that the first layer consists of many waters which are in the binding mode characterised in Figure 3.6[a] where the water hydrogen is bound to the terminal hydroxide oxygen and the bridging hydrogen to the water oxygen (hydrogens facing down slightly). This makes sense since it is the lowest energy configuration (see Table 3.3). This orientation does not have such a positive cosine value since the hydrogens are neither pointing towards nor away from the surface and is responsible for peak heights being much lower and opposite in direction for the first molecular adsorbed layer in the hydroxylated surface compared to the equivalent second layer of the non-hydroxylated surface. For the next water layer (hydroxylated surface), again there are a range of binding modes (not necessarily facing towards or away from the surface) but there is a small depletion, showing orientational ordering of this layer. This effect propagates throughout further water layers.

The negatively-charged hydroxylated surfaces show a different angular distribution to the neutral hydroxylated surface. Firstly, the cosine value remains below zero until the distance from the surface becomes large. On closer inspection it can be seen that the

ordering is similar to the non-hydroxylated surface, with peaks and depletions occurring at approximately the same distances.

This ordering is not so profound in the 12.5% surface as in the 25% surface. This shows that removal of some of the terminal hydroxyls will cause orientational preferences more like the non-hydroxylated surface than for the hydroxylated surface. The cosine distribution always stays below zero because of the affinity of hydrogens to the negatively-charged surface as in the negatively-charged non-hydroxylated surfaces.

There were two main objectives for this work. Firstly it was necassary to compare our results with those of Predota *et al.* to test whether the TIP3P water/rutile model could agree with SPC/E water/rutile model. Secondly, it is necessary to compare our results with experiment to give us an idea which surface (level of hydroxylation) and therefore which structural model could most accurately describe the system. In order to do this, the results have been tabulated in Tables 3.4 and 3.5. Note there are only X-ray experimental data for oxygens atoms.

Table 3.4: Vertical distances of oxygen from terminal titanium for this work, Predota *et al.* [2] and X-ray experiments [6]. The non-hydroxylated is shown as NH and the hydroxylated surface as H. Neutral and negative means that the value is the same for both neutral and negatively-charged surface. First and second layer means oxygens of the water in first and second layers perpendicular to the surface.

Oxygen type	z-distance O(Å)	Predota O(Å)	Experiment(Å)
Bridging, (NH) neutral and negative	1.3	1.3	1.2
Bridging, (H), neutral and negative	1.4	1.4	1.2
Terminal, (H), neutral and negative	1.9	2.0	2.1
First layer, (NH), neutral and negative	2.5	2.5	2.1
Second layer, (NH), neutral	3.8	3.8	3.5
Second layer, (NH), negative	4.0	3.8	3.5
First layer, (H), neutral and negative	3.6	3.7	3.5

It can be seen that all the peaks from this study have very similar positions to those of Predota *et al.*. TIP3P water can therefore match SPC/E water for modelling the rutile-water interface, especially given that, unlike SPC/E, the TIP3P model we use here explicitly models VDW effects for the hydrogens on water. The implication of this

Table 3.5: Vertical distances of hydrogen from terminal titanium for this work and that Predota *et al.* [2].

Hydrogen type	z-distance H(Å)	Predota H(Å)
bridging hydroxylated	1.8	2.1
terminal hydroxylated	2.4	2.5
first layer non-hydroxylated	3.0	2.9
second layer non-hydroxylated	4.4, 5.5	4.2, 5.3
first layer hydroxylated	3.2	3.2

is that it is possible to use the TIP3P model which can be used in conjunction with the Charmm27 force-field. Therefore the peptide/water/titania interface can be modelled using the Charmm27/TIP3P/Bandura potentials.

There is also a general agreement between the simulations and the crystal truncation rod experiments by Zhang *et al.* [6](see Table 3.4). X-ray results showed a peak at 1.2 Å corresponding to the bridging oxygen which is 1.4 Å in this study. A peak at 2.12 Å corresponds to the terminal oxygen which is at 1.9 Å for the fully hydroxylated surface or first layer water oxygen which is at 2.6 Å for the non-hydroxylated surface. There is a peak at 3.5 Å which correspond to the third water layer which is 4.0 Å for the non-hydroxylated surface and 3.6 Å for the hydroxylated surface. Both of these values are closer to the values for the hydroxylated surface which would suggest that the surface was hydroxylated. In light of the abundance of results which disagree over the hydroxylation state of the surface, we must not overinterpret this result. As discussed in Section 3.4.1.3, it is possible that for the minimum energy configuration, the water oxygen to 5-coordinated Ti distance is closer than the distance given using the present model. If this closer interaction was implemented into the force-field, it is possible that the axial density peak would resemble that of the X-ray peak. Also, the true surface probably takes into consideration a superposition of all the surfaces studied. There are effects which have not been taken into consideration such as pH effects and polarisation, all of which could be added in order to improve the model.

Whichever surface best describes the real surface, agreements between X-ray *in-situ*

experiments and simulations performed using the force-field have been shown. This force-field therefore can be taken forward for modelling the peptide/surface/water interface. In Chapter 5, such simulations will be shown. It will also be shown that analysis performed in this chapter will help interpretations of peptide/water/surface simulations.

3.5 Conclusion

In this chapter, a force-field which describes the interaction between the rutile TiO_2 (110) surface and TIP3P water was compared with analagous calculations using PDFT. Since the level and nature of hydroxylation of the rutile (110) surface is still in dispute, tests were made for two different situations, the non-hydroxylated and hydroxylated surfaces - the two extremes of hydroxylation. These tests involved the hydrogen degrees of freedom in the hydroxylated surface case and the interaction between both surfaces and water. CPMD and terminal hydrogen torsional profile calculations of the hydroxylated surface using the force-field showed good comparison with PDFT calculations giving validation that the force-field could accurately describe this aspect of the surface. Optimisations of water at both surfaces also showed agreement between the force-field and PDFT. It was therefore shown that the water-surface interactions could adequately be described by the force-field.

The next stage in the validation was to perform MD simulations using the force-field and to compare with previous simulations using SPC/E water and with *in-situ* X-ray standing wave experiments.

Simulations of water on six different surfaces were performed to model a range of hydroxylation states and gain insight into which case most accurately represented the real surface. The structure of water at the surfaces was analyzed by examining the axial density and angular distribution of water. The axial density profiles showed that both non-hydroxylated and hydroxylated surfaces give peaks in similar positions showing that the first layers of water on the non-hydroxylated surface were a good approxima-

tion for the hydroxyls of the hydroxylated surface. The results were in agreement with x-ray truncation rod studies although it was shown that the hydroxylated states better represented axial distances of water to the surface. It was suggested that this could be because of the model used rather than any phenomonological insight gained. Close agreements with the simulations of Predota *et al.* (who used SPC/E water) were also shown suggesting that TIP3P water was as good as SPC/E water at representing this interface. The angular distribution showed that the second layer waters for the neutral hydroxylated surfaces were orientated differently than second layer waters on non-hydroxylated surfaces showing that there are differences between the surfaces which may give differences when considering peptide binding. This seems to alter when terminal hydroxyls are removed as in the negatively-charged hydroxylated surfaces. The angular distribution results were also in agreement with simulations using SPC/E water. This work showed that TIP3P water could be used for modelling aqueous TiO_2 interfaces and it is therefore viable for simulations of peptides with TiO_2 in water using Charmm force-fields (Chapter 5).

The next chapter will depart from the titania surface and investigate the other part of the titania/water/peptide interaction, namely the water/peptide interaction.

Chapter 4

The behaviour of the RKLPDA peptide in water

In this chapter, the behaviour of the peptide in the bulk water will be explored. This could be an important factor in understanding peptide adsorption because the configurations which the peptide can adopt on the surface may be influenced by those which can be adopted in water. It is quite possible that the peptide configuration can change to accommodate adsorption and it is important to gain insight into which conformational degrees of freedom are more flexible and therefore will more be likely to change readily when the peptide is adsorbed into the surface. We will consider backbone torsions as the main degrees of freedom available for conformational change and will use the analysis of these torsions for understanding the conformational preferences of the peptide in water. Studying these conformational preferences in water is also a device for choosing possible binding configurations (and then putting the peptide on the surface in that conformation) and getting an idea about which torsional states are best for binding. This approach will be used in Chapter 5 and will be explained in more detail there.
It is also important to observe how the mutants' torsional states will differ from those of the wildtype. If different conformations are more favoured in the mutants than the wildtype, this could explain the difference in binding behaviours.

The stability of the different peptides in water may be important. For the peptide to adsorb, it must transfer from bulk water to the surface. If a particular peptide is thermodynamically stable in water, the gain in stability when adsorbing to the surface will be low compared to a peptide which is thermodynamically unstable in water.

As outlined in the introduction, the mutation of Pro, Asp and Arg have been found to have a lower binding affinity than the wildtype peptide [1]. The Lys-mutant however has been found to have a higher binding affinity. For Asp and Arg there would appear to be a trivial explanation for the reduction in binding affinity. These groups are directly involved in binding and without them the binding interaction is reduced, and therefore there should be less viable strong-binding configurations. It seems unlikely however that Pro is directly involved in binding (since it is neutral) and other explanations must be sought. Since Pro is well known to be a group that confers rigidity in peptides, the most obvious explanation for this difference is that this extra rigidity is responsible for strong-binding. Therefore the Pro-mutant has been concentrated on, and in order to gain insight into the effect of the change in conformational flexibility, the wildtype and Pro-mutant have been simulated and various analyses have been performed and comparisons have been made.

From first glance, the increase in binding affinity for the Lys-mutant with respect to the wildtype is not obvious to explain because Lys is known to bind to titania [85]. Under physiological pH, it is a positively-charged group, whereas titania is negatively-charged so an electrostatic interaction would indicate that this result was counter-intuitive. It is therefore postulated that there is also a conformational explanation for this increase in binding affinity for the Lys-mutant and for this reason, the Lys-mutant has also been concentrated on in this chapter. It will be shown that insight into this conformational change has been gained from performing simulations of the Lys-mutant in water and comparing with those of the wildtype.

Few simulations of peptides in water consider surface-binding peptides, most of the studies that do, study the water structuring and the thermodynamical change due to

changes in the solvent with binding. This is very useful but none of these studies investigate conformational factors and therefore completely neglect a vital contribution to adsorption of peptides to surfaces. This contribution will be studied here.

4.1 Background

This section will consist of relevant simulation and experimental work on peptides in water.

4.1.1 Simulation work

Simulation studies of peptides in water which highlight issues related to the present work will be presented here. Many simulation studies of peptides in water concentrate on folding of peptides for the understanding of protein folding [137, 138]. They are therefore simulations of certain folding motifs within proteins of interest. The rest of the studies are mainly more interested in the biophysics of peptides and tend to be studies of simpler peptides with no direct applications, but still of great interest because of the insights they give [139, 140, 141].

Brooks and Case reviewed peptide simulations which study conformational dynamics and thermodynamics and is a good reference to the early work in this field[142]. It also contains much original work. The computational studies which have been made using small model systems are interesting because these systems are simple enough to highlight some important principles.

Interestingly for the present study, work has been performed which studies the effect of mutation on helix formation for small model peptides. It was found for a short polyalanine peptide that when a Pro was mutated for one of the residues in the centre of the peptide, the change in the change in free energy of folding was calculated as +14 kJ/mol (3.4 kcal/mol) indicating that a Pro in this position does not support very compact conformations. When the Pro was mutated for an Ala at the N-terminus, the change in the

change in free energy of folding was calculated as -4 kJ/mol in the first helical position (N1) showing that helix formation is actually stabilised in this position. A value of +6 kJ/mol was obtained for analogous mutations at the second helical position (N2) [139]. The implications for these results will be outlined in the results section below.

Tobias and Brooks [140] studied the difference in free energy and conformation between AAA and VVV where V is valine, a branched-chain amino acid. Their calculations showed that the helical content was greater for AAA than VVV (free energy difference of forming the helix with mutation to Val was estimated as 4 kJ/mol). It was stated the reason for this was that for VVV, the turns region was stabilised with respect to the helix, in contrast to AAA, where the helix was favoured. This difference was put down to difference in solvation of particular residues in different transition states. This study therefore gives us insight into the role of water when considering the effect of mutation. These tri-peptides however are short and it should be envisaged that helical content cannot really be expressed but rather dihedral angles commensurate with helices.

Hermans *et al.* studied the difference in free energy of helix forming when mutating Ala tetrapeptide for the Leu tetrapeptide [141]. The authors predicted that the Leu residue is seen to be a poor helix former (free energy difference of forming the helix with mutation to Leu was estimated as +7.6 kJ/mol). This is probably because of steric factors.The work on mutations is interesting because it shows how secondary structure can be affected by sequence. It can be envisaged that this change in secondary structure can effect properties such as binding. This would add weight to the notion that the mutation of Pro and Lys (Sano and Shiba[1]) cause conformational changes, which in-turn affect function - in this case binding.

Studies of the thermodynamics of model β-sheets have also been performed (two β-strands hydrogen-bonded to each other connected by a turn) [143]. There were two points which came out of this study which were interesting for the present study. Firstly the authors calculated the free energy difference as a function of separation of β-strands and found a free energy minimum corresponding to the solvent-separated distance.

Solvent-separated interactions are found in the present work in relation to binding and will be outlined later. The second point was that it was found that the free energy of separation was affected by the side group, since the solvation is affected. This idea is at the heart of the present study since mutations can change solvation and therefore peptide behaviour.

More recent studies have tended to concentrate on larger peptides, probably because of greater computational resources (and codes) available for performing modelling on larger systems. Many of these simulations performed conventional MD for long simulation times and observed transitions between the main structural motifs. Some of the analysis methods that have been used to characterise the transitions were adapted for use in the present study *e.g.* hydrogen bond number and are therefore worth mentioning. Patel *et al.* performed MD simulations of an 11-mer peptide (TGAAKAVALVL) starting from three different conformations (α-helix, extended and polyproline) for more than 100 ns[138]. They found that the peptide showed transitions from α-helix to β-hairpin and postulated a mechanism mediated by α-turns. Diadone *et al.* performed MD simulations of a 14mer (MKHMAGAAAAGAVV) and 18 mer peptide (VHHQKLVFFAEDVGSNK) [137]. The simulations were started from an α-helix and it was found that there was a transition to β-hairpin in agreement with X-ray diffraction experiments. A microseconds length simulation was performed for a 13-residue peptide for simulations starting from extended and ideal α-helix conformation [144]. The authors state the importance of hydrogen-bonds between residue i and (i+3) or (i+4) in α-helix forming. This notation means there was a hydrogen bond between a carbonyl and NH, three and four residues apart respectively.

Other studies developed methods for increasing conformational sampling. Wu and Wang developed a method called self-guided MD (SGMD)[145] and it involves altered equations of motion, taking into consideration an average force. The method was tested with dialanine (measuring the Ramachandran plot) and a 16-residue peptide (AAQAAAAQAAAAQAAY) in water and vacuum. They reported accurate results for

the dialanine and a large increase in sampling for the 16-residue peptide. In another study by the same authors [146], the helix folding and unfolding of a 17mer peptide was studied. A 10 ns conventional MD simulation was performed and it was demonstrated that this was not long enough for folding or unfolding. Using SGMD, however the peptide folded within 10 ns. The authors also proposed a mechanism where a helix is propagated down the chain and showed that the propagation events occurred more often in the C-terminus end than the N-terminus end, showing the applicability of the method for the understanding of peptide behaviour. Methods of increasing sampling are vital to the field of peptide/protein simulation, especially when considering larger proteins where the significant events (*e.g.* folding) are intractable to standard MD. Similar techniques, if proved to be reliable could be used for studying peptides on surfaces, providing further insight into conformational changes upon adsorption.

Other studies have attempted to deal with sampling issues by treating the water implicitly. It is vitally important to test these methods to decide whether they are reliable compared with simulating explicit water molecules.

A 25-residue peptide was sampled by multi-canonical MD with explicit water and GB/SA using AMBER parm94 and parm96 [147]. They performed principal component analysis on the distances of the different combinations of residues. They then calculated the free energy as a function of the first two principle components. It was found that there were differences in the different models *i.e.* the most thermodynamically stable conformation from the GB/SA solvent was an α-helix, although that from the TIP3P solvent was a β-sheet.

Roe *et al.* compared replica exchange MD (REMD) simulations using TIP3P water with Poisson equation (PE) and three Generalised Born (GB) solvent models for 10-mer polyalanine [148]. It was found that the GB model supported more helical structure than explicit solvent and experiment. The free energy of solvation between α-helix, β-hairpin and polyproline II helix was calculated and it was found that PE was best at reproducing the differences which they state is important in reproducing explicit water

ensembles.

These types of studies are important since implicit solvent methods can increase the computational speed significantly. Testing these methods can give us confidence for their use and help us to develop better ways to treat the solvent implicitly. Implicit solvent methods will be discussed in relation to peptide on surface simulations.

Liang and Walsh performed MD simulations on glycyl alanine [149]. The differences between amoebapro, AMBER, CHARMM force-fields and CPMD calculations for the aspartyl-alanine dipeptide [150] were compared. Comparisons with the present work will be made below.

The simulation work reviewed has given some insight into the behaviour of peptides in water and have provided ideas for analysis of the simulations in the present studies. As well as simulation work, much experimental work has been performed in this field.

4.1.2 Experimental work

As mentioned in the Introduction, circular dichroism (CD) spectra can be used for studying the conformation of peptides. As for simulation studies, work has been performed for sequences relevant to proteins and for model systems. Studies for model systems can give relevant insights to the present work. Much of the issues discussed in this chapter such as helix stability and interactions between charged groups have been studied by CD spectroscopy. Some of the CD results relevant to the present study will be reviewed. Marqusee *et al.* used CD to study 16-mer peptides composed of Ala but also with Lys or Glu acid (in order to solubilise the peptides in water)[151]. It was found that peptides with three Lys or Glu residues adopted α-helix conformations but this helicity decreased with an increasing number of lysines (and therefore a decreasing number of alanines). The authors conclude that Ala has a high α-helix propensity. This can be tied into the present study since the effect of Ala-mutation on titania binding of certain residues of a peptide is considered. The secondary structure is certainly involved in many cases.

Marqusee *et al.* performed CD spectra on Ala-based peptides with mixed Lys and Glu[152]. It was found that helix stability was greater for peptides where Glu and Lys were 4 residues apart (i+4) than when they were 3 residues apart(i+3). They attribute this difference to the stabilisation of helices by salt bridges/ion pairs between the negatively-charged Glu and positively-charged Lys. This argument is strengthened by results which show that the helicity is at its maximum at pH 7; when the Glu is negatively-charged and Lys is positively-charged. In the present study, an Asp-Lys interaction is noticed and since Asp is very similar to Glu, this information is relevant. This will be discussed later.

The authors also suggest that helix formation is enthalpy-driven since helix formation is highest at 0 ^{o}C. This seems reasonable if an electrostatic interaction is dominant. This will be shown later that entropic versus energetic contributions to helix formation will be considered in relation to the RKLPDA peptide and its mutants.

A similar study was made where mutations of Ala for non-polar groups Leu, Val, Phe, and Ile were made [153]. The amount of helicity was ranked; Leu > Ala > Ile > Phe > Val. It was suggested that hydrophobicity was not such a significant factor since Ala and Leu had similar propensities. It was suggested that the restriction of side group rotation for more bulky groups when forming α-helices is the key factor. This would be an entropic effect, in contrast to the enthalpic effect of charged-group facilitation of α-helix formation. This highlights the difference between the effect of charged residues versus hydrophobic effects on the conformation of peptides.

It seems unusual that Leu has a higher propensity for helix forming than Ala considering how much more bulky Leu it is than Ala, and considering the opposite computational result by Hermans *et al.* [141] (shown above). This discrepancy highlights the need for the complementary use of experiment and theory in understanding the behaviour of peptides. Some of the issues introduced above will be explored in this chapter and Chapter 5. Most of these issues involve the effect of peptide sequence on the conformation of the peptide which is important in the understanding of peptide-surface binding.

4.2 Methods

MD simulations were performed using DLPOLY [154]. The Charmm27 [90] force-field was used for the peptide, TIP3P [4, 5] for water. The simulations were run with a time step of 1 fs with the frames being saved every 500 fs. Ewald summation was used for Coloumb interactions. All simulations were performed using the isobaric-isothermal (NPT) ensemble at 1 atmosphere pressure and a temperature of 298 K (after equilibration phase). The Leap-frog algorithm [100] and 12 Å cutoff were used for all simulations. The initial conformations were constructed using the protein module of TINKER. The conformations were chosen, always setting the ω-torsions (around the amide bond) to be 180°. 1623 water molecules were used in all simulations with an initial box size of 38.70 × 36.58 × 39.44. The ψ and ϕ torsions were set to be (−135°,135°) for a β-conformation and (-60°,-45°) for an α conformation. All β and all α starting conformations were used as well as mixtures of the two. Intuition was also used in order to find more unique conformations.

4.3 Results

4.4 General features of the wildtype peptide

In order to have an idea about the behaviour of the peptide before comparing the wild-type with its mutants, some of the general features will be presented. This will be separated into considerations of conformation and water structuring.

4.4.1 Conformation

Since there are so many degrees of freedom involved in the peptide, it is important to attempt to simplify the picture by uncovering some general trends. It was noticed that the backbone torsions adopted typical states which could be used for such a simplifica-

tion. Figure 4.1 shows the ω, ϕ and ψ angles around Arg during a simulation and gives an example of the typical states that the various backbone dihedrals of the peptide can adopt.

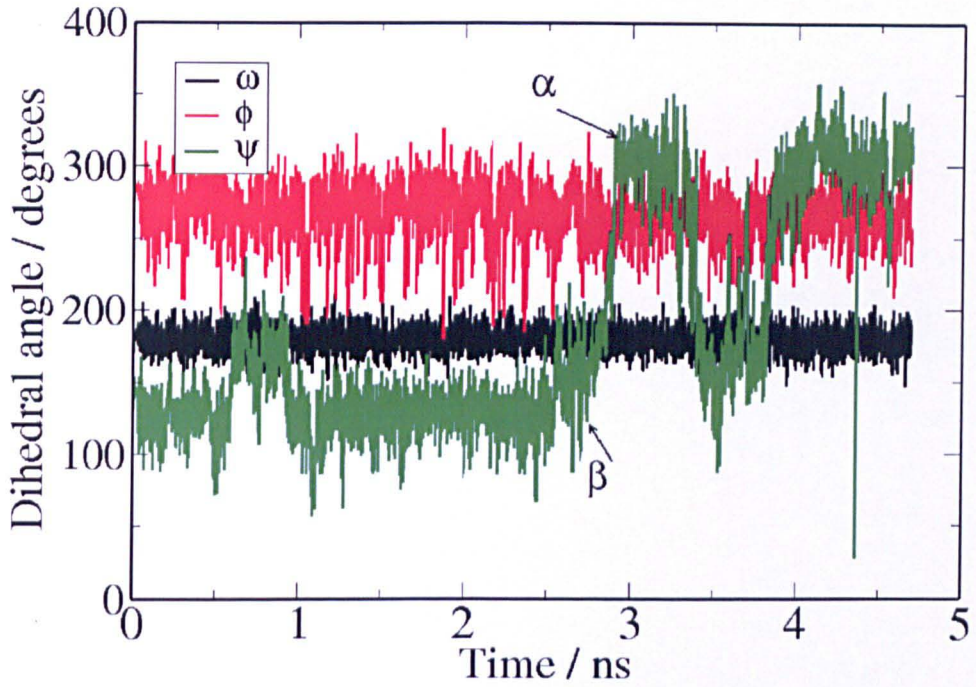

Figure 4.1: The ω, ϕ and ψ-angles around Arg of wildtype peptide versus time.

It can be seen that the ω oscillates slightly about 180° because it is an amide bond and is therefore planar and inflexible to change. The ϕ angle typically oscillates about 300°. In this case, the magnitude of oscillation is approximately 100° and is typical of the end groups, Arg and Ala. Usually Asp, Lys and Leu show less of a fluctuation with Pro showing a very low fluctuation. This can be seen in Figure 4.2, showing the distribution of ϕ angles for all the residues for the peptide starting in β-strand conformation.

It can be seen that the distribution is narrower for the Pro-ϕ than the other ϕ angles and the average is shifted 15° with respect to the other ϕ torsions. This indicates that the Pro has a different affect on backbone conformation than the other groups.

In Figure 4.1 the ψ angle accesses two states; α=300° , β=100°-200°. This is typical and it is usually only the ψ angle which defines the torsional state. Therefore we can

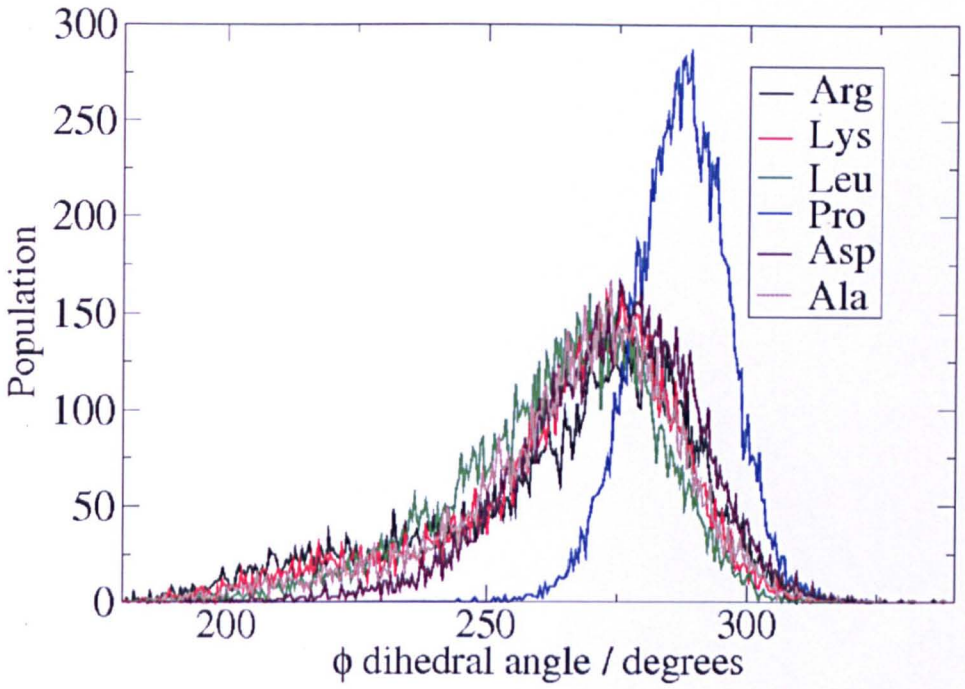

Figure 4.2: The distribution of ϕ torsions for the wildtype peptide starting in the all-β conformation.

coarsely describe the torsional state using a six-letter code where a β-strand is $\beta\beta\beta\beta\beta\beta$ and an α-helix is $\alpha\alpha\alpha\alpha\alpha\alpha$. There are 64 different permutations that can be obtained.

It was stated in the paper by Tobias and Brookes [140] that the transition from α to β occurs almost exclusively by a change in ψ. It is suggested that it follows a path of least conformational change since substantial changes in the ϕ are not necessary to take a peptide from extended to helical conformations (and vice versa). This is consistent with the analysis above.

The fluctuation of the Ala-ψ is typically larger than the other torsions. To demonstrate this, the ψ of Ala for the wildtype peptide starting at the all β conformation is shown in Figure 4.3[a]. This torsion fluctuates rapidly between α and β states in all the simulations run in this project although more time is spent in the α configuration overall. The reason for this fluctuation and therefore flexibility of this torsion is that it is at the end of the molecule and rotation is not restricted because it is a small, neutral group. Larger groups on the other hand are restricted because more solvent has to be displaced for

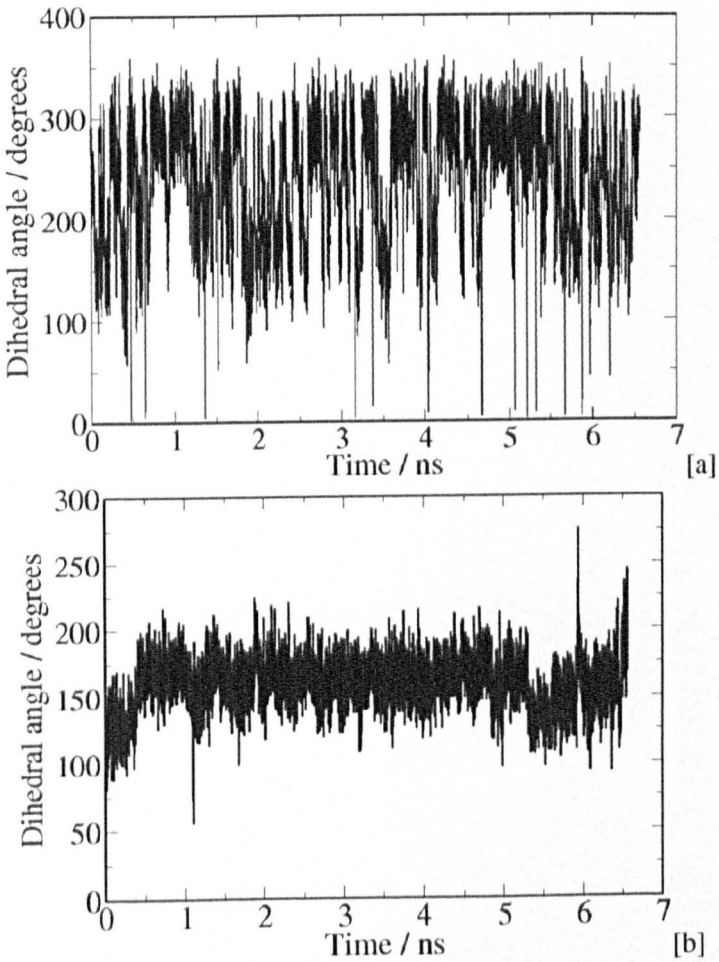

Figure 4.3: The ψ of Ala [a] and Arg [b] versus time for the wildtype peptide starting at all β conformation.

movement to occur. Charged groups will cause structuring of water and interact with different parts the peptide and will therefore have further restrictions. This is demonstrated in Figure 4.3[b] showing the ψ of Arg for the same simulation. It can be seen that although Arg is also on the end of the molecule, ψ does not fluctuate to the extent of the ψ of Ala because Arg is a large charged group. The water structuring will now be dealt with.

4.4.2 Water Structuring

In order to give insight into the effect of solvation on the conformation and behaviour of the peptide, the water structuring around the different groups in the peptide should be analysed. Water-peptide atom radial distribution functions (RDF) have been plotted for a 2 ns run of the peptide started off in the all β conformation to analyse the water structuring. For this purpose it will be assumed that the residues are independent and the water structure around them will not be affected by the other residues. This is probably not the case and will be investigated later.

Since the charged groups are postulated to be important for binding, it should be assumed that the structuring of water around these groups is important (especially considering the water structuring on the surface of titania). The RDF's of these groups will therefore be considered. Figure 4.4 shows the RDF for the Asp carboxylate oxygens with water oxygen and hydrogen.

It can be seen that the water is very structured around this group. The hydrogen RDF gives a peak at 1.9 Å. The oxygen peak is just as strong with a peak at 2.9 Å. The equality of peaks and the distance of the oxygen and hydrogen being about the same length as a hydrogen bond suggests that the hydrogen bonds are linear (this could be tested by measuring the angle between the Asp oxygen (OD), water hydrogen and water oxygen). The next hydrogen peak is at 3 Å; the other hydrogen of the coordinated water. There is another oxygen peak at 4.75 Å which relates to the waters in the second coordination shell *i.e.* those coordinated to hydrogen of the 3 Å hydrogen peak.

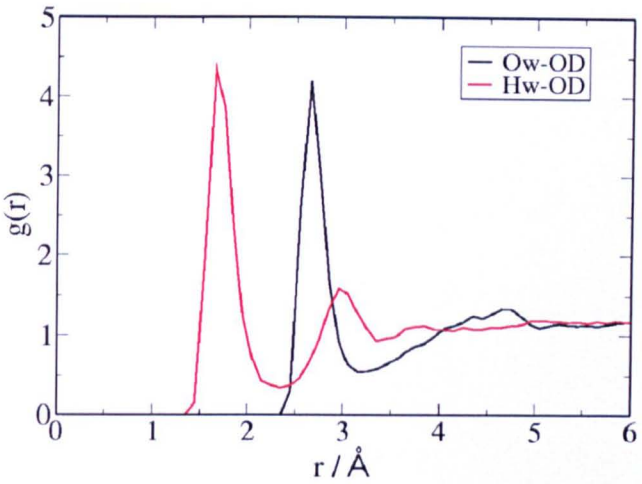

Figure 4.4: The RDF for the Asp carboxylate oxygens (OD) with water oxygen and hydrogen.

The distance between these peaks is that of a strong hydrogen bonded distance which shows that the spatial influence of the Asp on water is apparent out to 5 Å distance. The RDF shows agreement with the RDF of Liang and Walsh for the Asp group of aspartyl-alanine [150] and that of Song and Forciniti for the peptide DDIIDDII[155]. At this point, it would be useful to compare the peak positions/heights between different force-fields/methods and peptides. In the paper by Liang and Walsh (LW), the aspartyl-alanine (AD) peptide was studied using the AMOEBAPRO force-field (polarised) as well as AMBER/TIP3P and Charmm27/TIP3P. As expected, the OD-O_w and OD-H_w profiles were very similar for the present study and Charmm (LW) and AMBER (LW), except that the heights of the first peaks were larger in the present study, followed by Charmm (LW), then AMBER (LW). The reason for the difference between the two Charmm profiles must be environmental since the same force-field was used.

The AMOEBAPRO force-field gave smaller first peaks than Charmm and AMBER; Liang and Walsh state that the differences are due to conformational factors. The RDF's for Song and Forciniti, who use the Gromos/SPC/E force-field, yield similar peak heights and positions.

Figure 4.5 shows the RDF for the Lys nitrogen with water oxygen and hydrogens. It

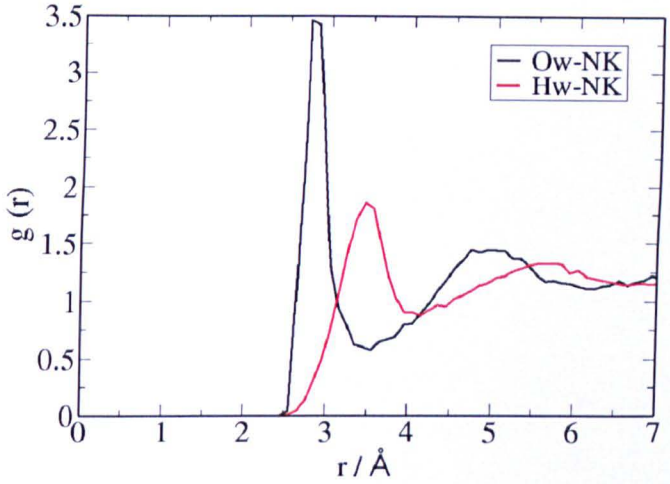

Figure 4.5: The RDF for the Lys end nitrogen (NK) with water oxygen and hydrogen.

shows that there is also structuring of water but there are differences compared with the Asp. Since it is an ammonium group, the water is associated with the hydrogens connected to this nitrogen. The first peak therefore is for oxygen at 2.7 Å. The second peak is for the hydrogens of the water in the first solvation shell. It is almost 1Å further out, but is broader (and not so high) showing that there is probably a distribution of angles for the hydrogen bond. The next coordination shell shows hydrogen and oxygen peaks at 5.0 and 5.9 Å respectively.

Figure 4.6 shows the RDF of nitrogens at the end of the Arg group.

The structuring of water appears to be less profound for Arg compared with Lys. The first oxygen peak at 2.5 Å is smaller than the analogous Lys peak. The separation to the first hydrogen peak however does show some hydrogen bond character. There is also structuring out to a second coordination shell.

In order to understand the lesser structuring of Arg compared with Lys, it is worth a review of the partial charges and Lennard-Jones parameters of the atoms in the groups. These are shown in Table 4.1.

Since the hydrogen charge of Lys is lower than that of Arg, we would expect the attraction to be stronger. However the nitrogen of Lys has a much lower charge than that of Arg (less than half) and the extra repulsion with the oxygen probably accounts for

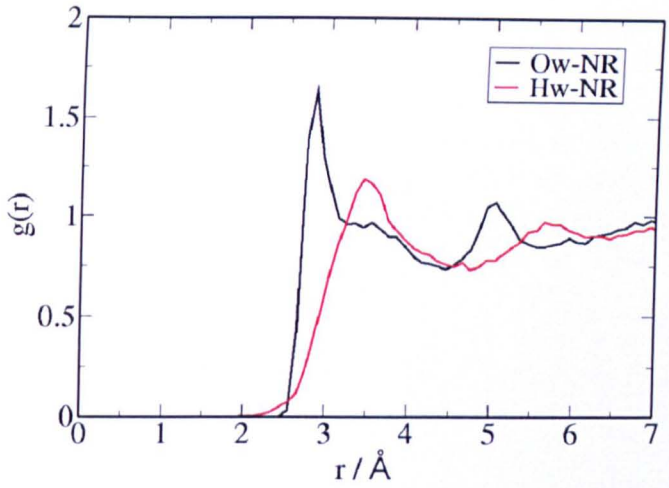

Figure 4.6: The RDF for the end nitrogens of Arg (NR) with water oxygen and hydrogen.

the difference in water structuring. Also the Arg nitrogen has two hydrogen atoms connected but the Lys nitrogen has three. An extra hydrogen would add extra structuring. In addition, there are two nitrogens of Arg but only one Lys nitrogen. It seems likely that the Lys nitrogen can be solvated more easily than the Arg nitrogen because of the space available for solvation; in Arg, the other nitrogen blocks water from solvating it. In order to test the contributions from the individual hydrogens of K and Arg, the RDF's of the respective hydrogens have been plotted in Figures 4.7 and 4.8.

The profiles are very similar showing a similar interaction. The peaks for Lys are slightly higher however, showing that all the contributions (differing charges, differing numbers of hydrogens and blocking by the other nitrogen) could be significant. It does suggest however that the structural differences are more important than the charge differences because the end-hydrogen RDF's should be more insensitive to structural differences since they are more similar *i.e.* terminating the side chain. The extra differences between the end-hydrogen RDF's may be due to the differences in charge or further structural differences. It seems that the differences in water structuring between the Lys and Arg could be significant in how the solvation effects the movement of these two groups.

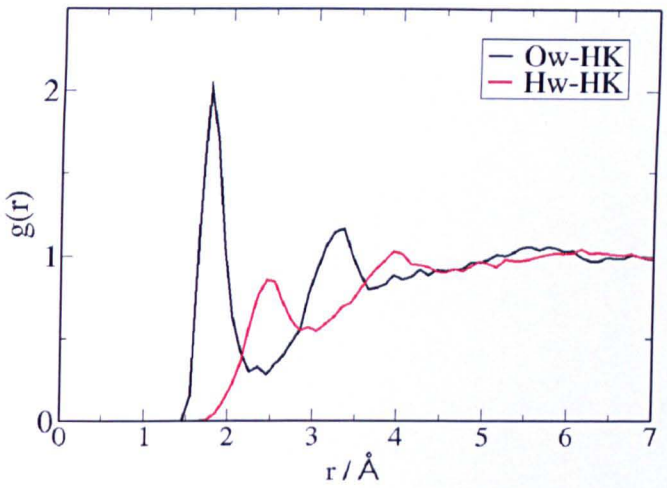

Figure 4.7: The RDF for the Lys ammonium hydrogens (HK) with water oxygen and hydrogen.

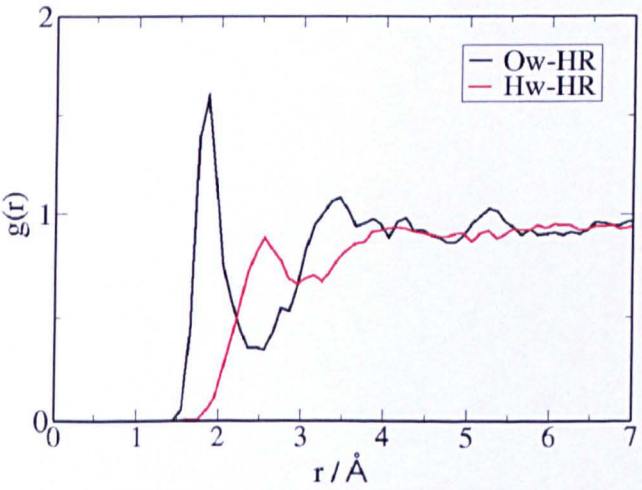

Figure 4.8: The RDF for the Arg group hydrogens (HR) with water oxygen and hydrogen.

Table 4.1: The charges and Lennard-Jones parameters on selected atoms in the peptide.

Atom type	charge	σ (kcal/mol)	ϵ (Å)
Leu C	-0.27	2.0600	0.0800
Leu H	0.09	1.3200	0.0220
Asp O	-0.76	1.7000	0.1200
Carbonyl O	-0.51	1.7000	0.1200
H (amide bond)	0.31	0.2245	0.0460
N (amide bond)	-0.47	1.8500	0.2000
Lys H	0.33	0.2245	0.0460
Lys N	-0.30	1.8500	0.2000
Arg H	0.46	0.2245	0.0460
Arg N	-0.80	1.8500	0.2000

The next group which will be considered is the Leu because it is a hydrocarbon group and should behave completely differently to charged groups. Figure 4.9 shows the RDF of the end carbons of Leu with water oxygens and hydrogens.

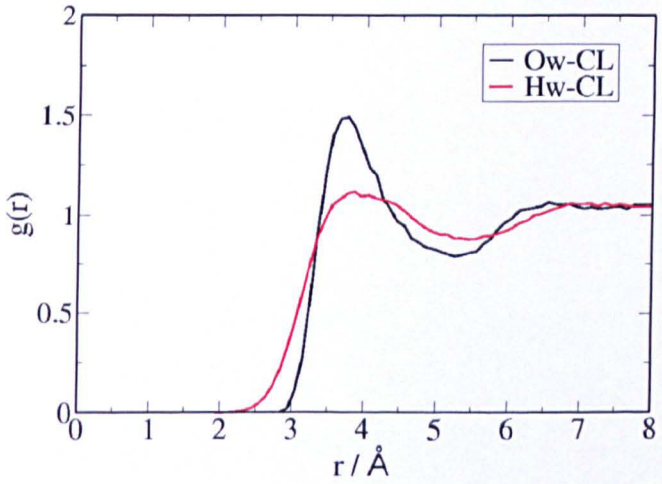

Figure 4.9: The RDF for the end carbons of Leu with water oxygen and hydrogen.

The first peak for both oxygen and hydrogen are situated at a distance of 3.6 Å. Since the peaks are at the same distance, it suggests that there is no electrostatic dependence and therefore no H-bonding. The peaks are due to repulsion and dispersion (van der Waals interactions). The lack of electrostatic dependence is due to the small partial charges as shown in Table 4.1. The lack of attraction between Leu and water would

mean that this group would be more influenced by entropic contributions than energetic ones. This will be discussed further in Chapter 5 in relation to the behaviour of Leu at the titania surface. Now the water structuring by the polar atoms of the backbone (backbone carbonyl and amide) will be considered. It is expected that this effect is important; especially when considering whether conformational aspects *e.g.* whether the solvation around the backbone is going to affect α-helix formation. Figure 4.10 shows the RDF for the nitrogens of the backbone with water oxygen and hydrogen.

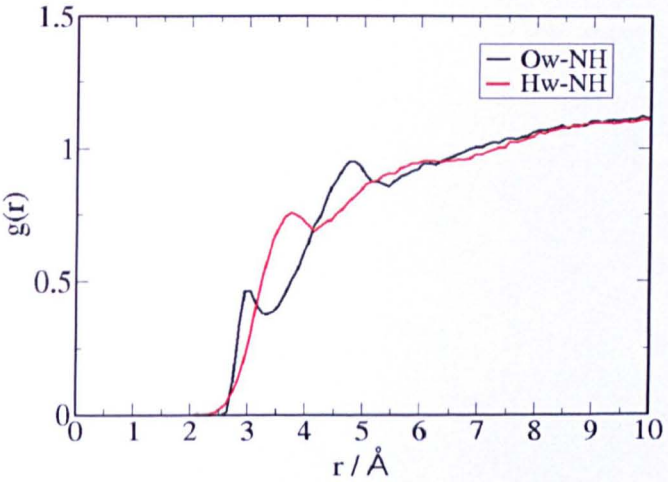

Figure 4.10: The RDF for the nitrogens of the backbone with water oxygen and hydrogen.

There is very little water structuring but there is some hydrogen bond character *i.e.* a separation in the oxygen and hydrogen peaks. This lack of structuring is due to an inability for waters to get sufficiently close to these groups, as well as interference of flanking groups.

In order to compare the hydrogens of the backbone amines with those of Lys, their RDFs have been plotted (Figure 4.11). It can be seen that the peaks are smaller for Lys compared with Arg. This verifies the idea of interference of other groups since the charges and Lennard-Jones parameters are very similar to those of Lys.

Figure 4.12 shows the RDF for the carbonyl oxygens of the backbone with water oxygen and hydrogen. This RDF should be compared with that of the Asp oxygen because

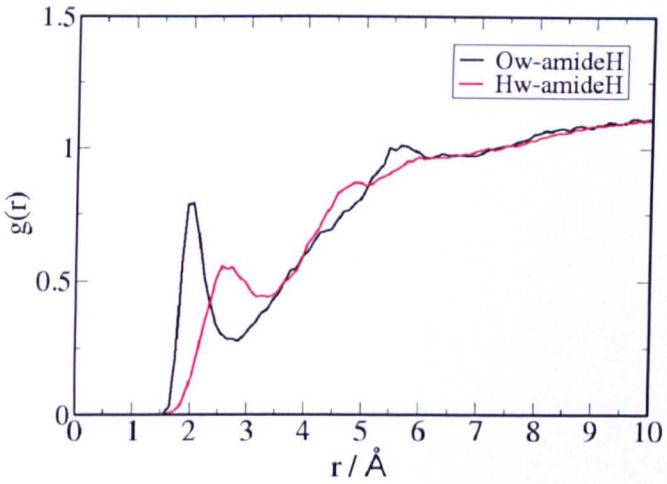

Figure 4.11: The RDF for backbone amide hydrogens (amideH) with water oxygen and hydrogen.

they are both oxygens, although they should be chemically different. The Carbonyls give smaller peaks than the Asp oxygens. This is because of a smaller charge on the carbonyl atom than that of the Asp oxygen (Lennard-Jones parameters are the same (see Table 4.1)) as well as Asp carrying an overall charge. Also for the carbonyl there is a blocking influence of other groups. For Asp it is conceivable that three or more waters can coordinate per atom but for the carbonyl there is only enough space for one water to coordinate.

The RDF plots have given an idea about the structuring of water around the different groups. It is now evident that the charged groups are highly-water structuring in nature, that Leu does not really interact very strongly with water and that the extent of hydration of the backbone is less than that of the side groups. This information is useful for the general understanding of the behaviour of the peptide in water and will be used when considering peptide binding (especially water-mediated binding) in Chapter 5.

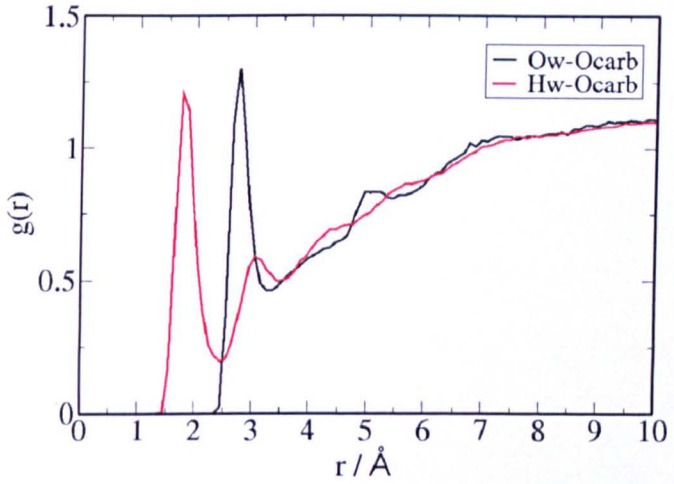

Figure 4.12: The RDF for the carbonyl oxygens (Ocarb) of the backbone with water oxygen and hydrogen.

4.5 Comparison between wildtype and Pro-mutant peptide

Since we postulate that the decrease in binding for the Pro-mutant compared to the wildtype is related to the conformational differences, analysis has been performed in order to compare the differences. It has been proposed that peptides that are more compact (because they have a less rigid backbone) are weaker binders [41]. This aspect will be tested for the Pro-mutant, which has been shown by experiment to be a weaker binder to the wildtype [1]. It is well known that the Pro confers rigidity and therefore could make the wildtype less compact.

4.5.1 Simulations starting in α-helix conformation

The α-helix conformation is a well-known conformation in peptides and many computational studies have been made involving the folding and unfolding of peptides. There are therefore many reference points for comparison in the literature and the peptide was started in this conformation as a result. Since it is a compact conformation and it has been postulated that compact structures are weaker binders, it is a good example to use for comparison of the stability of compact structures in the wildtype and Pro-mutant.

Figure 4.13 shows the wildtype and Pro-mutant peptide in the perfect α-conformation *i.e.* $\phi = 300°$ and $\psi = 315°$ for all torsions. It shows the analysis of the static structure only. It can be seen that for the Pro-mutated peptide there are four carbonyl-amide hydrogen bonds. The wildtype cannot however adopt the same conformation since the Pro-amide does not have a hydrogen.

A geometry optimisation of wild-type in vacuum was made to test whether peptide would find a more favourable conformation. The resulting conformation is shown in Figure 4.14.

It can be seen that there are now three hydrogen bonds, one of which is long. Therefore, even before a simulation is started, this type of conformation can be proposed to be more favourable for the Pro-mutant than the wildtype. The cause for this appears to be an energetic factor since it is energetically more stable to have four hydrogen bonds than three. It is likely that energetic contributions are most important especially considering the experimental results of Marquesse *et al.* showing the dominance of helix formation at 0° [151].

MD simulations were performed for the wildtype and Pro-mutant in order to test the stability and dynamical aspects of α-helices of respective peptides (see Section 4.2 for details). It was noticed that for the wildtype, after about 2 ns of simulation, the peptide was no longer in the α-helix configuration and the peptide had spontaneously undergone an unfolding event. After 5 ns, the Pro-mutant unfolded.

The fact that the Pro-mutant stays in the α conformation for a longer duration indicates that the Pro-mutant is more stable in the α-helix conformation than the wildtype. In order to demonstrate the unfolding process in both peptides, two analyses were made, radius of gyration and number of hydrogen bonds between backbone NH groups with backbone carbonyls. The radius of gyration is given by:

$$R_g^2 = \frac{1}{N}\sum_{k=1}^{N}(\mathbf{r}_k - \mathbf{r}_{mean})^2 \tag{4.1}$$

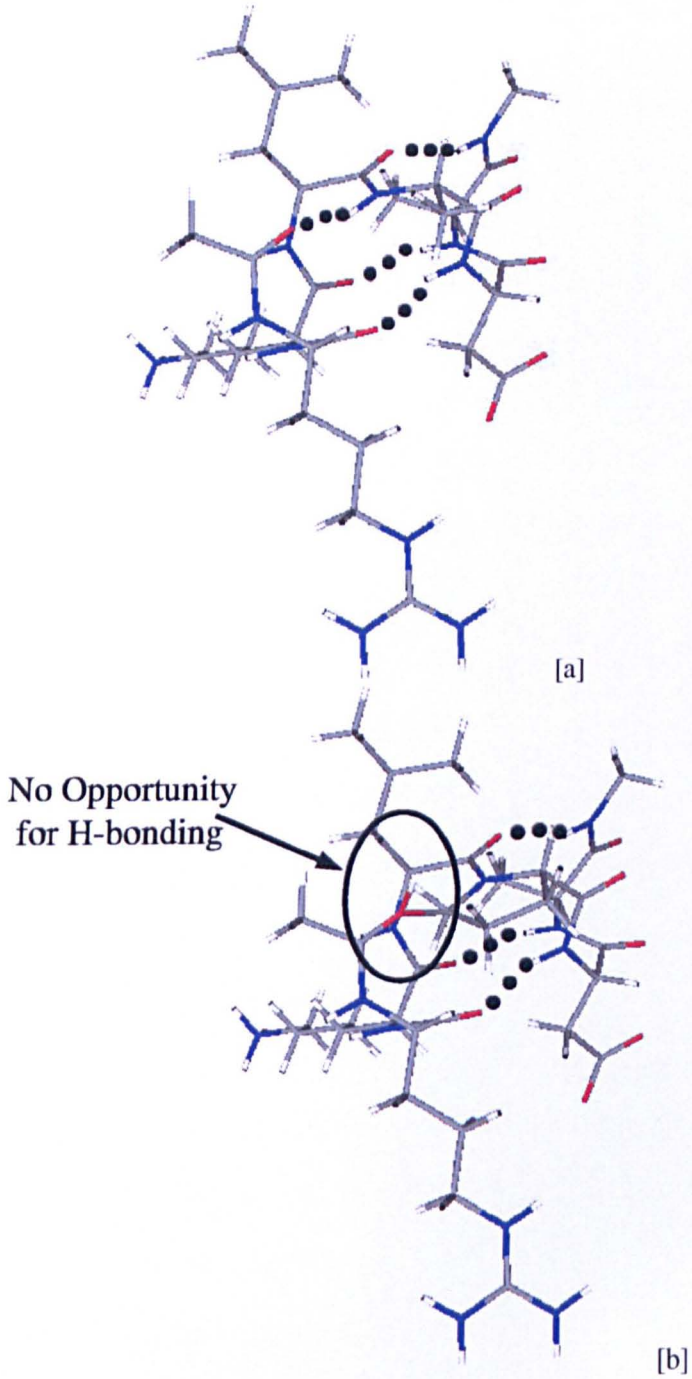

Figure 4.13: Pro-mutated [a] and wildtype peptide [b] in perfect α-helix conformation rendered as tubes for clarity.

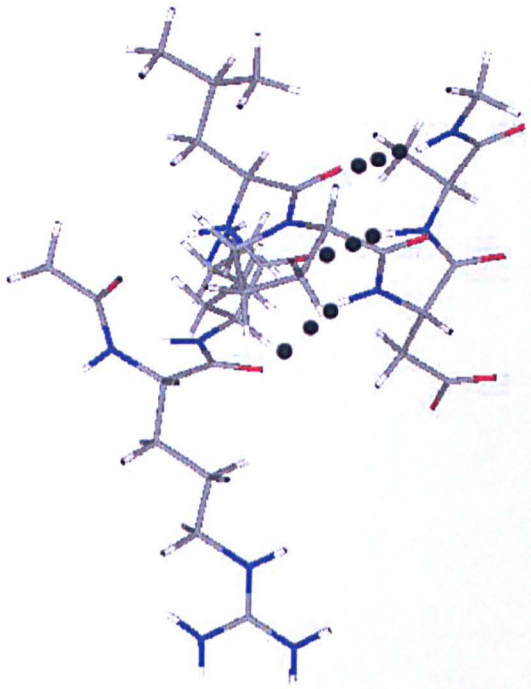

Figure 4.14: The conformation of the wildtype in the α-helix after geometry optimisation rendered as tubes for clarity.

where $\mathbf{r}_{mean}$ is the mean position of all the atoms in the peptide, N is the number of atoms, r_k is the position of the atoms. The radius of gyration gives a measure of how extended or compact the peptide is. To analyse the number of hydrogen bonds, a hydrogen bond is counted when a carbonyl and N-H group are within 2.2 Å of each other. The running average (per 20 ps) has been plotted for clarity and shown in Figure 4.16. Figure 4.15 shows the radius of gyration versus time for the wildtype [a] and Pro-mutant [b]. For the wildtype, it can be seen that there are two distinct jumps in the radius of gyration (R_g) at 2 ns and 3 ns corresponding to ψ torsion changes (shown later). R_g does however fluctuate considerably. For the Pro-mutant, R_g stays almost constant until 4ns, when it rapidly increases. Figure 4.16 shows the number of hydrogen bonds versus time for the wildype[a] and Pro-mutant[b].

For the Pro-mutant, the number of hydrogen bonds stays constant until the unfolding event at 4 ns (apart from a momentary decrease at 2.2 ns). At 4 ns, the number of hydrogen bonds rapidly decrease, just as R_g increases during the same time. The number of

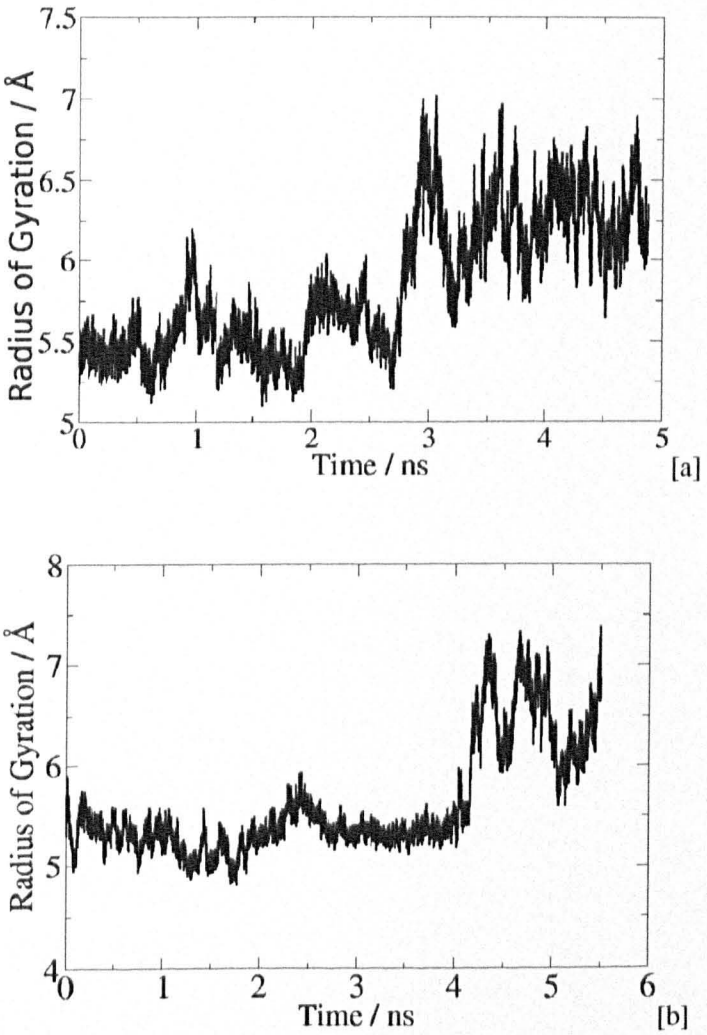

Figure 4.15: The radius of gyration of the wildtype peptide[a] and Pro-mutant[b] starting at all α-conformation.

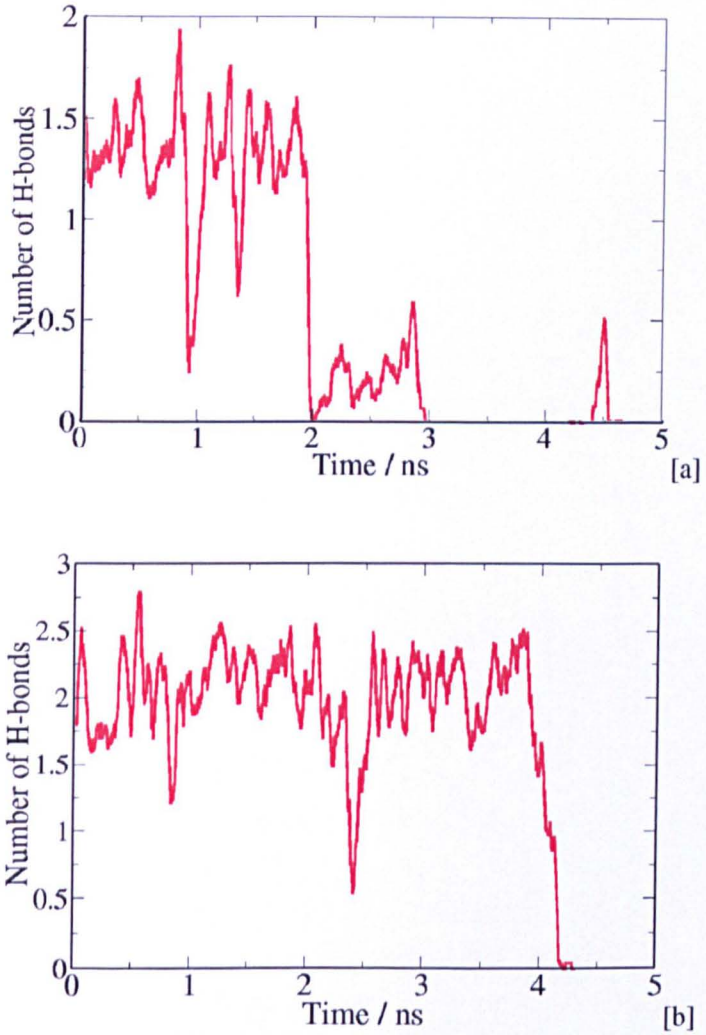

Figure 4.16: The running average of hydrogen bonds for the wildtype [a] and Pro-mutant [b] starting at all-α conformation.

hydrogen bonds for the wild-type is lower at the start as explained earlier. For the wild-type simulation the number of hydrogen bonds rapidly decreases at 2 ns. This value stays below 0.5 until 3 ns. During this time, the peptide is still compact (see Figure 4.15) and therefore does not really unfold at the precise moment when the hydrogen bonds break. This is because of the rigidity of the Pro holding the peptide in the folded position without the need for the stabilising effect of the hydrogen bonds. This rigidity therefore conceivably contributes an extra kinetic barrier to the unfolding (and probably folding).

To gain an understanding of the process by which the peptides unfold and to compare these mechanisms, the backbone torsional changes have been studied. Figure 4.17 shows the ψ of Asp, Pro and Lys as a function of time for the wildtype peptide starting in all-α configuration.

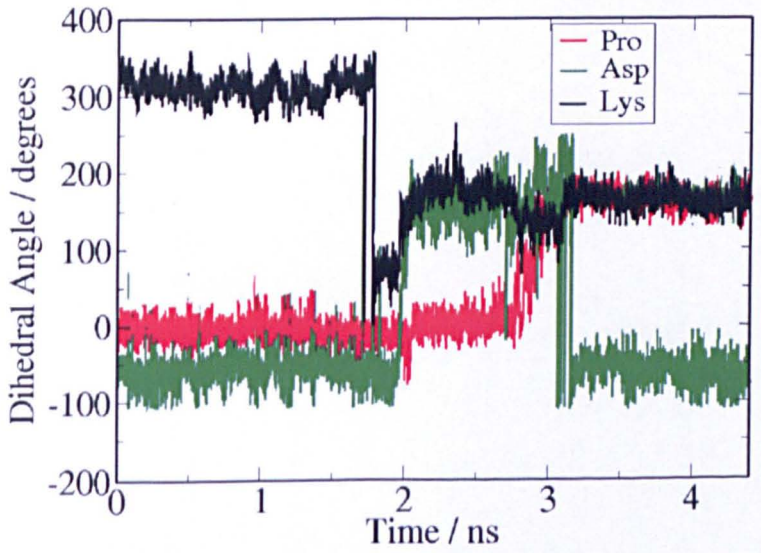

Figure 4.17: The ψ angle of Lys, Pro and Asp for the wildtype peptide starting in α-helix conformation.

The other ψ torsions stay constant and so are not involved in the unfolding process. At approximately 2ns, the Asp and Lys ψ torsions move from α to β classification. These changes occur at the same time as the hydrogen bond decrease and are therefore likely to be responsible for this change. At 3 ns, Pro moves from α to β. At the same time, Asp

shifts back to α conformation. This change takes place at the same time as the increase in radius of gyration and are therefore likely to be responsible for the actual unfolding (as opposed to the breaking of hydrogen bonds).

To compare the conformational change of the wildtype with the Pro-mutant, the ψ angles of L, D and "Pro" for the Pro-mutant starting in α-helix conformation are shown in Figure 4.18.

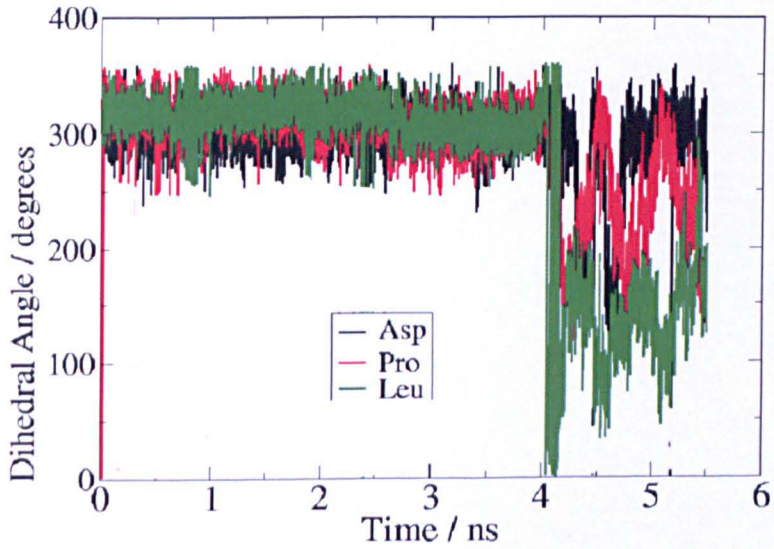

Figure 4.18: The ψ angle of Leu, Asp and "Pro"(Ala) for the Pro-mutant starting in α-helix conformation.

It can be seen that the these dihedrals stay almost constant until 4 ns when all three move to the β conformation. These changes occur at the same time as the radius of gyration increase and the hydrogen bond decrease showing that unfolding in this case is a sudden and immediate conformational change.

All the analyses shown above indicate that for the wildtype there is a gradual unfolding of the peptide and it seems that the main barrier to unfolding involves the stiffness of the backbone. The dihedrals that must change for unfolding to occur, do so at different times and relate to different changes in the number of H-bonds and the radius of gyration. For the Pro-mutant however, the unfolding event seems to occur very rapidly as all the relevant torsions simultaneously change from the equilibrium angle, the num-

ber of H-bonds rapidly decreases at the same time and the radius of gyration suddenly increases.

This information could be important when considering if the α-helix could spontaneously form in either peptide. It can be envisaged that the mechanism for forming the α-helix could be the same as for the unfolding mechanism. It seems as if there is less of a driving force for the wildtype to form the α-helix since it would have to form the intermediate where there are no hydrogen bonds before it moved into the all α conformation. For the Pro-mutant it seems more likely that if the peptide was in the correct conformation, it would spontaneously form the α-helix. This is because the torsions are more flexible and there is a stronger driving force since the number of hydrogen bonds in the α-helix is greater.

Both simulations were performed twice, starting from slightly different configurations. They demonstrating similar unfolding behaviour, showing that they were not 'one-off' events.

The results of these simulations are in agreement with the work by Yun *et al.* where the change in free energy of folding when Ala was mutated for Pro in the middle of the chain was calculated as 14 kJ/mol [139]. This shows that the presence of Pro reduces the stability of the helix; the present simulations suggest that the Pro-mutant is more stable than the wildtype in the α-helix configuration (at least because it takes longer for the unfolding to occur in the Pro-mutant than the wildtype).

It should be noted that the study of α-helix folding and unfolding may not be directly relevant to whether the peptide binds to the surface since it is unlikely that it is a dominant type of configuration. However, it does highlight important differences in behaviour for the Pro-mutant and wildtype. These differences may be important for understanding the differences in binding affinity between the two peptides. The α-helix conformation is the archetypal compact configuration. It is considered that compact configurations cannot bind to surfaces as effectively as extended ones since the surface area of a compact peptide is smaller than the surface area of an extended peptide.

Less peptide surface area would mean that there are less binding sites presented to the surface for interaction. Therefore if compact configurations are more favoured in the Pro-mutant, this could provide an explanation for the reduced binding affinity of this sequence to titania.

4.5.2 Simulations starting in the β-strand

The most obvious starting conformation is the β-strand conformation characterised as $\beta\beta\beta\beta\beta\beta$. Like the α-helix, the β-strand has also been well studied. The wildtype and Pro-mutant were therefore simulated and compared. Whereas the α conformation showed information about the dynamics of a particular event, the β simulations gave information about equilibrium properties such as peptide flexibility.

Following the previous results where the Pro-mutant was postulated to be more stable in the more compact α-helix conformation, the distributions of radius of gyration for the wildtype and Pro-mutant were plotted and shown in Figure 4.19.

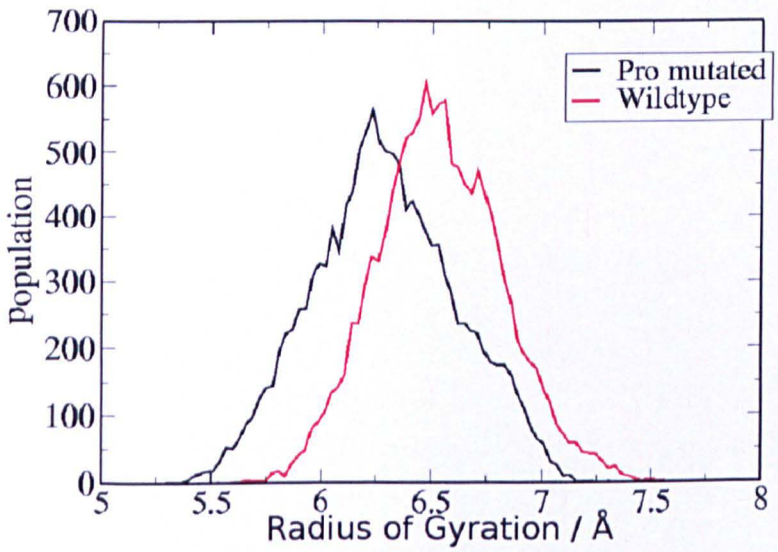

Figure 4.19: The distribution of radius of gyrations for wildtype and Pro-mutated peptide starting from β-strand.

It can be seen that the peak of the distribution is positioned further out in the wildtype case, showing a more extended equilibrium structure for the wildtype on average. This

could be due to the wildtype being held more rigid because of the Pro group. This would support the idea that the Pro-mutant is a weaker binder to titania because it is compact although it certainly is not conclusive evidence since it is only a small reduction.

In order to test the effect of mutation, the ψ-angles of Pro[a] and Leu[b] for the wildtype and Pro-mutant peptide (in this case the angle around Ala in position 3) starting from the all-β conformation were plotted and shown in Figure 4.20.

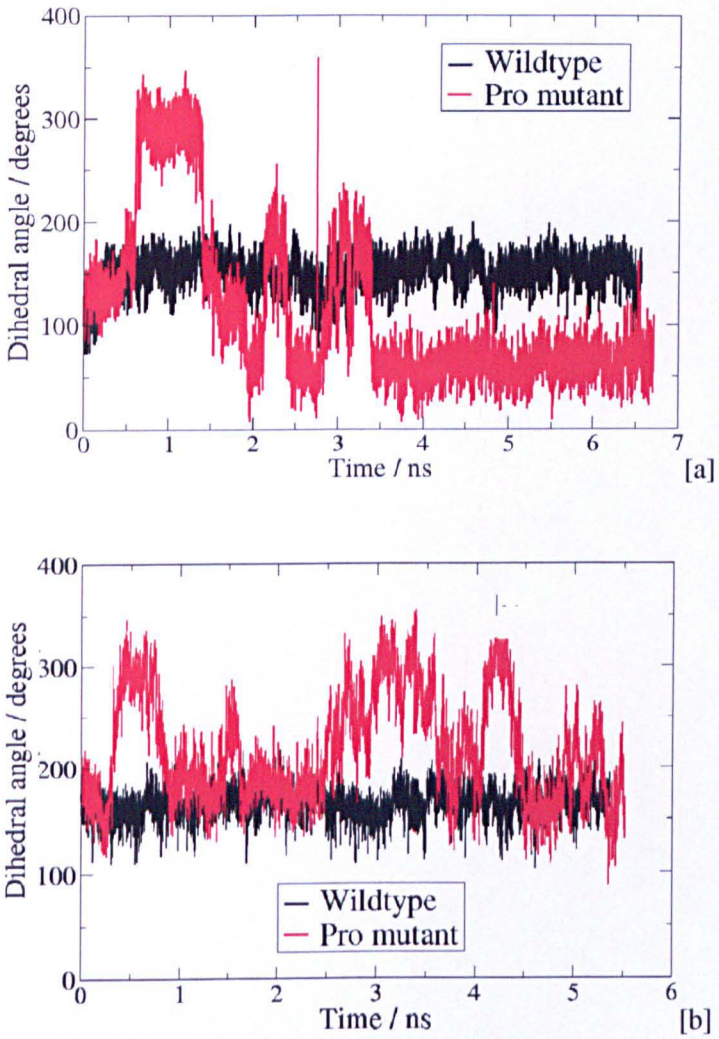

Figure 4.20: The ψ of Leu [a] and Pro [b] for wildtype and Pro-mutated peptide for the β-strand starting configuration, as a function of time.

These angles are the ones which were assumed to restrict the backbone conformation in

the wildtype. It can be seen that for the wildtype, these angles stay constant throughout the simulation. However, this is not the case for the Pro-mutant. Firstly the Pro-mutant 'Pro'-ψ seems to equilibrate for 3.5 ns when it then settles into a previously unseen state around 90° which will be called the 'opposite gauche' state. The Pro-mutant Leu-ψ fluctuates from α to β in contrast to the wildtype which stays constant. This shows that the mutation does not just affect the Pro (Ala in pos3) but also the Leu. This demonstrates the importance of Pro in maintaining peptide rigidity.

Figure 4.21 shows the distribution of ϕ-angles for the Pro-mutant starting at the all β configuration.

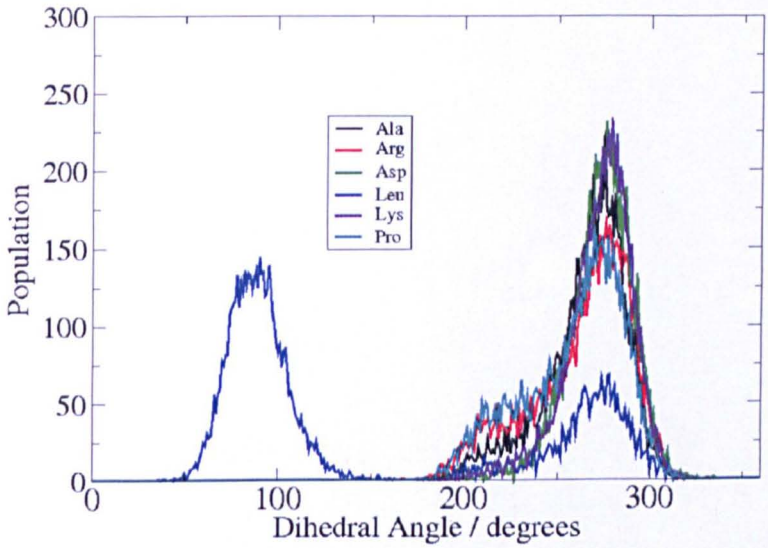

Figure 4.21: The distribution of ϕ-angles for the Pro-mutant starting at the all β configuration.

It should be expected that the Pro-ϕ in this case would change to a similar distribution to other ϕ torsions of the wildtype peptide shown in Figure 4.2. However all ϕ torsions have narrow distributions similar to the Pro torsions of the wild-type . This shows a subtle difference due to the mutation. In speculation, the reason for this difference could be that the restriction of the backbone torsion angles of Leu and Pro in the wildtype would cause the rest of the ϕ-angles to change to a greater extent. When there is less restriction however, ϕ fluctuation is not so necessary. The extra state at 90° is due to the

'opposite gauche' conformation of Leu.

This section has shown that there is a general difference between the wildtype and Pro-mutant and that the rigidity of the Pro is responsible for these differences. It is likely that these differences are responsible for the decreased binding in the Pro-mutant; this will be explored further in Chapter 5.

4.6 Interaction between Lys and the rest of the molecule

As stated earlier and in the Introduction, when the Lys was mutated, the binding affinity of the peptide to titania increased. It was postulated that there must be a reason related to conformation since Lys should be a binding group and therefore mutating it should decrease the binding affinity. Therefore studying the behaviour of the Lys group in water is worthwhile since insight can be gained. One aspect of this is how the Lys group interacts with other groups in the molecule.

It was noticed many times that the Lys interacts with other parts of the molecule and several examples will be given to demonstrate this phenomenon. Figure 4.22 shows a configuration (started from a simulation in water where all torsions were in the 'opposite gauche' state) where the Lys and Asp are very close and this close association is further stabilised by an interaction between the Pro-Leu carbonyl and Lys. To show the

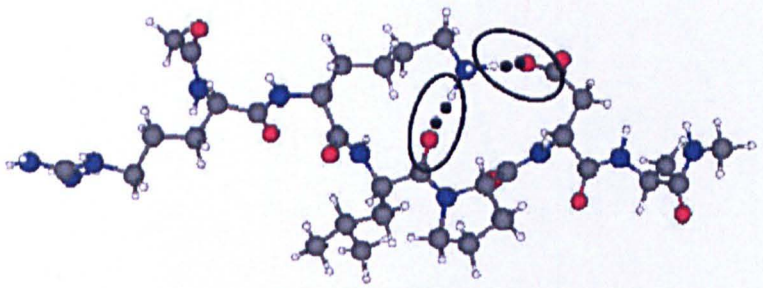

Figure 4.22: A snapshot showing the Asp very close to the Lys for the wildtype peptide in the all-'opposite gauche' conformation. An interaction between Lys and carbonyls 6 and Asp can be seen and is circled.

persistence of this interaction, the D-K distance versus time has been plotted and shown

in Figure 4.23. There are long periods of close contact between these two groups.

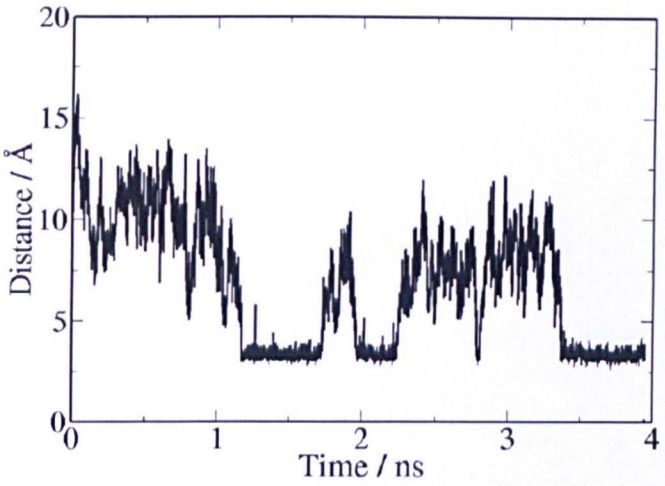

Figure 4.23: The Asp-Lys distance versus time for the wildtype peptide starting in the all-'opposite gauche conformation'.

When a simulation of the wildtype peptide was started in the $\beta\beta\alpha\beta\beta\beta$ conformation, it also showed an interaction of Lys with a part of the molecule. Figure 4.24 shows a snapshot of the peptide in this configuration and it can be seen that there is an interaction between the Lys and the two carbonyl groups at the Asp end of the molecule.

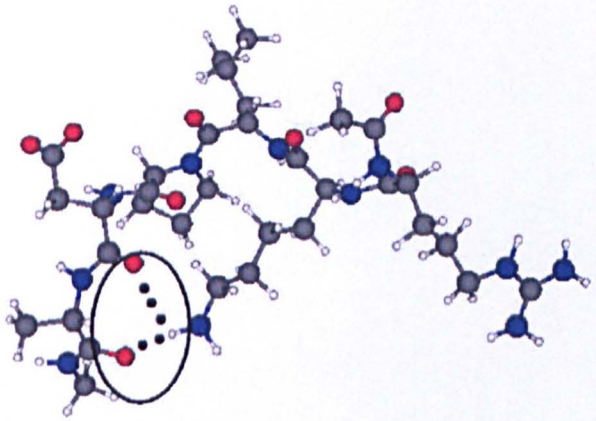

Figure 4.24: A typical conformation of the peptide in the $\beta\beta\alpha\beta\beta\beta$ configuration. An interaction between Lys and carbonyls 6 and 7 can be seen and is circled.

This is highlighted in Figure 4.25 which shows the distance from the end of Lys to carbonyls 6 and 7 as a function of time, in the $\beta\beta\alpha\beta\beta\beta$ configuration. It can be seen that

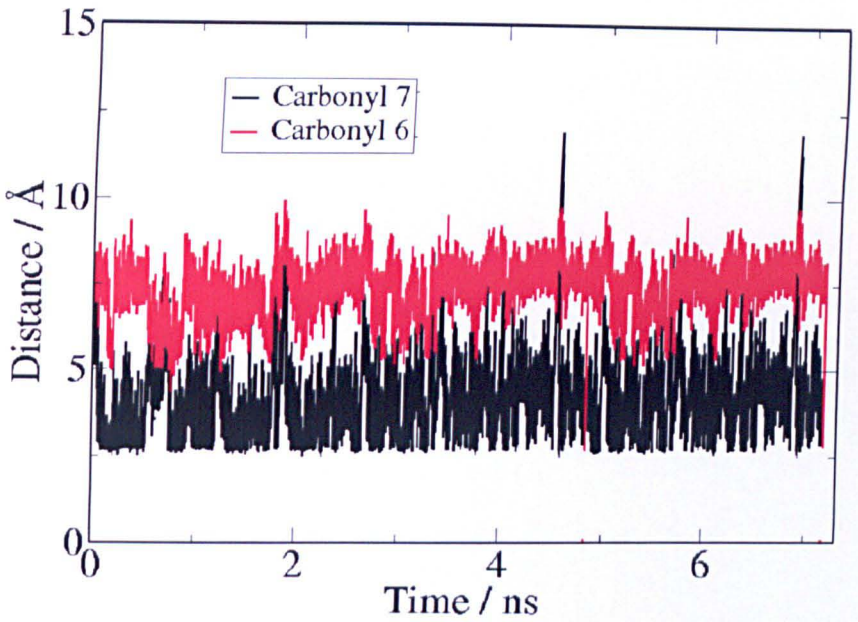

Figure 4.25: The distances from the end of Lys to carbonyls at position 6 and 7 as a function of time for the wildtype peptide in $\beta\beta\alpha\beta\beta\beta$ configuration.

the Lys spends most of the simulation time (7.5 ns) within 5 Å of these groups. The Asp-carbonyl distances fluctuate but do not increase to the point of separation.

For the duration of the simulation, the wildtype peptide conformation does not change much which indicates that it is a stable conformation. For example the Leu stays in the α configuration. It is likely that there is an energetic advantage of this interaction occurring. If is also likely that there is an energetic advantage of peptide-adsorption; the Asp-carbonyl interaction would reduce this effect by reducing the difference in energy between the adsorbed-peptide and free-peptide states. Therefore this could mean that the interaction with the surface would lead to a lower gain in stability compared with the the Lys-mutant. This would provide a reason for the higher binding affinity in the Lys-mutant with respect to the wildtype. It would be useful to simulate the Lys-mutant starting in the $\beta\beta\alpha\beta\beta\beta$ configuration for comparison of conformational stability.

If the Lys and Asp do interact with each other, it is possible that the interaction of the Asp group with the surface would be partially blocked, less able to bind and therefore cause a reduction in binding affinity. This effect would not occur upon Lys mutation,

leading to an increased binding affinity. It is possible that there are only a limited number of configurations that can actually bind to the surface (see Chapter 5). The interaction of the Lys with Asp and carbonyl groups may restrict the conformation in such a way as to reduce the population of possible binding configurations, again reducing the binding affinity.

There is also some evidence in the literature to support such interactions between Lys with Asp. For example, it has been shown both experimentally (NMR)[156] and theoretically (MD using Charmm22 and TIP3P) [157] that salt bridges between Asp and Lys are formed in amyloid β-proteins. Also, as highlighted in the Introduction, it was found by CD spectroscopy that for Ala based peptides, with Glu and Lys separated by 4 residues (i+4) and 3 residues (i+3), greater helicity was found for i+4 than i+3 [152]. This is significant because it was postulated that interactions between Glu and Lys, stabilised the α-helices. This adds weight to the hypothesis that Lys and Asp interactions in the RKLPDA peptide are significant since Glu and Asp are very similar. It also shows that these interactions influence secondary structure. In the case of the RKLPDA peptide, the Lys and Asp are 3 residues apart (i+3) and therefore should not have such a strong interaction. Glu however is longer than Asp (has one more carbon in the chain). This could mean that the shorter (i+3) (as opposed to (i+4)) interaction is stronger when Glu is substituted for the shorter Asp residue.

These experiments give further evidence that these interactions are possible and likely to play a part in peptide behaviour. If helix formation was stabilised by these interactions, more compact conformations would be possible for the wildtype than the Lys-mutant. The same argument as for the Pro-mutant versus wildtype would apply; a more compact conformation should be less strongly bound than an extended one. Therefore mutating the Lys would make the peptide less compact and potentially increase the binding affinity. In order to test this, the Lys-mutant should be simulated starting in the all α-conformation to test whether it unfolds quicker than the wildtype.

Several possible reasons have been suggested for explaining why the Lys-mutant does

not support a lower binding affinity than the wildtype in terms of Lys-Asp and Lys-carbonyl intrapeptide interactions. These include an increased stability (and therefore decreased stability gain upon adsorption), a reduction in the population of possible binding configurations and an increase in the number of compact conformations for the wildtype peptide compared to the Lys-mutant. It is possible that these effects, although not massive when noted individually, combine into a significant effect overall. There are probably other reasons which we have not explored since we have only taken the conformation of the peptide in water into consideration. Further evidence will be shown in Chapter 5 where the presence of the surface has also been taken into consideration.

4.7 Interaction between Arg and the rest of the molecule

Considering the possible importance of the interaction between Lys and different groups, it should be thought that Arg (also a positively-charged group) would also support the same kind of interactions. We have found configurations where the Arg seems to interact with carbonyl groups and an example is shown in Figure 4.26, a configuration of the wildtype peptide starting at $\beta\alpha\beta\beta\beta\beta$ configuration (after 0.6 ns of simulation in bulk water).

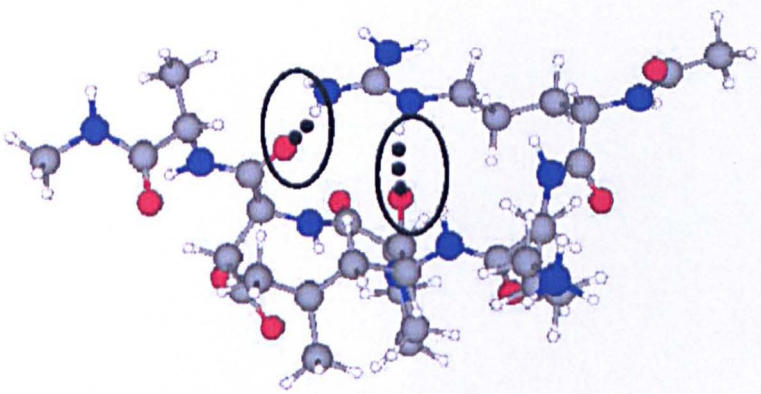

Figure 4.26: A conformation of the wildtype peptide starting at $\beta\alpha\beta\beta\beta\beta$ configuration at 0.6 ns, showing the Arg-carbonyl interaction (circled).

It shows that the two hydrogens of the Arg group are hydrogen bonding with backbone

carbonyls (Carbonyls 4 and 6).

Figure 4.27 shows the distance from the end carbon of Arg to two of the carbonyls shown in Figure 4.26. It can be seen that there is a close interaction until approxi-

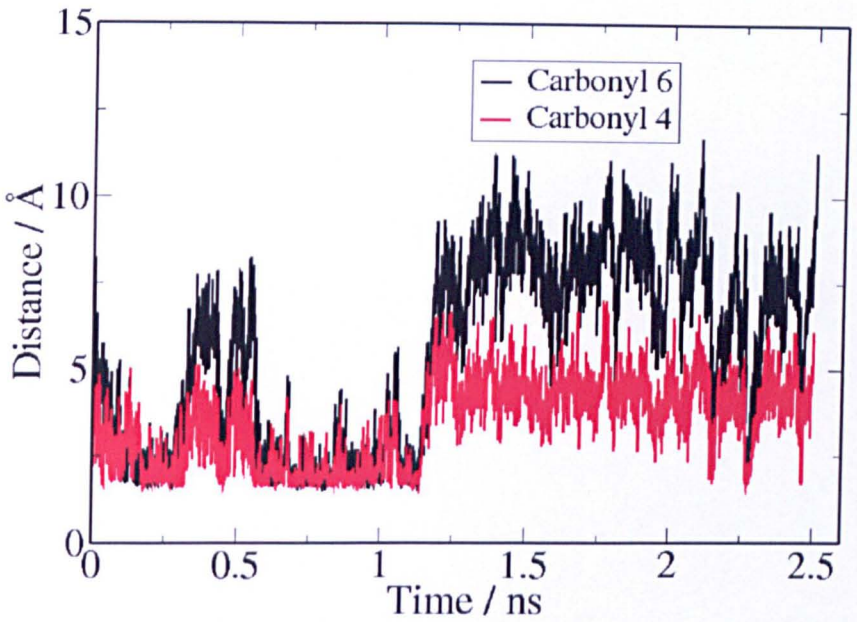

Figure 4.27: The distances from the end carbon of Arg to carbonyls, 4 and 6, as a function of time for the wildtype peptide in $\beta\alpha\beta\beta\beta\beta$ configuration.

mately 1.3ns after which, this interaction breaks. This example shows that the Arg-carbonyl interaction may not be as favoured as the Lys-carbonyl interaction (since the Arg-carbonyl groups come apart) and therefore does not not effect peptide-surface adsorption so much. The reason for this could be that the interaction is not so strong *c.f.* RDFs suggest that the Arg-water structuring is not as strong as the Lys-water structuring (see Figures 4.7 and 4.8). It could also be caused by the fact that Lys and Arg are in different positions in the peptide molecules (position 2 and 1 respectively); it may be more favourable for a group second from the end to associate with Asp/carbonyls than a group located at the end of the peptide. To test this, these two residues could be swapped and simulations repeated. It must be noted that this is just one example; the conformation of the peptide is different from the example given for the Lys-Asp/carbonyl examples and this could play a role. More simulations and analysis would be needed to test this

further. Despite these issues, this was the only configuration found where there is an Arg-Asp/carbonyl interaction and this did break. This does suggest that the interaction of Arg with the rest of the molecule is not so important as the interaction of Lys with the rest of the molecule. If this was the case, it would provide an explanation for the increase in binding affinity for Lys mutation but not upon Arg mutation.

4.8 Characterising the peptide conformations

Some specific aspects of the effect of mutation have been investigated but it was also desirable to study a more general aspect, especially the conformational sampling of the different mutants. Therefore, the type of macrostates that were sampled were analysed. The main information which we hoped to gain from this analysis was the number of 6-letter macrostates sampled and the spread of these macrostates since this would give us information about the general conformational behaviour of the mutants.

Also, studying the separate torsions gives no information about the combinations of macrostates that are actually being sampled and nothing about how the torsional state of one group affects the torsional state of another group. In an attempt to study the correlation between the torsions, tables of the populations of conformations sampled using the six-letter code are shown. The population was counted by characterising each configuration (saved every 500 steps, so each 500th configuration). This was done by calculating each ψ dihedral angle; if ($220° < \psi < 50°$) the state was considered α. If ($220° > \psi > 50°$) the state considered β. Every time a particular 6-letter permutation was found, it was counted.

Table 4.2 shows the populations starting at the all β conformation for the wildtype and Pro-mutant. The conformations are ranked in the order with which they first appeared in the simulation. First of all it can be seen that there are many more conformations adopted for the Pro-mutant than the wildtype. This is because the Leu and the Pro were able to change into α conformations in the Pro-mutant but not in the wildtype. It

Table 4.2: Conformations of Pro-mutant and wildtype peptide started from $\beta\beta\beta\beta\beta\beta$ configurations ranked in the order which the configuration first appeared. The frequency is the number of times a particular conformation appeared.

Pro-mutant		Wildtype	
frequency	config	frequency	config
513	$\beta\beta\beta\beta\beta\beta$	2530	$\beta\beta\beta\beta\beta\alpha$
373	$\beta\beta\beta\alpha\beta\beta$	1937	$\beta\beta\beta\beta\beta\beta$
667	$\beta\beta\beta\beta\beta\alpha$	2710	$\beta\beta\beta\beta\alpha\beta$
333	$\beta\beta\beta\alpha\beta\alpha$	5569	$\beta\beta\beta\beta\alpha\alpha$
21	$\beta\beta\beta\beta\alpha\alpha$	20	$\beta\beta\beta\alpha\alpha\beta$
18	$\beta\beta\beta\beta\alpha\beta$	60	$\beta\beta\beta\alpha\alpha\alpha$
66	$\beta\beta\alpha\beta\beta\alpha$	1	$\beta\alpha\beta\alpha\alpha\alpha$
106	$\beta\beta\alpha\beta\beta\beta$	2	$\beta\beta\beta\alpha\beta\alpha$
79	$\beta\beta\alpha\alpha\beta\beta$	4	$\beta\beta\beta\alpha\beta\beta$
472	$\beta\beta\alpha\beta\alpha\beta$	2	$\alpha\beta\beta\beta\alpha\beta$
892	$\beta\beta\alpha\beta\alpha\alpha$	14	$\alpha\beta\beta\beta\beta\alpha$
42	$\beta\beta\alpha\alpha\alpha\alpha$	28	$\beta\alpha\beta\beta\beta\alpha$
49	$\beta\beta\alpha\alpha\alpha\beta$	34	$\beta\alpha\beta\beta\beta\beta$
77	$\beta\beta\alpha\alpha\beta\alpha$	1	$\alpha\alpha\beta\beta\beta\beta$
44	$\alpha\alpha\alpha\alpha\alpha\alpha$	43	$\beta\alpha\beta\beta\alpha\beta$
219	$\beta\beta\beta\alpha\alpha\alpha$	150	$\beta\alpha\beta\beta\alpha\alpha$
256	$\beta\beta\beta\alpha\alpha\beta$	14	$\alpha\alpha\beta\beta\alpha\alpha$
452	$\beta\alpha\beta\alpha\beta\beta$		
425	$\beta\alpha\beta\alpha\beta\alpha$		
78	$\beta\alpha\alpha\alpha\beta\alpha$		
122	$\beta\alpha\alpha\alpha\beta\beta$		
562	$\beta\alpha\beta\beta\beta\alpha$		
437	$\beta\alpha\beta\beta\beta\beta$		
120	$\beta\alpha\alpha\beta\beta\beta$		
157	$\beta\alpha\alpha\beta\beta\alpha$		
65	$\beta\alpha\alpha\alpha\alpha\alpha$		
110	$\beta\alpha\beta\alpha\alpha\alpha$		
66	$\beta\alpha\beta\alpha\alpha\beta$		
486	$\beta\alpha\beta\beta\alpha\alpha$		
524	$\beta\alpha\beta\beta\alpha\beta$		
104	$\beta\alpha\alpha\beta\alpha\beta$		
110	$\beta\alpha\alpha\beta\alpha\alpha$		
21	$\beta\alpha\alpha\alpha\alpha\beta$		
1	$\alpha\alpha\beta\alpha\beta\alpha$		
1	$\alpha\alpha\beta\beta\alpha\alpha$		
2	$\alpha\alpha\alpha\beta\alpha\beta$		
1	$\alpha\alpha\beta\beta\alpha\beta$		
1	$\alpha\alpha\beta\beta\beta\beta$		

can be seen that for the wildtype peptide, the main conformations have the first four amino acids in the β state and it is the Asp and Asp that mainly change. There are also some states where the Pro and Lys change but these are only a small percentage of configurations. The largest population is $\beta\beta\beta\beta\alpha\alpha$. The Leu did not move from β to α and the Pro is in the α state in only a few configurations therefore limiting the number of conformations the wildtype could adopt. For the Pro-mutant however, the Leu was able to move to α showing that the Pro has an effect on the Leu ψ-angle. The largest population had an α "Pro" and the ability to adopt two states for Pro and Leu allowed a larger range of conformations to be adopted. It also resulted in a more even spread of conformations. The Arg α population in this case is not highly populated which was the main limiting factor in exploring all 64 conformations.

The populations of conformations for Arg, Lys and Leu mutated peptides starting in the all β conformation were also analysed and shown in Figure 4.3. It can be seen that in contrast to the wildtype and Pro-mutant, the "Arg" group adopts the Arg-α configuration in the Arg-mutant. This is because the Ala interacts less strongly with water than Arg and therefore does not restrict its movement so much. The Lys-mutant shows the same trend with the largest population for the Lys-α conformations.

Surprisingly, the Leu-mutant showed a similar number of conformations as the other mutants (except Pro-mutant). The mutation did not seem to increase the chance of Leu-switching to the α configuration showing that it is mainly the Pro which causes a restriction in the rotation of the Leu-ψ torsion, and not steric effects of the bulky Leu group. This is probably because the Leu group does not really interact with water and therefore allows flexibility. The largest population was $\beta\beta\beta\beta\alpha\alpha$; the same as the wildtype. Again this shows that the substitution of the Leu has less profound effects than substitution of the Pro. This agrees with the work of Sano and Shiba since the experimental binding affinity did not change when Leu was mutated.

The main result of this analysis is the number of configurations which have appeared for each peptide. Most of the peptides sampled less than 20 conformations. The Pro-mutant

Table 4.3: Populations of conformations for Arg, Lys and Leu mutated peptide started from the all-β conformation ranked in the order which the configuration first appeared.

Arg-mutant		Lys-mutant		Leu-mutant	
frequency	config	frequency	config	frequency	config
399	$\beta\beta\beta\beta\beta\alpha$	119	$\beta\beta\beta\beta\beta\beta$	1128	$\beta\beta\beta\beta\beta\beta$
1	$\beta\beta\beta\alpha\beta\alpha$	130	$\beta\beta\beta\beta\beta\alpha$	1437	$\beta\beta\beta\beta\beta\alpha$
372	$\beta\beta\beta\beta\beta\beta$	190	$\beta\beta\beta\beta\alpha\beta$	3487	$\beta\beta\beta\beta\alpha\alpha$
402	$\alpha\beta\beta\beta\beta\beta$	390	$\beta\beta\beta\beta\alpha\alpha$	0	$\alpha\beta\beta\beta\beta\alpha$
1004	$\alpha\beta\beta\beta\alpha\beta$	14	$\beta\beta\beta\alpha\beta\alpha$	1549	$\beta\beta\beta\beta\alpha\beta$
25	$\alpha\beta\beta\alpha\beta\beta$	112	$\beta\beta\beta\alpha\beta\beta$	20	$\beta\alpha\beta\beta\alpha\alpha$
6	$\alpha\beta\beta\alpha\beta\alpha$	19	$\beta\alpha\beta\alpha\beta\beta$	523	$\beta\beta\beta\alpha\beta\beta$
1	$\alpha\beta\beta\alpha\alpha\beta$	143	$\beta\beta\beta\alpha\alpha\alpha$	145	$\beta\beta\beta\alpha\alpha\beta$
730	$\alpha\beta\beta\beta\beta\alpha$	234	$\beta\beta\beta\alpha\alpha\beta$	655	$\beta\beta\beta\alpha\beta\alpha$
2657	$\alpha\beta\beta\beta\alpha\alpha$	3	$\beta\alpha\beta\alpha\alpha\alpha$	31	$\beta\beta\beta\alpha\alpha\alpha$
1850	$\beta\beta\beta\beta\alpha\alpha$	3	$\beta\alpha\beta\alpha\alpha\beta$	3	$\beta\alpha\beta\alpha\beta\beta$
692	$\beta\beta\beta\beta\alpha\beta$	2738	$\beta\alpha\beta\beta\alpha\alpha$	4	$\alpha\beta\beta\beta\alpha\beta$
3	$\alpha\alpha\beta\beta\alpha\alpha$	1159	$\beta\alpha\beta\beta\alpha\beta$	2	$\beta\alpha\beta\beta\beta\alpha$
2	$\alpha\alpha\beta\beta\alpha\beta$	820	$\beta\alpha\beta\beta\beta\alpha$	1	$\alpha\beta\beta\beta\alpha\alpha$
1	$\alpha\alpha\beta\beta\beta\alpha$	1092	$\beta\alpha\beta\beta\beta\beta$	16	$\beta\alpha\beta\beta\alpha\beta$
3	$\beta\alpha\beta\beta\alpha\alpha$	2	$\alpha\alpha\beta\beta\beta\beta$		
1	$\beta\alpha\beta\beta\beta\beta$	2	$\alpha\alpha\beta\beta\alpha\alpha$		
1	$\beta\alpha\beta\beta\alpha\beta$				

on the other hand sampled 36 conformations showing completely different behaviour to the other mutants and wildtype. This leads us to the conclusion that the Pro has a massive effect on conformation and helps us to speculate on why the Pro-mutant is a weaker binder to titania than the wildtype peptide. It could be argued that the Pro-mutant has a larger amount of conformational entropy than the wildtype because it can sample a larger number of conformations. If this is the case, it would lose a greater amount of conformational entropy upon adsorption (as the conformation is restricted) than the wildtype and adsorption would be unfavoured with respect the wildtype. More suggestions for this effect will be given in Chapter 5.

4.9 Conclusion

In this chapter, the behaviour of the RKLPDA peptide and its mutants in water were studied. The main motivation behind this part of the project was to gain insight into the strength of binding of the peptide and how mutation changes this binding. Obviously since the surface was not present, the strength of particular binding configurations could not be gauged. The point was however that the experimental changes in binding affinity when the Lys and Pro were mutated must be explained by conformational differences between the wildtype and Lys and Pro-mutants. Therefore, the conformational differences in water were studied.

The chapter started with general features of the wildtype peptide. It was noticed that there were two main states for the peptide to be in; α and β and this mainly depended on the ψ torsion. This dihedral was therefore used to characterise the macrostate of the peptides throughout the chapter. This notation will also be shown to be useful next chapter.

The water structuring around various groups was studied. It was shown that the charged groups, especially Asp, caused structuring of water. It was shown that this structuring had an effect on the behaviour of the groups *e.g.* the Arg was less flexible than Ala

even though both groups are on respective ends of the peptide. The Leu group on the other hand showed some structuring but the peak positions of water oxygen and hydrogen were at the same radial distance indicating a lack of hydrogen bonding. This information will be shown to be useful when considering the behaviour of the peptide at the titania surface (especially water-mediated binding configurations). It also helps us to get a general feeling for the driving forces involved when considering the behaviour of the peptide in water.

Comparisons were made between simulations of the wildtype and Pro mutant for the peptides started in the all α and all β configurations. There are obviously many more configurations which needed to be tested for a comprehensive study of the differences between the wildtype and Pro-mutant but from these two examples it was shown that there were fundamental differences between these two peptides. For the α-helix, there was unfolding in both cases but it occurred more rapidly for the wildtype suggesting that the α-helix was more unstable for the wildtype than the Pro-mutant. Also the unfolding mechanism seemed quite different for both peptides . For the wildtype, the unfolding was staggered, the peptide remaining in the helix despite the lack of H-bond stabilisation. For the Pro-mutant however, the unfolding happened very rapidly with all torsions responsible changing at once, with an increase in radius of gyration and H-bond decrease occurring simultaneously. It was argued that it was unlikely that the wildtype would spontaneously move into the α-helix conformation because (assuming the folding mechanism was similar to the unfolding mechanism) it would have to first form an intermediate that was not stabilised by any hydrogen bonds. This information was considered important because the α-helix conformation is the archetypal compact configuration. It is considered that compact configurations cannot bind to surfaces as effectively as extended ones. Therefore if compact configurations are more favoured in the Pro-mutant, this could provide an explanation for its reduced binding affinity to titania.

For the all β configuration, there were differences in the ψ torsions of Leu and Pro.

It was shown that these torsions were much more flexible for the Pro-mutant than the wildtype. This extra flexibility manifested itself in the greater sampling of the peptide shown by a much greater number and range of 6-letter macrostates observed in a single simulation for the Pro-mutant than the wildtype. It was suggested that this would mean a greater entropy for the Pro-mutant and therefore a greater entropy loss upon adsorption for the Pro-mutant than the wildtype. Whatever the reason, it is apparent that this change in flexibility is highly significant and probably responsible for the decrease in binding affinity with Pro-mutation.

It was shown that there were interactions between Lys and Asp and between Lys and backbone carbonyls. It was considered that this could be highly significant for the adsorption of the peptide onto the surface since it would considerably affect the conformation of the peptide. It was therefore suggested that these interactions could be responsible for the lower binding affinity of the wildtype compared with the Lys-mutant. Several possible reasons were suggested for explaining this phenomenon. These include an increased stability and therefore decreased stability gain upon adsorption, a reduction in the population of possible binding configurations and an increase in compact conformations for the wildtype peptide compared to the Lys-mutant. It is possible that these effects, although not massive individually, combine into a significant overall effect.

The issues raised in this chapter, especially those concerning the mutation of Pro and Lys have helped to guide some of the work in the next chapter. The next chapter will explore these issues further, concentrating on the interaction of the peptide (and its mutants) with the surface.

Chapter 5

Interaction between the peptide and surface

As outlined in Chapter 1, Sano and Shiba measured the binding affinities of a peptide (RKLPDA) and the corresponding Ala mutants, and found profound differences between them. Binding affinity is a property that not just reveals how strongly-bound a particular configuration is, but takes into consideration a large number of molecules over a large time-scale. It is therefore a property of a very large number of configurations. In this study, conventional MD was used. Since conventional MD cannot model such length- and time-scales, the binding affinity and binding affinity differences have to be extrapolated from intuitive examples. If the peptide stays bound to surface for an appreciable amount of time, tractable within a simulation, it at least shows that this molecule has some binding capacity. If, when mutated, the molecule comes free from the surface, it indicates that the mutated group was essential for the binding in that particular configuration. This would then remove one possible binding configuration. With enough of these examples, it is hoped that useful information can be gained to explain binding affinity differences. Sano and Shiba proposed a simplified binding mechanism but did not explain most of the phenomena observed [1]. For example, Sano and Shiba offered no concrete explanation for the Pro-mutant being a much weaker binder than

the wild-type and no explanation for the Lys-mutant to be a stronger binder despite this peptide containing fewer binding opportunities *i.e.* less positively-charged groups. One of the aims of this Chapter is therefore to continue where the last chapter left off in shedding light on these phenomena. It was shown in Chapter 3 that the titania surface causes structuring of water. In this Chapter, we aim to highlight the implications of this structuring for the interaction of the peptide with the surface. It will be shown that multiple binding configurations are possible and that the peptide can bind via the structured water layers. It is also an aim to unfold some of the detailed mechanisms behind adsorption, remodelling events and desorption of the peptide on the surface.

5.1 Background

Over the past few years, computational studies of the interaction between peptides (and proteins) with surfaces have started to appear in the literature. A review of these studies will be made with emphasis on the studies more relevant to the present study.

5.1.1 Peptides on titania

The most relevant studies are ones where simulations of peptides on titania. These give us further information about the mode of peptide binding to the titania, the surface studied here. They can be particularly revealing if the peptides contain the same residues, giving vital information on specific modes of binding.

Carravetta and Monti [158] studied Ala-ACE, Ala-NME and dipeptides Ala-Lys and Ala-Glu on TiO_2 using TIP3P water and the AMBER protein force-field. The authors placed Ala-ACE and Ala-NME directly onto the surface and computed the distances of the carbonyl, carboxylate and amine groups to the surface and the peptide-surface interaction energies. Their data suggested that the Ala-ACE is more strongly bound than Ala-NME but this is probably because Ala-ACE has two carbonyl groups but Ala-NME only one. They show similar analysis for the dipeptides Ala-Glu and Ala-Lys;

for Ala-Glu they find that the end carboxylate group stays close to surface and the Glu carboxylate group remains further from the surface. However, it is suspected that their findings are strongly biased by their initial configurations; these authors made no attempt to explore these effects. The authors compare the backbone torsions of Ala-Lys and Ala-Glu and show that that the ψ is more flexible for Ala-Glu than Ala-Lys. From the atom-surface distances it was shown that the Lys started close to the surface and moved to the bulk water before settling down to around 6 Å distance from the surface, which they attribute to the flexibility of the Lys group. It will be shown that in agreement, Lys has been seen to attach to and desorb from the surface in the present study. In this paper the effects of structured layers of water are neglected and the authors seem to assume that the only possible binding configurations are those with direct contact of charged groups with the surface. It will be shown later that water-mediated configurations may be very important for binding of peptides to surfaces.

Recently, Monti *et al.* studied the interaction of the dipeptides AK and AE with titania using MD (AMBER, TIP3P)[159]. In this work many peptides were put on the surface simultaneously in order to test how the interaction between peptides on the surface, affected adsorption. The backbone torsions were measured and a range of behaviours were observed *i.e.* some molecules had restricted backbones due to surface-peptide interactions, some peptide conformations were more free because only one group was attached to the surface. Binding modes involved Lys, carbonyl groups, N-terminus groups and the Glu group (which is similar to Asp).

The two papers just outlined are certainly relevant to the present work since they study the same surface and show binding of peptides containing the similar residues, Glu and Lys. It will be shown that Asp (a similar group to Glu) and Lys are important in binding in the present study. The authors do not really consider the binding of the side groups but concentrate on the carbonyl and end carboxylate binding. The terminal groups may not be so important in larger peptides since they are statistically less significant. The importance of backbone carbonyls will be shown later. Similar to the present study, there

is also analysis of the conformations; backbone torsions and intra-molecular H-bonds are computed and it was found that they can affect the binding modes and the binding in turn affects the conformational mobility. The work visited a previously unstudied area (by atomistic simulation) when intermolecular interactions between adjacent peptides were studied. This is very interesting since these interactions have been found to affect adsorption experimentally [29]. In fact, the authors were attempting to understand the self organisation of peptides containing Lys and Glu [88, 89]. It seems as if this study was very preliminary but some interesting results were obtained. It was found that AK were more tightly packed and there were H-bonds between terminus-backbone interactions and terminus-side chain interactions compared to AE. They state that AK have a stronger tendency to self organise but further work certainly would have to be performed to confirm this finding since this property would be strongly influenced by starting configuration.

Simulations by Monti were reported for a segment of a collagen peptide (a triple helical protein important for biocompatibility) in water on TiO_2 [160]. Monti studied a region without charged side groups in order to test if the protein could bind without electrostatic interactions. The peptide was put onto direct contact with the surface in six different configurations (rotated around the axis parallel to the surface). Water structuring was mentioned in this paper but binding of the peptide to this water was not considered *i.e.* the author states that the peptide blocks adsorption of water. However, this could be an artifact of starting configuration. The binding of the peptide was shown to be due to side-chain hydroxyl oxygens of Hyp (hydroxyproline) and Ser with titanium atoms (RHO–Ti) and to bridging oxygens (ROH–O).

Another interesting and relevant modelling study was by Langrel and Menken [161] who modelled the interface between TiO_2 rutile (100) and (110) surfaces with amino acids, glycine, methionine, Ser and Cys in water using first principles molecular dynamics. The main emphasis of this study was to investigate the implications of deprotonation/protonation of side-groups, carboxyl, amine and surface groups (hydroxy-

lated and non-hydroxylated). The authors relate pKa and experimental results to certain modes of binding. One example is for the zwitterionic methionine (a sulphur-containing residue), adsorbed on the (110) surface, where a proton of the NH_3^+ group was transferred to a surface bridging O, consistent with the pKa for H on TiO_2 being lower than that of the amino acid. This is interesting because it highlights a phenomenon which has previously (and since) not been addressed by modelling studies namely the proton dissociation of certain groups on the surface and therefore proton transfer.

Another interesting aspect which was highlighted was chemisorption. The chemisorption by ester condensation of the carboxyl group and a surface hydroxyl group was proposed and it was shown that it was energetically favourable. It was also shown that a bond between a deprotonated hydroxyl or thiol group of Ser or Cys, respectively and a surface Ti formed when it is adsorbed onto the non-hydroxylated surface but not onto the partially hydroxylated surface.

This work is interesting because it used a technique which can deal with proton dissociation and chemical bonding, both of which cannot be dealt with by classical simulations. These effects could be fundamental to the interaction of the peptides with such surfaces and this could highlight a limitation of the present study. To put this limitation into perspective however it must be pointed out that studies by *ab initio* MD are severely limited by computational cost, the size of the system that can be studied and the amount of simulation time that can be sampled. This highlights the need for testing the validity of simpler, computationally cheap models and the importance of these effects for describing such systems. However, it can certainly be considered that work like this could add further insight to peptide-surface interactions

5.1.2 Other surfaces

Previous work which does not involve titania surfaces is interesting for two reasons. Firstly, some general features of binding can still be distilled from these studies, especially those such as conformational, water structuring, electrostatic and hydrophobic

interactions. Secondly, these studies show different methods for simulation and analysis which are available for studying the adsorption of peptides on surfaces. These have certainly been useful for choosing analysis methods for the present study.

5.1.2.1 Peptides on other surfaces

The first studies which will be reviewed are those involving small peptides on surfaces. For the study of the adsorption of peptides onto surfaces, especially for understanding binding affinities, it is highly desirable to calculate the free energy of adsorption. This would tell us the binding affinity of the peptide on the surface using the model in question. Many studies calculate what they call the free energy of adsorption. This involves calculating the vertical displacement of the peptide above the surface and using this to calculate the free energy (see Chapter 2). These studies rely on complete sampling of the conformation of peptide but many of them do not use any method to ensure this sampling and do not test their conformational sampling. Also, it should be assumed that unless the interaction is very weak, the peptide will spend most of the time sampling just one binding configuration and neglecting other important configurations. Despite these limitations, some qualitative trends have been gained and interesting ideas have been highlighted. For example the effect of water on the adsorption of peptides onto surfaces has been discussed in these studies, an effect which is central to the present study.

One such study was made by Raut *et al.*[162]. Raut *et al.* studied 9-mer peptides GGGGKGGGG and GGGGGGGGG on OH, COOH and Oligoetylene oxide (OEG) functionalized alkanethiol self-assembled mono-layers (SAM) on gold using the AMBER force-field. The application for such studies is that SAMs can be used to modify surfaces in order to make them more biocompatible. It was shown that peptides did not bind to the OH-SAM but both peptides showed binding to COOH SAM via NH_3^+ groups of Lys and the N-terminus mediated by a water layer. Therefore the Lys containing peptide was a stronger binder. There were also hydrophobic interactions between

CH_2 groups of the Gly and Lys side-chain and those of the SAMs. The magnitude of binding for OEG SAMs was intermediate with respect to OH and COOH SAMs. This study brought out some important issues involving the nature of the interaction of different peptides to surfaces of differing chemical properties.

In a study by Schravendijk *et al.* [163], the free energy of adsorption was also calculated but there were less limitations since they used only amino acids, making conformational sampling less challenging. Also, an extra force was used in order to hold the peptide at different distances from the surface, and the potential of mean force (PMF) was calculated. This eliminates the sampling problem created when the peptide is immobilised onto the surface although bias potentials can create artifacts.

Schravendijk *et al.* studied amino acids on Ni(111) surface in water using MD and used *ab initio* and Langevin dynamics (LD) calculations to iteratively improve their potential. For the amino acid-surface interaction, attractive Morse and repulsive 10-4 potentials were chosen. PMF calculations were made for Ala and Phe and for Ala it was found that the free energy of adsorption was weak and independent of the atom used to constrain it to the surface. For Phe, the ΔG_{ads} was more attractive but when the ring was used as a constraint point, the ΔG was largely positive despite the interaction energy (and *ab initio* interaction energy) being largely negatively-charged. The authors account for this by stating that the water-surface interaction energy is stronger than the peptide-surface interaction, which means that it is unfavourable for water to be displaced and the peptide to adsorb very close to the surface (many waters would have to be displaced for the phenyl group to get close to the surface). The PMF is highly negative using LD in vacuum which supports this view, the authors state that explicit water is necessary for peptide-(hydrophilic)surface simulations. This point will be argued further in relation to the present study.

Similar to the present study, some studies have been performed to understand the strength of binders which have been found by phage display. Kantarci *et al.* [164] performed molecular dynamics simulations of four different peptides with the Pt(111) surface in

water. These peptides were found by phage display to be strong binders (1-CPTSTGEAC, 2-CGSVTSTKC, 3-CVRTSTTAC, 3-CIMRDGPMC) to Pt. The authors calculated radial distribution functions (RDF) between waters and side groups in bulk water and found that the TST region (hydroxide containing side chains, noble metals binders contain such groups) in peptides 1 and 2 (experimentally strong binding) were more solvated than in peptide 3 (a weaker binding peptide). The RDF of the TST region of peptide 1, 2 and 3 adsorbed onto the surface showed a closer contact of this group for the strong binding peptides than the weak binding peptide 3. Torsional angle autocorrelation functions of backbone atoms showed that the torsions around TST are the most flexible. The authors suggest that this flexibility as well as the close contact to the surface is responsible for the strong binding. However, the authors also mention that the flexibility is hindered by adsorption. It seems as if this would decrease the conformational entropy on binding and make it more unfavourable. However this could possibly be offset by increases in solvent entropy. The authors give no explanation for this phenomenon but this goes back to the question asked in the introduction about why some binders are good because of their flexibility yet others are good because they contain Pro and are therefore rigid. An explanation for the latter will be given later.

Oren *et al.* modelled the interaction between experimentally determined strong, medium and weak binding polypeptides and different crystallographic faces of Pt using a Lennard-Jones potential [165] in vacuum. Low energy configurations were found by rotating the peptide on the surface and optimising, interaction energies were then compared. It was found that there was a good agreement between the interaction energies and the experimental strength of binding for all surfaces. The authors acknowledge however that no electrostatics are involved but state they could be unimportant. However the paper lacks evidence for this statement. This work only gives potential energies of the "global minimum" whereas binding is probably a property of an ensemble of states.

Simulations investigating the adsorption of peptides using a distributed multipole forcefield (AMOEABAPRO) on carbon nanotubes (CNT) were performed [166] with the aim

of reproducing results from the experimental study by Wang *et al.* [44]. A distributed multipole model was used to model the electrostatics because a CNT is a neutral material with only one atomic type, distributed charges would make the surface highly charged, a highly undesirable situation. In order to address the need for describing electrostatics (as opposed to a simple VDW model) and for validation of the force-field, interaction energies of different small groups which mimic W, H, and R as well as benzene were computed. Different methods were used (LDA, PBE, Hartree Fock and Wilson Levy (HFWL), periodic LDA, AMOEABAPRO and a force-field with only VDW surface-peptide interaction parameters) and compared. Quite different interaction energies were found for the VDW force-field compared to other methods especially for the H and R mimics, showing how vital electrostatics are and putting studies which do not consider them into doubt.

Two of the strong binding peptides found by phage display [44] (HWKHPWGAWDTL and HWSAWWIRSNQS) and a non-binder (LPPSNASVADYS) on carbon were studied by MD using the AMOEABAPRO force-field in implicit solvent. It was found that the two binders gave a considerably lower average interaction energy than the non-binder showing comparison with experiment. It was stated that it is the presence of aromatic groups lying parallel to the surface which is responsible for the binding. One issue that was discussed in this paper was the need for using explicit solvent molecules. It was found that the hydrophilic groups extended away from the surface and it was stated that this showed the correct solvation effect *i.e.* the water would solvate the hydrophilic groups and cause them to move away from the surface and that this effect was captured with the implicit solvent. This is a different situation to peptides on titania because unlike titania, CNT's are hydrophobic and there should be little water structuring. Titania on the other hand is hydrophilic and water structuring is important meaning explicit water molecules are essential.

In order to address such questions, a study was made into the effectiveness of certain implicit solvents on peptide interaction with surfaces [167] but it only really compared

the difference between different types of implicit solvent and DFT/self-consistent reaction field implicit solvent (it did not compare these methods with simulations containing explicit solvent). Studies like this however are important for the development and improvement of implicit solvent models for use in peptide/surface simulations.

Other studies of peptides on surfaces, were not driven so much by experimental results or direct applications but were more interested in model systems which could gain insight into the general principles of peptide binding and develop simulation and analysis techniques. These studies usually use homopolymers (peptides with the same amino acid) or simple derivatives of homopolymers and flat model surfaces.

Two studies, both involving peptides consisting of Ile and Asp and a generic charged surface were made [155, 168]. In these studies, the surface-peptide interaction was modelled by a Lennard-Jones potential, SPC for water and GROMACS force-field for the peptide intramolecular potential. These studies are interesting for the present study since they contain Asp, which will be shown later in the Chapter to be a binder to titania. Also the water structuring around the peptide in bulk water and on the surface was studied. Comparisons with the present study will be shown later. The authors speculated about the entropy changes due to changes in water structuring and conformation due to adsorption *i.e.* that adsorption causes surface structured water to be released therefore increasing entropy. This is an effect which has to be taken into consideration in the present study especially considering the water structuring on the surface shown in Chapter 3.

The first study, by Song and Forciniti studied the interaction between an octapeptide (DDIIDDII) and concentrated on the water structuring [155]. The RDF's of different atoms with water were calculated in water alone and in the presence of the surface. It showed that there was structuring of water around the Asp in agreement with results from the last chapter. The authors also calculated the RDF's when the peptide was adsorbed onto the surface and found that the hydration of Asp decreased compared to the hydration in bulk water. This was due to direct contact of the Asp groups with the

surface which therefore limited water contact with these groups.

A paper by Mungikar and Forciniti [168] concentrated on the conformation of the peptide. It was found that when the peptide adsorbs, it spreads on the surface and water gets in-between the surface and peptide, influencing conformation. This was shown when the H-bonding network was studied and intramolecular H-bonds were found to be broken and replaced by H-bonds with water, indicating a transition from an α conformation to more extended one. Also the 'free energy' of adsorption was calculated by fixing the peptide at different distances and integrating the average force. Mungikar and Forciniti state that the conformational entropy increases with adsorption as the H-bonds break leading to a favourable process.

Another paper by Mijajlovic and Biggs also studied conformational change of peptides when adsorbed onto a surface, this time of the alanine hexapeptide and on a smooth uncharged surface [169] using a genetic searching algorithm. The authors sequentially changed the surface energy (the interaction between surface and peptide) and found that the conformation changed in a discrete switching manner as a function of surface energy magnitude. These involved changes from α-helices to less compact α-helices with a larger RMSD which spread out to greater extent as surface energy increased. It was stated that the reason for these steps in conformation was that H-bonds were broken and reformed in a discrete manner. Much work has been performed for poly-alanine in water (see Chapter 4) and this work shows its behaviour when adsorbed on surfaces. It also ties in with the present work which has also investigated the effect of the surface on the conformation as well as the conformations required for strong binding.

5.1.3 Proteins on surfaces

As seen in the introduction, there has been a lot of experimental work concerning peptides on surfaces. Modelling studies of whole proteins on surfaces have been made to gain insight into the factors affecting such processes and many of the same aspects have been considered [170]. These studies usually have to compromise on detail due to com-

putational considerations; some of these studies will be reviewed. In these studies, it is usually important to consider the objective of the simulation *i.e.* what the protein is used for and why the interaction with the surface is important. Studies have been made which test the same factors such as ion concentration and pH changes which are also tested in experiment. Validations can be made with such studies as well as gaining extra detail inaccessible to experimental techniques.

Ravichandran *et al.* studied hen egg-white lysosome on a charged solid interface using an atomistic model, holding the whole protein rigid and propagating the simulation with Brownian dynamics[171]. This study seems to a test of method *i.e.* whether a rigid model can be used for study of a protein on a surface. Lysosomes are very rigid proteins so are good proteins for such a test. Analysis of the time taken for the protein to reach the surface was made and it was found that when the salt concentration was increased, the frequency of adsorption decreased suggesting an electrostatic interaction was crucial for binding. This was shown by the decrease in frequency when electrostatic contributions were removed. The authors also analysed the frequency of residues closest to the adsorption surface and found that the two Asp groups are important for binding.

The work by Ravichandran *et al.* is related to the present study since they considered a negatively-charged surface and Asp is important for binding. It gives us an idea about how the residue studied here could interact with the surface if it was part of a larger, more rigid protein. The methodology in testing the effect of salt concentration shows a comparison with methodologies adopted in experiment.

Zhou *et al.* studied the adsorption of antibody proteins onto charged surfaces using different levels of coarse graining. A united residue model was used to study the adsorption of immunoglobins on charged surfaces (SAM's) using MC [172]. The united residue model involved considering each amino-acid residue as an interaction site with the charges assumed to be -1 for Glu and Asp and +1 for Arg and Lys. VDW parameters were found by fitting an interaction energy-distance curve for each residue on the

surface to an empirical equation.

Zhou *et al.* also studied antibody adsorption using a colloid model which considered a bead as being a domain of the protein, each bead having different charges [173]. The authors modified the charges in order to take into consideration changes in pH and different immunoglobins. These charges manifested themselves as different dipoles and it was found that when the magnitude of the dipole was increased, the significance of end-on adsorption for positively charged surfaces increased. This model was very coarse grained and the whole protein was considered. Atomistic calculations were also made and qualitative agreement was found with the colloid model and united residue model.

It was found in three levels of coarse graining that electrostatic contributions dominated at low salt concentrations and high surface concentrations, exhibiting limited binding configurations. At high salt concentrations and low surface concentrations dispersion dominated since the salt ions screened the electrostatic interactions. This is agreement with experiment. It was suggested that directed mutagenesis of charged groups onto the end of the proteins could therefore be used in order to increase the controlled adsorption for biosensor applications since this was found to increase the interaction via end-on adsorption. This is in the same vein as the work by Dai *et al.* [32] (controlled immobilisation of enzyme onto surface), the mutagenesis experiments highlighted in the Introduction and the mutagenesis modelling studies of the present study. It emphasises the need for finding strong binding peptides for such applications and the role of modelling for making such predictions.

The work by Zhou *et al.* is also interesting because it simulates the response of immunoglobins to negatively- and positively charges surfaces. Immunoglobins are important in biocompatibility and biosensors, the motivations for the present study. The work spans many length scales and therefore is an example of a multiscale methodology. The agreement between the different levels of coarse graining and experiment showed that this kind of approach could be made viable for such a study.

Other investigations were made into the conformational change of proteins in line with experimental work as well as considerations of enzyme/biosensor denaturisation. They are also related to the present work since we have considered conformational change upon adsorption on the smaller scale which may influence conformation change on the larger scale.

Raffaini and Ganazzoli aimed to study the interaction between blood proteins to graphite. The authors hoped to gain insight into the pyrolytic carbon, widely used in certain implants such as cardiac valves. The two studies concentrated on residues with only α-helices and one with only β-sheets, which made these studies interesting from a biophysical point of view. Raffaini and Ganazzoli studied the interaction of a module of fibronectin, a blood protein thought to be involved in the late stages of blood clotting (a 93 residue peptide comprising of β-sheets) on graphite surfaces[174]. They chose six different binding conformations, optimised them and performed MD . They found two kinds of adsorption, a reversible adsorption where the peptide showed only small reversible changes in secondary structure with continuous breaking and reforming of β-sheets. They also observed an irreversible interaction where the peptide denatured and sat flat on the surface, maximising surface area. Raffaini and Ganazzoli also studied albumen sub-domains (α-helical) on flat graphite [175]. They found denaturisation and spreading onto the surface in this case also. The secondary structure was found to be particularly pronounced for the hydrophobic α-helices

In these studies, the procedure used involved using an implicit water model and the authors state that water has little effect on the conformation coming back to the discussion earlier. However, they do not observe the spreading of the protein when water is present and claim it is beyond their computational ability.

The idea that the hydrophobic regions show the most conformational change is interesting since it is known that hydrophobic surfaces denature proteins the most since hydrophobic groups bind the strongest to hydrophobic surfaces and have to move from the centre of the protein, therefore unfolding the protein. Again this was discussed in

the Introduction in relation to experimental work and shows how modelling can be used to gain insight into such processes.

The previous work in the simulation outlined has covered many aspects of protein/peptide adsorption. Many studies involve small peptides on various surfaces and help us to understand the effect of sequence of peptide on adsorption. These studies are also diverse in the type of surface which they study and help us to understand how peptides bind to different kinds of surfaces. It can be seen from many of these studies that modelling studies can be used to complement experiment and look into further detail about some of the considerations of peptide/protein binding to surfaces.

This gives us confidence that the modelling used in this study is a worthwhile pursuit and leads into the methodology and results section.

5.2 Methodology

In the present work, MD simulations were performed using DLPOLY [154]. The Charmm27 [90] force field was used for the peptide, the modified TIP3P [4, 5] for water and the Bandura force-field [3] for the TiO_2 surface. Lorenz-Berthelot mixing rules were used to assign Lennard-Jones potentials between the peptide and surface. The non-hydroxylated surface was used with cell parameters of 38.990 Å 37.12Å and 60 Å for the x, y and z dimensions respectively. Ewald summation was used for electrostatic interactions. All simulations were performed using the isobaric-isothermal (NPT) ensemble at 1 atm pressure and a temperature of 298 K (after equilibration stage). A time step of 1 fs was used and the frames were saved every 500 fs. The Leap-frog integration algorithm and 12 Å cutoff were used for all simulations. The initial configurations for the peptide were generated using a variety of methods. The first approach involved running simulations with implicit solvent (ASP) with the peptide on the surface and finding low-energy unique conformations. These configurations were then used to construct a simulation cell by placing the peptide configuration on the surface and soaking the cell

with TIP3P water. In this method, additional starting configurations were generated by vertically shifting (in the z-direction) the peptide by 2Å and 3Å before soaking and simulating. The second method involved performing MD simulations of the peptide in water and choosing configurations that should bind using intuitive knowledge gained through the previous simulations. Interface simulations were equilibrated by holding the peptide fixed and simulating for 20 ps. The peptide was then relaxed and simulations at 0, 50, 100, 150, 200, 250K were run for 20 ps each before simulating at 298K. This procedure will be called procedure 1. Lastly, extra starting configurations were generated by starting the simulation with the peptide in the centre of the cell and applying a harmonic tethering potential (in the z-coordinate) between different parts of the peptide and the surface. This approach was employed to gain insight into the mechanism of binding. 2123 water molecules were used in all simulations. The simulations for the mutated peptides were set up by taking a configuration where the peptide was adsorbed onto the surface and mutating the particular group keeping the water in place (it was assumed that since Ala is smaller than any other group, there will be no overlaps with water due to this mutation). The simulation was then restarted. In some cases, when there was a lot of movement at the start of the simulation due to large forces, procedure 1 was used.

PDFT optimisations were also made for alanine on the non-hydroxylated rutile TiO_2 surface using CASTEP to test the force-field. The cell size was (12.998 × 12.3748 × 22.000) Å and a cutoff energy of 400 ev and 111 k-point grid were used. Ultrasoft pseudopotentials were also used for these calculations [108]. Initial conditions were generated by performing optimisations using the force-field using TINKER and inputing the final configuration into the PDFT optimisation.

In this study, the non-hydroxylated surface was used even though as discussed in Chapter 3 the hydroxylated surface was discovered to give a closer approximation to experiment. The choice to use the non-hydroxylated surface was made because of its simplicity. When the peptide on surface simulations were started, the conformational

preferences were unknown for the peptide. It was therefore desired that the simplest surface which was static would be used since a flexible surface would add new degrees of freedom. This would add a massive amount of extra complexity to an already massively complex challenge. The aim is to move onto the more complicated hydroxylated surface once we have some knowledge of what was required for binding to such surfaces. Also as mentioned a lot of work has been performed for peptide adsorption on the non-hydroxylated surface which means that useful comparisons can be made. We assume that the qualitative results will be similar for the hydroxylated and non-hydroxylated (neutral and negative) since the water structuring peaks have just been shifted (see axial density subsection in Chapter 3) and that we can gain valuable insight into the interaction between titania/peptide/water interface by studying peptide adsorption on the non-hydroxylated surface.

5.3 Results and Discussion

The simulations in this chapter contain the final ingredient, the peptide-surface-water interaction and use insight gained during the previous chapters *e.g.* understanding the water structuring on the surface and around the different peptide groups will help us to understand the effect of water on the peptide adsorption to the surface.

5.3.1 Validation of force-field

We have seen in previous work and the previous chapters that the need for a correct force-field is vital. Here is therefore an attempt for validation of the force-field for the peptide-surface interaction parameters. As mentioned, we used Lorentz-Berthelot mixing rules for the VDW interactions between the peptide and surface. This of course is not ideal and it would be useful to have a better idea about whether this model can be used to correctly represent these interactions.

Geometry optimisations were performed for blocked alanine (ACE-Ala-NME) on the

non-hydroxylated TiO_2 surface and a result will be shown in this section. Figure 5.1 shows blocked alanine adsorbed onto the non-hydroxylated TiO_2 surface after minimisation using PDFT and the force-field.

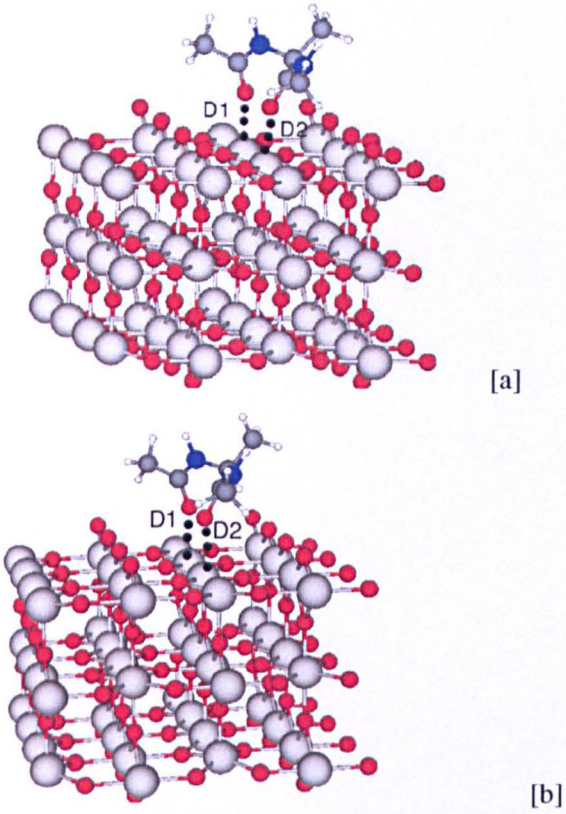

Figure 5.1: The force-field [a] and PDFT [b] optimised structures of alanine adsorbed on the non-hydroxylated TiO_2 rutile (110) surface.

It can be seen that geometry is very similar for the force-field and DFT calculations. The carbonyl-Ti distances, D1 and D2 are shown in Table 5.1.

Table 5.1: Distances of two carbonyl-Ti distances after optimisations with force-field and PDFT.

	Force-field	DFT
D1 /Å	2.31	2.35
D2 /Å	2.37	2.35

They show a close agreement between PDFT and the force-field calculations. This is

not conclusive evidence because it is only one configuration. The reason that more work was not performed in this area was that these simulations were very expensive. It does however show that the force-field can reproduce the electrostatic contribution (the carbonyl-Ti attraction) and gets the van der Waals repulsion correct.

We can compare this work to that of Carravetta *et al.* [158]. They performed similar PDFT calculations of alanine on the non-hydroxylated surface. A two layer slab was used but it was shown by Zhang and Lindan [120] and Bates *et al.* that adsorption energies are very sensitive to slab thickness[176]. Thinner slabs can mean that there are interactions between opposite faces. They also used the PW91 functional and 340 eV cutoff (*c.f.* RPBE, 400 eV cutoff, 3-layer surface - present study). The authors found Ti-O distances of 2.02 Å and 1.98 Å (did not state which ones were which). The results show a tighter binding to the present study, probably due to the 2-layer surface *ie.* the binding decreases with thickness [176, 108]. Also, the authors were not entirely clear about whether they used blocked or unblocked alanine and use a less accurate basis set and a different functional. The discrepancy could also be a result of different starting configurations or slight differences in structural model.

Monti *et al.* do not compare these minimisations with force-field calculations but consider mean distances between peptide and surface during a simulation of ACE-Ala and NME-Ala of 2.12 Å and 2.10 Å respectively. These could give different distances however because of solvent and equilibrium effects. It is interesting that in the present study there is no difference in the DFT distances of the different carbonyls in the molecule. These results show differences with previous work but it must be considered that the methods used (cut-off energy, slab width *etc.*). It should also be considered that this validation work is for the non-hydroxylated surface; the other hydroxylation states have not been considered.

Further work should be performed for further validation of such interactions perhaps for different amino acids, different surfaces and different functionals.

5.3.2 Molecular Dynamics simulations

The force-field was assumed to give a reasonable description of the interface, and was used for performing MD simulations. This is not to say that further work would not be put into improving the force-field but considering other inaccuracies and sampling issues, it was decided the force-field should only be improved once it was established how accurate it needed to be. It will be shown that insights have been gained and agreements made with experiments demonstrating the validity of the current model.
The aim of this work was to gain an insight into the peptide-surface interface just as insights into various peptide-surface systems have been found in the literature.
The results will be separated into three sections concentrating on different aspects. First, the effect of water on binding will be studied, and the reasons for this will be highlighted next. The sections after that will concentrate on binding configurations and dynamics/mechanism. The objective for studying binding configurations is to find stable/metastable macrostates and to explore the region of configuration space which contain such macrostates. The dynamical studies are more focussed on the processes involved in the adsorption.

5.3.2.1 Effect of Water structuring on the TiO_2 surface

As mentioned throughout this thesis, it is thought that the water structuring has a significant effect on peptide binding, especially when considering hydrophilic surfaces, where surface-induced water structuring is at its greatest. In Chapter 3, it was shown that the water structuring on the titania surface both in the position and angular distribution were significant and validation with experiment was made. In this section, it will be shown how this water structuring affects the binding of the peptide on the surface. This is of course related to the water structuring around peptide groups (shown in Chapter 4) since the structuring of water at the surface can be disrupted by water structuring around peptide groups and vice-versa. This can then affect conformational preferences. In order to show the effect of water structuring for peptide adsorption, the axial density

profile for water oxygen and atoms of Asp and Arg has been plotted for the RKLPDA peptide on the surface and can be seen in Figure 5.2.

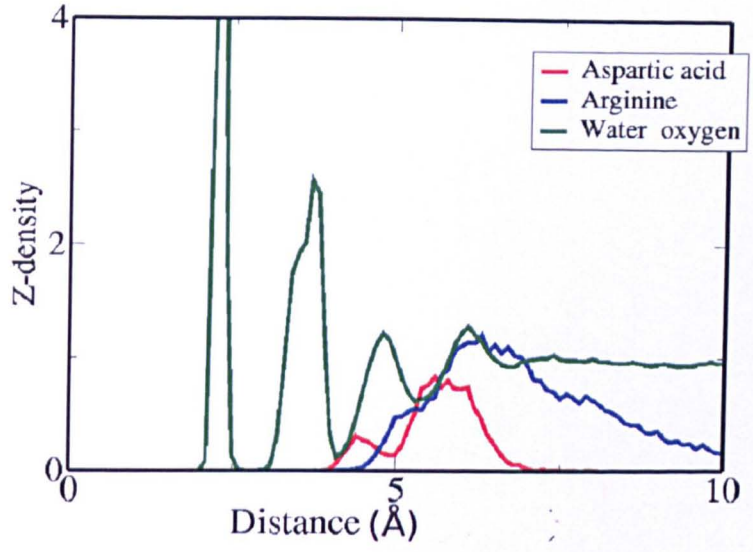

Figure 5.2: The z-density (vertical density) profiles for water oxygen, Asp and Arg on the non-hydroxylated TiO_2(110) surface.

In the particular simulation used to generate Figure 5.2, the Asp and Arg groups were bound to the surface via the first and second layers of water and did not penetrate into the first and second layers. This simulation was run for 1 ns after equilibration which suggests peptide stability on the surface. This stability will be investigated further in Section 5.3.4.

To get a better idea of the water structuring, its effect and the effect of the peptide on the water, the lateral density has been plotted and shown in Figure 5.3. The lateral density shows the density of water for a particular layer as a function of surface plane coordinates *i.e.* in the x-y plane as if one is looking down onto the surface.

Lateral density plots were first shown in the paper by Predota *et al.* [2] and for this reason, they were not shown in Chapter 2. The lateral density plots will be shown here with the emphasis on their implications for peptide binding.

The first water layer is very localised and could almost be called a crystalline layer. The water oxygens in this case are bound to the 5-coordinated titanium atoms. It there-

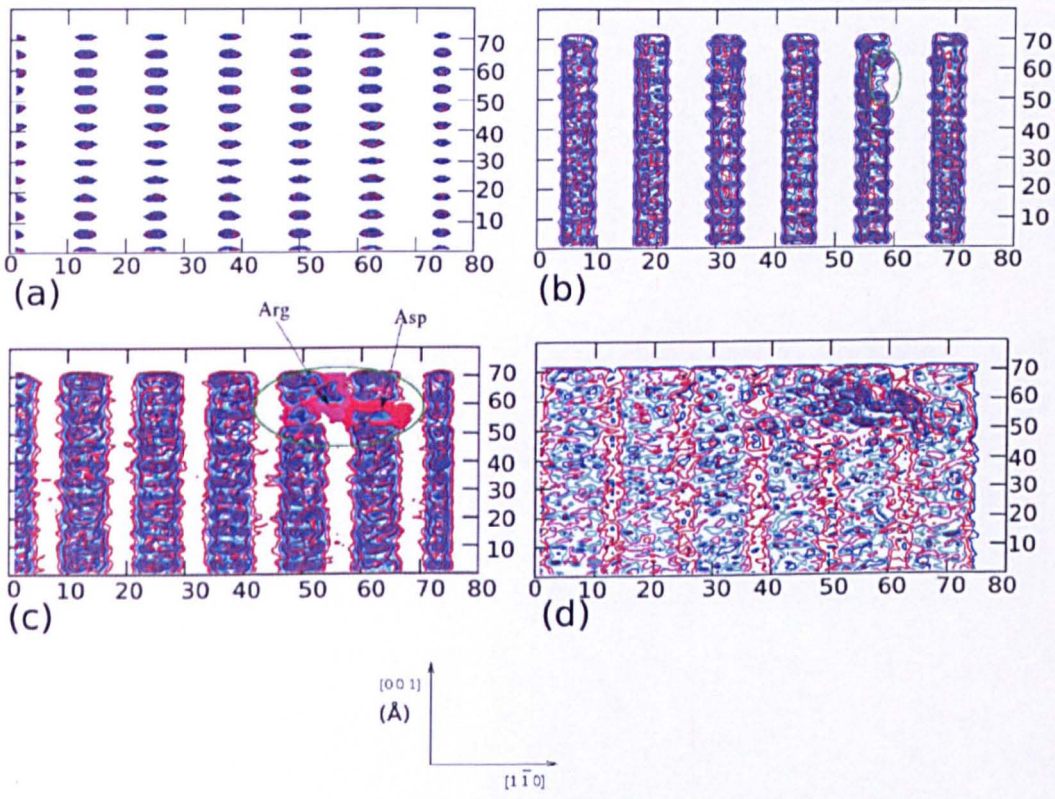

Figure 5.3: The lateral density profiles for (a) first water layer (b) second layer (circle shows where Asp deforms the water structure) (c) third layer (Arg and Asp are labelled) (d) fourth layer.

fore seems reasonable that the peptide groups could not displace these waters especially since the interaction energy between water and the surface is very favourable (approximately 20 kcal mol^{-1} per water). The second layer of water is also structured. In this case the waters hydrogens are bound to the surface bridging oxygens. It can be seen that they are less localised with two regions of density per oxygen; this is caused by the water oxygens interacting with hydrogens of the first layers. There is a small amount of deformation of the structure due to the Asp group which is bound to it; showing that although the Asp group can effect the second layer density, it does not have a great effect. The third layer is still structured although the Asp and Arg are present in this layer. The fourth layer also shows structuring and contains much of the peptide.

To further emphasise the effect of water, a simulation in which the peptide starts flat to the surface but gradually changes so that the centre of the molecule moves away from the surface will be described. At this point, it should be noted that a structure reminiscent of the 'horseshoe' structure (proposed by Sano and Shiba) was observed in many occasions. The next analysis serves as an introduction to this phenomena as well as an attempt to explain it. More water-mediated 'horseshoe' structures will be shown later. It is proposed that water structuring is responsible for this change to the 'horseshoe' structure and this will be investigated further. If the peptide is flat on the surface, it should be thought that backbone carbonyls are bound to the surface. During the transition to 'horseshoe', the central carbonyls should desorb from the surface. To characterise the transition from the peptide being flat on the surface to being in the 'horseshoe' structure , the z-distances of the backbone carbonyl of a simulation as a function of simulation time was plotted and shown in Figure 5.4.

At the start of the simulation, four carbonyl oxygens are directly bound to the 5-coordinated Ti on the surface; the two carbonyls on the C-terminus end of the molecule, the N-terminus carbonyl and Pro-Leu carbonyl. The other carbonyls are bound to the surface via the hydrogens of the first layer of water (the hydrogens are facing away from the surface, see Chapter 3) . It can be seen that at 100 ps and 440 ps the NME

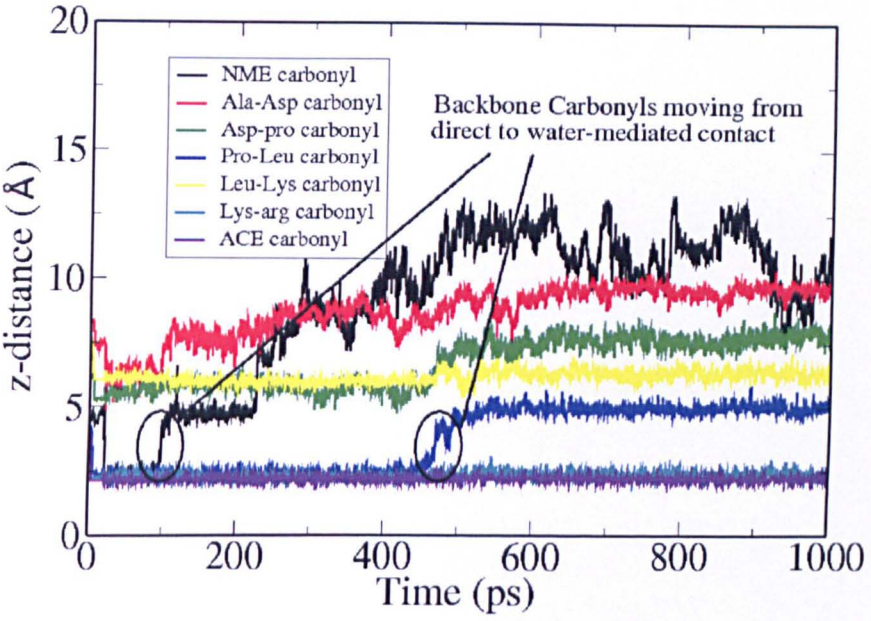

Figure 5.4: The vertical distances of the carbonyl groups to the surface, 5-coordinated Ti.

and Pro-Leu carbonyls respectively move from direct binding to water mediated binding. This transition occurs in a stepwise fashion *i.e.* there seem to be discrete vertical distance states for carbonyl oxygen as they move from direct surface contact to first layer contact. At this stage, the waters replace the carbonyls as binders. At 200 ps the NME carbonyl moves from the first water layer binding to fourth layer binding also in a stepwise fashion and then proceeds to the bulk layers of water.

The transition shown results in the carbonyls in the centre of the peptide to move from direct contact to water mediated contact and even to further water layers. This therefore demonstrates the peptide moving into a 'horseshoe' type structure. The stepwise fashion of the vertical distance states suggests that the water structuring is responsible for the change and hence the 'horseshoe' structure.

In order to gain insight into the driving forces behind the change shown in Figure 5.4, some of the individual contributions to the potential energy as a function of simulation time are shown in Figure 5.5. The interaction energy of the peptide and surface is the difference in energy between the surface and peptide, and the surface alone and the

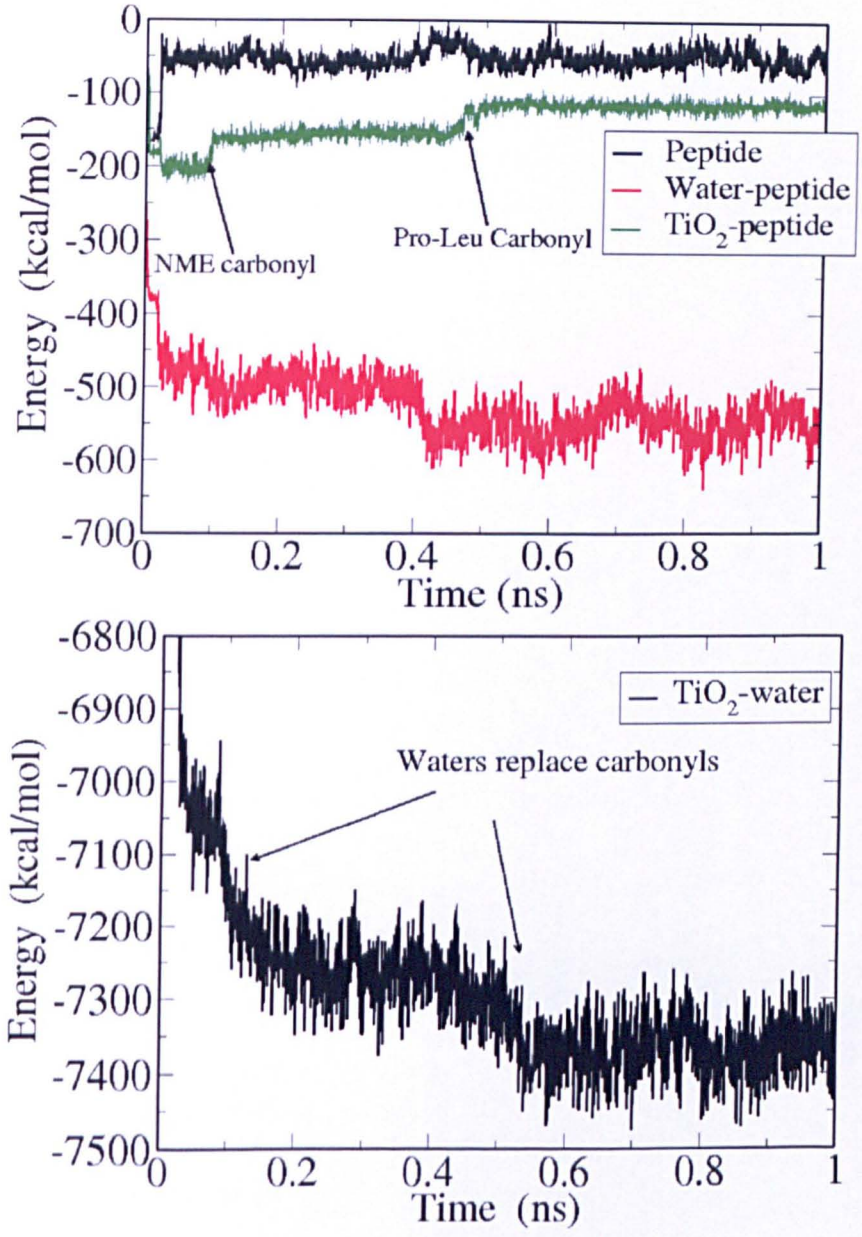

Figure 5.5: The individual contributions to the potential energy as a function of simulation time.

peptide alone and tells us the effect of the surface itself on the peptide. The peptide-water energy is the difference between the water and peptide and, peptide and water alone and gives us an idea about the effect of hydration of the peptide. The peptide intra-molecular energy gives the bonding, angle, torsion and intramolecular Lennard-Jones and electrostatic contributions and gives an idea about how stable the particular conformation of the peptide is. The surface-water interaction energy gives us an idea about the effect of hydration of the surface. By consideration of all these contributions, it was hoped that some of the reasons for certain behaviours could be uncovered; in this case, the movement from the peptide being flat on the surface to the 'horseshoe' structure (see later and work by Sano and Shiba).

The surface-peptide interaction energy increases as the carbonyls move from direct contact with the surface to through water contact. As this occurs, the peptide-water interaction energy decreases to compensate. The peptide-water interaction energy fluctuates more relative to the other contributions and seems to decrease before the surface-peptide interaction energy increases. This suggests that the peptide-water interaction is a driving force for the carbonyls moving from the surface. As the Pro-Leu carbonyl moves from the surface there is a change in the peptide intramolecular energy showing peptide reorganisation during this process.

The water-surface interaction energy is much more negative than the other interaction energies so had to be plotted on a separate graph (the scale is exactly the same). This highly negative energy is because it takes all the surface into consideration (many waters interacting with all the surface). However, only the surface and water close to the peptide should be considered. Nevertheless, the interaction energy change can be considered for gaining useful information. It can be seen that the water-surface energy tends to change to a greater extent than the other interaction energies as the carbonyls move from the surface showing that it is a major factor when considering the energetics of adsorption.

The free-energy calculations of Schravendijk *et al.* [163] stated that the free-energy of

adsorption of certain groups was positive despite a favourable interaction of the groups with the surface. They stated that the favourable interaction of the water for the surface was responsible. This work agrees with this finding and shows that the water-surface interaction energy is probably an important contribution to the free energy of adsorption. This would be especially true if the the group in question was not as strong binding as the water is for the surface. This is a possible explanation for the 'horseshoe' structure which has groups in the centre which will not interact with the surface very strongly since they are neutral (Leu and Pro). In this study, the solvation of the peptide has also been considered and it is also quite likely to be an important contribution in the free energy of adsorption.

There are also other influences which could be involved which have not been considered such as solvent entropy and conformational entropy (also discussed by Song and Forciniti [155]). It is likely that if the peptide displaced very structured waters, there would be a gain in solvent entropy as the waters became more disordered. However, the peptide would become more ordered in this process and the conformational entropy would decrease. It will be discussed later that the more rigid the peptide, the less decrease there would be in conformation entropy and the more favourable the adsorption would possibly be.

Other effects include water-water interaction energy *i.e.* how second layer water interacts with first layer water and how this changes with adsorption. These issues should be further investigated for greater understanding of peptide adsorption.

This section reinforces how vital explicit water is for the model for two related reasons. Firstly, since the water/peptide and water/surface energies both change significantly, this effect could not be represented explicitly. It has also been shown that there is great structuring of water, again this is too complicated to represent implicitly.

This section has introduced the possible effects of water on peptide binding. The effect of water on binding however will be a central theme throughout the rest of the chapter. The next section will concentrate on water-mediated binding configurations; water

structuring is obviously related.

5.3.3 Binding configurations

As stated in the methodology section, different ways of generating configurations were attempted for sampling configuration space and to find suitable starting configurations. Two binding configurations which were found by taking implicit solvent generated configurations will be explained in detail. They are not the only configurations but they were found to be interesting because they were mediated by water. These studies also showed a favourable comparison with the 'horseshoe' configuration proposed by Sano and Shiba and seem to be representative of such a structure. This is interesting because the 'horseshoe' configuration was arrived at independently from that of Sano and Shiba *i.e.* formed spontaneously during a simulation (by a similar process as shown in Section 5.3.2.1, Figure 5.4). This adds some validity to the model.

These two configurations are shown in Figure 5.6, are typical and will be used throughout this chapter for testing various peptide-binding behaviour *e.g.* for testing the effect of mutation. Figure 5.6 shows one typical configuration from each simulation and the first and second layers of water; the other waters have been made invisible to make visualisation easier.

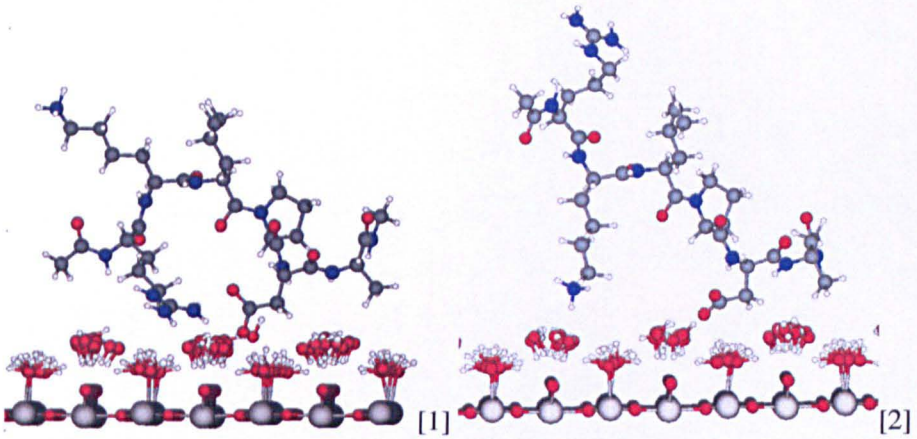

Figure 5.6: Binding configurations. [1] will be labelled Config DR [2] labelled Config DK. All waters except those in layers one and two have been rendered invisible.

For both of these configurations, Asp is bound to the first or second layers of water via the water hydrogens. One of the positively-charged groups (Arg or Lys) is also bound via water oxygens of the second layer. As stated the structures are reminiscent of the structure proposed by Sano and Shiba [1] where the peptide is attached via the charged groups with the rest of the peptide moving into the more unstructured layers of water forming a 'horseshoe'. We should also go back to the many experimental results which state that the interaction between peptides with titania surfaces are electrostatic in nature [86, 27, 85, 84, 87] and note the agreement *i.e.* the charged groups interacting with the surface strongly suggest an electrostatic interaction. Some of the reasons for specific aspects of these configurations will be given.

It can be seen that the Leu group tends to move into the unstructured water layers. This is because it is a long aliphatic group and interacts with water less strongly than water does with itself. This can be explained further when considering the RDF of Leu and water oxygen in Chapter 4 (Figure 4.9), where the Leu-water RDFs suggested little water structuring and therefore interaction of Leu with water. A lack of interaction would indicate that Leu should be more stabilised by entropic factors than energetic ones. The unstructured waters are more accommodating to Leu than the structured waters since they offer more conformational possibilities. The structured waters will not be affected by Leu so the Leu will only be able move amongst a rigid frame caused by these waters. The unstructured waters however, will move more freely allowing a greater number of vacancies (between waters) for Leu to fill.

The charged groups on the other hand gain energetic advantage of being immobilised to the structured layers due to electrostatic interactions. Firstly, the Asp oxygen interacts with the water hydrogens in the first layer. This can also be demonstrated by reference to the RDF work of Chapter 4 (Figure 4.4) and the angular distribution plots of Chapter 3 (Figure 3.9[a]). The RDF of Asp oxygens with water hydrogens shows a high peak, indicating a strong interaction, which can be assumed the same when applied to any water in close proximity. The angular distribution of the first layer of water on the

surface shows that the hydrogens are pointing away from the surface and therefore are available for interaction with Asp which is pointing its oxygens down towards the surface. The hydrogens of the second layer waters are also available for binding because they are less orientationally structured and their hydrogens do not always face towards the surface. The presence of the Asp possibly influences the second layer waters and causes their hydrogens to face the Asp oxygens.

In the case of the Lys and Arg, there is an interaction between the end hydrogens of the charged group and the second layer water, and this can also be demonstrated by reference to the RDF work of Chapter 4 (Figure 4.7 and 4.8) and the angular distribution plots of Chapter 3 (Figure 3.9[a]). The end hydrogen-water oxygen RDF shows a peak indicating an interaction. The angular distribution of the second layer of water on the surface shows that the hydrogens are predominantly facing towards the surface and therefore the oxygens are free to hydrogen bond with the water oxygen.

It has been found that Asp is the most crucial charged group for binding (its strength of binding will be demonstrated later) and this can be explained by a few factors. The RDF's of Chapter 4 indicate that the strength of interaction with water in general for Asp (oxygen-water hydrogen) compared with Lys and Arg (hydrogen-water oxygen) is much stronger (first peaks are much higher). Secondly, the Asp is bound to the first layer which is much more structured than the second layer of water which Lys and Arg are bound to; meaning greater stability for Asp. Also the first layer is more orientationally structured than the second water layer, again giving more stability. Asp also has the opportunity for binding to second-layer water hydrogens whereas Lys and Arg are limited to second layer oxygens since first layer oxygens are completely shielded from them. This extra binding opportunity can presumably increase the binding strength by increasing the volume of configuration space available for binding.

From visual inspection of the trajectories, it is apparent that the peptide stays close to the surface for longer than 2 ns for all configurations and it is conceivable that the peptide will stay there for much longer. To actually quantify the degree of peptide immo-

bilisation, we calculated the root mean squared deviation (RMSD) of the z-coordinate (vertical distance from the surface) of the three charged groups as well as the centre of mass (COM) of the peptide. We performed this analysis for the bound peptide-surface configurations and compared this with data for the free peptide (in bulk water) when started in exactly the same configuration. There is also another bar which will be described in the next section. The RMSD is calclated using

$$RMSD = \frac{\sum_{i=1}^{n} \sqrt{(z_i - \bar{z})^2}}{n} \tag{5.1}$$

where $\bar{z}$ is the average surface-atom distance and z_i is the instantaneous surface-atom distance. n is the number of frames that the value is calculated over. This is plotted as a bar chart and is shown in Figure 5.7.

It can be seen that for both configurations, the RMSD values were considerably lower for the peptide on the surface than when the peptide was in bulk water. This demonstrates that the immobilisation is due to the surface and not inherent to the conformation of the peptide alone. It can also be seen that for the surface simulations, the Asp shows the lowest fluctuation. This is because it is the strongest binder and is the most stable group on the surface. The reason for this was explained earlier. It can be seen that for Config DK, the Asp and Lys are bound to the structured water as the Arg RMSD is greater than the Lys. In Config DR the Arg is bound and so the RMSD is lower than Lys.

The way that the peptide binds to the surface has been established but it is important to understand the conformation of the peptide in the binding configurations. In Chapter 4, a 6-letter code was adopted to roughly characterise the conformations of the peptide in bulk water. The same approach was also used for the peptide on the surface in order to distil some rules for deciding which conformation was necessary for binding to the surface. The 6-letter macrostate of the binding configurations 1 and 2 are shown in Table 5.2.

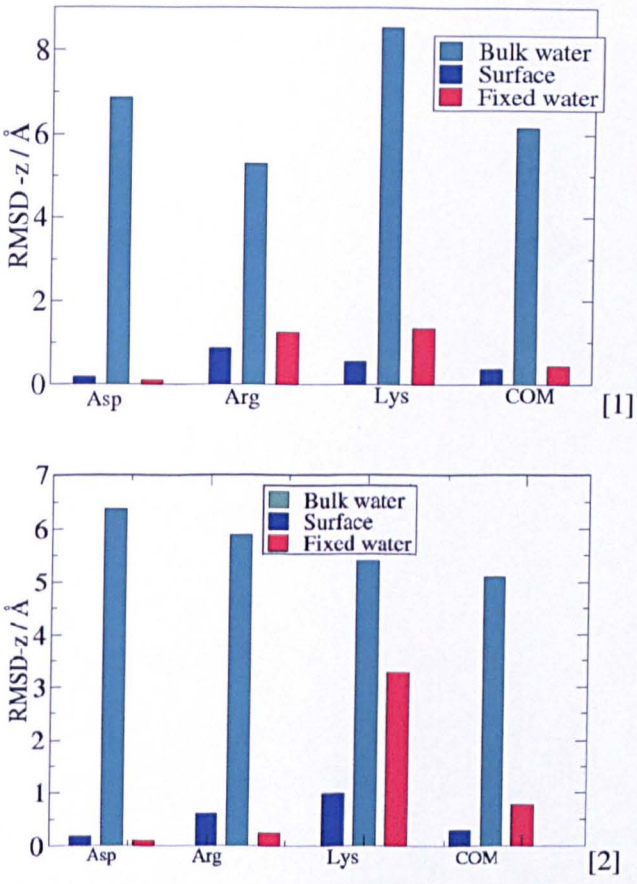

Figure 5.7: The surface-group vertical distance RMSD of the two binding configurations bound to the surface (blue), in bulk water (Turquoise) and with the surface removed but first two water layers held fixed (red). [1] Config DK [2] Config DR.

Table 5.2: The 6-letter macrostate of the binding configurations DK and DR.

Config DK	$\beta\beta\beta\beta\alpha\beta$
Config DR	$\beta\alpha\beta\beta\alpha\beta$

From Table 5.2 and studying conformations of peptides which were systematically changed, insight into the conformations that the peptide would need to adopt in order to bind was found.

If we start with the β-strand ($\beta\beta\beta\beta\beta\beta$) (Fig 1.4[a] in Chapter 1), it can be seen that the Arg and Asp are both on the same side of the molecule, which should yield favourable binding. However, the Leu is also on the same side, which may lead to steric clashes with the surface (see discussion of Leu earlier). It can be envisaged that in order for the Arg and Asp to be on the same side of the molecule and Leu to be on the opposite side, there have to be two α-turns in between Asp and Arg or on the Asp or Arg ψ torsions: observed in Config DR ($\beta\alpha\beta\beta\alpha\beta$). In order to have Asp and Lys on the same side of the molecule there has to be one such α-turn; observed in Config DK ($\beta\beta\beta\beta\alpha\beta$). This analysis has helped to simplify the picture when considering possible binding configurations. It seems as if a binding configuration has to have a specific backbone conformation to be a binder. This means that there may not actually be as large a number of binders as first anticipated. This insight can be also be used to find new binding configurations and this will be shown in Section 5.3.6.

There are also other conformational factors which will be mentioned because they may be important for later discussion. As described in Section 5.3.2.1, solvation is probably a key factor in the formation of the 'horseshoe' shape. It can be suggested (as Sano and Shiba proposed) that the two charged groups on either end of the peptide (Arg and Asp) are responsible for the ends of the peptide to stay bound and that it is more stable for the rest of the peptide to be solvated (as alluded to in the discussion on the possible contribution of water-surface and water-peptide interaction energies to the free energy of adsorption in Section 5.3.2.1). It is likely that Pro, as a rigid group, is implicated

(as shown in Chapter 3) and holds the peptide in this bent 'horseshoe' configuration, by enforcing a kink in the backbone. It will be shown later that when the Pro was mutated for Ala, this horseshoe shape disappeared.

For Config DR, the Asp group is very close to the Arg. It is possible that there is co-operation between these two groups and that this interaction is an important aspect in the binding mechanism. Charged group-charged group interactions and their significance will be investigated further in the mechanistic section of this chapter. The next section will show work performed with the aim of further understanding the role of the structured water for these configurations.

5.3.4 Fixed water simulations

Since the peptide in Configs DK and DR were not bound directly to the surface, but to water, it was considered whether the surface-peptide interaction was actually necessary for the binding. Was it just the structured layers of water that were actually required? In order to test this, the surface was removed and the first two layers of water were held fixed. The system was simulated with the peptide starting in the same configuration as Configs DK and DR. It was also thought that the nature of binding could be further probed by such studies. The result of this can be seen in the red bars of Figure 5.7.

Firstly it can be seen that the RMSD's of all the bound groups and COM were much lower than for bulk water showing that the peptide was immobilised to structured water. This showed that indeed the surface itself was not necessary for binding of the peptide in water mediated binding configurations. The surface is necessary in an indirect sense however because it causes the water structuring in the first place. It can be noticed that in both cases, the Asp RMSD is actually lower for the fixed water simulations than those with the surface. It is possible that this is because the first and second layer waters are completely fixed as opposed to in the presence of the surface where they fluctuate.

To summarise, these configurations each had charged groups bound to the structured water layers. This work has covered some important aspects of the binding of these

configurations; how the groups bind to the structured water, the role of the water and surface in this binding and the backbone conformations of the peptide which are likely to be favourable for binding. The next section will further investigate the possibility of direct-contact binding configurations.

5.3.5 Direct contact flat configurations

The binding configurations shown so far have been examples of water-mediated binding configurations. Of course, it is not completely essential for the binding that they are in such a configuration. In fact when this simulation work was originally started, the most obvious choice of starting configuration were ones where the peptide was flat on the surface. These configurations were the first ones simulated because they were the minimum energy configurations found by implicit solvent simulations. The reason these were found really highlighted the need for using explicit water molecules; without them, the peptide adsorbs flat onto the surface. Some of these configurations will be shown to give an idea about the kind of binding possible.

The last configuration of each simulation (Dir1-Dir4) will be shown with little dynamic information because this subsection is meant to give a flavour of the configurations possible . All simulations were run for more than 1 ns, and the main change from their initial configuration occurred within the first 200 ps. The configurations are shown in Figure 5.8.

The first point to note is that all configurations are directly bound via the Asp, in keeping with previous findings and providing further evidence about how essential the Asp is for binding (direct or water-mediated). They are all also bound via a different number of backbone carbonyls to 5-coordinated titanium atoms. These are end carbonyls in all configurations except Dir4; with Dir1 and Dir2 being in 'horseshoe' type configurations. For Dir2, the Lys is also attached to a bridging oxygen. Dir3 is bound via Asp, the two end carbonyls (on the Arg side) and the Arg is bound to a bridging oxygen. Lastly, Dir4 stayed a truly flat configuration and was completely locked to the surface

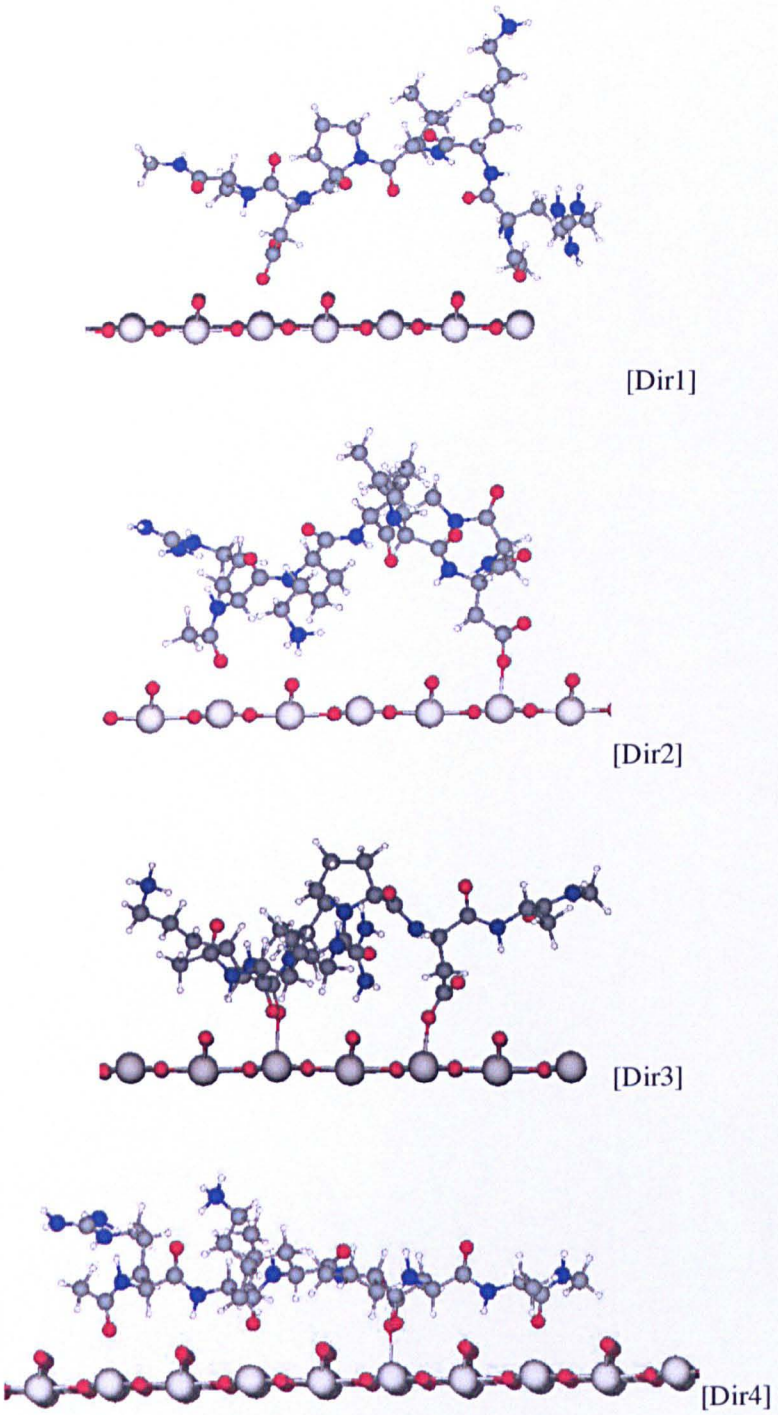

Figure 5.8: Snapshots at the end of 1 ns simulations for direct contact simulations. All waters have been rendered invisible.

by interactions between alternate carbonyls and 5-coordinated titaniums. There is also an interaction between backbone amine hydrogens and bridging oxygens.

For these configurations, the torsions were analysed but the 6-letter macrostates could not be defined since unusual torsions (*e.g.* intermediate between α and β) were observed (not shown). It is likely that for the direct contact configurations, the close interaction held the peptide in a strained conformation quite different to conformations found in bulk water. This seems a reasonable assumption when we consider that the backbone carbonyls are attached to the 5-coordinated titaniums in a very specific manner which would completely dictate the backbone configuration. This is in contrast to the non-direct (non carbonyl) binders which have conformations much more similar to those found in bulk water. This could mean that very flat binding configurations are unlikely to be formed because it would take too much of a conformational change from bulk water to surface bound configurations. It could also mean that the non-direct binders are intermediates. They may be formed first; easily because little conformational change is necessary, followed by conformational change into more flat, direct binders where the interaction is strong enough to offset any conformational barriers.

In order to investigate such issues, the contributions of the energy of Dir4 are shown in Fig 5.9. This has been chosen because it is considered as an extreme case (almost

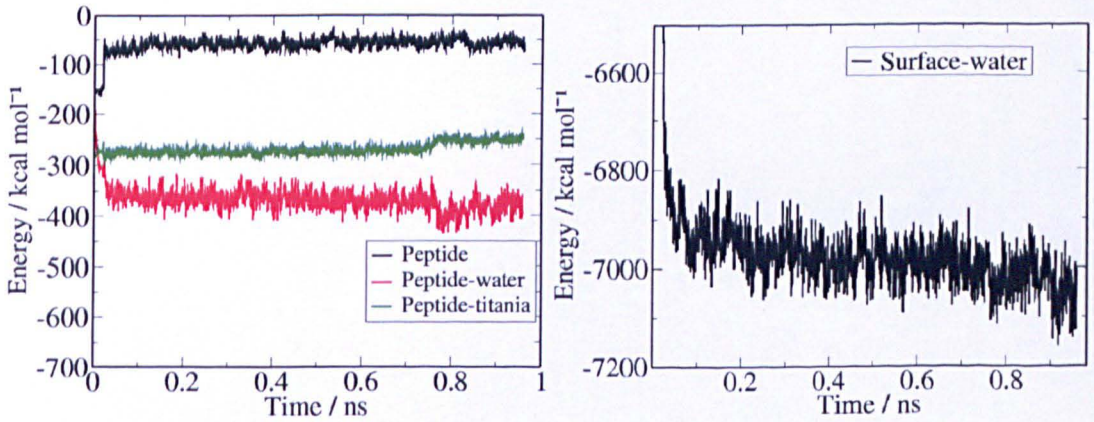

Figure 5.9: The individual contributions of the total potential energy of Dir4.

completely flat); it is useful to compare the energy at the end of this simulation with

energies at the end of the simulation shown earlier in Fig 5.5 (termed ex1) where only 2 carbonyls are attached to the surface.

The peptide-surface interaction energy is much lower for Dir4 (-250 kcal mol^{-1}) than ex1 (-100 kcal mol^{-1}) but this is compensated by the peptide-water (-350 kcal mol^{-1} for dir4 and -470 kcal mol^{-1}for ex1) and water-surface (-7000 kcal mol^{-1} for Dir4 and -7350 kcal mol^{-1}for ex1) interaction energies. The peptide-water and water-surface interaction energies add up to a much larger effect in favour of a less direct contact configuration.

This gives an argument for suggesting that the optimum configuration is not when the peptide lies flat on the surface in the way indicated by Dir4. It can also be noticed that at 0.7 ns, the surface-peptide energy increases and the peptide-water and water-surface energies decrease. This is due to the Arg moving from direct contact to water-mediated contact.

These energetic questions are important but the previous argument makes assumptions. It assumes that there are no other factors involved which could be added for improvement of the model. The suitability of the model for describing amorphous titania (to compare with Sano and Shiba [1]) has to also be considered.

The configurations which stay flat depend on the periodicity of the surface. When considering the rutile surface as a model system for amorphous titania, the most general binding modes should be taken to be the most important (the sites for binding (Ti and bridging oxygen) for rutile will not be situated in the same place for amorphous titania as rutile (110)). In order to test this, experimental binding affinity of perfect rutile (110) surfaces would be useful. It should however be assumed that amorphous titania has no regular periodicity so configurations which depend on this will not be important.

The water mediated configurations at least will take into consideration the possibility of hydroxylation. Even though there are differences between hydroxylated and non-hydroxylated surfaces, the recognition of the peptide for first layer of water could be similar to the bridging hydrogen (see Chapter 3). Direct contact on the other hand as-

sumes no hydroxylation and therefore fits into a more limited number of cases. This is especially true with the flat configurations since it requires a larger section of non-hydroxylated surface.

Despite these arguments, direct-contact and water-mediated configurations could account for irreversible and reversible adsorption respectively as introduced in Chapter 1. One example of this is the irreversible binding of cytochrome c to titania[18]. It is conceivable that cytochrome c is more likely to displace the structured water layers and directly bind to the surface than the RKLPDA peptide. It is a large, rigid protein and would therefore not have an unfavourable decrease in conformational entropy upon adsorption as a hexapeptide would. A second example is the observation of irreversible of binding of the Asp containing peptides but only reversible binding of the peptide containing no Asp residues [86] (discussed in Chapter 1). This could be explained in terms of Asp groups being able to directly bind to the surface and therefore being responsible for the irreversible binding. Imamura *et al.* however account for the ionisation of Asp and the positively-charged surface at acidic pH (this effect was only seen below pH=7) for the high affinity showing a gulf between experimental and the theoretical capabilities at the moment *i.e.* the model used here cannot account for dissociation.

It is still unclear whether direct contact is possible but modelling evidence suggests that very flat binding configurations are not favoured. There is no evidence to suggest that configurations where the charged groups only bind directly to the surface do not exist however.

5.3.6 Extra configurations found from bulk water simulations

As mentioned, extra configurations were searched for by taking configurations from bulk water simulations. The reason for this search was to find water-mediated binding configurations which had a different conformation but were still bound to the surface via the charged groups.

The following method was used which calculated three torsions. Torsion 1 was defined

by the end carbon of Asp, its α-carbon, the end carbon of Arg and its α-carbon. Torsion 2 was defined by the end carbon of Asp, its α-carbon, the end carbon of Lys and its α-carbon. Torsion 3 was defined by the end carbon of Asp, its α-carbon, the end carbon of Leu and its α-carbon. If Asp was on the same side as either Lys or Arg (torsion1 or torsion2 : 45°-320°) and on different sides to Leu (torsion3 : 0°-45° or 320°-360°), the configuration was classed as a possible binder.

This criteria (Criteria 1) was therefore used to simplify the search and several new binding configurations were found by visual inspection.

The first configuration of interest was $\alpha\beta\alpha\beta\alpha\alpha$. This however did not bind to the surface and will be outlined later in relation to Lys mutation. The other configurations that were found were ones derived from all-α and all-β configurations. These configurations do not conform to the criteria imposed by simply considering the macrostates (α or β). They did however conform to Criteria1. These configurations can be seen in Figure 5.10 and are labelled 3 and 4 to depict Config 3 and Config 4.

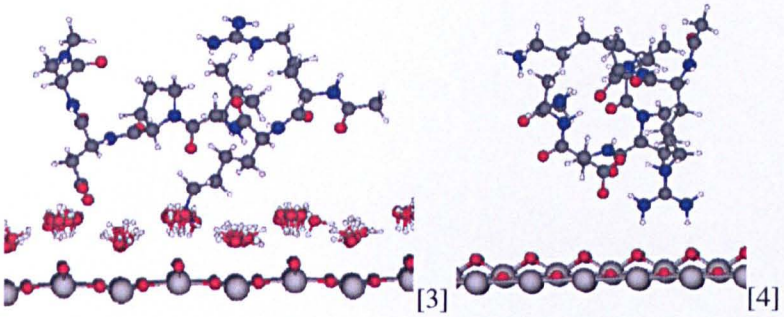

Figure 5.10: Binding configurations 3 and 4. For Config 3, waters except those in layers one and two are made invisible. For Config 4, all waters are made invisible to show direct binding of Arg.

In Config 3, the conformation is all β and is an interesting example because the Lys starts off very close and leaves the surface. This can be seen in the vertical distance plot shown in Figure 5.11. It can be seen that the Lys is in direct contact with the surface until 1.1 ns where it moves to water mediated contact and further from the surface. This suggests that the Lys-surface interaction is not overwhelmingly strong compared with

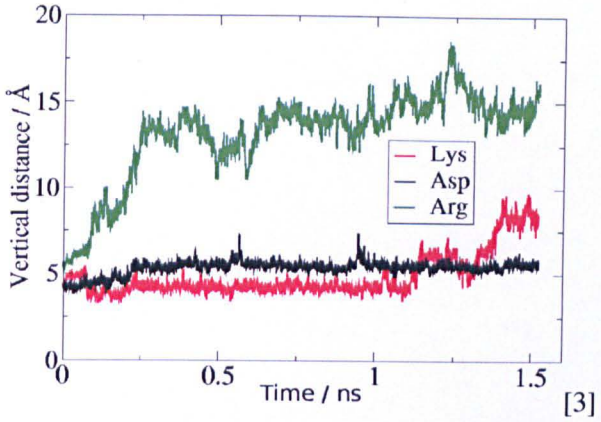

[3]

Figure 5.11: The vertical distances of charged groups from the surface.

other factors. It is suspected that these factors could be conformational. This suggests that the Lys may not be vital to the binding, which would offer a partial explanation for the lack of binding affinity decrease with mutation [1] (see later for more explanation). The Lys moving away from the titania surface was also noticed by Carravetta and Monti [158].

During the simulation, the configuration changed from $\beta\beta\beta\beta\beta\beta$ to $\beta\beta\beta\beta\alpha\beta$. This is exactly the same as Config DK. This gives further evidence to the generality of Config DK and DR and the suggestion that there are only a limited number of water mediated binding configurations possible.

Config 4 is almost an α configuration, and is therefore very compact. This configuration is shown because it is was also found by the method described above and was found to stay bound to the surface for more than 2 ns. In this configuration, the Arg NH_2 groups line up to bridging oxygens directly and Asp oxygens line up to the Arg NH_2 groups. The interaction between the Asp and Arg and between Arg and surface probably stabilises the configuration. It is a possibility that although in Chapter 4, it was suggested that this type of configuration is not stable, the interaction with the surface could help its stability. To test this, this simulation should be run for longer.

These two configurations were shown because they were found using a different method and they started with ideal cases of all-α and all-β configurations, configurations which

were predicted to not be able to bind to the surface. It can be envisaged that this kind of method could be used to find many more configurations (if many more binding configuration do exist).

5.3.7 Binding of the peptide further from the surface

One binding configuration was found which was situated further away from the surface but seemed stable (Config 5). This configuration was found from a simulation where Config1 had been heated, causing the peptide to move further from the surface. A configuration was taken and the simulation started using procedure 1 (as outlined in Section 5.2). The vertical group to the surface distances of the charged groups are shown in Figure 5.12.

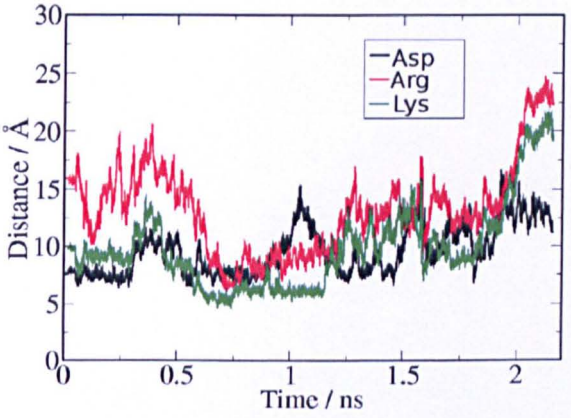

Figure 5.12: The vertical distance of the charged groups to the surface as a function of simulation time for Config 5.

At the start of the simulation, the Asp is 7.5 Å away from the surface and is attached to the third solvation layer, the Lys is about 9 Å away from the surface but from visualisation of the trajectory, it can be seen that it is interacting with the Asp. The significance of this will be highlighted in the Lys mutation section (Section 5.5.2). The Arg starts further from the surface but by 0.6 ns, the Arg and Lys are bound to the second layer of water. A snapshot at 730 ns is shown in Figure 5.13.

Lys and Arg bind to the second layer for about 0.5 ns and the Asp binds to the third

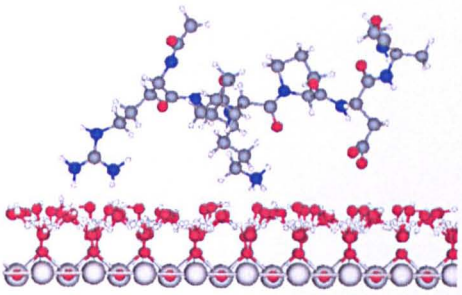

Figure 5.13: A snapshot at 730 ns showing Config 5.

layer for about 1.5 ns which shows that there is some stability. The Asp briefly leaves the surface (0.9 ns) but comes back (1.25 ns); during this period, the Arg and Lys are bound. This shows that Arg and Lys can be important for holding the peptide close to the surface while the Asp repositions itself. This could be a reason why Arg was found vital for binding experimentally.

This example shows a possibility for binding further away from the surface and could be important as an intermediate to adsorption/desorption. Eventually however, the peptide does leave the surface, again showing how important Asp actually is for the binding (at least in this model) *i.e.* when Asp was not bound to the first and second layers, the peptide was able to desorb.

In this section, a large variety of possible binding configurations have been shown. These involve different conformations as well as the possibility of binding directly to the surface or to further layers of water. It seems likely that a strong binding peptide is one which does not have one individual strong binding configuration but supports many of these strong binding configurations. This is because the more binding options there are, the more opportunity there will be for successful binding. It will be shown later that this is highly significant when considering the addition/removal of binding configurations with mutation and how this causes changes in binding affinity.

A central theme in this section has been the water structuring, how that affects the conformation and how the peptide actually binds to the surface. The next section will con-

centrate on the mechanism of binding of the peptide on the surface. It will be assumed that the water structure is important aspect when considering adsorption/desorption mechanisms but it will not be explicitly analysed.

5.4 Mechanistic considerations

In the last sections, the stability of certain binding configurations and the effect of water structuring were assessed. Information can however be derived from how the binding configuration is formed because it gives us clues into what makes it a good binder. If a particular group is involved in the mechanism yet is not directly involved in the binding, its removal may still affect the rate of adsorption.

The rate of adsorption and desorption can affect binding affinity and this can be explained if we consider the ratio of the rates of adsorption to rate of desorption. If the rate of adsorption is much greater than that of desorption, the binding affinity will be high and vice-versa. The adsorption equilibrium constant, K_{ads} is given by;

$$K_{ads} = \frac{k_a}{k_d} \tag{5.2}$$

where k_a is the forward reaction rate constant (rate of adsorption) and k_d is the reverse reaction rate constant (rate of desorption). This is argued in the paper by Tamerler *et al.* [45], which measured the rate of adsorption and desorption for a gold binding peptide on Au and Pt and found that the rate of desorption was lower for Au than Pt by a factor of 10 and the rate of adsorption was greater for Au than Pt by a factor of 2. This expressed itself as a larger binding constant for Au than Pt (see the Introduction). The rate can also involve the diffusion of the peptide to the surface. In this study, no quantitative measure will be attempted for these rates since they are beyond the timescale of such simulations but insight into the mechanism of adsorption and desorption has been found. These mechanisms can help us to speculate on the rate of adsorption and desorption and therefore gain an understanding of binding affinity and binding affinity differences

between different peptides.

5.4.1 Adsorption mechanisms

In this section, two simulations will be outlined where the peptide has started in a configuration unsuitable for binding, has experienced some conformational or rotational remodelling before moving into a binding configuration. It can be suggested that this remodelling is crucial for the the binding configuration and that these simulations highlight some important aspects of the binding mechanisms. A variety of analysis methods have been employed in order to characterise such processes *i.e.* whether this remodelling involves rotation of the whole molecule (bulk rotation) or conformational change. Figure 5.14 shows configurations at different points of the simulation which leads to binding Config DR.

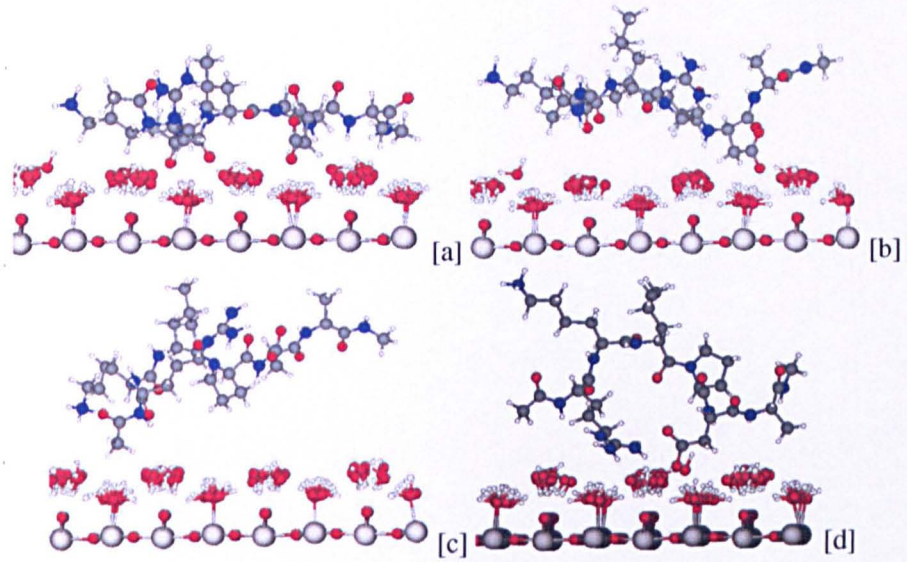

Figure 5.14: Structures of the peptide on the surface at the start of the simulation[a] and after 400 ps[b] and 750 ps[c] and 1500 ps[d].

At the start of the simulation, the peptide is very flat on the surface since it has been started from an implicit solvent simulation (but vertically displaced by 3 Å). The Asp is able to bind to the structured water and stays bound for 500 ps. This can be seen in Fig

5.15 which shows the z-distances of the charged groups to the 5-coordinated titanium. Figure 5.14[b] shows a configuration at 400 ps while the Asp is still bound. At 500

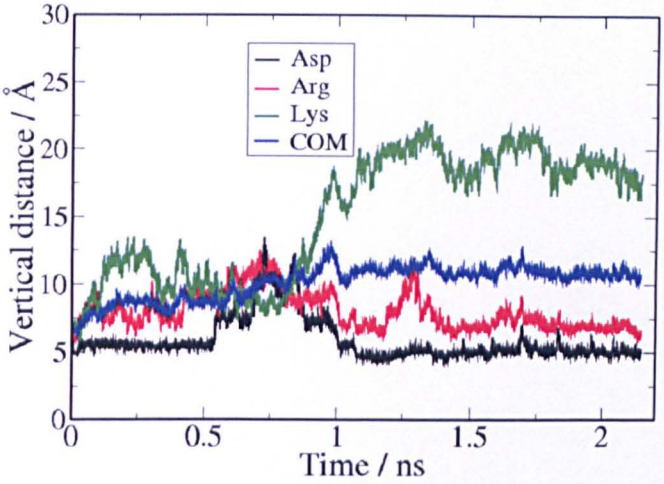

Figure 5.15: Vertical distance between charged groups and surface for Config DR.

ps, the Asp moves away from the surface. Figure 5.14[c] shows the peptide at the 750 ps and it can be seen that the Asp group is facing away from the surface. The Asp returns to the surface by 1000 ps. It could be assumed that there was a rearrangement of the conformation during the desorption/re-adsorption process. However, from studying the backbone torsions, it is evident that this does not occur. Therefore it was reasoned that the remodelling must involve peptide bulk rotation and a series of analyses were performed to test this. These included tests for different axes of rotation.

Fig 5.16 shows the z-component of the vector between the centre of mass and the end carbon of Asp. This gives an idea about the z-position of the Asp compared with the centre of mass and can tell us whether the 'horseshoe' structure is lying in-plane with the surface (not good for binding) or it is facing perpendicular to the surface as in the binding configuration 1. The schematic in Figure 5.16 (right) shows that the magnitude of the z-component of this vector tells us about the rotation of the molecule as a whole about an axis along the length of the molecule. A value of zero will tell us that the Asp and COM are on the same vertical level, a positive value, that the Asp is facing away from the surface and a negative value tells us that the Asp is facing towards the surface

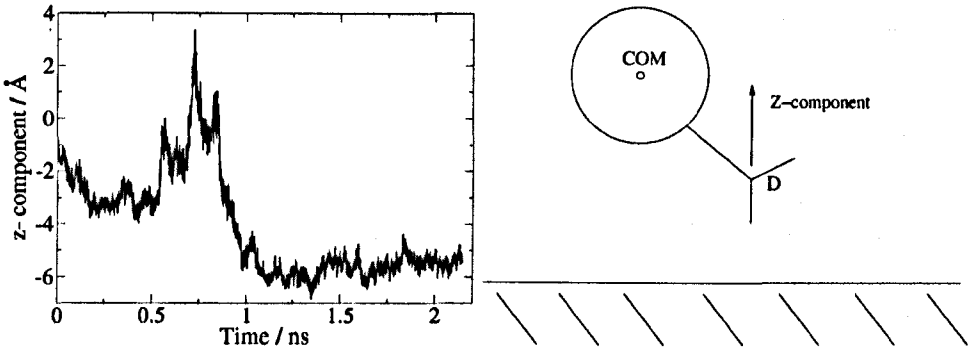

Figure 5.16: z-component of vector between the centre of mass and the end carbon of Asp for Config DR (left) and a schematic showing how the z-component relates the the bulk rotation (right). The axis of rotation is through the length of the peptide and is perpendicular to the page.

with respect to the rest of the molecule. If we compare Figure 5.16 with Figure 5.15, it can be seen that between 500 and 1000 ps, when the Asp comes free from the surface and moves back respectively (Figure 5.15), the z-component of the vector (Figure 5.16) follows a similar pattern *i.e.* there seems to be correlation between the z-distance of Asp and z-component of the vector. This suggests that this rotation is largely responsible for the peptide desorption and re-adsorption. When the Asp is the furthest away from the surface (750 ps), the z-component of the vector is positive and so is facing away from the surface, it returns to negative at the end of the simulation as the Asp faces towards the surface with the peptide in a "horseshoe" structure.

In order to gain further insight into the bulk rotation of the peptide during the simulation, different components of the vector between the α-carbon of Lys and Asp have been calculated. The Lys and Asp have been chosen because they are the second residues from opposite ends of the molecule whereas the torsions of the end residues (Arg and Ala) are much more flexible and so will give a less reliable measure than Lys and Asp due to a greater fluctuation in the vector. Figure 5.17 shows the z-component of this vector.

The schematic in Figure 5.17 (right) shows that the value of the z-component gives an idea about how upright or flat the peptide is. A zero value means that Lys α-carbon

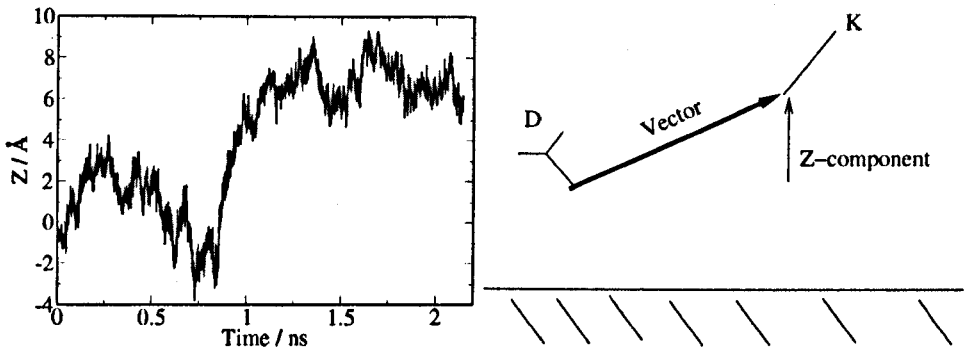

Figure 5.17: The z-component of the vector between the Lys and Asp α-carbons for Config DK (left). A schematic is shown to indicate how the z-component of this vector relates to bulk rotation. The axis of the vector along the length of the molecule is in the plane of the page.

and Asp α-carbon are at the same vertical position and so the peptide is more flat with respect to these groups. A positive value means that the Asp α-carbon is closer to the surface than Lys α-carbon, a negative value shows that the Lys α-carbon is closer to the surface than Asp α-carbon. Figure 5.17 (left) shows that at 750 ps where the peptide is not bound, a negative value is given showing that the peptide is in a rotational state that allows the Lys α-carbon to be closer to the surface than the Asp α-carbon. As the peptide is re-adsorbed, this value becomes positive, meaning there is rotation allowing the Asp to get closer to the surface. At this stage this value, is around 8 Å because the Asp is close to the surface and the Lys is facing into the bulk water.

Figure 5.18 shows the angle between the x and y components of the vector between the Asp and Lys α-carbons.

The schematic in Figure 5.18[B] shows that this angle characterises the peptides rotational state in the x-y plane (parallel to the surface plane). A zero value means that the peptide is sitting across the rails (of bridging oxygens) and a value of 90° means that it is sitting in between the rails or on top of a rail made by the bridging oxygen. The peptide moves freely among these states throughout the simulation, despite being adsorbed onto the surface. It can be very important for the peptide to be able to rotate but still stay bound to the surface because the more configurations that are available for

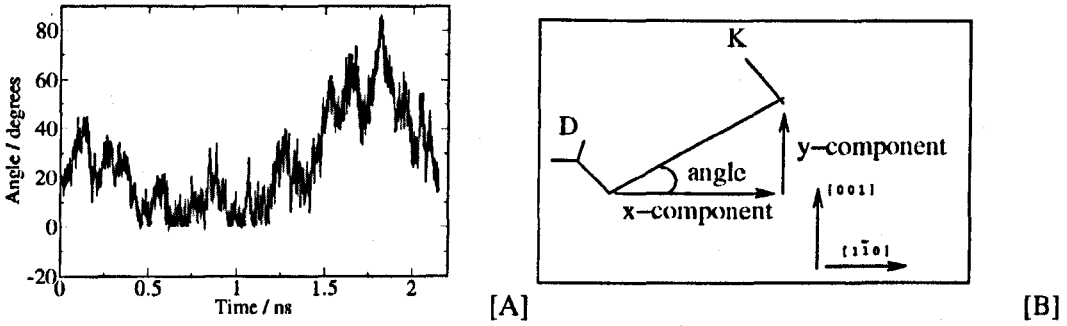

Figure 5.18: The angle between the x and y components of the vector between the Lys and Asp α-carbons for Config DR (left). A schematic is shown to indicate how this angle relates to bulk rotation (right). The surface is in the plane of the page.

the binding, the greater the opportunity for binding and therefore the greater the binding affinity.

These metrics highlight the significance of rotation of the molecule as a whole in adsorption/desorption mechanisms. Since it has been observed that bulk rotation is a faster process than conformational change, it can be conceived that rotation is important in fine-tuning the orientation of the peptide with respect to the surface. Of course, it cannot be stated that conformational remodelling is not important in remodelling of the peptide since it may not be accessible within the timescale of conventional MD. Methods for increasing the sampling such as metadynamics [104] should be developed to study such conformational remodelling.

Bulk rotation is also important in the second possible adsorption mechanism which will be highlighted, but there was also another aspect which involved the initiation via interaction of the backbone carbonyls to the structured water. Figure 5.19 shows three configurations during an unconstrained simulation that followed a tethered simulation where a harmonic potential in the z-direction was added to three points of the backbone (the Arg, Asp and Pro α-carbons) *i.e.* the result shows normal MD after release of the tether.

It can be seen in Figure 5.19[a] and [b] that at the start of the untethered phase, the two

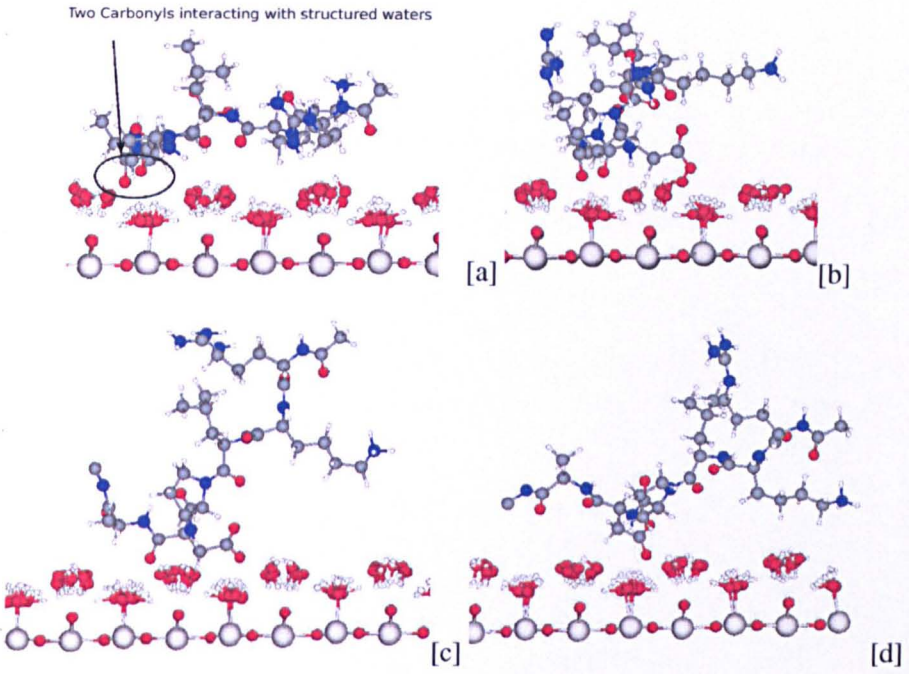

Figure 5.19: Configurations of the peptide on the surface at 0 ps[a], 300 ps[b], 700 ps[c] and 1500 ps[d], from a post-tethered unconstrained simulation.

carbonyls at the Asp end of the peptide are bound to the structured water. In order to analyse this binding, the vertical distance of these carbonyls to the surface have been plotted and shown in Figure 5.20. The vertical distances of the charged groups have also been plotted and shown in Figure 5.21. At the start of the simulation, both carbonyl-surface distances are about 5 Å away. At this point, the Asp is further from the surface (Figure 5.21). After 100 ps, the Asp is closer and stays bound to the structured water throughout the simulation. Figure 5.19[b] shows the peptide after 300 ps of simulation with the Asp and two carbonyls bound to the structured water. Figure 5.20 shows that at 600 ps, the first carbonyl comes free from the surface and Figure 5.19[b] shows a configuration when only one of the carbonyls and Asp is bound to the structured water. At around 950 ps, the second carbonyl comes free from the surface, which can be seen by an increase in the vertical distance of the carbonyl in Figure 5.20. A configuration after this event is shown in Figure 5.19[d]

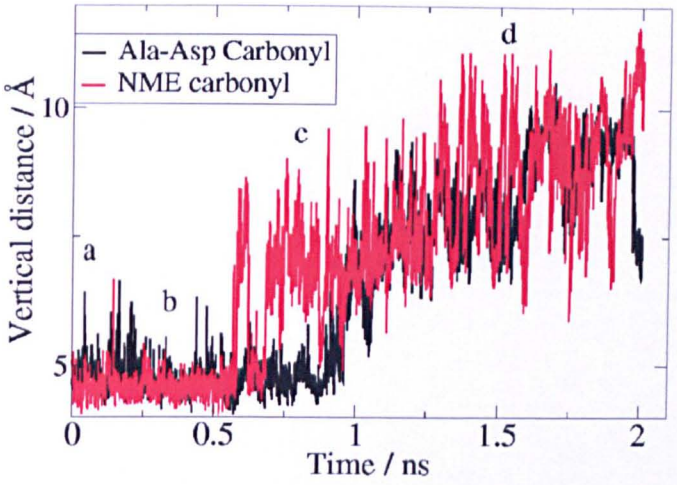

Figure 5.20: The vertical distance of the Ala-Asp and NME carbonyls to the surface versus time. The markings a,b,c and d correspond with the snapshots in time shown in Figure 5.19.

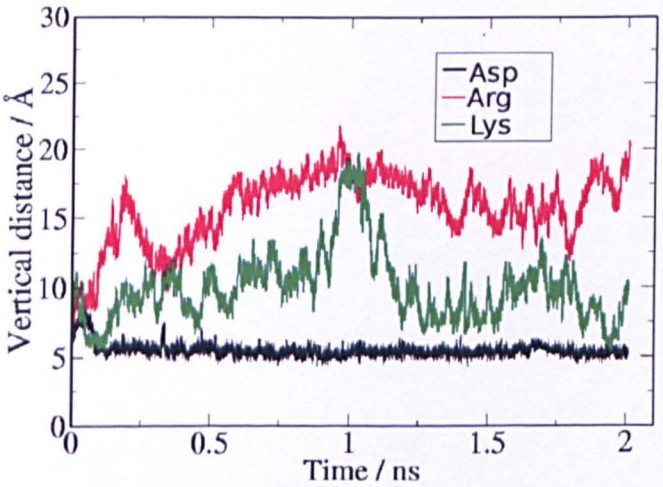

Figure 5.21: The z-distance of Asp, Arg and Lys to the surface versus time.

In order to gain a further understanding of the mechanism, the z- component of the vector between the Asp and Lys α-carbons (Figure 5.22) and the angle between the x and y components (Figure 5.23) have been plotted to give information about how upright the molecule is and the molecules alignment in the x-y plane respectively (bulk rotation analysis).

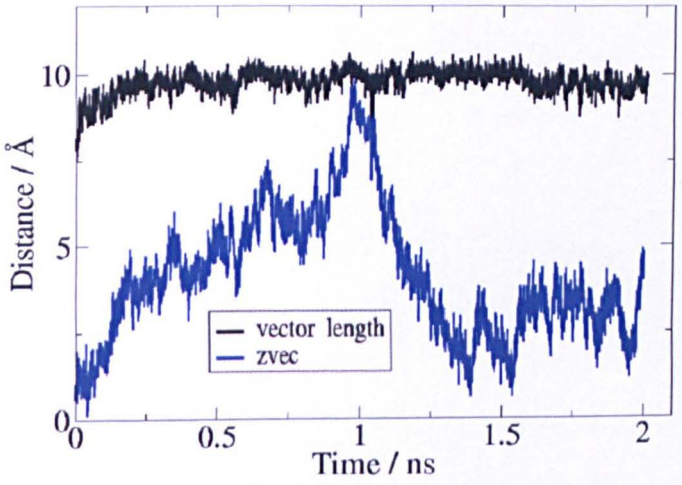

Figure 5.22: The z-component and the length of the vector between the Asp and Lys α-carbons (zvec). See Figure 5.17 for a definition of this vector.

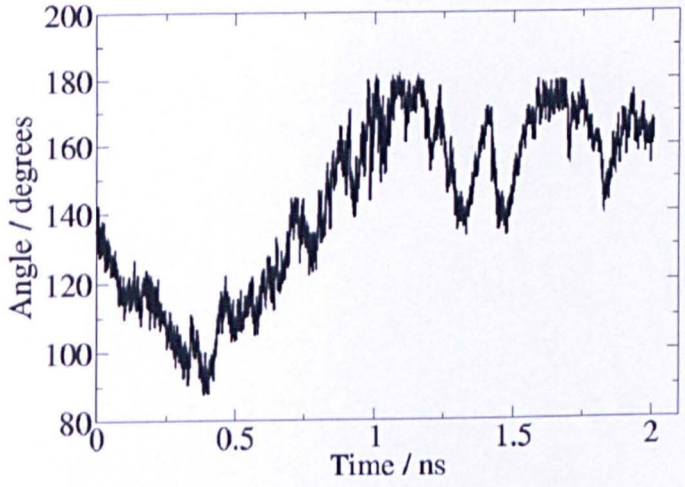

Figure 5.23: The angle between the x and y components of the vector between the Asp and Lys-α-carbons. See Figure 5.18 for a definition of this vector.

From 0 to 1 ns, there is an increase in the z-component (Figure 5.22) as the axis along

the length of the molecule orientates itself perpendicular to the surface plane. The configuration where the z-component is at its maximum is shown in Figure 5.19[c]. Also at this time, the Lys-surface and Arg-surface distances (Figure 5.21) increase and approach maxima at the same time as the z-component of the vector. The z-component decreases again until 1400 ps after which, it levels off for the rest of the simulation. During the time of decrease in z-component, the peptide becomes less upright and moves into a configuration reminiscent of those in Figure 5.6 where the Lys is bound to the structured water.

It should be noted that the z-component stays positive throughout the simulation because the Asp is always closer to the surface than the other groups. It does however become more positive as the peptide becomes more upright on the surface.

The correspondence of the Lys-surface and Arg-surface distances with the z-vector as well as the constancy of the vector length demonstrate that the driving force of the mechanism is not internal motion but overall bulk rotation of the whole molecule.

Figure 5.23 shows that at the start of the simulation, the long axis of the peptide is diagonal to the surface *i.e.* angle is 130 °. From 0 to 400ps, the peptide rotates to almost 90° and so lines up with the the y-axis as in figure 5.19[b]. From 400ps to 1100 ps, the angle moves to 180°. During this stage, the two carbonyls move from the first water layer binding to bulk layers. It could be suggested that these two events are related. The two carbonyls at the start of the simulation sit in between the rails of bridging oxygens and are bound to the first layer of water hydrogens (above the 5-coordinated Ti) . As the whole molecule is rotated in the x-y plane, the end carbonyl moves above the bridging oxygen instead of the first-layer water-hydrogens above the 5-coordinated titanium and can not bind anymore. Therefore it is likely that this rotation is responsible for the breaking of the carbonyl-structured water interaction. The second carbonyl experiences a similar event at 900 ps when it moves above the bridging oxygen and consequently moves away from the surface. The z-component of the vector reaches its maximum at approximately the same time as the x-y angle reaches 180° suggesting a concerted

movement. After 1100 ps however, there is no consistent rotation (but oscillation) in the x-y plane and only a flattening of the peptide on the surface as mentioned earlier.

The simulation analysed here is a good example of one of the mechanisms possible for peptide binding. It highlights the importance of the carbonyls in this mechanism. It was thought that the carbonyls have no part to play in peptide adsorption because all peptide sequences have carbonyls and so it can be argued they do not confer specificity. However this mechanism shows that when combined with specific elements (in this case a strong binding Asp) they can assist in the binding mechanism in a secondary way. When the peptide approaches the surface, the end carbonyls will sometimes be the first groups to come close to the surface. If the carbonyls then hold the peptide close to the surface for long enough for conformational/rotational organisation, it gives an additional binding mechanism to the mechanism where the Asp is the first group to approach the surface (also a possible mechanism) giving it more opportunities to bind. In the mechanism just discussed, the carbonyls held the peptide in position before the Asp moved and started to bind. Once the Asp had bound, these carbonyls were no longer necessary and eventually came free. The peptide reorganised its overall orientation and eventually the Lys became involved in the binding. This aspect of the mechanism where the carbonyls held the peptide close to the surface is similar to situations where the other charged groups (Arg and Lys) hold the peptide close to the surface giving the Asp the opportunity for binding.

This section has highlighted some of the features involved in the adsorption mechanism. It has mainly concentrated on bulk rotation since this is within the timescale of these simulations. Further work would have to performed, perhaps accelerated sampling or coarse-grained simulations in order to gain insight into the conformational changes necessary for binding. The question still arises about whether the peptide reorients itself when bound to the surface or whether it must be in the correct configuration before it approaches the surface.

The kinetics of bulk rotation vs the kinetics of conformational change were discussed

by Agashe *et.al.* [177]. The Fibrongen γ-Chain was modelled on SAM surfaces containing different head groups using MD. It was found that the protein did not change its conformation but rotated in order to find a preferred conformation. The authors concluded that the kinetics of orientational changes are much quicker than that of conformational changes; this is in agreement with the present work. Agashe *et.al.* suggested that this difference in kinetics could provide two time-separable mechanisms to control the adsorption of proteins on surfaces by manipulation of the surface (although this could equally involve manipulation of the peptide/protein). This would mean that the orientation of the peptide/protein could be controlled first, followed by the control of conformation. However, if the kinetics were on the same time scale, no control of orientation could be achieved as the conformation would change leaving no opportunity for orientational change. In the present study, it is indicated that the bulk rotation is on a different timescale to conformational change because bulk rotation has been observed in the conventional MD studies but conformational changes have not. Insight into the bulk rotation/conformational kinetics of strong binding peptides onto surfaces has been gained in the present study. This insight may therefore contribute to the control of adsorption of peptides/proteins in the future.

One of the most important issues and main reasons for studying the binding mechanisms is to get an insight into the specificity of binding. We must therefore ask if there are aspects of the mechanisms which would not be available for other peptide sequences. There seems no obvious answer concerning the first mechanism (shown in Figure 5.14) but it can be thought that a different sequence would be solvated in a different way and therefore rotate in a different way. For the second mechanism (shown in Figure 5.19), it seems that it is crucial for the Asp to be at the end of the molecule for this mechanism to be valid since it is the carbonyls at the end which first bind.

5.4.2 Desorption

As mentioned earlier, desorption mechanisms are important when considering binding of peptides to a surface. In the present study, desorption events have been noticed, they are therefore within the nanosecond timescale. One of the mechanisms found will be highlighted here. Figure 5.24 shows the z-distances of the ends of the charged groups versus time for a particular simulation.

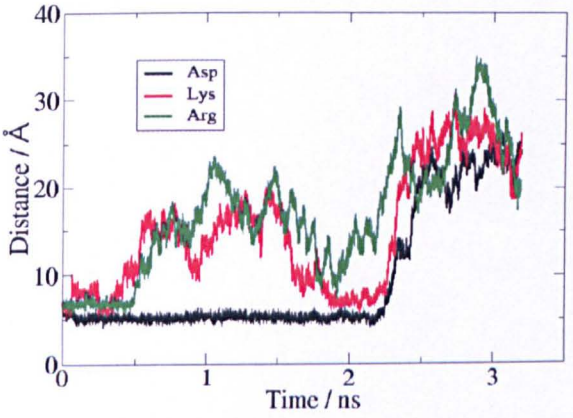

Figure 5.24: The z-distance of Arg, Asp and Lys to the surface.

At the start of the simulation, the peptide was flat on the surface and therefore all groups were close to the surface. Arg and Lys moved from the surface (0.4 ns) and eventually moved back to the surface by 1.8 ns. All the charged groups moved away from the surface after 2.3 ns indicating that the peptide had desorbed from the surface.

It was noticed that at 2 ns, there was a close interaction between the Lys and the Asp and the Lys and Leu-Pro Carbonyl. A configuration during this period (2 ns) is shown in figure 5.25.

It can be seen that the Leu-Pro carbonyl are at a distance from each other which indicates a close interaction. At the same time the Lys-Asp distance becomes typical of one where there is a water bridge between these groups (see Figure 5.26).

This is where the work of Chapter 4 helped us *i.e.* when these close interactions were noticed, it was postulated that these interactions could be responsible for the desorption.

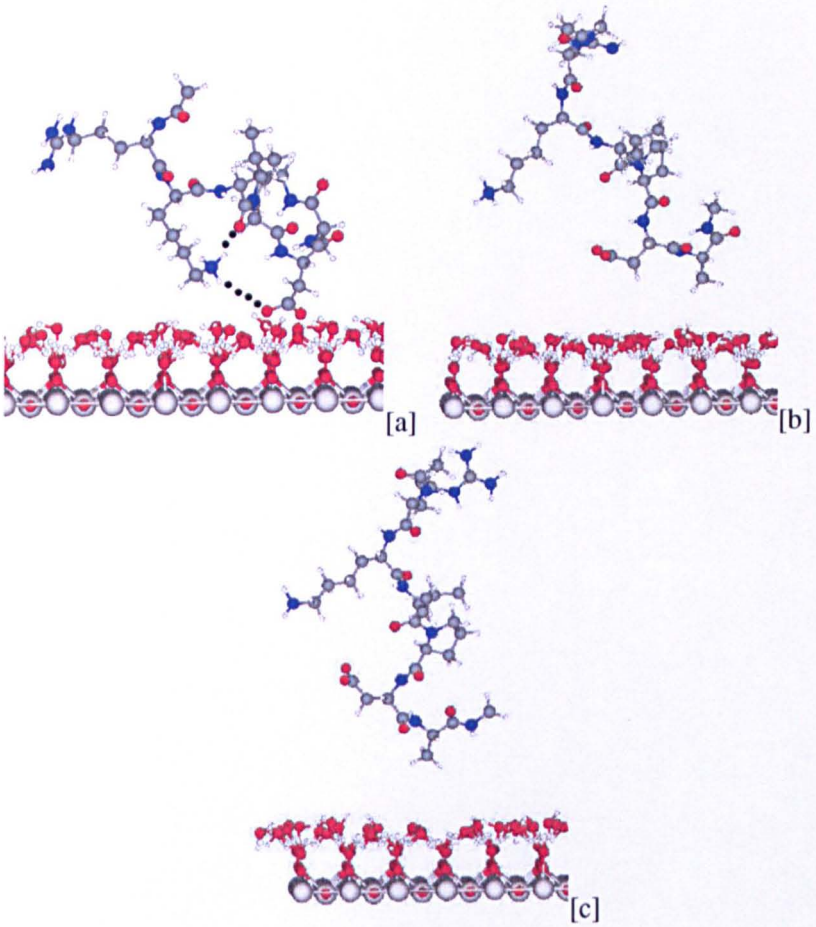

Figure 5.25: The configuration discussed in Section 5.4.2 at 2 ns[a], 2.25 ns[b] and 2.4 ns[c].

In order to characterise these interactions, the Asp-Lys and Asp-carbonyl distances are shown in Figure 5.26.

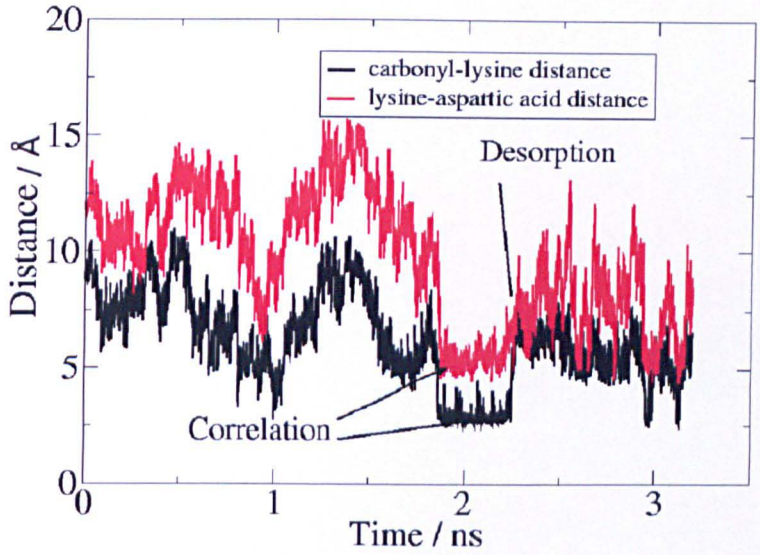

Figure 5.26: The Lys-Carbonyl and Lys-Asp distance.

It can be seen in Figure 5.26 that the two distances are correlated with each other from 1.9 ns to 2.3 ns (even prior to this point, they change in relation with each other). The Asp vertical-distance increases at 2.3 ns as the peptide leaves the surface (see Figure 5.24). The Lys-Asp and Lys-carbonyl distances also increase as the peptide desorbs indicating a correlation between the three events. This correlation strongly suggests that the three-way intramolecular interaction is key to this desorption mechanism.

This leads to further questions of the effect of Lys and why the Lys mutant (where Lys is replaced with Ala) has been found experimentally to yield a greater binding affinity. It is a possibility that the Lys can be responsible for the desorption and therefore mutating it would remove this mechanism and increase the affinity for adsorption. Later on in the chapter it will shown that such a mutation does indeed have this effect (at least using the model employed here).

The process by which the peptide desorbed has been characterised. Figure 5.25[b] and [c] show configurations at 2.2 ns and 2.4 ns as the peptide is desorbing from the surface.

It is apparent that bulk rotation was also important in this desorption mechanism. The peptide rotated so that the peptide was upright. The important point however was that as the peptide rotated away, the Lys was still in a position to interact with the Asp group as evidenced in Figure 5.26. It is possible that this interaction was responsible for pulling the Asp away from interaction with the structured layers of water. This would offer an explanation for the implication of this interaction in causing the desorption.

This section on adsorption/desorption mechanisms has shown the significance of bulk rotation for the peptide moving onto and off of the surface. No quantitative information about the kinetics of adsorption/desorption can obviously be obtained from these examples but insight has been gained into these processes, the possible causes for the mechanisms and peptide behaviour on surfaces in general.

5.5 Mutation of peptide on the surface

As mentioned earlier, Sano and Shiba performed alanine mutations and observed changes in binding affinity for particular mutations. In the previous chapter, the mutants were studied in water. In this section, results of simulations of the mutants on the surface will be shown. It will also be shown how they differ to simulations of the wildtype peptide on the surface and that insight has been gained into the effect of such mutations. As in the last chapter, the Pro and Lys-mutants will be concentrated on because the effect of these mutations are the least straightforward to rationalise. Since Lys is a likely candidate for surface binding, the gain in binding affinity with mutation seems counter-intuitive. Since Pro does not directly contribute to binding (it is a neutral group), the decrease in binding affinity for the Pro-mutant is also difficult to explain. Some of the binding configurations were taken, mutated, simulated and compared with the analogous wildtype simulations to test the effect of mutation on binding.

It should be noted that a lot of detail will be shown for these examples and this may seem unusual if only considering the effect of mutation. However, much analysis has

been performed not only to show this effect but also out of fundamental interest. Further mechanistic details and considerations can be highlighted in order to increase our knowledge of the behaviour of peptides on surfaces in general.

5.5.1 Pro mutation

5.5.1.1 Config DK mutation

The first interesting simulation is related to the last chapter where the wildtype and Pro-mutant starting in the α configuration, showed different behaviour. It was shown that the wildtype unwinded at a faster rate than the Pro-mutant and it was argued that the wildtype would not spontaneously adopt the α conformation.

In the following example, the Pro in Config DK was mutated into Ala, and the simulation was started immediately at 298K. It was later discovered that this procedure introduced problems because the water was not equilibrated at the start of the simulation. Nonetheless, interesting behaviour emerged which is worth presenting.

Figure 5.27 shows the running average of the number of backbone hydrogen bonds versus simulation time defined in the same way as in Section 4.5.1 (a hydrogen bond is counted when a carbonyl and N-H group are within 2.2 Å) for Config DK after mutation of Pro with Ala.

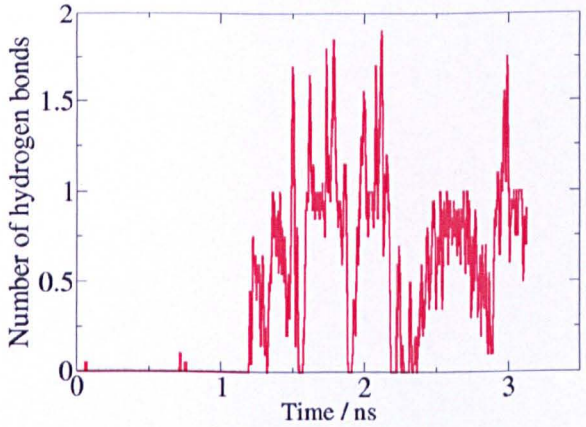

Figure 5.27: The running average of the number of backbone hydrogen bonds versus simulation time for Config DK after mutation of Pro with Ala on the surface.

It can be seen that there is an appearance of backbone hydrogen-bonds at 1.2 ns. It is assumed that the formation of backbone hydrogen bonds is not a result of the erroneous starting conditions because the system should have reached equilibration by 1.2 ns. After that, there are mainly one or two H-bonds denoted (i,i+4) and (i,i+7). This notation means there was a hydrogen bond between a carbonyl and NH, four and seven residues apart respectively. This would indicate that an α-helix has been formed, which is confirmed by the conformation at the end of the simulation, which is $\beta\alpha\alpha\alpha\beta\alpha$. The number of H-bonds for the wildtype is shown in Figure 5.28 for comparison.

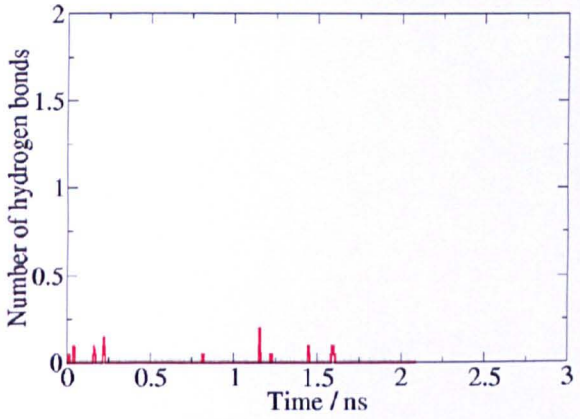

Figure 5.28: The running average of the number of backbone hydrogen bonds versus simulation time for Config DK wildtype on the surface.

It can be seen that although there is an appearance of H-bonds for the wildtype, they are transient whereas for the Pro-mutant they persist throughout the simulation. It should be noted that one or two H-bonds are highly significant for a such a small peptide. A configuration of the Pro-mutant on the surface has been shown in Figure 5.29.
This figure is included to give an idea of how compact the peptide is on the surface.
To further characterise this compactness, the radius of gyration of the peptide, Figure 5.30 has been plotted It starts at 7 Å and quickly decreases due to the starting conditions. The radius of gyration follows similar trends to the H-bond number, reaching a minimum when, the first H-bond starts to appear and increasing again momentarily when the H-bond decreases.

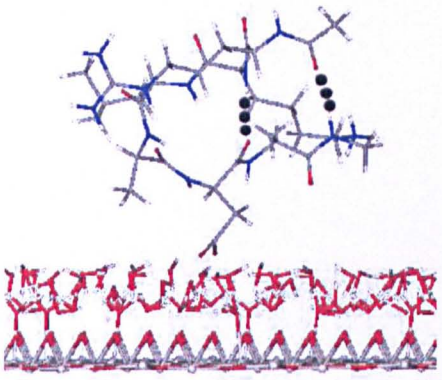

Figure 5.29: Configuration of Pro-mutated peptide after folding into α-helix. The molecule has been rendered as sticks for clarity.

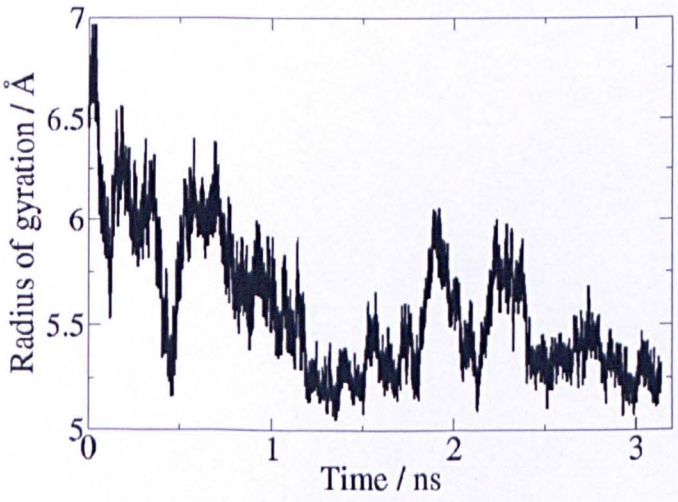

Figure 5.30: The radius of gyration of Config DK after mutation of Pro with Ala.

As emphasised, the starting conditions were not correct so we cannot definitely say that this would not happen for the wildtype (although for previous reason it has been suggested that it is unlikely). In order to test this, the peptide could be mutated back at around 1 ns (before it has started to form any H-bonds) and simulated. The results of this simulation cannot be used for direct comparison but are presented because they are interesting, show progression of work and highlight the issues involved in reaching equilibrium in a controlled way. They also show α-helix formation on the surface even after equilibrium has been reached (evidenced by H-bond formation). α-helix formation/unfolding on surfaces is a well studied area both computationally [169, 168] and experimentally [30, 28]. The other computational studies however showed α-helices becoming less compact and H-bonds breaking when adsorbed onto surfaces. The difference in behaviour could be related to the peptide sequence or surface type such as reported for polyalanine on an uncharged surface [169]) and the sequence DDIIDDII on a generic charged surface [168]). Mijajlovic and Biggs [169] found that the peptide became less compact with surface energy; perhaps the water-mediated nature of the interaction makes the surface energy weak enough for an α-helix to form. Mungikar and Forciniti also found unfolding on the surface. It was a suggested above (Config 4) that α-helices can be stabilised by certain interactions and this could be important *i.e.* perhaps no such interactions were present in the studies mentioned. This seems likely since polyalanine or DDIIDDII although may be able to interact with the surface, will not have the opportunity to self-interact (since they do not contain oppositely charged residues; probably a vital ingredient for surface-induced helix stabilization. Experimental results have shown α-helix promotion in certain proteins (α-chymotrysin adsorbed on a teflon surface [30]); this type of mechanism may be important in such proteins (although the hydrophobic teflon surface is quite different to hydrophilic titania). The starting configuration could also be important *i.e.* the peptide may have started in a favourable configuration for H-bonds to form. More work needs be performed for investigation of α-helix stability and formation on different surfaces and with different

sequences.

In order to start the simulation without introducing non-equilibrium effects, the previous simulation was brought to equilibrium slowly by using Procedure 1 (as outlined in Section 5.2). The initial motivation behind this was to test if the α-helix formation would happen if the water was able to solvate the peptide properly before letting the peptide move. It did have profound effects and the result was that the peptide desorbed from the surface. This can be seen by the vertical distance plot of Figure 5.31, where the Asp detaches from the surface at 0.2 ns and the Lys moves away at 0.5 ns.

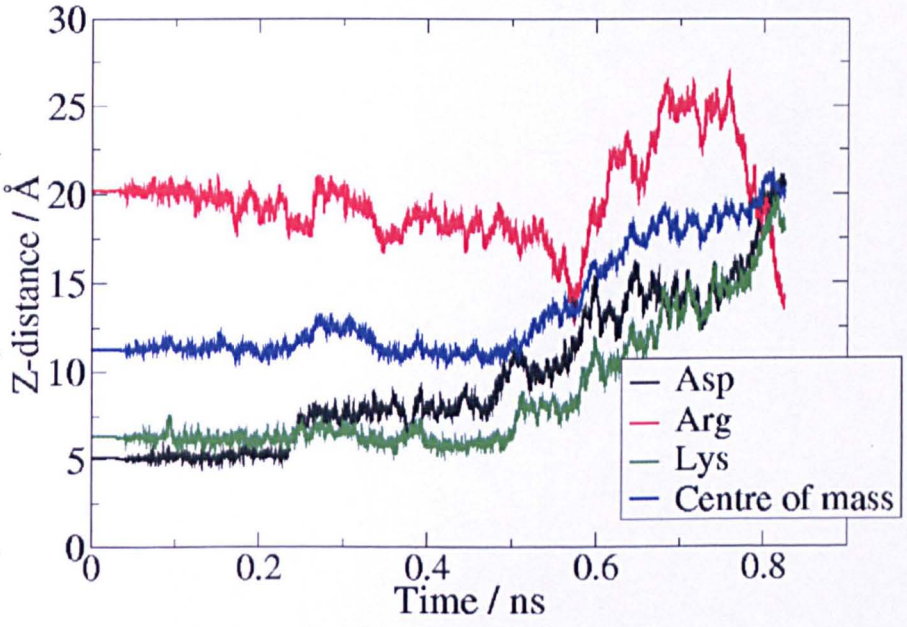

Figure 5.31: The vertical distance of Asp, Lys and Arg to the surface for the Pro-mutated peptide starting in Config DK, using Procedure 1.

It seems a reasonable explanation that the mutation of the Pro is responsible for the desorption, due to resultant additional flexibility of the backbone in the mutant case. In order to demonstrate this, the ϕ, ψ and ω angles of Pro(Ala) and Leu have been plotted and shown in Figures 5.32 and 5.34.

These are compared with analogous torsions in the wildtype in Figures 5.33 and 5.35. It can be seen that the "Pro"-ϕ fluctuates much more than is seen in the wildtype case. This could certainly have a destabilising effect on the binding configuration. Also there

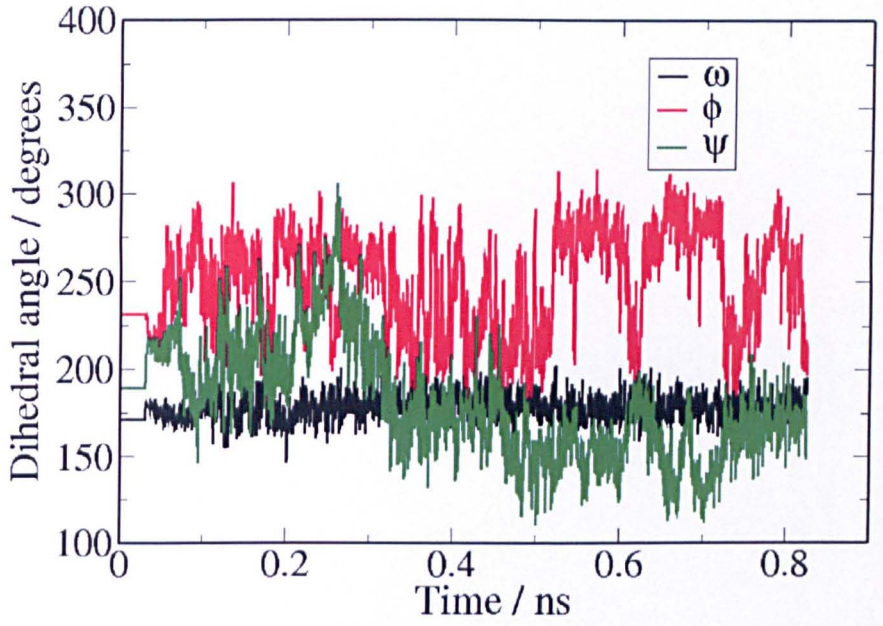

Figure 5.32: The ϕ, ψ and ω angles of 'Pro' for the Pro-mutant in Config DK.

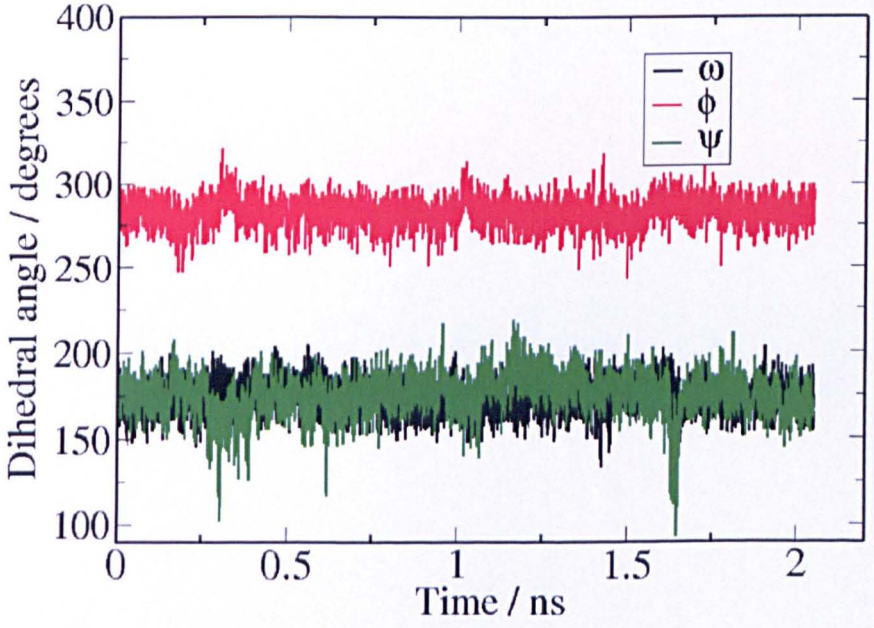

Figure 5.33: The ϕ, ψ and ω angles of Pro for the wildtype in Config DK.

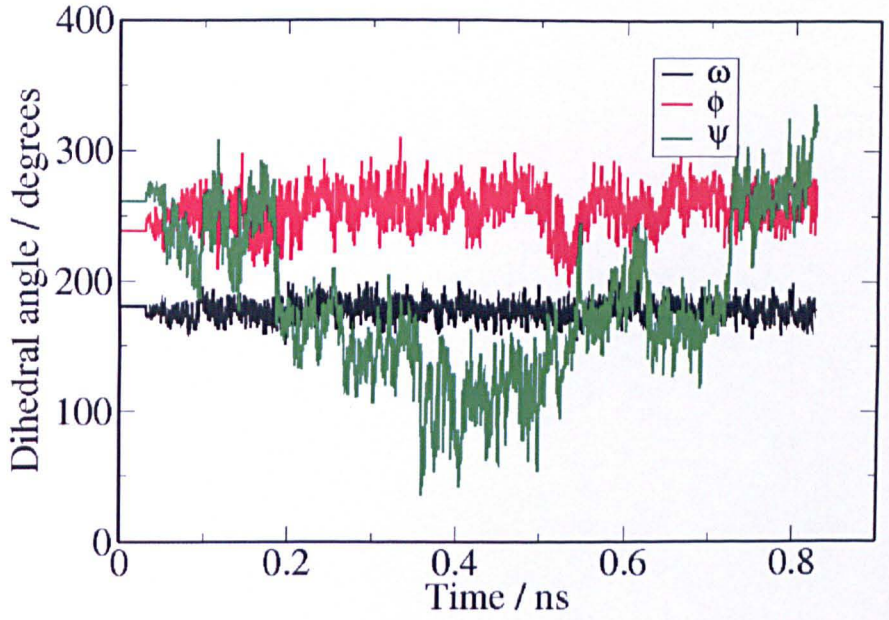

Figure 5.34: The ϕ, ψ and ω angles of Leu for the Pro-mutant in Config DK.

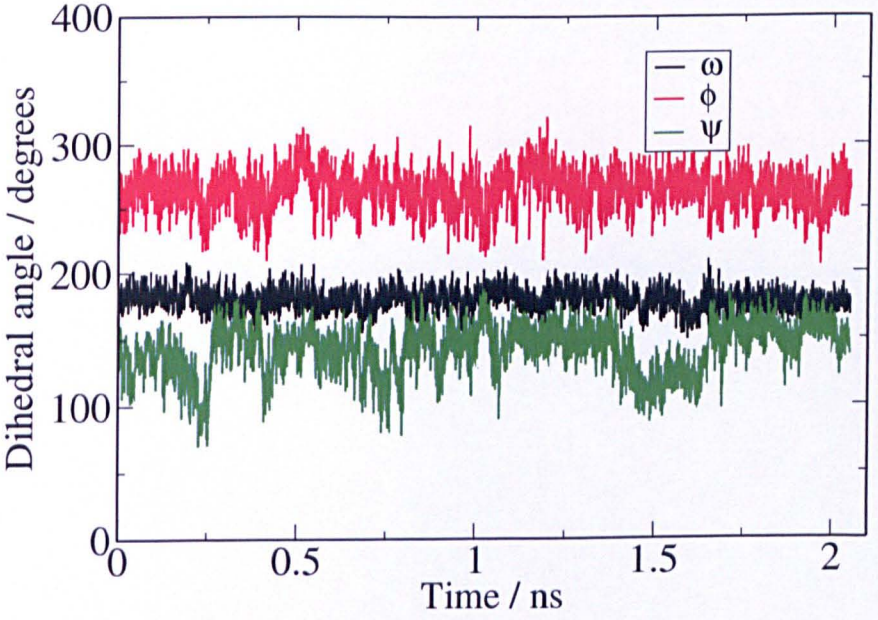

Figure 5.35: The ϕ, ψ and ω angles of Leu for the wildtype in Config DK.

are large jumps in both Leu and "Pro"-ψ angles corresponding to the desorption *i.e.* when Asp detaches from the surface. It can be seen (Figure 5.32 and 5.34) that these angles fluctuate significantly throughout the simulation, destabilising the binding configuration and causing a desorption event. For the wildtype however, the ϕ and ψ angles stay constant throughout the simulation and the ψ of Pro fluctuates a lot less (fluctuation of about 25° in the wildtype compared to about 100° in the Pro-mutant). This is a direct example of a situation where the wildtype binds to the surface but the Pro-mutant does not. It offers an explanation of why the binding affinity decreases after Pro mutation. As expected, it is the reduction in conformational stability which causes the desorption and it is feasible that the rigidity of the Pro is required to hold the binding groups in place. Since this binding configuration is available for the wildtype but not for the Pro-mutant, this suggests that there is a reduction in the number of binding configurations when Pro is mutated. We have already discussed that a large binding affinity may be due to many strong binding configurations. The effect discussed in this section could therefore occur for many binding configurations causing a significant reduction in the binding affinity. Also, it shows a desorption mechanism which is available for the Pro-mutant but not the wildtype. This could therefore cause an increase in desorption rate and significantly decrease the binding affinity (see discussion of adsorption/desorption rates above).

5.5.1.2 Config DR mutation

In order to further emphasise the effect of the Pro mutation on the binding of the peptide, the Pro-mutated Config DR will be considered. This is not quite as compelling as the previous example because there is not complete desorption due to Pro mutation, but it does show that the mutation has an effect which causes a conformational change and therefore affects binding. One point to note in this simulation is that the Arg and Asp are spatially very close. This means there is inherent stability in the structure and the Pro is not quite as essential for holding the binding structure rigid. This could be the reason why it does not desorb completely. In this example, particular detail will

be shown because there is a large conformational change on the surface, something which is rare when using conventional MD. This change will be deconvoluted into individual backbone torsion changes in an attempt to explain this change and further our knowledge of such processes. This feeds back to the sequence specificity since one residue may be less/more restrictive to the key torsion involved in the conformational change.

Firstly, snapshots at 2 ns, 2.1 ns and 2.35 ns of the simulation which started with Config DR but with the Pro mutated to Ala are shown in Figure 5.36. It can be seen that

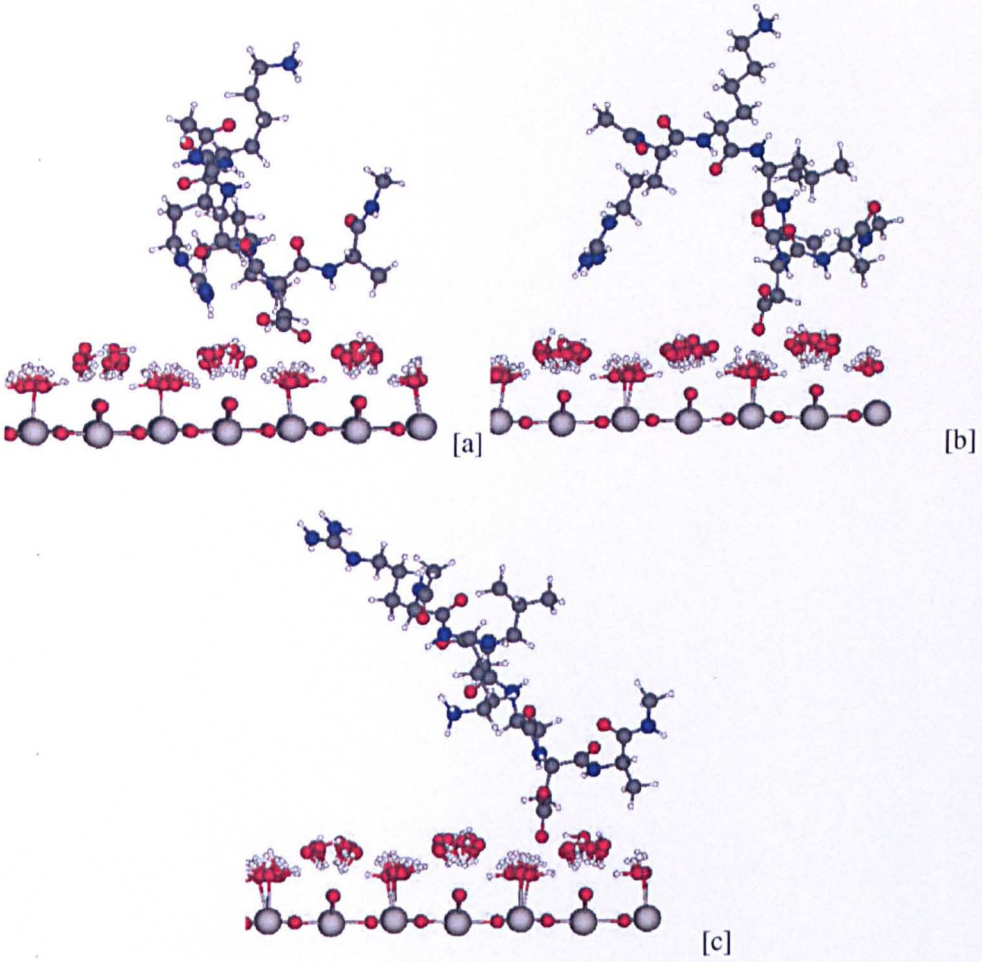

Figure 5.36: Snapshots at 2 ns[a], 2.1 ns[b] and 2.35 ns[c] during a simulation starting with the Pro-mutated Config DR.

throughout the simulation, the Arg moves away from the Asp and from the surface. This can be seen in Figure 5.37 which shows the vertical distances of the charged groups to the surface versus simulation time and Figure 5.38 which shows the distance of the Asp to the Arg versus time.

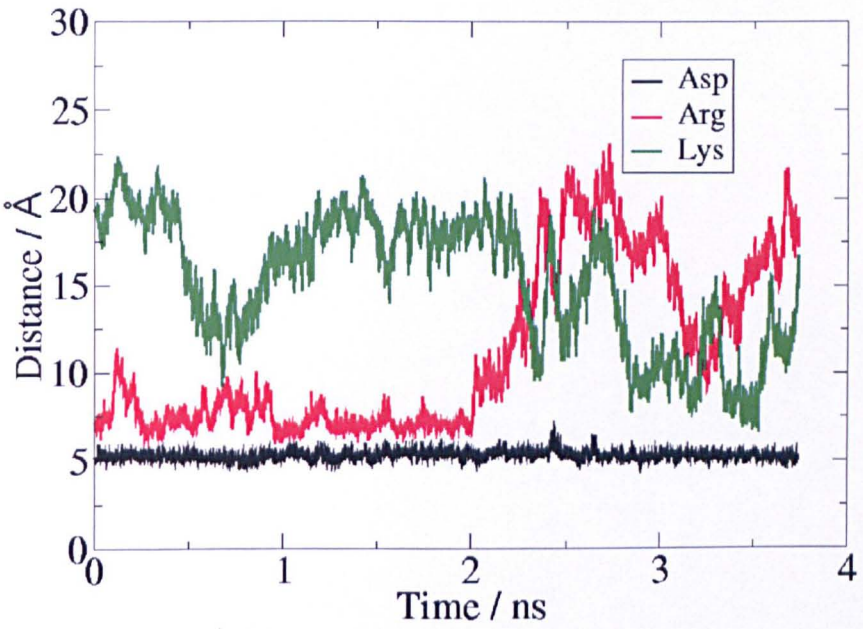

Figure 5.37: The vertical distance of Asp, Lys and Arg to the surface for the Pro-mutated peptide starting in Config DR.

It can be seen (Figure 5.37) that throughout this simulation, the Asp is bound to the surface. The main point however is that the Arg moves away from the surface at 2 ns and that the mutation of the Pro for Ala is probably responsible since this does not happen in the wildtype. It is likely that the absence of the Arg-surface interaction would make the interaction of the peptide with the surface weaker and this effect could contribute to a loss in binding affinity.

The Arg moving from the surface is also shown by an increase in the Arg-Asp distance, also at 2 ns (see Figure 5.38). The radius of gyration (defined in Section 4.5.1) was also plotted for further characterisation and shown in Figure 5.39.

It can be seen that there was a decrease in radius of gyration at about 400 ns and it was considered whether this collapse is due to the extra flexibility attributed to the mutation

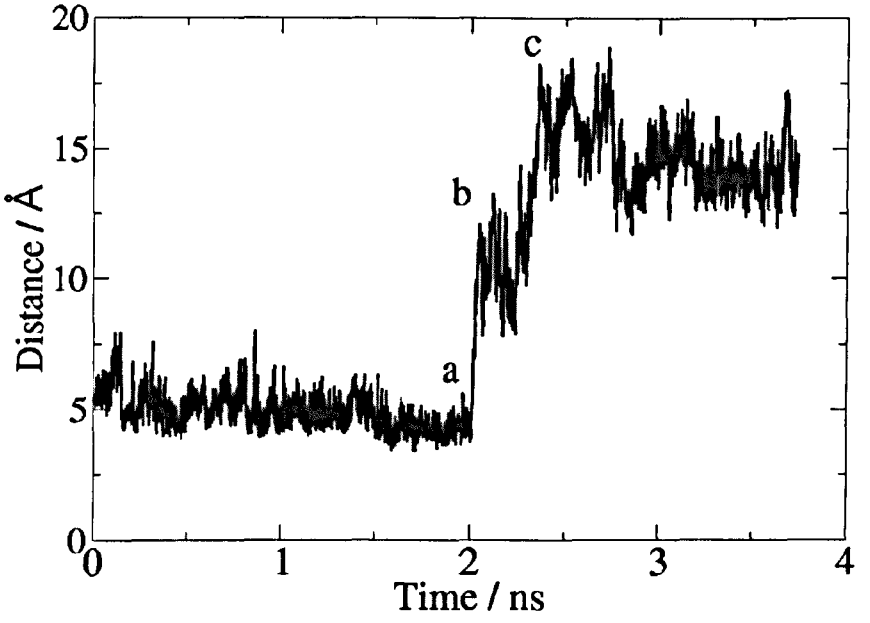

Figure 5.38: The Asp-Arg distance versus time for the pro-mutated peptide starting in Config DR. The annotated letters relate to snapshots in Figure 5.36.

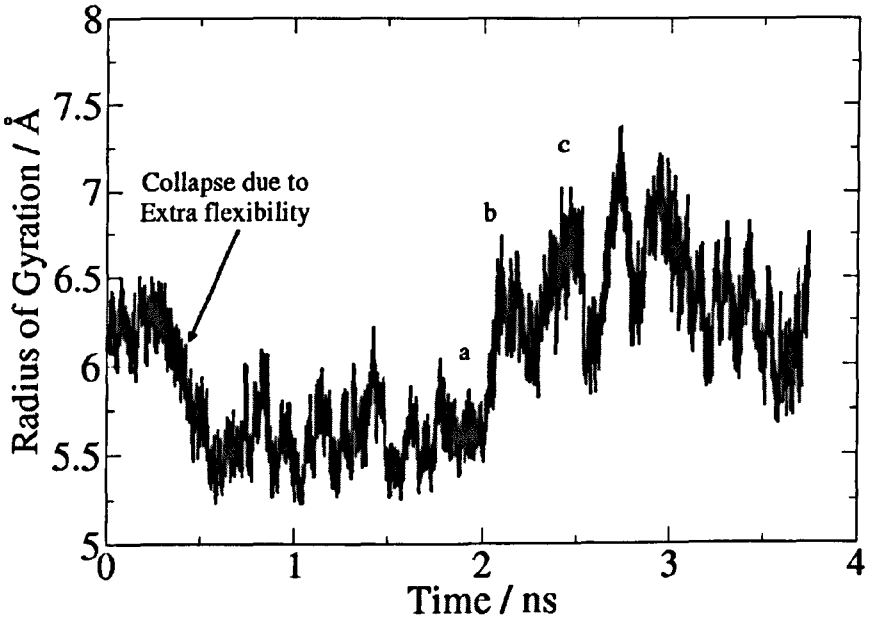

Figure 5.39: The radius of gyration versus time for the Pro-mutated peptide starting in Config DR. The annotated letters relate to snapshots in Figure 5.36.

of Pro. It can be noticed that the change in radius of gyration (from 2 - 2.7 ns) follows the same pattern as the change in Asp-Arg distance and the vertical distance of Arg from the surface.

In order to test whether a conformational change is responsible for the collapse and the Arg moving from the surface, the backbone torsions were considered. As in the last section, Pro and Leu torsions for the mutant (Figure 5.42 Pro, Figure 5.40 Leu) and wildtype (Figure 5.43 Pro, Figure 5.41 Leu) are shown.

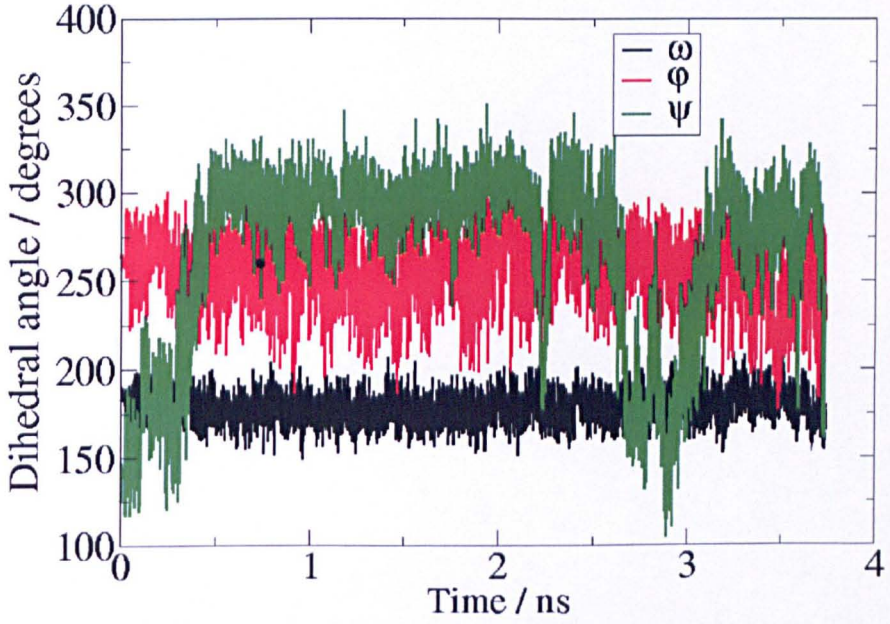

Figure 5.40: The torsion angles around Leu of the Pro-mutated peptide starting in Config DR.

The other torsions do not really change so are not shown. Before considering whether there were any sudden torsional changes which were responsible for the conformational change, it should be noted that the fluctuations in the Pro and Leu torsions were greater for the Pro-mutant than for the wildtype, especially the ϕ torsions. This is similar to other examples in the Pro-mutation section and the same arguments apply.

The conformational change of the Pro-mutant will now be explained. Since the conformational change is large, it seems likely that there are large torsional changes responsible. Therefore the torsions which showed a large change are shown. These include the

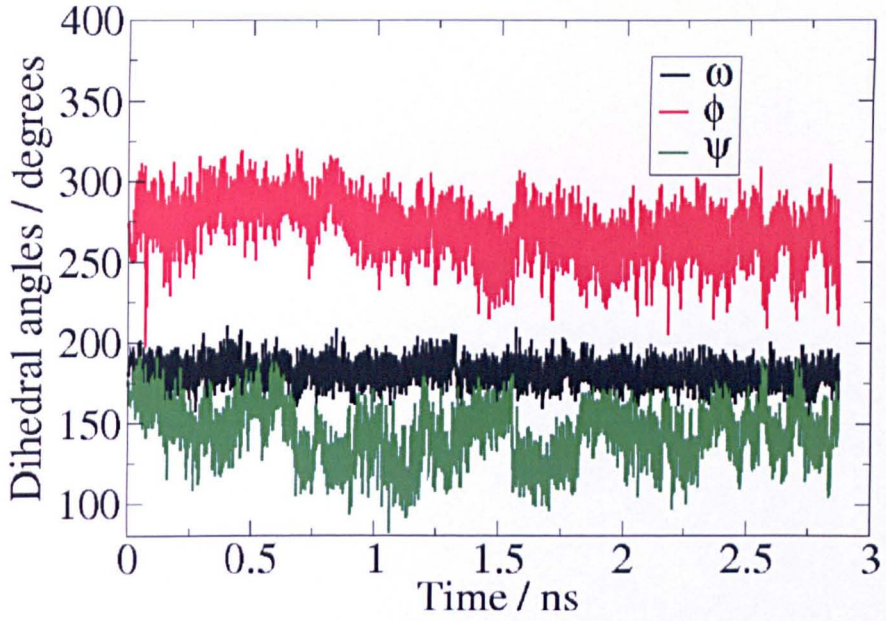

Figure 5.41: The torsion angles around Leu of the wildtype peptide in Config DR.

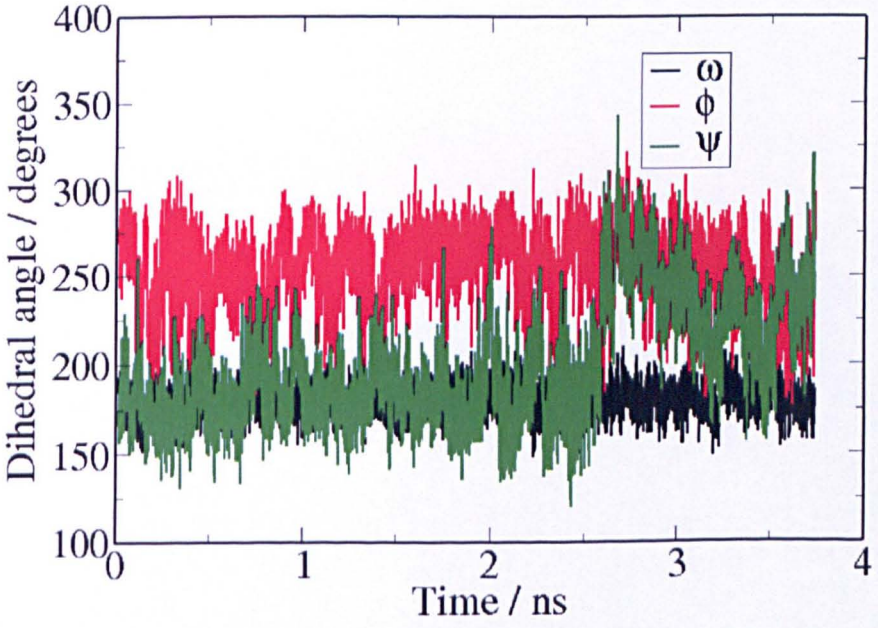

Figure 5.42: The torsion angles around "Pro" of the Pro-mutated peptide starting in Config DR.

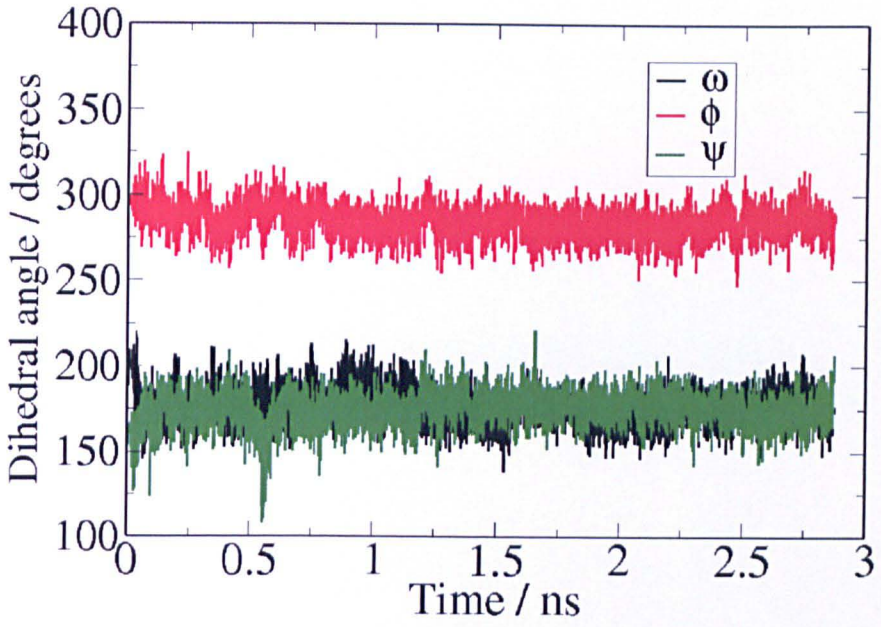

Figure 5.43: The torsion angles around Pro of the wildtype peptide in Config DR.

Leu and Pro torsions already shown and the torsions of Lys as seen in Figure 5.44.

The conformational change started at 2 ns (Figures 5.38, 5.39, 5.37) and at this point, there was a momentary increase in the Pro-ψ followed by a momentary decrease in Lys-ψ, which was then followed by a momentary decrease in Leu-ψ. At the end of this sequence of torsional events, the dihedrals are almost the same as they were before, yet the conformation is quite different, since the Arg is now further away from the Asp (distance increased from 5Å to 13Å). This is a good example of how conformational changes can occur without large changes in any one individual torsional angle but a cumulative effect of many torsional angles. It seems that this change is convoluted within the regular fluctuation of the other torsions (ϕ and ψ) in a highly correlated and complex way. This gives extra evidence to the suggestion that the mutation of the Pro can cause knock-on effects to the whole conformation, because the extra fluctuation available to these dihedrals after the mutation offers greater opportunity for torsional changes. These occur in a cumulative way and help to initiate changes in the other dihedral angles. During this period it can actually be seen (Figure 5.42) that the 'Pro'-ϕ

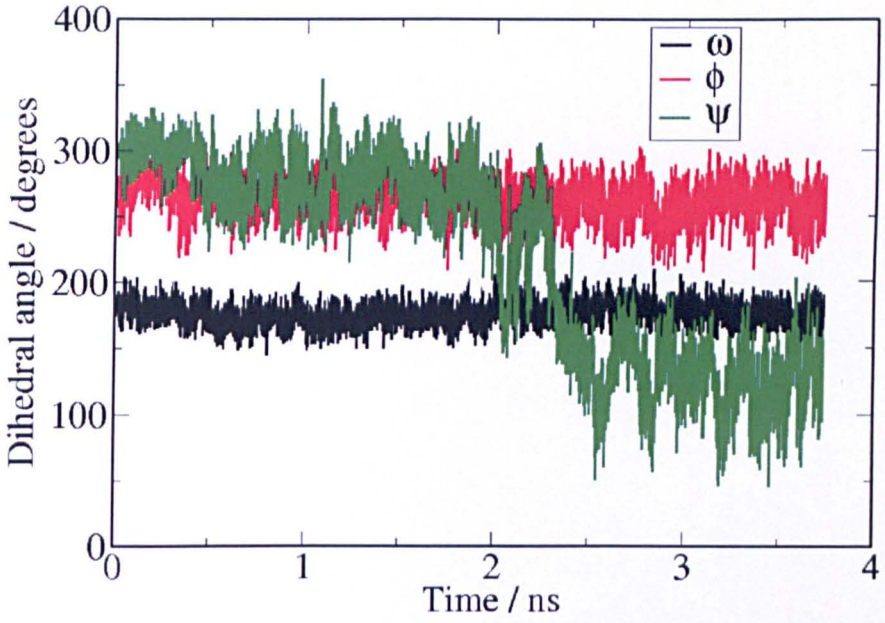

Figure 5.44: The torsion angles around Lys of the Pro-mutated peptide in configuration DR.

changes in an irregular way.

The remaining conformational change corresponding to the Asp-Arg distance increasing to 17.5 Å is possibly due to a large change in the Lys-ψ during the period from 2.2 ns to 2.6 ns. There are also changes in the Leu-ψ and Pro-ψ after 2.6 ns and these changes could be responsible for further changes in Asp-Arg distance, Arg vertical distance and radius of gyration.

This simulation shows that the mutation of Pro has effects beyond what was originally anticipated. For the wildtype, it seems unlikely that the Asp and Arg would come apart in the same way as the Pro-mutant had done. This is because of the rigidity of the Pro-torsions reinforcing the interaction of the Arg with the surface and Asp *i.e.* the Pro rigidity adds extra support to the binding structure. With the Pro-mutant however, this rigidity is not there and if the Arg momentarily moves away from the Asp, it is possible for the two groups to come apart.

The mutations of Config DK and Config DR have both shown differences to the wildtype. Both show situations which can offer an explanation for the experimental reduc-

tion in binding affinity with mutation of Pro for Ala.

5.5.2 Lys mutation

As mentioned earlier, the binding affinity increased when Lys was mutated. It was suggested that the interaction between Lys and Asp was responsible. A likely candidate for binding (wildtype) was found when performing a simulation of the peptide in water which had the $\beta\beta\alpha\beta\alpha\beta$ conformation. This conformation fulfils the coarse-grained criteria for an RD binder (that there are two α-torsions between Asp and Arg) as well as criteria 1 (see Section 5.3.6). The wildtype peptide was put on the surface on three separate occasions and given every chance to adsorb onto the surface by using Procedure 1. Every effort was made in order to get it to adsorb because it was hoped that it could be used as a further binding configuration. The peptide was rotated and translated on several occasions to generate many different initial conditions. The peptide did not stay bound to the surface however. This configuration starts in $\beta\beta\alpha\beta\alpha\beta$ conformation and can be seen in Figure 5.45.

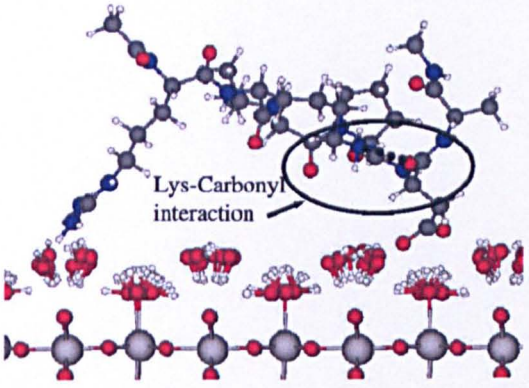

Figure 5.45: The Leu-α wildtype on the surface at 250 ps.

This is a snapshot at 250 ps, just before it comes off the surface. It seems to be in a favourable 'horseshoe' type configuration with the Asp and Arg bound to the surface

mediated by structured water. To demonstrate its desorption, the vertical distance versus time is shown in Figure 5.46

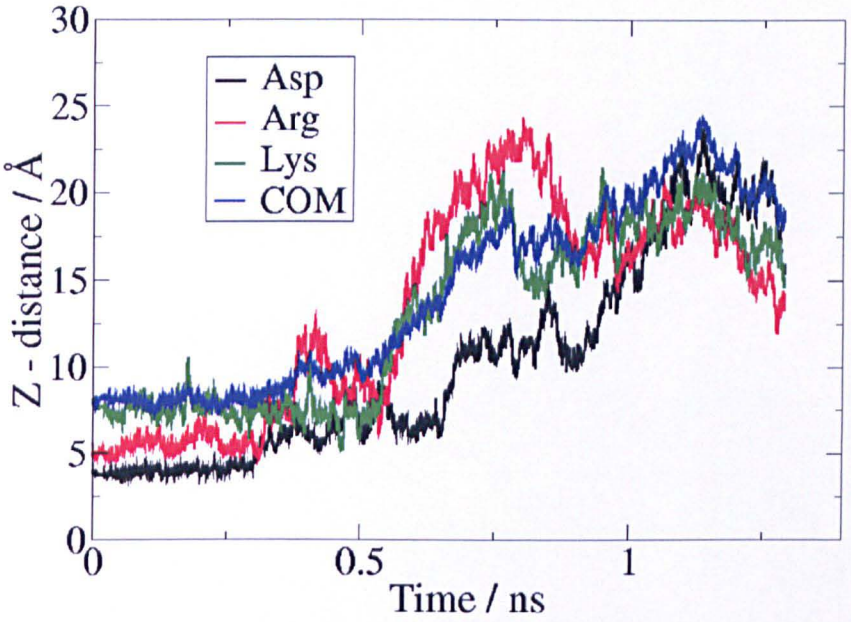

Figure 5.46: The vertical-distance versus time for Leu-α wildtype on the surface.

It shows that the wildtype is not stable on the surface and desorbed within 300 ns (at 300 ns the Asp moves away from the surface). This seemed surprising since it was considered a very likely binder. It was noticed that the Lys becomes very close to the Asp-Ala carbonyl and this is indicated in Figure 5.45. It was then considered whether this interaction was responsible for the desorption.

In order to test this, the Lys-mutant was put in the same starting configuration. It was found that the Lys-mutant did not desorb in the same way. Figure 5.47 shows the Arg and Asp vertical distance from the surface versus time and it can be seen that the Asp stays very close to the surface and the Arg continually moves on and off the surface for more than 2 ns. This suggests that there might be longer-term stability for the Lys-mutant than the wildtype. A configuration of the Lys-mutant is shown in Figure 5.48.

The stability of the binding configuration compared with the wildtype suggests that the Lys is involved in this desorption mechanism since when it is absent (and therefore

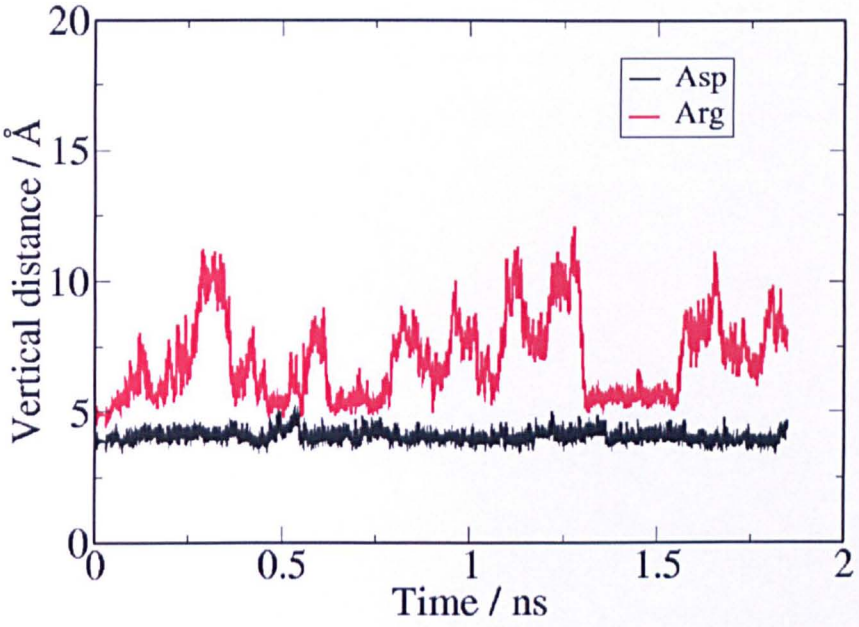

Figure 5.47: The z-distance versus time for Leu-α Lys-mutant on the surface.

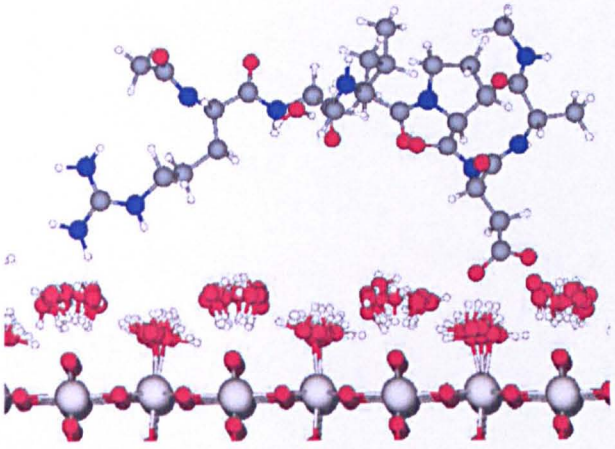

Figure 5.48: The Structure of the Leu-α Lys-mutant on the surface at 1.5 ns.

there is no Lys-Asp/carbonyl interaction) it does not desorb and would help yet again to explain the increase in binding affinity found by Sano and Shiba when the Lys is mutated for Ala. If this binding configuration is available for the Lys-mutant but not the wildtype, this would increase the binding affinity by providing an extra opportunity for binding. We could also extrapolate this result for other binding configurations and can envisage that the Lys-carbonyl interaction could have a similar influence. It has actually been observed on other occasions (see Section 5.4.2) that this interaction is possibly implicated in the desorption mechanism; this adds weight to the idea.

In order to rationalise the effect of the Lys-mutation, it would be helpful to analyse the mechanism of desorption and how the Lys is involved. The most obvious mechanism is that there is some sort of conformational or bulk rotational change. From analysis of torsions/bulk rotation analysis and visualisation however, it was evident that there were no major torsional changes or bulk rotational changes. It can be seen in Figure 5.45 that the peptide seems to be in a favourable configuration. However it moves off the surface without any appreciable torsional change or bulk rotation. It seems as if the peptide moves off the surface by a bulk translation, another possible desorption/adsorption mechanism (albeit a trivial one).

5.6 Other mutations

Simulations of the other mutants of Config DR and Config DK were also made. They showed binding which was very similar to the wildtype, except for the Asp-mutants which came free from the surface. The centre of mass of Asp-mutants starting with Config DR and Config DK are shown in Figure 5.49 to demonstrate this.

It can be seen that in both situations, the vertical distance of the centre of mass increased to a value greater than 15 Å showing that the Asp-mutated peptide detaches from the surface. This shows that the Asp is essential for binding of the peptide to the surface (when mediated by the structured water) and is in agreement with the experiment which

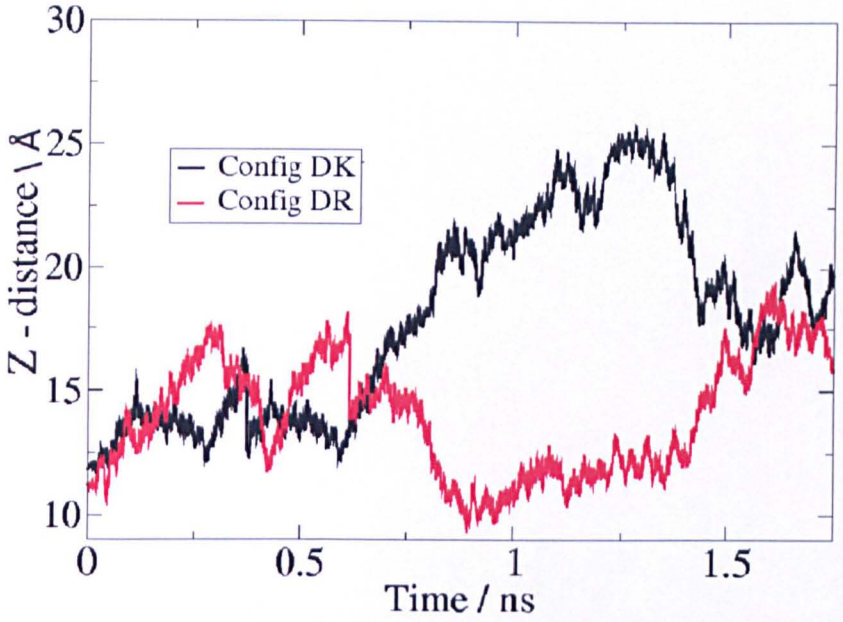

Figure 5.49: The vertical distance from the centre of mass to the surface for the Asp-mutants for Config DR and Config DK.

states that the binding affinity decreases when Asp is mutated. It may be still possible for binding of the the Asp-mutant to occur with direct contact with the surface. However it seems likely that at the very least, water mediated binding is an intermediate state for direct contact binding and therefore mutation removes this intermediate state, decreases the rate of binding and decreases the binding affinity.

The other mutation of interest was that of the Arg-mutation. This however was not as conclusive as the Asp-mutation because the Asp was still bound to the surface and therefore the peptide did not desorb on the simulation time scale. The binding affinity decreased however when Arg was mutated for Ala and speculations can be made on why this was the case. It should be thought that the interaction of the peptide with the surface would not be as strong without Arg *e.g.* Config DR would not be possible and would leave only DK binding configurations and ones where only Asp is bound to the surface. This would reduce the number of binding configurations and the strength of individual binding configurations and cause a reduction in binding affinity. Also, Arg may be may be implicated in the binding mechanism *i.e.* it may be the first group to

attach to the surface holding the peptide in position before Asp binds to the surface. It may also prevent a desorption mechanism *i.e.* if the Asp comes free, it may stop the peptide from desorbing allowing reattachment of Asp. All of these possible explanations seem plausible and would cause a decrease in the binding affinity for the Arg-mutant compared with wildtype.

The mutation simulations have shown agreement with experimental trends in binding affinity. This suggests that the model used has some validity and it has therefore been used to come up with explanations for the changes in binding affinity with mutation.

5.7 Conclusion

This chapter covered a range of important aspects when considering peptide binding to titania. These included, the effect of water structuring, validity of the force-field, the nature of binding to the surface, the mechanistic aspects of binding and the effect of Ala mutation on binding affinity.

Firstly, PDFT and force-field geometry optimisations of alanine on the non-hydroxylated surface were presented for comparison and validation of the force-field. Similar geometries were found for both optimisations in the likely global minimum. This gave some evidence that the force-field could be used although it is acknowledged that much more work needs to be performed in this area. Also in light of the simulation work showing water mediated binding, it may not be completely essential for the surface-peptide interaction to be completely accurate since the peptide, in water mediated configurations, binds to the water rather than the surface itself. The issue of direct versus water mediated binding however is still in question and depends on the dissociation state of the surface.

The effect of water structuring on peptide binding was investigated. It was found that the first two layers were highly structured and in the simulations presented, the peptide did not appear to be able to penetrate into these layers. It was shown that the two

charged groups Asp and Arg appeared in the third layers. The Asp oxygens were bound to the first layer waters whose hydrogens were facing away from the surface and second layer waters which are orientationally less ordered. It was argued that it is the strength of the interaction with water (shown by RDF's) and possibility for binding to different layers of water that makes the Asp such an important ingredient in the binding of the RKLPDA peptide to titania. The Arg hydrogens bind to the second layers of water but are not quite as crucial for binding in the simulation shown (An Asp-'surface water' interaction is always observed in stable water mediated binders in comparison to Arg-'surface water' interactions which have been observed to dissociate more readily).

Simulations were shown where the peptide started in a flat configuration with direct contact carbonyl-surface interactions. In one example, it was shown that the carbonyls however moved away from the surface and it was suggested that the driving force behind this was the displacement of these carbonyls by waters. This resulted in a 'horseshoe' type configuration. The interaction energies between the different components of the system were plotted and it was shown that although the surface-peptide binding decreased during this process, the water-peptide and water-surface binding increased to a greater extent. This suggested that the driving force behind the transition was the solvation of the peptide and surface. This put into doubt whether flat, direct contact configurations could be formed although says nothing about whether direct contact configurations are possible *i.e.* ones with only a few direct contact points. Of the other flat, direct contact simulations, most of these moved into a 'horseshoe' type configuration with only two or three direct binding points. This added extra evidence for suggesting the unfavourability of very flat configurations. One configuration however remained very flat after 1 ns. The different interaction energies were calculated and compared with the example earlier. It was shown that the favourable peptide-surface interaction energy of the flat configuration (compared with 'horseshoe' type structure) was far outweighed by the unfavourable peptide-water and water-surface energies. Again, this added extra evidence for suggesting that very flat configurations are unfavoured.

Two typical water-mediated binding configurations were shown. In both cases, the Asp was bound to the structured water. In Config DR, the Arg was also bound, in Config DK, the Lys was bound. It was shown that these groups were stable by calculating the RMSD and comparing with simulations made for these configurations in bulk water. Also simulations were performed where the surface was removed and the first two layers of water were held fixed. The peptide was still shown to be stable, indicating that in water mediated binding, the surface itself is not essential for binding. The surface however causes the water structuring so is indirectly responsible for the binding.

Another configuration was found where the Asp was bound via further layers of water. This type of configuration could be important for the binding mechanism although in this case, the peptide ended up desorbing from the surface. The fact that the peptide desorbed when there was no interaction between the Asp and first two layers of water at least showed how essential the Asp is for binding compared with the other groups. In this case, the interaction with the Lys and Arg and the surface was not enough for the peptide to stay bound to the surface.

Adsorption and desorption mechanisms were considered. These are important because a fast adsorption rate and slow desorption rate would mean a high binding affinity and vice versa. It is important to gain insight into the mechanisms for understanding which sequence makes a good binder. Two adsorption mechanisms were shown, both of them involved bulk rotation as a way of fine-tuning the peptide position for effective binding. Conformational changes were mostly beyond the timescale of conventional MD, so this aspect was not considered in this study.

A simulation showing a desorption event was highlighted. It was noticed that the Lys seemed to interact with the Asp and the Pro-Leu carbonyl. The distances between these groups and Lys was therefore plotted. It was shown that there was correlation between these two distances. Both the carbonyl-Lys and Asp-Lys distances became very close and eventually moved further from each other. At the same time, the peptide moved from the surface. This suggested that this interaction was implicated in the desorption

event. This insight helped us to suggest that these interactions are the reason the binding affinity does not decrease when the Lys is mutated experimentally.

Changes in binding affinity with mutation were further investigated by performing simulations of mutants on the surface. Lys and Pro were concentrated on because the changes in binding affinity with mutation were more difficult to explain and were thought to involve conformational factors. For Pro, the two water-mediated binding configurations were mutated and simulated. It was shown that in Config DK, the Pro-mutated peptide actually desorbed from the surface. It was suggested that the extra flexibility in Leu and Pro caused by the mutation was responsible for the destabilization of the binding configuration and desorption. This offered an explanation for the decrease in binding affinity in the Pro-mutant especially when considering that this effect could occur for many binding configurations, removing opportunities for binding. For Config DR, the peptide did not desorb but there was a conformational change which led to the Arg group moving from the surface. It was suggested that this conformational change did not occur in the wildtype because of the rigidity caused by the Pro. It is very likely that the Arg moving from the surface would decrease the strength of the interaction and therefore gives further insight into the cause of the diminished binding affinity with mutation of the Pro for Ala.

A simulation of a Lys-mutant was also performed and compared with the wildtype. It was found that whereas the wildtype desorbed, the Lys-mutant stayed bound to the surface. This gave evidence that interactions of Lys with different parts of the molecule are responsible for the decrease in binding affinity with mutation. It at least shows that this effect could contribute to a decrease in binding affinity even if there are also other causes.

Lastly, mutations of Asp for the two water-mediated binding configurations were made. It was shown for both configurations that this mutation caused desorption, agreeing with experimental binding affinity measurements.

The aim of this chapter was to gain insight into the binding of the RKLPDA peptide. It

was hoped that the reasons why this peptide is particularly strong binding to the surface would be illuminated. It was also hoped that the reasons for changes in binding affinity with mutation would be found. These are obviously related since mutations change the sequence and this helps the understanding of the binding (this is why Sano and Shiba performed these experiments). It has been found by this study that the peptide binds to the surface in a specific manner via charged groups. This is backed up by experiments that show binding of these charged groups to titania and mutagenesis experiments that show the importance of Asp and Arg in the binding.

The 'horseshoe' structure was first proposed by Sano and Shiba and a similar structure was independently found in the present study. Plausible explanations for effects of Lys and Pro mutations on binding affinities have also been made. These explanations originated from information gained from simulations using the model. These all show validation of the model and allow us to go further in predicting the behaviour of the peptide on the surface. One of the main results shown is that binding affinity does not just depend on the sum of the individual binding groups but involves comformational factors too. This work has therefore helped to highlight why sequence and not only amino acid composition generally dictates the binding.

The results obtained in this chapter have helped the understanding of the adsorption process and will hopefully help us to design peptides with the desired binding properties to titania and to surfaces in general.

Chapter 6

Conclusion and Outlook

The main aim of this thesis was to help to understand the interactions of peptides with surfaces so that we can potentially exploit this information in the control of adsorption of biomolecules on surfaces. Whether this is to prevent undesired adsorption or for biotechnological applications, it is important to understand what causes certain proteins/peptides to bind to certain surfaces so that either peptide or surface can be modified for the desired effect.

This thesis concentrated on titania surfaces which have specific applications in biosensors and titania implants. It is important to understand how peptides bind to the implant surface since interaction of various proteins can govern their biocompatability. Titania biosensors involve the immobilization of enzymes and it is possible to insert strong binding peptides into proteins and increase their binding affinity[32]. Therefore, it is important to find peptides which are strong binding, understand why they are strong binding and ultimately be able to fine-tune enzyme binding to titania. In this thesis, insight into the key characteristics of binding has been found. These have included electrostatic and conformational factors.

The key experimental work which this study was attempting to compare with and gain insight into was that by Sano and Shiba [1]. In this study, a strong binding peptide, RKLPDA was found by phage display. Changes in binding affinity were found when

certain residues were mutated for alanine. One of the main aims of this project was to understand why RKLPDA was strong binding and why the mutations caused changes in binding affinity. Molecular modelling, specifically classical molecular dynamics was employed for this aim. The results of the thesis were split into three chapters each concentrating on different aspects of the peptide/water/surface interface.

Chapter 3 involved the interaction of the rutile (110) surface with water. This is a complicated interaction since the surface is reactive to water and it is still unclear to what extent dissociation of water takes place. In order to address this, a model which could take a range of dissociation states into consideration was used. Chapter 3 was absolutely essential for this thesis for many reasons. Firstly, validation of the force-field (with respect to water-surface interactions) was made by comparing force-field calculations with analogous PDFT calculations. Also MD simulations (using TIP3P) were performed and compared with previous MD simulations using SPC/E water. Agreement was shown and the significance of this was that it showed that TIP3P was as good as SPC/E water for describing the water/titania interface and could be used in simulations of the peptide on the surface using the Charmm protein force-field. Agreements were also shown with in-situ x-ray data, again showing validation. This validation was essential for us to have confidence in our model.

The water structuring perpendicular to the surface as well as orientation caused by the surface was determined. This helped us to postulate that these structured layers of water would not only be a barrier to direct contact of the peptide with the surface but may actually present a surface of its own, which the peptide can interact with. It also helped to put this work in the context of the real surface. Even though the interaction of the peptide with the other surfaces (hydroxylated and negative) was not studied, it can be appreciated that the real surface may have subtleties beyond the scope of this project.

Chapter 4 studied the behaviour of the peptide in water. It concentrated on conformational aspects of the peptide considering how this could potentially affect the peptide adsorption onto the titania surface. The cases of mutation of Lys and Pro with Ala were

concentrated on because the explanations of how the binding affinity changes upon mutation were more difficult to understand in terms of reduction in viable binding groups. The binding affinity of the peptide increased when Lys was mutated for Ala even though it is known to be a binder to titania and the binding affinity decreased when Pro was mutated despite it being a neutral group. It was therefore considered that these changes must be conformational in nature. It was noticed on many occasions that Lys bound to Asp and the end-carbonyls and was considered whether these interactions caused the decrease in binding affinity. Reasons for this change that were suggested were 1) an increased stability of the peptide in water and therefore a decreased stability gain upon adsorption, 2) a reduction in the population of possible binding configurations and 3) an increase in compact conformations for the wildtype peptide compared to the Lys-mutant.

It was shown that there was an increase in the flexibility of the backbone when the Pro was mutated for Ala. It was suggested that this extra flexibility would mean that the conformational entropy was greater in the Pro-mutant than the wildtype and this would lead to a greater entropy loss upon adsorption of the Pro-mutant to the surface compared with the wildtype.

Chapter 4 was useful for this project because it helped to highlight certain issues which could then be considered when modelling the peptide/water/surface interface. It was suggested in this chapter that when studying binding affinities we not only have to consider the behaviour of peptides when adsorbed onto surfaces but also their behaviour in bulk water since they must transfer from bulk water to the surface in order to bind.

Chapter 5 showed the results of simulations of the peptide and selected mutants on the non-hydroxylated titania surface. It was found that the charged groups bound to the surface via the structured water which agreed with the many experimental studies indicating charged-group to titania interactions. The 'horseshoe' structure, first proposed by Sano and Shiba, was found to be important. It was also shown that the surface in itself was not essential for binding but rather that the peptide is bound to the structured

water above the surface.

Adsorption and desorption mechanisms were studied and it was shown that in the timescale of simulation the main modes of adsorption and desorption were bulk rotation of the whole molecule. It was proposed that this bulk rotation is a way of fine-tuning the peptide position for effective binding.

Mutations of Pro were made for the binding configurations and different behaviour was found between the Pro-mutant and wildtype. In one example, the Pro-mutant peptide desorbed and in another example, a conformational change occurred causing the Arg to detach from the surface, thereby weakening the interaction of the peptide with the surface. It was shown that the fluctuation of the backbone dihedrals of the peptides on the surface was much greater for the Pro-mutant than wildtype. It was suggested that these extra fluctuations are responsible for the destabilization of the binding configuration, specifically the 'horseshoe' configuration.

Simulations comparing the wildtype and Lys-mutant showed an example where the Lys-mutant bound to the surface, yet the wildtype did not. The difference between them was a Lys-carbonyl interaction which further indicated that these interactions were responsible for the lower binding affinity of the wildtype compared with the Lys-mutant. Many different factors were suggested to account for the differences in binding affinity of Lys and Pro-mutants compared with the wildtype peptide in both Chapters 4 and 5. It is possible that all of these factors have a small affect but when they are combined, large changes in binding affinity can be observed. These effects may not always be all in the same direction. For example it is very possible that Lys does bind to the surface but other conformational factors dominate in order to make the Lys-mutant bind with a greater affinity to the surface than the wildtype. This shows how complicated peptide-surface binding actually is, especially when conformational aspects dominate. It demonstrates that the binding affinity of a particular peptide does not just depend on how many binding groups there are, but also conformational factors which will probably be sequence specific. This work has therefore helped to highlight why sequence and not

only residue composition generally dictates the binding.

This thesis has covered many aspects which need to be considered for the understanding of peptide binding to titania surfaces and surfaces in general. It has has given insight into the nature of the water-surface interface, the conformational behaviour of surface-binding peptides and the binding of said peptides to the titania surface.

Obviously, more work could to be done for fuller understanding of this complicated field. These can be divided into short term work and long-term work. Short term work is that which can be achieved with the model already available or work to improve the model. Long-term work will involve taking into consideration what we actually want to achieve scientifically and devising models (and experiments) for the achievement of these aims.

For the short term, the obvious next step would be to put the peptide on the hydroxylated surface to test whether there are any differences in binding. The negatively-charged surfaces would also be interesting especially since the TiO_2 surface has been found to be negatively-charged under physiological pH.

Other work which could be performed would be further improvement and validation of the force-field, especially the peptide-surface interaction parameters. It would also be helpful to perform simulations which could increase the sampling of peptide conformations when bound on the surface and be able to calculate the changes in free energy of adsorption. This would give us more definite answers to whether our model was correct since we could then compare with experimental data such as SPR experiments. The more complicated contributions such as entropic contributions could also be quantified and we could gain greater understanding of the system.

To analyse the longer-term future work, we should evaluate the aims of the project. In order to understand the implications of peptide binding to the biocompatability of Ti implants, it is important to further understand the effects of the binding of specific proteins to the surface. How does the binding of certain proteins actually cause biocompatibility or a lack of biocompatibility? It is possible that the similar electrostatic contributions to

the ones studied here are responsible for the binding of whole proteins to the surface? We could modify the surface in such a way as to reduce these electrostatic contributions and eventually test these surfaces for their biocompatibility (*in-vitro*). Obviously, it would be helpful to model these systems in order to understand which materials are good at limiting or increasing the binding. It is also important to understand the true nature of the titanium dioxide on the surface of titanium metal when it is oxidised. What is the phase of the titania? What surface is actually exposed? Is the surface flat or stepped? How would these factors affect the binding? Could we treat the titanium differently to obtain the phase/surface *etc* which give us the desired binding affinity?
For biosensors applications, it is more of a defined challenge since the proteins and kind of surface used can be controlled and chosen. It is still important to understand the nature of the different phases/surfaces and how peptides bind to these surfaces in order to be able to choose the best surface materials for such biosensors. It can be envisaged that peptides like the RKLPDA peptide can be inserted into enzymes (as in earlier experimental work [81, 82]) and therefore it would be important to find and understand binders with different binding affinities to further control this process.
One of the main aims of the project was to gain fundamental understanding of peptide adsorption. This study has done this and the knowledge obtained will hopefully help us to develop technologies which can successfully exploit peptide adsorption to inorganic surfaces.

References

[1] K. I. Sano and K. Shiba. J. Am. Chem. Soc. **125**, 14234 (2003).

[2] M. Predota, A. V. Bandura, P. T. Cummings, J. D. Kubicki, D. J. Wesolowski, A. A. Chialvo, and M. L. Machesky. J. Phys. Chem. B **108**, 12049 (2004).

[3] A. V. Bandura and J. D. Kubicki. J. Phys. Chem. B. **107**, 11072 (2003).

[4] W. L. Jorgenson. J. Am. Chem. Soc. **103**, 335 (1981).

[5] P. Mark and L. Nilsson. J. Phys. Chem. A **105** (2002).

[6] Z. Zhang, P. Fenter, L. Cheng, N. C. Sturchio, M. J. Bedzyk, M. Predota, A. Bandura, O. J. D. Kubicki, P. T. C. S. N. Lvov, A. A. Chialvo, M. K. Ridley, P. Banazeth, L. A. D. A. Palmer, M. L. Machesky, and D. J. Wesolowski. Langmuir **20**, 4954 (2004).

[7] B. K. Ho, A. Thomas, and R. Brasseur. Prot. Sci. **12**, 2508 (2003).

[8] M. Sarikaya, C. Tamerler, A. K. Y. Jen, K. Schulten, and F.Baneyx. Nat. Mater. **2**, 577 (2003).

[9] K. Nakanishi, T. Sakiyama, and K. Imamura. J. Biosci. Bioeng. **91**, 233 (2001).

[10] V. Hlady and J. Buijs. Curr. Opin. Biotechnol. **7**, 72 (1996).

[11] M. Malmsten, D. Muller, and B. Lassen. J. Colloid Interface Sci. **193**, 88 (1997).

[12] S. Yamamoto and T. Ishihara. Sep. Sci. Technol. **35**, 1707 (2000).

[13] B. C. Robertson and A. L. Zydney. J. Colloid Interface Sci. **134**, 563 (1990).

[14] M. R. Duncan, J. M. Lee, and M. P. Warchol. Int. J. Pharm. **120**, 179 (1995).

[15] S. R. Whaley, D. S. English, E. L. Hu, P. F. Barbara, and A. M. Belcher. Nature **405**, 665 (2000).

[16] A. M. Belcher, X. H. Wu, R. J. Christensen, P. K. Hansma, G. D. Stucky, and D. E. Morse. Nature **381**, 56 (1996).

[17] S. Brown, M. Sarikaya, and E. Johnson. J. Mol. Biol. **299**, 725 (2000).

[18] E. Topoglidis, A. E. G. Cass, B. O'Regan, and J. R.Durrant. J. Elec. Anal. Chem. **517**, 20 (2001).

[19] E. Topoglidis, C. J. Campbell, A. E. G. Cass, and J. R. Durrant. Langmuir **17**, 7899 (2001).

[20] E. Topoglidis, T. Lutz, R. L. Willis, C. J. Barnet, A. E. G. Cass, and J. R. Durrant. Faraday. Discuss. **116**, 35 (2000).

[21] E. Topoglidis, A. E. G. Cass, G. Gilardi, N. B. S. Sadeghi, and J. R. Durrant. Anal. Chem. **70**, 5111 (1998).

[22] M. Tirrell, E. Kokkoli, and M. Biesalski. Surf. Sci. **500**, 61 (2002).

[23] J. M. Berg, J. L. Tymoczko, and L. Stryer. W. H. Freeman and Company, New York **Sixth edition** (2007).

[24] P. E. Wright, H. J. Dyson, and R. A. Lerner. Biochemistry **27**, 7167 (1988).

[25] H. J. Dyson and P. E. Wright. Annu. Rev. Biophys. Biophys. Chem. **20**, 519 (1991).

[26] S. Brahms and J. Brahms. J. Mol. Biol. **138**, 149 (1980).

[27] A. D. Roddick-Lanzilotta and A. J. McQuillan. J. Colloid Interface Sci. **217**,, 194 (1999).

[28] D. R. Lu and K. Park. J. Colloid Interface Sci. **144**, 271 (1991).

[29] D. C. Cullen and C. R. Lowe. J. Colloid Interface Sci. **166**, 102 (1994).

[30] T. Zoungrana, G. H. Findenegg, , and W. Norde. J. Colloid Interface. Sci. **190**, 437 (1997).

[31] M. H. Baron, M. Revault, S. Servagent-Noinville, J. Abadie, and H. Quiquampoix. J. Colloid Interface Sci. **214**, 319 (1999).

[32] H. Dai, W.-S. Choe, C. K. Thai, M. Sarikaya, B. A. Traxler, F. Baneyx, and D. T. Schwartz. J. Am. Chem. Soc. **127**, 15637 (2005).

[33] N. C. Seeman and A. M. Belcher. Proc. Natl. Acad. Sci. U.S.A. **99**, 6451 (2002).

[34] J. J. Gray. Cur. Opin. Stuct. Biol. p. 110 (2004).

[35] W. Yue, A. N. Kulak, and F. C. Meldrum. J. Mater. Chem. **16** (2005).

[36] R. J. Parka and F. C. Meldrum. J. Mater. Chem. **14**, 2291 (2004).

[37] F. C. Meldrum and S. T. Hyde. J. Cryst. Growth **231**, 544 (2001).

[38] M. L. S. Thachepan, S. A. Davis, and S. Mann. Chem. Mater. **18**, 3557 (2006).

[39] J. B. Thompson, G. T. Paloczi, J. H. Kindt, M. Michenfelder, B. L. Smith, G. Stucky, D. E. Morse, and P. K. Hansma. Biophys. J . **79**, 3307 (2000).

[40] J. L. Kulp, T. Minamisawa, K. Shiba, M. Terjana, and J. S. Evans. Langmuir **23** (2007).

[41] S. Collino and J. S. Evans. Biomacromolecules **8** (2007).

[42] R. R. Naik, S. J. Stringer, G. Agarwal, S. E. Jones, and M. O. Stone. Nat. Mater. **1**, 169 (2002).

[43] D. J. H. Gaskin, K. Starck, and E. N. Vulfson. Biotechnol. Lett. **22**, 1211 (2000).

[44] S. Wang, E. S. Humphreys, S.-Y. Chung, D. f. Delduco, S. R. Lustig, H. Wang, K. N. Parker, N. W. Rizzo, S. Subramoney, Y.-M. Chiang, and A. Jagota. Nat. Mater. p. 196 (2003).

[45] C. Tamerler, M. Duman, E. E. Oren, M. Gungormus, X. Xiong, T. Kacar, B. A. Parviz, and M. Sarikaya. Small **2**, 1372 (2006).

[46] S.-W. Lee, C. Mao, C. E. Flynn, and A. M. Belcher. Science **296**, 892 (2002).

[47] G. M. Whitesides, J. P. Mathias, and C. T. Seto. Science **254**, 1312 (1991).

[48] G. M. Whitesides and B. Grzybowski. Science **292**, 2418 (2002).

[49] C. E. Giacomelli and W. Norde. J. Colloid Interface Sci. **233**, 234 (2001).

[50] T. R. Walsh. Unpublished (2007).

[51] W. Norde and A. C. I. Anusiem. Colloids Surf. **66**, 73 (1992).

[52] B. Liedberg, B. Ivarsson, P. O. Hegg, and I. Lundstrom. J. Colloid Interface Sci. **114**, 386 (1986).

[53] P. A. Mulheran and D. A. Robbie. Phys. Rev. B **64** (2001).

[54] J. J. Ramsden. Chem. Soc. Rev. p. 73 (1995).

[55] T. Sakayama, I. Tanino, M. Urakawa, K. Imamura, T. Takahashi, T. Naga, and K. Nakanishi. J. Biosci. Bioeng. **88**, 536 (1999).

[56] F. Baneyx and D. T. Schwartz. Curr. Opin. Biotechnol. **18**, 312 (2007).

[57] U. Kriplani and B. K. Kay. Curr. Opin. Biotechnol. **16**, 470 (2005).

[58] C. Tamerler, S. Dincer, D. Heidel, H. Zareie, and M. Sarikaya. Prog. Org. Coat. **47**, 267 (2003).

[59] S. Brown. Proc. Natl. Acad. Sci. **89**, 8651 (1992).

[60] S. Brown. Nat. Biotechnol. **15**, 8651 (1997).

[61] S. Nygaard, R. Wendelbo, and S. Brown. Adv. Mater. **14**, 1853 (2002).

[62] C. K. Thai, H. Dai, M. S. R. Sastry, M. Sarikaya, D. T. Schwartz, and F. Baneyx. Biotechnol. Bioeng. **87**, 129 (2004).

[63] K. Kjaergaard, J. K. Sorensen, M. A. Schembri, and P. Klemm. Appl. Env. Micro. **66**, 10 (2000).

[64] E. Eteshola, L. J. Brillson, and S. C. Lee. Biomol. Eng **22**, 201 (2005).

[65] E. E. Oren, C. Tamerler, D. Sahin, M. Hnilova, U. O. Safak, M. Sarikaya, and R. Samudrala. Bioinformatics (2007).

[66] K. Goede, P. Busch, and M. Grundmann. Nano lett. **4**, 2115 (2004).

[67] D. Kase, J. L. K. III, M. Yudasaka, J. S. Spenser, S. Iijima, and K. Shiba. Langmuir **20**, 8989 (2004).

[68] U. Diebold. Surf. Sci. Rep. p. 53 (2003).

[69] T. J. Beck, A. Klust, M. Batzill, U. Diebold, C. Valentin, and A.Selloni. Phys. Rev. Lett. **93**, 3 (2004).

[70] U. Diebold. Appl. Phys. A **76**, 681 (2003).

[71] D. Dobson, P. A. Connor, and A. J. McQuillan. Langmuir **13**, 2614 (1997).

[72] P. A. Connor, K. D. Dobson, and A. J. McQuillan. Langmuir **15**, 2402 (1999,).

[73] S.-J. Xiao, M. Textor, and N. D. Spencer. Langmuir **14**, 5507 (1998).

[74] T. Albrektsson and H.-A. Hansson. Biomaterials **7**, 7986 (1986).

[75] B. Kasemo and J. Gold. Adv. Dent. Res. p. 8 (1999).

[76] D. A. Puleo and A. Nanci. Biomaterials **20**, 2311 (1999).

[77] C. E. Giacomelli, M. J. Esplandiu, P. I. Ortiz, M. J. Avena, and C. P. D. Pauli. J. Colloid Interface Sci. **193**, 88 (1999).

[78] V. Ball, A. Bentaleb, J. Hemmerle, J. C. Voegel, and P. Schaaf. Langmuir **12**, 1614 (1996).

[79] S. E. Moultona, J. N. Bariscia, A. J. McQuillanb, and G. G. Wallace. Colloids Surf., A **220**, 159 (2003).

[80] M. B. Hugenschmidt, L. Gamble, and C. T. Campbell. Surf. Sci. **302**, 329 (1994).

[81] T. Hayashi, K. Sano, K. Shiba, Y. Kumashiro, K. Iwahori, I. Yamashita, and M. Hara. Nano lett. **6**, 515 (2006).

[82] K. Sano, K. Ajima, K. Iwahori, M. Yudasaka, S. I. amd I. Yamashita, and K. Shiba. Small **1**, 826 (2005).

[83] K. Sano, H. Sasaki, and K. Shiba. Langmuir **21**, 3090 (2005).

[84] A. D. Roddick-Lanzilotta and A. J. McQuillan. J. Colloid Interface Sci. **227**, 48 (2000).

[85] A. D. Roddick-Lanzilotta, P. A. Connor, and A. J. McQuillan. Langmuir **14**, 6479 (1998).

[86] K. Imamura, Y. Kawasaki, T. Nagayasu, T. Sakiyama, and K. Nakanishi. J. Biosci. Bioeng. **103** (2007).

[87] H. Chen, X. Su, K.-G. Neoh, and W.-S. Choe. Anal. Chem. **78**, 487 (2006).

[88] G. Polzonetti, C. Battocchio, G. Iucci, M. Dettin, R. Gambaretto, C. D. Bello, and V. Carravetta. Mater. Sci. Eng. **26**, 929 (2006).

[89] G. Iucci, C. Battocchio, M. Dettin, R. Gambaretto, C. D. Bello, F. Borgatti, V. Carravetta, S. Monti, and G. Polzonetti. Surf. Sci. **601**, 3843 (2007).

[90] J. A. D. MacKerell, D. B. M. Bellott, R. L. Dunbrack, Jr., J. D. Evanseck, M. J. Field, S. Fischer, J. Gao, H. Guo, S. Ha, D. Joseph-McCarthy, L. Kuchnir, K. Kuczera, F. T. K. Laux, C. Mattos, S. Michnick, T. Ngo, D. T. Nguyen, B. Prodhom, I. W. E. Reiher, B. Roux, M. Schlenkrich, J. C. Smith, R. Stote, J. Straub, M. Watanabe, J. Wiorkiewicz-Kuczera, D. Yin, and M. Karplus. J. Phys. Chem. B **102**, 3586 (1998).

[91] M. Matsui and M. Akaogi. Mol. Simulat. **6**, 239 (1991).

[92] A. R. Leach. Pearson Education Limited **2nd Edition** (2001).

[93] P. Hohenberg and W. Kohn. Phys. Rev. **136**, 864 (1964).

[94] W. Kohn and L. J. Sham. Phys. Rev. **140**, 1133 (1965).

[95] T. Bucko, J. Hafner, and L. Benco. J. Phys. Chem. B **109**, 7345 (2005).

[96] J. W. Ponder and D. A.Case. Adv. Protein. Chem **66**, 27 (2003).

[97] J. G. Traylor, H. G. Smith, R. M. Nicklow, and M. K. Wilkinson. Phys. Rev. B **3**, 3457 (1971).

[98] D. W. Kim, N. Enomoto, Z. Nakagawa, and K. Kawamura. J. Am. Chem. Soc. **79**, 1095 (1996).

[99] S. Fleming, A. Rohl, M.-Y. Lee, J. Gale, and G. Parkinson. J. Cryst. Growth. **209**, 159 (2000).

[100] L. Verlet. Phys. Rev. **159**, 98 (1967).

[101] S. Nosé. J. Chem. Phys. **81**, 511 (1984).

[102] S. Nosé. Mol. Phys. **52**, 255 (1984).

[103] G. H. Hoover. Phys. Rev. A **31**, 1695 (1985).

[104] A. Laio and M. Parrinello. Phys. Rev. Lett. **92**, 170601 (2002).

[105] L. Wesson and D. Eisenberg. Protein Sci. **1**, 227 (1992).

[106] F. C. Bernstein, T. F. Koetzle, G. J. Williams, E. F. Meyer, M. D. Rodgers, O. Kennard, T. Shimanouchi, and M. Tasumi. J. Mol. Biol. **112**, 535 (1977).

[107] W.Stumm. Chemistry of the Solid-Water Interface, John Wiley and Sons (1992).

[108] M. Ramamoorthy and D. Vanderbilt. Phys. Rev. B. **49**, 16721 (1994).

[109] F. Allegretti, S. O'Brien, M. Polcik, D. I. Sayago, and D. P. Woodruff. Surf. Sci. (2006).

[110] V. E. Henrich, G. Dresselhaus, and H. J. Zeiger. Solid State Commun. **24**, 623 (1977).

[111] D. Brinkley, M. Dietrich, P. Farrall, G. Gantner, A. Schafer, and A. Szuchmacher. Surf. Sci. **395**, 292 (1998).

[112] M. A. Henderson. Surf. Sci. **355** (1996).

[113] W. D. Clendening, J. A. Rodriguez, J. M. Campbell, and C. T. Campbell. Surf. Sci. **2**, 429 (1989).

[114] R. Schaub, P. Thostrup, N. Lopez, E. Logsgaard, I. Stensgaard, J. K. Norskov, and F. Besenbache. Phys. Rev. Lett. **87**, 266104 (2001).

[115] P. J. D. Lindan, J. Muscat, S. Bates, N. M. Harrison, and M. Gillan. Faraday Discuss. **106**, 135 (1997).

[116] P. J. D. Lindan, N. M. Harrison, J. M. Holender, and M. J. Gillan. Chem. Phys. Lett. **261**, 246 (1996).

[117] P. J. D. Lindan, N. M. Harrison, and M. J. Gillan. Phys. Rev. Lett. **80**, 762 (1998).

[118] A. Fahmi and C. Minot. Surf. Sci. **304**, 343 (1994).

[119] T. Bredow and K. Jug. Surf. Sci. **327**, 398 (1995).

[120] C. Zhang and P. J. D. Lindan. J. Chem. Phys. **118**, 4620 (2003).

[121] A. S. Barnard, P. Zapol, and L. A. Curtiss. Surf. Sci. **582**, 173 (2005).

[122] M. Casarin, C. Maccato, and A. Vittadini. Appl. Surf. Sci. **142**, 196 (1999).

[123] M. Casarin, C. Maccato, and A. Vittadini. J. Phys. Chem. B **102**, 10745 (1998).

[124] Z. Zhang, P. Fenter, L. Cheng, N. C. Sturchio, M. J. Bedzyk, M. L. Machesky, and D. J. Wesolowski. J. Surf. Sci. Lett. **554**, L95 (2004).

[125] M. Predota and L. Vlcek. J. Phys. Chem. B **comments** (2007).

[126] M. Predota, P. T. Cummings, and D. J. Wesolowski. Phys. Chem. C **111**, 3071 (2007).

[127] E. Mamontov, L. Vlcek, D. J. Wesolowski, P. T. Cummings, W. Wang, L. M. Anovitz, and J. Rosenqvist. Langmuir **23**, 4925 (2007).

[128] M. Predota, Z. Zhang, P. Fenter, D. J. Wesolowski, and P.T.Cummings. J. Phys. Chem. B **108**, 12061 (2004).

[129] V. N. Koparde and P. T. Cummings. J. Phys. Chem. C. **111**, 6920 (2007).

[130] J. W. Ponder, S. Rubenstein, C. Kundrot, S. Hustonand, M. Dudek, Y. Kong, R. Hart, M. Hodsdon, R. Pappu, W. Mooij, G. Loeffler, M. Vorobieva, N. Sokolova, P. Bagossi, P. Ren, A. Carlsson, A. Kutepov, A. Grossfield, and M. Schnieders. TINKER **Version 4.2** (2004).

[131] M. D. Segall, P. J. D. Lindan, M. J. Probert, C. J. Pickard, P. J. Hasnip, S. J. Clark, and M. C. Payne. J. Phys.: Cond. Matt. **14**, 2717 (2002).

[132] H. J. Monkhurst and J. D. Pack. Phys. Rev. **13**, 5188 (1976).

[133] B. Hammer, L. B. Hansen, and L. K. Norskov. Phys. Rev. B. **59**, 7413 (1999).

[134] E. Spohr. J. Chem. Phys. **107**, 6342 (1997).

[135] S. C. Abrahams and J. L. Bernstein. J. Am. Chem. Soc. **55**, 3206 (1971).

[136] J. K. Burdett, T. Hughbanks, G. J. Miller, J. W. Richardson, and J. V. Smith. J. Am. Chem. Soc. **109**, 3639 (1987).

[137] I. Daidone, F. Simona, D. Roccatano, R. A. Broglia, G. Tiana, G. Colombo, and A. DiNola. Proteins **57** (2004).

[138] S. Patel, P. V. Balaji, and Y. U. Sasidhar. J. Peptide Sci. **13**, 314 (2007).

[139] R. H. Yun, A. Anderson, and D. J. Hermans. Proteins: Structure, Function, and Genetics **10**, 219 (2004).

[140] D. J. Tobias and C. L. Brooks. Biochemistry **30**, 6059 (1991,).

[141] J. Hermans, A. G. Anderson, and R. H. Yun. Biochemistry **31**, 5646 (1992,).

[142] C. L. Brooks and D. A. Case. Chem. Rev. **93**, 2487 (1993).

[143] D. J. Tobias, S. F. Sneddon, and C. L. Brooks. J. Mol. Biol. **227**, 1244 (1992).

[144] L. Monticelli, D. P. Tieleman, and G. Colombo. J. Phys. Chem. B **109,**, 20064 (2005,).

[145] X. Wu and S. Wang. J. Phys. Chem. B, **102,**, 1998 (1998).

[146] X. Wu and S. Wang. J. Phys. Chem. B **105,**, 2227 (2001,).

[147] D. Mitomo, Yukihisa, Watanabe, N. Kamiya, and J. Higo. Chem. Phys. Lett. **427**, 399 (2006).

[148] D. R. Roe, A. Okur, L. Wickstrom, V. Hornak, and C. Simmerling. J. Phys. Chem. B **111**, 1846 (2007).

[149] T. Liang and T. Walsh. Mol. Simulat. **33**, 337 (2007)).

[150] T. Liang and T. R. Walsh. Phys. Chem. Chem. Phys. **8**, 4410 (2006).

[151] S. Marqusee, V. H. Robbins, and R. L. Baldwin. Proc. Natl. Acad. Sci. USA **86**, 5286 (1989).

[152] S. Marqusee and R. L. Baldwin. Proc. Natl. Acad. Sci. USA **84**, 8898 (1987).

[153] S. Padmanabhan, S. Marqusee, T. Ridgeway, T. M. Laue, and R. L. Baldwin. Nature **344**, 268 (1990).

[154] (), DL_POLY is a molecular dynamics simulation package written by W. Smith, T.R. Forester and I.T. Todorov and has been obtained from STFC's Daresbury Laboratory via the website http://www.ccp5.ac.uk/DL_POLY.

[155] D. Song and D. Forcinitia. J. Chem. Phys. p. 8089 (2001).

[156] T. L. Luhrs, C. Ritter, M. Adrian, D. Riek-Loher, B. Bohrmann, H. D. Dubeli, D. Schubert, and R. Riek. Proc. Natl. Acad. Sci. USA **102**, 17342 (2005).

[157] B. Tarus, J. E. Straub, and D. Thirumalai. J. Am. Chem. Soc. **128**, 16159 (2006).

[158] V. Carravetta and S. Monti. J. Phys. Chem. B p. 6160 (2006).

[159] S. Monti, V. Carravetta, W. Zhang, and J. Yang. J. Phys. Chem. C **111**, 7765 (7765).

[160] S. Monti. J. Phys. Chem. C **111**, 6086 (2007).

[161] L. M. W. Langrel. Surf. Sci. **538**, 1 (2003).

[162] V. P. Raut., M. A. Agashe, S. J. Stuart, and R. A. Latour. Langmuir **21**, 1629 (2005).

[163] P. Schravendijk, L. M. Ghiringhelli, L. D. Site, and N. F. A. van der Vegt. J. Phys. Chem. C **111**, 2631 (2007).

[164] N. Kantarci, C. Tamerler, M. Sarikaya, T. Haliloglu, and P. Doruka. Polymer **46**, 4307 (2005).

[165] E. E. Oren, C. Tamerler, and M. Sarikaya. Nano lett. **5**, 415 (2004).

[166] S. D. M. Tomasio and T. R. Walsh. Mol. Phys. **105**, 221 (2007).

[167] Y. Sun and A. Latour. J. Comput. Chem. **27** (2006).

[168] A. A. Mungikar and D. Forciniti. Biomacromolecules **5**, 2147 (2004).

[169] M. Mijajlovic and M. J. Biggs. J. Phys. Chem. **111**, 15839 (2007).

[170] V. Noinville, C. Vidal-Madjar, and B. Sebille. J. Phys. Chem. **99**, 1516 (1995).

[171] S. Ravichandran, J. D. Madura, and J. Talbot. J. Phys. Chem. B **105**, 3610 (2001).

[172] J. Zhou, S. Chen, and S. Jiang. Langmuir **19**, 3472 (2003).

[173] J. Zhou, H. Tsao, Y. Sheng, and S. Jiang. J. Chem. Phys. **121**, 1050 (2004).

[174] G. Raffaini and F. Ganazzoli. Langmuir **20**, 3371 (2004).

[175] G. Raffaini and F. Ganazzoli. Langmuir **19**, 3403 (2003).

[176] S. P. Bates, G. Kresse, and M. J. Gillan. Surf. Sci. **409**, 336 (1998).

[177] M. Agashe, V. Raut, S. J. Stuart, and R. A. Latour. Langmuir **21**, 1103 (2005).